Steady flows of viscoelastics fluids due to moving surface with heat transfer

By

Anum Shafiq

Supervised By

Prof. Dr. Tasawar Hayat

Department of Mathematics
Quaid-I-Azam University
Islamabad, Pakistan
2016

Steady flows of viscoelastics fluids due to moving surface with heat transfer

By

Anum Shafiq

A THESIS SUBMITTED IN THE PARTIAL FULFILLMENT OF THE REQUIREMENT FOR THE DEGREE OF

DOCTOR OF PHILOSOPHY

IN

MATHEMATICS

Supervised By

Prof. Dr. Tasawar Hayat

Department of Mathematics
Quaid-I-Azam University
Islamabad, Pakistan
2016

Steady flows of viscoelastics fluids due to moving surface with heat transfer

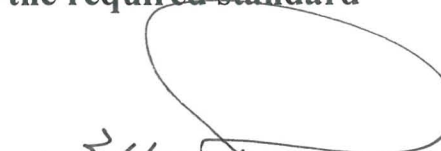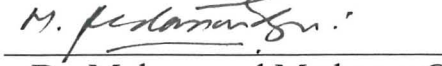## By

Anum Shafiq

CERTIFICATE

A DISSERTATION SUBMITTED IN THE PARTIAL FULFILLMENT OF THE REQUIREMENTS FOR THE DEGREE OF THE DOCTOR OF PHILOSOPHY

We accept this dissertation as conforming to the required standard

1. _____ 18/5/16
   Prof. Dr. Tasawar Hayat
   (Supervisor)

2. _____ 18/5/16
   Prof. Dr. Tasawar Hayat
   (Chairman)

3. _____
   Dr. Rahmat Ellahi   18/5/16
   (External Examiner)

4. _____
   Dr. Muhammad Mudassar Gulzar
   (External Examiner)

Department of Mathematics
Quaid-I-Azam University
Islamabad, Pakistan
2016

ACKNOWLEDGEMENT

Preface

In recent times the analysis of non-Newtonian fluids has acquired a special status due to complex modeling and computations. This motivation stems through the fact that non-Newtonian fluids have widespread applications in geophysics, biological sciences, chemical and petroleum industries. The well-known Navier-Stokes theory is inadequate for the behavior of non-Newtonian materials especially in engineering and biological processes. However such materials in view of their diverse characteristics cannot be described through one constitutive relationship between shear stress and deformation rate. This fact of non-Newtonian materials is quite distinct than the viscous fluid. Besides this the governing equations of non-Newtonian materials in general are higher order than the Navier-Stokes equations. Thus additional boundary or initial conditions are necessary in obtaining a unique solutionfor the arising differential systems. Further the flow of non-Newtonian materials over a moving surface with heat transfer is specifically significant in the extrusion processes, cooling of continuous strips or filaments, paper production, food processes, metallurgical processes and many others.It is due to the fact that the investigators are interested to increase the efficiency of various machines by increasing the rate of heat transfer.The properties of final product also depend greatly upon heat transfer rate at the stretching surface. The cooling rate depends on physical properties of cooling medium including thermal conductivity. To further improve the mechanical properties of the fiber/plastic sheet through better cooling rate, it is necessary that we have to control its viscoelasticity by using polymeric additives. By using such additives the viscosity of the fluid is increased and it slows down the rate of solidification. Having such in mind this thesis develops models analyzing the stretched flows of viscoelastic materials in presence of heat transfer. This thesis is arranged in the form of eleven chapters.

Chapter one comprises literature survey of the previous published works and laws of the conservation of mass, linear momentum, energy and mass transport. Mathematical modeling and boundary layer equations of Walters-B, second-grade and third-grade fluids are presented. Homotopy analysis method is also outlined briefly.

Chapter two concentrates on the flow of Walters-B fluid over a stretching surface with Newtonianheating. The governing partial differential equations are first simplified through boundary layer approximations and then reduced into ordinary differential equations by using the

appropriate substitutions. The resulting problems have been solved for the series solutions by homotopic approach. Convergence analysis is performed. Graphical results for the dimensionless velocity and temperature are presented and discussed for various physical parameters. In addition the expressions of skin friction coefficient and the local Nusselt number are presented. The dimensionless expressions of wall shear stress and wall mass flux are analyzed graphically and numerically. The outcomes of this chapter are published in **Zeitschrift Fur Naturforschung A70 (5) (2015) 317-324.**

Chapter three focuses on melting heat transfer in the stagnation point flow ofWalter-B fluid toward an impermeable stretching sheet. Flow analysis is explored with mixed convection, viscous dissipation and Joule heating. Suitable transformations are employed to achieve the systems of ordinary differential equations. Arising nonlinear problems are solved successfully for the convergent series solutions. Characteristics of various pertinent parameters on the velocity and temperature distributions, skin friction coefficient and Nusselt number are examined. It is found that velocity has opposite behavior for melting parameter and Weissenberg number. The analysis of this chapter has been submitted for publication in **Bulletin of the Polish Academy of Sciences.**

Chapter four investigated the magnetohydrodynamic (MHD) Falkner-Skan flow of second gradenanofluid. The flow is caused by a stretching wedge with melting heat transfer and heat generation/absorption. A system of ordinary differential equations is obtained by using suitable transformations. Convergent series solutions are derived. Influence of various pertinent para-meters on the velocity, temperature and concentration is evaluated. Analysis of the obtained results shows that fluid flow enhances with the increase of wedge and second grade fluid parameters. Also thermophoresis and Brownian motion parameters have reverse behavior on thetemperature and concentration fields.The contents of chapter four are published in **Journal of Molecular Liquid 215 (2016) 664-670.**

Chapter five looks at the heat transfer effects in magnetohydrodynamic (MHD) axisymmetric flow of third-grade fluid between the stretching sheets. Viscous and Joule heating effects are given due attention. The resulting nonlinear problem is computed for the velocity and temperature fields. Expressions of skin friction coefficient and local Nusselt number are calculated. Dimensionless results of velocity and temperature fields are examined for various

parameters of interest. Numerical values of skin friction coefficient and Nusselt number are obtained and analyzed. The investigation of this chapter is published in **Computers and Fluid 86 (2013) 103-108.**

Chapter six addresses the boundary layer flow of third grade fluid over an unsteady permeable stretching sheet with heat transfer. The magnetic and electric fields in the momentum equations are considered. Thermal boundary layer equation includes both viscous and Ohmic dissipations. The related nonlinear partial differential system is reduced first into ordinary differential system and then solved for the series solutions. The dependence of velocity and temperature profiles on the various parameters are shown and discussed by sketching graphs. Expressions of skin friction coefficient and local Nusselt number are calculated and analyzed. Numerical values of skin friction coefficient and Nusselt number are tabulated and examined. It is observed that both velocity and temperature increase in presence of electric field. Further the temperature is increased due to the radiation parameter. Thermal boundary layer thickness enhances by increasing Eckert number. The outcomes of chapter six published in **Plos One 9(1) (2014) 0083153.**

Chapter sevenlooks at the analysis of mixed convective boundary layer flow of third grade fluid with variable thermal conductivity. Thermal conductivity is taken temperature dependent. The flow is caused by an exponential stretching surface. The convergent series solutions for the velocity and temperature are first constructed and then analyzed. Numerical values of local skin friction coefficient and local Nusselt numbers are examined through tabulated values.The results of chapter seven are submitted for publication in **Bulgarian Chemical Communication.**

Chapter eight addresses the magnetohydrodynamic (MHD) stagnation point flow of third-grade fluid by a stretching cylinder. Thermal radiation effectis considered in the analysis of heat transfer phenomenon. Joule heating and viscous dissipation effects are also retained. The resulting nonlinear system is computed for the series solutions. Influence of various physical parameters on the velocity and temperature profiles are scrutinized graphically. A comparative study between Newtonian and third-grade fluids is made. Velocity and temperature profiles in the presence/absence of stagnation point are discussed graphically. Numerical values of skin friction and Nusselt number are also computed and interpreted.The results of this chapter are submitted for publication in **Pramana Journal of Physics.**

Chapter nine addresses the effects of inclined magnetic field and heat transfer in the flow of third-grade fluid due to an exponentially stretching sheet. Formulation and analysis are given in the presence of heat source and sink. The variable thermal conductivity is taken temperature dependent. The governing boundary layer equations and boundary conditions are simplified through appropriate transformations. Resulting equations are solved for the approximate solutions. Convergence of derived solutions is explicitly discussed. Influences of various dimensionless parameters on the flow and thermal fields are discussed. Numerical values of local skin friction coefficient and the local Nusselt number are analyzed. The outcomes of chapter nine are published in **AIP Advances 5 (2015) 087108.**

Chapter ten focuses on the mathematical modeling and analysis of magnetohydrodynamic (MHD) mixed convection stagnation point flow by radially stretching surface. Problem formulation involves the constitutive equations of an incompressible third-grade fluid. In addition heat transfer analysis is examined in presence of Joule heating and Soret and Dufour effects. Adequate transformations lead to the nonlinear ordinary differential systems. Homotopic approach is employed for the convergent series solutions of the resulting problems. Interval of convergence is explicitly determined. The velocity, temperature and concentration are analyzed with respect to different parameters of interest. The skin friction coefficient, Nusselt andSherwood numbers are numerically examined. The contents of this chapter are submitted for publication in Journal of **Applied and Computational Mathematics.**

The main objective of chapter eleven is to model and analyze the characteristics of homogeneous heterogeneous reactions in the magnetohydrodynamic (MHD) flow of third grade fluid over a stretching surface. Both magnetic and electric fields are cosidered. Advanced heat transfer technique (i.e. Newtonian heating) and heat generation/absorption effects are used in the formulation. Homogeneous and heterogeneous reactions are considered within the fluid and at the boundary respectively. Production of heat during chemical reaction is assumed negligible. Approximate convergent solutions are constructed. Influences of various pertinent parameters on the velocity, temperature and concentration distributions are analyzed and discussed. Numerical values of skin friction and local Nusselt number are computed. Concentration distributions for homogeneous and heterogeneous reaction parameters are found opposite. The results of chapter eleven are accepted in **Plos One.**

Contents

Chapter 1

Literature review and basic equations

1.1 Introduction

This chapter comprises literature survey of the previous work related to the viscoelastic fluid, heat transfer, Newtonian heating, melting heat phenomenon and homogeneous-heterogeneous reactions. Governing equations for boundary layer flows of Walters-B, second grade and third grade fluids are also presented. The basic idea of homotopy analysis method (HAM) is also included.

1.2 Background

There is a substantial interest of the recent researchers in the flows of non-Newtonian fluids. Such motivation in these fluids is mainly because of their use in the industrial and technological applications. Many materials like mud, personal care products, ice cream, paints, oils, cheese, asphalt etc. are non-Newtonian fluids. Most biological fluids with higher molecular weight components are non-Newtonian in nature. The usual properties of polymer melts and solutions together with the desirable attributes of many polymeric solids have given rise to the world-wide industry of polymer processing. The non-Newtonian fluids in particular have key importance in geophysics, chemical and nuclear industries, material processing, oil reservoir engineering, bioengineering and many others. Rheological properties of all the non-Newtonian fluids cannot be predicted using single constitutive equation. Therefore many models of non-Newtonian fluids are based either on "natural" modifications of established macroscopic theories or molecular considerations. The additional rheological parameters in the constitutive equations of non-Newtonian fluids are the main culprit for the lack of analytical solutions. The resulting equations are more complex and higher order than the Navier-Stokes equation. Instead the more general Cauchy momentum equation with a proper constitutive law must be adopted. For instance Loureiroa and Freirea [1] studied the asymptotic analysis of turbulent boundary layer flow of purely non-Newtonian fluids. Keimanesha et al. [2] examined the flow of a third grade fluid between two parallel plates using the multi-step differential transform method. Mustafa et al. [3] analyzed the stagnation-point flow and heat transfer of a Casson fluid over a stretched surface. Abbasbandy and Hayat [4] studied the series solution for unsteady boundary layer equations with special third grade fluid. Mahmoud [5] reported the slip velocity effect

in the flow of a power-law fluid over a moving permeable surface with heat generation. Hayat et al. [6] investigated the boundary layer flow of Jeffrey fluid in the presence of convective boundary conditions. Renardy and Wang [7] studied the boundary layer flow of the upper convected Maxwell fluid. Ramzan et al. [8] presented the magnetohydrodynamic three dimensional flow of couple stress fluid in the presence of Newtonian heating. Sahoo and Labropulu [9] analyzed the steady Homann flow and heat transfer of an electrically conducting fluid. A subclass of non-Newtonian fluids is viscoelastic fluid. Such fluids exhibit both viscous and elastic characteristics. The importance of viscoelastic flow is increasing day by day in paper and petroleum industries, chemical technology and geophysical fluid dynamics. The viscoelastic features of non-Newtonian fluids in general are classified by three categories namely the differential, rate and integral types. The simplest subclass of differential type materials is second-grade. It should be noted that second-grade fluid captures the normal stress effect whereas the shear thinning and shear thickening properties even in steady flow situation can be only analyzed by third-grade fluid. In this thesis we studied the viscoelastic fluids like Walters-B [10-13], second grade [14-17] and third grade [18-21] fluids.

Magnetohydrodynamics (MHD) is a study of the interaction of electrically conducting fluids and electromagnetic forces. The MHD fluid was first introduced by Swedish Physicist, Alfven [22]. Hartman and Lazarus [23] studied the effects of a transverse uniform magnetic field in the flow of an incompressible viscous fluid between two infinite insulating parallel plates. In recent years the study of magnetohydrodynamic flow of an electrically conducting fluid past a heated surface has attracted the attention of many researchers. This is because of its considerable applications in many engineering problems such as plasma studies, petroleum industries, MHD power generators, cooling of nuclear reactors, the boundary layer control in aerodynamics and crystal growth. Extensive literature on the MHD flows in presence of applied magnetic field exists now. For example Rashidi et al. [24] considered the MHD flow of nanofluid induced by a rotating disk. Shehzad et al. [25] analyzed the hydromagnetic flow of Maxwell fluid over a bidirectional stretching surface with variable thermal conditions. Turkyilmazoglu [26] analyzed the exact solution of magnetohydrodynamic viscous fluid by a rotating disk. Hayat et al. [27] discussed the buoyancy driven MHD flow of thixotropic fluid. They also examined the effects of thermophoresis and Joule heating in this investigation. An applied magnetic field effect in natural convection flow of nanofluid is studied by Sheikholeslami et al. [28]. Dandapat and Mukhopadhyay [29] discussed the stability characteristics of a thin conducting liquid film flowing and a non-conducting plane in the presence of electromagnetic field. Hayat et al. [30] investigated the series solution of magnetohydrodynamic axisymmetric flow of third grade fluid between porous disks with heat transfer. Unsteady magnetohydrodynamic mixed convection stagnation point flow of viscoelastic fluid towards a vertical surface is discussed by Ahmad and Nazar [31]. Magnetohydrodynamic Jeffery Hamel nanofluid flow through non-parallel walls is investigated analytically by Hatami et al. [32]. They used different base fluids and nanoparticle. Sheikholeslami et al. [33] considered the effect of MHD in an inclined L-shape enclosure filled with nanofluid. Analytical solution of boundary layer magnetohydrodynamic free convective flow over a vertical porous plate has been studied by Raju et al. [34]. They also considered the heat transfer analysis with thermal radiation and chemical reaction. Three dimensional boundary layer flow of Maxwell fluid is investigated

by Awais et al. [35]. Freidoonimehr et al. [36] has studied the effect of uniform magnetic field on a free convective boundary layer flow of nanofluid. Sheikholeslami et al. [37] reported the effects of radiation and magnetohydrodynamics in flow of nanofluid. Sheikholeslami and Ganji [38] investigated the hydrothermal behavior of nanofluid with variable magnetic field.

Heat transfer in flows induced by a continuously stretching surface is significant in industrial engineering processes like cooling of the cutting tools during machining operations, cooling of electronic components in computers, the generation and condensation of steam in a thermal power plant, heating and cooling of the buildings and thermal control of reentering of the space craft. In view of above mentioned physical situation several investigations through numerous flow configurations have been carried out. Recently melting effects for heat transfer is given much attention. This is due to the fact that it has applications in permafrost melting, preparation of semi-conductor material and solidification of magma flows. Pedroso and Domoto [39] devised methodology for calculating melting rates based on the diffusion/melting. Afterwards some studies have been presented to analyze the effect of melting heat transfer. Epstein [40] investigated the effect of melting on heat transfer to submerged bodies. Melting heat transfer in a steady laminar flow of viscous fluids over a plate has been considered by Epstein and Cho [41]. Kazmierczak et al. [42] explored characteristics of melting heat transfer in the flow of dissimilar fluid by a vertical plate in porous medium. Cheng and Lin [43, 44] studied combined effects of melting and mixed convection in steady and unsteady flows due to a vertical plate saturated with porous medium. Ishak et al. [45] analyzed the effect of melting in flow over a surface with parallel free stream. Bachok et al. [46] examined melting phenomenon in the stagnation point flow towards a stretching/shrinking surface. Yacob et al. [47] studied the steady boundary layer stagnation-point flow of micropolar fluid towards a horizontal linearly stretching/shrinking surface. The authors employed Runge Kutta-Fehlberg method with shooting technique for the numerical solution. Gorla et al. [48] investigated the melting heat transfer in a nanofluid flow towards a permeable continuous moving sheet. Abdel-Rahman et al. [49] numerically analyzed the problem of magnetohydrodynamic steady laminar flow and heat transfer from a warm laminar liquid flow to a melting moving surface in the presence of thermal radiation. Numerical solution by implicit finite difference method (FDM) is given. Hayat et al. [50] considered the problem to study the characteristics of melting heat transfer in the boundary layer stagnation point flow of third grade fluid past a stretching surface. Boundary layer stagnation point flow of second grade fluid towards a stretching sheet with Dufour and Soret effects combined with melting heat transfer has been examined by Hayat et al. [51]. Awais et al. [52] presented the analytical and numerical solutions for the melting heat transfer in boundary layer stagnation-point flow with thermal-diffusion and diffusion-thermo effects. Hayat et al. [53] also investigated the characteristics of melting heat transfer in the stagnation-point flow of Maxwell fluid with double-diffusive convection. Combined effects of radiation and melting in magnetohydrodynamic boundary layer flow past a moving surface is disclosed by Das [54].

Four different types of heat transfer from wall to ambient fluid was first considered by Merkin [55] i.e., (a) constant or prescribed surface temperature, (b) constant or prescribed surface heat flux, (c) conjugate boundary conditions and (d) Newtonian heating in which heat transfer from bounding surface

with a finite heat capacity is proportional to the local surface temperature. Researchers utilized the Newtonian heating process in their practical applications such as to design heat exchanger, conjugate heat transfer around fins and also in convection flows setup where bounding surfaces absorb heat by solar radiations. Lesic et al. [56] studied free convective boundary layer flow of viscous fluid towards a horizontal surface embedded in a porous medium with Newtonian heating. Behavior of heat transport in the flow of viscous fluid towards a sheet with Newtonian heating and porous medium is reported by Lesic et al. [57]. Salleh et al. [58] studied forced convection stagnation point flow of viscous fluid with Newtonian heating. Further Salleh et al. [59] examined heat transfer characteristics in flow of viscous fluid over a stretching surface with Newtonian heating. Magnetohydrodynamic boundary layer flow of nanofluid past a vertical flat plate with Newtonian heating is investigated by Uddin et al. [60]. Hayat et al. [61] discussed mixed convective heat transport in the Falkner-Skan flow of Maxwell fluid with Newtonian heating. Hayat et al. [62] analyzed the flow of second grade fluid towards a stretching surface with Newtonian heating. Makinde [63] constructed the computational modelling for unsteady MHD flow of viscous fluid past a flat plate with Newtonian heating and Navier slip effects. Ramzan et al. [64] discussed the magnetohydrodynamic three dimensional flow of couple stress fluid in the presence of Newtonian heating. Viscous dissipation effect in the flow of nanofluid with Newtonian heating was studied by Makinde [65]. Sarif et al. [66] examined boundary layer flow induced by stretching sheet with Newtonian heating.

The natural processes of chemical reactions involve both homogeneous and heterogeneous reactions. Some of the reactions have the ability to proceed very slowly or not at all, except in the presence of a catalyst. The interaction between the homogeneous and heterogeneous reactions is very complex involving the production and consumption of reactant species at different rates both within the fluid and on the catalyst surface such as reactions occurring in combustion, catalysis and biochemical systems. Merkin [67, 68] studied the isothermal model for homogeneous heterogeneous reactions in the boundary layer flow with equal and different diffusivities of reactant and autocatalyst. Further Chaudhary and Merkin [69] analyzed the characteristics of homogeneous-hetrogeneous reactions in the boundary layer flow with loss of reactant. Khan and Pop [70] examined the problem of stagnation point flow of viscous fluid over a permeable wall in the presence of homogeneous-hetrogeneous reaction. Characteristics of homogeneous-hetrogeneous reactions in the stagnation point flow of viscous fluid towards a stretched surface is investigated by Bachok et al. [71]. Shaw et al. [72] investigated the effects of homogeneous-heterogeneous reactions in the flow of micropolar fluid induced by stretching/shrinking sheet embedded in a porous medium. The analysis of homogeneous-heterogeneous reactions in flow of nanofluid past a permeable stretching sheet was examined by Kaneswaran et al. [73].

1.3 Fundamental laws

1.3.1 Conservation law of mass

Law of mass conservation states that mass neither be created nor destroyed. Mathematically, for compressible fluid it can be expressed as

$$\frac{\partial \rho}{\partial t} + \boldsymbol{\nabla}.\left(\rho \mathbf{V}\right) = 0. \tag{1.1}$$

In above expression, ρ indicates the density of fluid and $\mathbf{V}$ the velocity field.

For incompressible fluid, we have

$$\boldsymbol{\nabla}.\mathbf{V} = 0. \tag{1.2}$$

In Cartesian coordinates, one can write it as follows:

$$\frac{\partial u}{\partial x} + \frac{\partial v}{\partial y} + \frac{\partial w}{\partial z} = 0, \tag{1.3}$$

while in cylindrical coordinates we have

$$\frac{1}{r}\frac{\partial}{\partial r}\left(rv_r\right) + \frac{1}{r}\frac{\partial}{\partial \theta}\left(v_\theta\right) + \frac{\partial}{\partial z}\left(v_z\right) = 0. \tag{1.4}$$

1.3.2 Conservation law of linear momentum

This law states that total linear momentum of the system is conserved. It is derived from Newton's second law. Mathematically we have

$$\rho\frac{d\mathbf{V}}{dt} = \boldsymbol{\nabla}.\boldsymbol{\tau} + \rho\mathbf{b}. \tag{1.5}$$

Here left hand side (L. H. S.) of Eq. (1.5) represents inertial forces while on right hand side (R. H. S.) first term represents surface forces and second term represents body forces. In the above expression $\frac{d}{dt}$ denotes material time derivative, ρ denotes density, $\mathbf{V}$ denotes velocity field, $\boldsymbol{\tau}$ represents Cauchy stress tensor and $\mathbf{b}$ represents body force. For incompressible fluid Cauchy stress tensor is defined as

$$\boldsymbol{\tau} = -p\mathbf{I} + \mathbf{S}. \tag{1.6}$$

Here p denotes pressure, $\mathbf{I}$ denotes identity tensor and $\mathbf{S}$ denotes extra stress tensor.

Using velocity field $\mathbf{V} = \left[u\left(x,y,z,t\right), v\left(x,y,z,t\right), w\left(x,y,z,t\right)\right]$, momentum equations in Cartesian coordinates can be expressed in the following forms

$$\rho\left(\frac{\partial u}{\partial t} + u\frac{\partial u}{\partial x} + v\frac{\partial u}{\partial y} + w\frac{\partial u}{\partial z}\right) = \frac{\partial \tau_{xx}}{\partial x} + \frac{\partial \tau_{xy}}{\partial y} + \frac{\partial \tau_{xz}}{\partial z} + \rho b_x, \tag{1.7}$$

$$\rho\left(\frac{\partial v}{\partial t} + u\frac{\partial v}{\partial x} + v\frac{\partial v}{\partial y} + w\frac{\partial v}{\partial z}\right) = \frac{\partial \tau_{yx}}{\partial x} + \frac{\partial \tau_{yy}}{\partial y} + \frac{\partial \tau_{yz}}{\partial z} + \rho b_y, \tag{1.8}$$

$$\rho\left(\frac{\partial w}{\partial t} + u\frac{\partial w}{\partial x} + v\frac{\partial w}{\partial y} + w\frac{\partial w}{\partial z}\right) = \frac{\partial \tau_{zx}}{\partial x} + \frac{\partial \tau_{zy}}{\partial y} + \frac{\partial \tau_{zz}}{\partial z} + \rho b_z, \tag{1.9}$$

where $\tau_{xx}, \tau_{xy}, \tau_{xz}, \tau_{yx}, \tau_{yy}, \tau_{yz}, \tau_{zx}, \tau_{zy}$ and τ_{zz} represent the components of Cauchy stress tensor and b_x, b_y and b_z represent components of body force.

Using velocity field $\mathbf{V} = [v_r(r, \theta, z, t), v_\theta(r, \theta, z, t), v_x(r, \theta, z, t)]$ momentum equations in cylindrical coordinates can be written as follows:

$$\rho \left(\frac{\partial v_r}{\partial t} + v_r \frac{\partial v_r}{\partial r} + \frac{v_\theta}{r} \frac{\partial v_r}{\partial \theta} - \frac{v_\theta^2}{r} + v_z \frac{\partial v_r}{\partial z} \right) = \frac{1}{r} \frac{\partial}{\partial r} (r \tau_{rr}) + \frac{1}{r} \frac{\partial}{\partial \theta} (\tau_{r\theta}) + \frac{\partial}{\partial x} (\tau_{rz}) - \frac{\tau_{\theta\theta}}{r} + \rho b_r, \quad (1.10)$$

$$\rho \left(\frac{\partial v_\theta}{\partial t} + v_r \frac{\partial v_\theta}{\partial r} + \frac{v_\theta}{r} \frac{\partial v_\theta}{\partial \theta} - \frac{v_r v_\theta}{r} + v_z \frac{\partial v_\theta}{\partial z} \right) = \frac{1}{r^2} \frac{\partial}{\partial r} (r^2 \tau_{\theta r}) + \frac{1}{r} \frac{\partial}{\partial \theta} (\tau_{\theta\theta}) + \frac{\partial}{\partial z} (\tau_{\theta z}) + \rho b_\theta, \quad (1.11)$$

$$\rho \left(\frac{\partial v_z}{\partial t} + v_r \frac{\partial v_z}{\partial r} + \frac{v_\theta}{r} \frac{\partial v_z}{\partial \theta} + v_z \frac{\partial v_z}{\partial z} \right) = \frac{1}{r} \frac{\partial}{\partial r} (r \tau_{zr}) + \frac{1}{r} \frac{\partial}{\partial \theta} (\tau_{z\theta}) + \frac{\partial}{\partial z} (\tau_{zz}) + \rho b_z, \quad (1.12)$$

in which $\tau_{rr}, \tau_{r\theta}, \tau_{rz}, \tau_{\theta r}, \tau_{\theta\theta}, \tau_{\theta z}, \tau_{zr}, \tau_{z\theta}$ and τ_{zz} represent the components of Cauchy stress tensor and b_r, b_θ and b_z represent components of body force.

1.3.3 Conservation law of energy

The conservation law of energy physically depicts that total energy of the system remains constant. It is derived from first law of thermodynamics. Mathematical form of this law can express as follows:

$$\rho c_p \frac{dT}{dt} = \boldsymbol{\tau}.\mathbf{L} - \operatorname{div} \mathbf{q} - \operatorname{div} \mathbf{q}_r. \quad (1.13)$$

The term on the L.H.S. of Eq. (1.13) denotes internal energy, first term on R.H.S. denotes viscous dissipation while the second and third terms represent thermal and radiative heat fluxes respectively. ρ the density, c_p the specific heat at constant pressure, T the temperature of fluid, $\boldsymbol{\tau}$ the Cauchy stress tensor and $\mathbf{q}$ and $\mathbf{q}_r$ depict thermal and radiative heat fluxes respectively. These thermal and radiative heat fluxes are defined by Fourier's law of heat conduction and Stefan Boltzman law respectively.

1.3.4 Equation of mass transfer

This law describes that total concentration of the system under observation remains constant. It is derived from Fick's second law. Mathematically it can be written in the absence of chemical reaction as

$$\frac{dC}{dt} = -\boldsymbol{\nabla}.\mathbf{j}. \quad (1.14)$$

From Fick's first law we have

$$\mathbf{j} = -D\boldsymbol{\nabla}C. \quad (1.15)$$

Hence equation of mass transfer becomes

$$\frac{dC}{dt} = D\boldsymbol{\nabla}^2 C, \quad (1.16)$$

where C denotes concentration of specie, D denotes mass diffusivity and $\mathbf{j}$ denotes mass flux.

1.4 Boundary layer constitutive equations

This thesis is based on the description of boundary layer flows of Walters-B, second grade and third grade fluids. Therefore we briefly explain the mathematical modeling of these fluid models.

1.4.1 Walters B fluid

Walters [10-13] has presented an elegant model for the rheological equation of state of a viscoelastic fluid. This model can accurately simulate the complex flow behavior of various polymer solutions, hydrocarbons, paints and other industrial liquids. The Walters-B model generates highly non-linear flow equations which are an order higher than the classical Navier–Stokes equations. It also introduces elastic properties of the fluid which are important in extensional behavior of polymers. The extra stress tensor $\mathbf{S}$ for Walters-B fluid is defined as:

$$\mathbf{S} = 2\mu_0 \mathbf{A}_1 - 2k_0 \frac{d\mathbf{A}_1}{dt}, \tag{1.17}$$

where

$$\frac{d\mathbf{A}_1}{dt} = \frac{\partial \mathbf{A}_1}{\partial t} + \mathbf{V}.\boldsymbol{\nabla}\mathbf{A}_1 - \mathbf{A}_1.\boldsymbol{\nabla}\mathbf{V} - (\boldsymbol{\nabla}\mathbf{V})^{t^*}.\mathbf{A}_1, \tag{1.18}$$

in which $\mathbf{A}_1$ denotes rate of strain tensor, $\mathbf{V}$ denotes the velocity field of fluid, $\frac{d\mathbf{A}_1}{dt}$ denotes the covariant derivatives of the rate of strain tensor in relation to the material in motion, μ_0 denotes the limiting viscosity and k_0 denotes the short memory coefficient. The values of μ_0 and k_0 are defined as follows:

$$\mu_0 = \int_0^\infty N(\kappa)\, d\kappa, \tag{1.19}$$

$$k_0 = \int_0^\infty \kappa N(\kappa)\, d\kappa, \tag{1.20}$$

where $N(\kappa)$ denotes the distribution function with relaxation time κ. By taking short term memory into account the following term

$$\int_0^\infty \kappa^s N(\kappa)\, d\kappa, \qquad s \geq 2, \tag{1.21}$$

is neglected in case of Walters-B fluid.

Components of Cauchy stress tensor of Walters-B fluid are

$$\tau_{xx} = -p + 2\mu_0 \frac{\partial u}{\partial x} - 2k_0 \left(u\frac{\partial^2 u}{\partial x^2} + v\frac{\partial^2 u}{\partial x \partial y} - 2\left(\frac{\partial u}{\partial x}\right)^2 - \frac{\partial u}{\partial y}\left(\frac{\partial v}{\partial x} + \frac{\partial u}{\partial y}\right)\right), \tag{1.22}$$

$$\tau_{yy} = -p + 2\mu_0 \frac{\partial v}{\partial y} - 2k_0 \left(u\frac{\partial^2 v}{\partial x \partial y} + v\frac{\partial^2 v}{\partial y^2} - 2\left(\frac{\partial v}{\partial y}\right)^2 - \frac{\partial v}{\partial x}\left(\frac{\partial v}{\partial x} + \frac{\partial u}{\partial y}\right)\right), \tag{1.23}$$

$$\tau_{xy} = \tau_{yx} = \mu_0 \left(\frac{\partial u}{\partial y} + \frac{\partial v}{\partial x} \right) - k_0 \left[u \left(\frac{\partial^2 u}{\partial x \partial y} + \frac{\partial^2 v}{\partial x^2} \right) \right.$$
$$\left. + v \left(\frac{\partial^2 u}{\partial y^2} + \frac{\partial^2 v}{\partial x \partial y} \right) - 2 \frac{\partial u}{\partial x} \frac{\partial v}{\partial x} - 2 \frac{\partial u}{\partial y} \frac{\partial v}{\partial y} \right]. \tag{1.24}$$

Invoking the components of Cauchy stress tensor in equation of motion and applying the boundary layer approximations $(u = O(1), \; x = O(1), \; v = O(\delta), \; y = O(\delta))$, we have

$$u \frac{\partial u}{\partial x} + v \frac{\partial u}{\partial y} = -\frac{1}{\rho} \frac{\partial p}{\partial x} + \nu \frac{\partial^2 u}{\partial y^2} - \frac{k_0}{\rho} \left[u \frac{\partial^3 u}{\partial x \partial y^2} + v \frac{\partial^3 u}{\partial y^3} + \frac{\partial u}{\partial x} \frac{\partial^2 u}{\partial y^2} - \frac{\partial u}{\partial y} \frac{\partial^2 u}{\partial x \partial y} \right]. \tag{1.25}$$

1.4.2 Second grade fluid

The constitutive equation for the Cauchy stress in a second-grade fluid is [14–17]:

$$\tau = -p\mathbf{I} + \mu \mathbf{A}_1 + \alpha_1^* \mathbf{A}_2 + \alpha_2^* \mathbf{A}_1^2, \tag{1.26}$$

where p denotes scalar pressure, $\mathbf{I}$ denotes the identity tensor and μ denotes the coefficient of viscosity. The first two kinematic tensors $\mathbf{A}_1$ and $\mathbf{A}_2$ are

$$\mathbf{A}_1 = \nabla \mathbf{V} + (\nabla \mathbf{V})^{t^*}, \tag{1.27}$$

$$\mathbf{A}_2 = \frac{d\mathbf{A}_1}{dt} + \mathbf{A}_1 (\nabla \mathbf{V}) + (\nabla \mathbf{V})^{t^*} \mathbf{A}_1, \tag{1.28}$$

in which $\mathbf{V}$ denotes the fluid velocity, $\frac{d}{dt}$ is the material derivative and α_1^* and α_2^* are respectively the viscoelasticity and cross-viscosity of the fluid. According to Dunn and Fosdick [14] and Fosdick and Rajagopal [15] the equation (1.26) is compatible with thermodynamics in the sense that all motions satisfy the Clausius-Duhem inequality and the assumption that at constant temperature the specific Helmholtz free energy is a minimum in equilibrium then the material moduli must satisfy the conditions given below:

$$\mu \geq 0, \;\; \alpha_1^* > 0, \qquad \alpha_1^* + \alpha_2^* = 0. \tag{1.29}$$

Component form of two-dimensional steady flow of second-grade fluid are

$$u \frac{\partial u}{\partial x} + v \frac{\partial u}{\partial y} = -\frac{1}{\rho} \frac{\partial p}{\partial x} + \nu \left(\frac{\partial^2 u}{\partial x^2} + \frac{\partial^2 u}{\partial y^2} \right) + \frac{\alpha_1^*}{\rho} \left[5 \frac{\partial u}{\partial x} \frac{\partial^2 u}{\partial x^2} + u \frac{\partial^3 u}{\partial x^3} + v \frac{\partial^3 u}{\partial x^2 \partial y} + u \frac{\partial^3 u}{\partial y^2 \partial x} \right.$$
$$\left. + \frac{\partial u}{\partial y} \frac{\partial^2 u}{\partial y \partial x} + \frac{\partial u}{\partial x} \frac{\partial^2 u}{\partial y^2} + v \frac{\partial^3 u}{\partial y^3} + \frac{\partial u}{\partial y} \frac{\partial^2 v}{\partial x^2} + 2 \frac{\partial v}{\partial x} \frac{\partial^2 v}{\partial x^2} \right], \tag{1.30}$$

$$u \frac{\partial v}{\partial x} + v \frac{\partial v}{\partial y} = -\frac{1}{\rho} \frac{\partial p}{\partial y} + \nu \left(\frac{\partial^2 v}{\partial x^2} + \frac{\partial^2 v}{\partial y^2} \right) + \frac{\alpha_1^*}{\rho} \left[2 \frac{\partial u}{\partial y} \frac{\partial^2 u}{\partial y^2} + \frac{\partial v}{\partial x} \frac{\partial^2 u}{\partial y^2} + u \frac{\partial^3 v}{\partial x^3} + v \frac{\partial^3 v}{\partial x^2 \partial y} + \frac{\partial v}{\partial x} \frac{\partial^2 v}{\partial y \partial x} \right.$$
$$\left. + u \frac{\partial^3 v}{\partial y^2 \partial x} + \frac{\partial v}{\partial y} \frac{\partial^2 v}{\partial x^2} + 5 \frac{\partial v}{\partial y} \frac{\partial^2 v}{\partial y^2} + v \frac{\partial^3 v}{\partial y^3} \right]. \tag{1.31}$$

After using the boundary layer approximations, we have

$$u\frac{\partial u}{\partial x} + v\frac{\partial u}{\partial y} = -\frac{1}{\rho}\frac{\partial p}{\partial x} + \nu\frac{\partial^2 u}{\partial y^2} + \frac{\alpha_1^*}{\rho}\left(\frac{\partial u}{\partial x}\frac{\partial^2 u}{\partial y^2} + u\frac{\partial^3 u}{\partial x\partial y^2} - \frac{\partial u}{\partial y}\frac{\partial^2 v}{\partial y^2} + v\frac{\partial^3 u}{\partial y^3}\right). \tag{1.32}$$

1.4.3 Third grade fluid

The Cauchy stress tensor $\boldsymbol{\tau}$ in third grade fluid is

$$\boldsymbol{\tau} = -p\mathbf{I} + \mu\mathbf{A}_1 + \alpha_1^*\mathbf{A}_2 + \alpha_2^*\mathbf{A}_1^2 + \beta_1\mathbf{A}_3 + \beta_2\left(\mathbf{A}_1\mathbf{A}_2 + \mathbf{A}_2\mathbf{A}_1\right) + \beta_3\left(tr\mathbf{A}_1^2\right)\mathbf{A}_1, \tag{1.33}$$

in which $\mathbf{I}$ is the identity tensor, μ is the fluid dynamic viscosity and α_1^*, α_2^*, β_1, β_2, β_3 are the material constants of third-grade fluid. Note that Eq. (1.33) is compatible with thermodynamics when the material constants satisfy

$$\mu \geq 0, \ \alpha_1^* \geq 0, \ \beta_1 = \beta_2 = 0, \ \beta_3 \geq 0, \ \alpha_1^* + \alpha_2^* \leq \sqrt{24\mu\beta_3}. \tag{1.34}$$

The expression for Rivlin-Ericksen tensors $\mathbf{A}_1$, $\mathbf{A}_2$ and $\mathbf{A}_3$ are

$$\mathbf{A}_1 = \nabla\mathbf{V} + (\nabla\mathbf{V})^T, \tag{1.35}$$

$$\mathbf{A}_2 = \frac{d\mathbf{A}_1}{dt} + \mathbf{A}_1(\nabla\mathbf{V}) + (\nabla\mathbf{V})^T\mathbf{A}_1, \tag{1.36}$$

$$\mathbf{A}_n = \frac{d\mathbf{A}_{n-1}}{dt} + \mathbf{A}_{n-1}(\nabla\mathbf{V}) + (\nabla\mathbf{V})^T\mathbf{A}_{n-1}. \tag{1.37}$$

Component form of two dimensional steady flow of third-grade fluid are given below:

$$\begin{aligned}
\rho\left(u\frac{\partial u}{\partial x} + v\frac{\partial u}{\partial y}\right) = & -\frac{\partial p}{\partial x} + \mu\left(\frac{\partial^2 u}{\partial x^2} + \frac{\partial^2 u}{\partial y^2}\right) + \alpha_1^*\left\{\frac{\partial u}{\partial x}\frac{\partial^2 u}{\partial y^2} + 13\frac{\partial^2 u}{\partial x^2} + 3\frac{\partial u}{\partial y}\frac{\partial^2 u}{\partial x\partial y}\right.\\
& + 3\frac{\partial u}{\partial y}\frac{\partial^2 v}{\partial x^2} + 2\frac{\partial v}{\partial x}\frac{\partial^2 u}{\partial x\partial y} + 4\frac{\partial v}{\partial x}\frac{\partial^2 v}{\partial x^2} + v\frac{\partial^3 u}{\partial y^3} + v\frac{\partial^3 u}{\partial x^2\partial y} + u\frac{\partial^3 u}{\partial y^2\partial x}\\
& \left. + u\frac{\partial^3 u}{\partial x^3}\right\} + \alpha_2^*\left\{8\frac{\partial u}{\partial x}\frac{\partial^2 u}{\partial x^2} + 2\left(\frac{\partial u}{\partial y} + \frac{\partial v}{\partial x}\right)\left(\frac{\partial^2 u}{\partial x\partial y} + \frac{\partial^2 v}{\partial x^2}\right)\right\}\\
& + 2\beta_3\left\{4\frac{\partial^2 u}{\partial y^2}\left(\frac{\partial u}{\partial x}\right)^2 + 3\frac{\partial^2 u}{\partial y^2}\left(\frac{\partial v}{\partial x}\right)^2 + 3\frac{\partial^2 u}{\partial y^2}\left(\frac{\partial u}{\partial y}\right)^2\right.\\
& + 4\frac{\partial v}{\partial x}\left(\frac{\partial u}{\partial x}\frac{\partial^2 v}{\partial x^2} + 3\frac{\partial u}{\partial x}\frac{\partial^2 u}{\partial x\partial y}\right) + 2\frac{\partial u}{\partial y}\frac{\partial v}{\partial x}\left(3\frac{\partial^2 u}{\partial y^2} - \frac{\partial^2 u}{\partial x^2}\right)\\
& \left. + 2\frac{\partial u}{\partial x}\left(3\frac{\partial^2 u}{\partial x\partial y} + \frac{\partial^2 v}{\partial x^2}\right) + \frac{\partial^2 u}{\partial x^2}\left(20\left(\frac{\partial u}{\partial x}\right)^2 - \left(\frac{\partial v}{\partial x}\right)^2 - \left(\frac{\partial u}{\partial y}\right)^2\right)\right\},
\end{aligned}$$
$$\tag{1.38}$$

$$\begin{aligned}
\rho\left(u\frac{\partial v}{\partial x} + v\frac{\partial v}{\partial y}\right) = & -\frac{\partial p}{\partial y} + \mu\left(\frac{\partial^2 v}{\partial x^2} + \frac{\partial^2 u}{\partial x\partial y}\right) + \alpha_1^*\left\{\frac{\partial u}{\partial y}\left(4\frac{\partial^2 u}{\partial y^2} - 2\frac{\partial^2 u}{\partial x^2}\right) - \frac{\partial^2 v}{\partial x^2}\frac{\partial u}{\partial x}\right.\\
& \left. + 13\frac{\partial u}{\partial x}\frac{\partial^2 u}{\partial x\partial y} + 3\left(\frac{\partial^2 u}{\partial y^2} - \frac{\partial^2 u}{\partial x^2}\right) - v\left(\frac{\partial^3 u}{\partial y^2\partial x} + \frac{\partial^3 u}{\partial x^3}\right) + u\left(\frac{\partial^3 v}{\partial x^3} - \frac{\partial^3 u}{\partial x^2\partial y}\right)\right\}
\end{aligned}$$

$$+\alpha_2^* \left\{ 8\frac{\partial u}{\partial x}\frac{\partial^2 u}{\partial x \partial y} + 2\left(\frac{\partial u}{\partial y} + \frac{\partial v}{\partial x}\right)\left(\frac{\partial^2 u}{\partial y^2} - \frac{\partial^2 u}{\partial x^2}\right) \right\}$$

$$+2\beta_3 \left\{ 4\frac{\partial u}{\partial x}\frac{\partial v}{\partial x}\left(3\frac{\partial^2 u}{\partial x^2} - \frac{\partial^2 u}{\partial y^2}\right) + 4\frac{\partial^2 u}{\partial x^2}\left(\frac{\partial^2 v}{\partial x^2} - 5\frac{\partial^2 u}{\partial x \partial y}\right) + 12\frac{\partial u}{\partial y}\frac{\partial^3 u}{\partial x^3} \right.$$

$$+ \left(\frac{\partial v}{\partial x}\right)^2\left(\frac{\partial^2 u}{\partial x \partial y} + 3\frac{\partial^2 v}{\partial x^2}\right) + 6\frac{\partial u}{\partial y}\frac{\partial v}{\partial x}\frac{\partial^2 v}{\partial x^2} + \left(\frac{\partial u}{\partial y}\right)^2\left(\frac{\partial^2 u}{\partial x \partial y} + 3\frac{\partial^2 v}{\partial x^2}\right.$$

$$\left. \left. -4\frac{\partial u}{\partial x}\frac{\partial^2 u}{\partial y^2} + 2\frac{\partial^2 u}{\partial x \partial y}\frac{\partial v}{\partial x}\right) \right\}. \tag{1.39}$$

After using the boundary layer approximations, we have

$$u\frac{\partial u}{\partial x} + v\frac{\partial u}{\partial y} = -\frac{1}{\rho}\frac{\partial p}{\partial x} + \nu\frac{\partial^2 u}{\partial y^2} + \frac{\alpha_1^*}{\rho}\left[u\frac{\partial^3 u}{\partial x \partial y^2} + \frac{\partial u}{\partial x}\frac{\partial^2 u}{\partial y^2} + 3\frac{\partial u}{\partial y}\frac{\partial^2 v}{\partial y^2} + v\frac{\partial^3 u}{\partial y^3}\right]$$

$$+2\frac{\alpha_2^*}{\rho}\frac{\partial u}{\partial y}\frac{\partial^2 v}{\partial y^2} + 6\frac{\beta_3}{\rho}\left(\frac{\partial u}{\partial y}\right)^2\frac{\partial^2 u}{\partial y^2}. \tag{1.40}$$

In cylinderical co-ordinates, component form of two-dimensional steady flow of third-grade fluid are given below:

$$\rho\left(u\frac{\partial u}{\partial r} + w\frac{\partial u}{\partial z}\right) = -\frac{\partial p}{\partial r} + \mu\left(\frac{\partial^2 u}{\partial r^2} + \frac{\partial^2 u}{\partial z^2} + \frac{1}{r}\frac{\partial u}{\partial r} - \frac{u}{r^2}\right)$$

$$+\alpha_1^*\left[-\frac{2u^2}{r^3} - 2\frac{w}{r^2}\frac{\partial u}{\partial z} + \frac{4}{r}\left(\frac{\partial u}{\partial r}\right)^2 + \frac{\partial u}{\partial z}\frac{\partial^2 w}{\partial z^2} + w\frac{\partial^3 u}{\partial z^3} - 2\frac{u}{r^2}\frac{\partial u}{\partial r}\right.$$

$$+3\frac{\partial u}{\partial r}\frac{\partial^2 u}{\partial z^2} + 3\frac{\partial w}{\partial r}\frac{\partial^2 w}{\partial z^2} + \frac{2}{r}\left(\frac{\partial w}{\partial r}\right)^2 + \frac{2w}{r}\frac{\partial^2 u}{\partial r \partial z} + 5\frac{\partial w}{\partial r}\frac{\partial^2 u}{\partial r \partial z}$$

$$+4\frac{\partial w}{\partial z}\frac{\partial^2 w}{\partial r \partial z} + \frac{\partial u}{\partial r}\frac{\partial^2 w}{\partial r \partial z} + u\frac{\partial^3 u}{\partial r \partial z^2} + w\frac{\partial^3 w}{\partial r \partial z^2} + \frac{2u}{r}\frac{\partial^2 u}{\partial r^2}$$

$$+10\frac{\partial u}{\partial r}\frac{\partial^2 u}{\partial r^2} + 3\frac{\partial u}{\partial z}\frac{\partial^2 w}{\partial r^2} + 4\frac{\partial w}{\partial r}\frac{\partial^2 w}{\partial r^2} + 2w\frac{\partial^3 u}{\partial r^2 \partial z} + u\frac{\partial^3 w}{\partial r^2 \partial z} + 2u\frac{\partial^3 u}{\partial r^3}$$

$$+\frac{2}{r}\frac{\partial u}{\partial z}\frac{\partial w}{\partial r} + 2\frac{\partial w}{\partial z}\frac{\partial^2 u}{\partial z^2} + 4\frac{\partial u}{\partial z}\frac{\partial^2 u}{\partial r \partial z}\right] + \alpha_2^*\left[-\frac{4u^2}{r^3} + \frac{4}{r}\left(\frac{\partial u}{\partial r}\right)^2 + 2\frac{\partial u}{\partial z}\frac{\partial^2 w}{\partial z^2}\right.$$

$$+2\frac{\partial u}{\partial r}\frac{\partial^2 u}{\partial z^2} + 2\frac{\partial w}{\partial r}\frac{\partial^2 w}{\partial z^2} + 4\frac{\partial w}{\partial r}\frac{\partial^2 u}{\partial r \partial z} + \frac{1}{r}\left(\frac{\partial w}{\partial r}\right)^2 + \frac{1}{r}\left(\frac{\partial u}{\partial z}\right)^2 + 2\frac{\partial u}{\partial r}\frac{\partial^2 w}{\partial r \partial z}$$

$$+2\frac{\partial w}{\partial z} + 2\frac{\partial u}{\partial z}\frac{\partial^2 u}{\partial r \partial z} + 8\frac{\partial u}{\partial r}\frac{\partial^2 u}{\partial r^2} + 2\frac{\partial u}{\partial z}\frac{\partial^2 w}{\partial r^2} + 2\frac{\partial w}{\partial r}\frac{\partial^2 w}{\partial r^2}$$

$$\left. +\frac{2}{r}\frac{\partial u}{\partial z}\frac{\partial w}{\partial r} + 2\frac{\partial w}{\partial z}\frac{\partial^2 u}{\partial z^2} + 4\frac{\partial u}{\partial z}\frac{\partial^2 u}{\partial r \partial z}\right] + \beta_3\left[-\frac{8u^3}{r^4} + \frac{8}{r}\left(\frac{\partial u}{\partial r}\right)^3 - \frac{8u^2}{r^3}\frac{\partial u}{\partial r}\right.$$

$$+\frac{8}{r}\frac{\partial u}{\partial r}\left(\frac{\partial w}{\partial z}\right)^2 + \frac{4}{r}\frac{\partial u}{\partial r}\left(\frac{\partial u}{\partial z}\right)^2 + \frac{4}{r}\frac{\partial u}{\partial r}\left(\frac{\partial w}{\partial r}\right)^2 + \frac{8}{r}\frac{\partial u}{\partial r}\frac{\partial u}{\partial z}\frac{\partial w}{\partial r}$$

$$+24\left(\frac{\partial u}{\partial r}\right)^2\frac{\partial^2 u}{\partial r^2} + \frac{8u^2}{r^2}\frac{\partial^2 u}{\partial r^2} + \frac{16u}{r^2}\frac{\partial u}{\partial r} + 8\left(\frac{\partial w}{\partial z}\right)^2\frac{\partial^2 u}{\partial r^2} + 16\frac{\partial u}{\partial r}\frac{\partial w}{\partial z}\frac{\partial^2 w}{\partial r \partial z}$$

$$+4\frac{\partial u}{\partial z}\frac{\partial^2 u}{\partial r^2} + 4\frac{\partial w}{\partial r}\frac{\partial^2 u}{\partial r^2} + 16\frac{\partial u}{\partial r}\frac{\partial u}{\partial z}\frac{\partial^2 u}{\partial r \partial z} + 8\frac{\partial u}{\partial r}\frac{\partial u}{\partial z}\frac{\partial^2 w}{\partial r^2}$$

$$+16\frac{\partial u}{\partial r}\frac{\partial w}{\partial r}\frac{\partial^2 u}{\partial r \partial z} + 8\frac{\partial u}{\partial r}\frac{\partial w}{\partial r}\frac{\partial^2 w}{\partial r^2} + 4\left(\frac{\partial u}{\partial r}\right)^2\frac{\partial^2 u}{\partial z^2} + 4\left(\frac{\partial u}{\partial r}\right)^2\frac{\partial^2 w}{\partial r \partial z} + \frac{4u^2}{r^2}\frac{\partial^2 u}{\partial z^2}$$

$$+\frac{4u^2}{r^2}\frac{\partial^2 w}{\partial r \partial z} + \frac{4u}{r^2}\left(\frac{\partial u}{\partial z}\right)^2 + 8\frac{\partial u}{\partial z}\frac{\partial w}{\partial z}\frac{\partial^2 w}{\partial z^2} + 8\frac{\partial w}{\partial r}\frac{\partial w}{\partial z}\frac{\partial^2 w}{\partial z^2} + 4\left(\frac{\partial w}{\partial z}\right)^2\frac{\partial^2 u}{\partial z^2}$$

$$+4\left(\frac{\partial w}{\partial z}\right)^2\frac{\partial^2 w}{\partial r \partial z} + 6\left(\frac{\partial u}{\partial z}\right)^2\frac{\partial^2 u}{\partial z^2} + 6\left(\frac{\partial w}{\partial r}\right)^2\frac{\partial^2 u}{\partial z^2} + 12\frac{\partial u}{\partial z}\frac{\partial w}{\partial r}\frac{\partial^2 w}{\partial r \partial z}$$

14

$$+12\frac{\partial u}{\partial z}\frac{\partial w}{\partial r}\frac{\partial^2 u}{\partial z^2} - \frac{8u}{r^2}\left(\frac{\partial u}{\partial r}\right)^2 - \frac{8u}{r^2}\left(\frac{\partial w}{\partial z}\right)^2 - \frac{4u}{r^2}\left(\frac{\partial w}{\partial r}\right)^2$$

$$+6\left(\frac{\partial u}{\partial z}\right)^2\frac{\partial^2 w}{\partial r\partial z} + 6\left(\frac{\partial w}{\partial r}\right)^2\frac{\partial^2 w}{\partial r\partial z}\Bigg], \tag{1.41}$$

$$
\begin{aligned}
\rho\left(u\frac{\partial w}{\partial r} + w\frac{\partial w}{\partial z}\right) &= -\frac{\partial p}{\partial z} + \mu\left[\frac{1}{r}\frac{\partial w}{\partial r} + \frac{\partial^2 w}{\partial r^2} + \frac{\partial^2 w}{\partial z^2}\right] \\
&+ \alpha_1^*\left[\frac{u}{r}\frac{\partial^2 w}{\partial r^2} + \frac{w}{r}\frac{\partial^2 u}{\partial z^2} + \frac{u}{r}\frac{\partial^2 u}{\partial r\partial z} + \frac{w}{r}\frac{\partial^2 w}{\partial r\partial z} + \frac{3}{r}\frac{\partial u}{\partial r}\frac{\partial u}{\partial z}\right. \\
&+ \frac{3}{r}\frac{\partial w}{\partial r}\frac{\partial w}{\partial z} + \frac{1}{r}\frac{\partial u}{\partial z}\frac{\partial w}{\partial z} + \frac{1}{r}\frac{\partial u}{\partial r}\frac{\partial w}{\partial r} + 2\frac{\partial u}{\partial r}\frac{\partial^2 w}{\partial r^2} + u\frac{\partial^3 w}{\partial r^3} \\
&+ 3\frac{\partial w}{\partial r}\frac{\partial^2 u}{\partial z^2} + w\frac{\partial^3 u}{\partial r\partial z^2} + 4\frac{\partial u}{\partial r}\frac{\partial^2 u}{\partial r\partial z} + u\frac{\partial^3 u}{\partial r^2\partial z} + 4\frac{\partial w}{\partial r}\frac{\partial^2 w}{\partial r\partial z} \\
&+ w\frac{\partial^3 w}{\partial r^2\partial z} + 3\frac{\partial u}{\partial z}\frac{\partial^2 u}{\partial r^2} + 3\frac{\partial w}{\partial z}\frac{\partial^2 w}{\partial r^2} + 5\frac{\partial u}{\partial z}\frac{\partial^2 w}{\partial r\partial z} + \frac{\partial w}{\partial z}\frac{\partial^2 u}{\partial r\partial z} \\
&+ \frac{\partial w}{\partial r}\frac{\partial^2 u}{\partial r^2} + 2u\frac{\partial^3 w}{\partial r\partial z^2} + 2\frac{\partial w}{\partial z}\frac{\partial^2 u}{\partial z^2} + 2w\frac{\partial^3 w}{\partial z^3} + 8\frac{\partial w}{\partial z}\frac{\partial^2 w}{\partial z^2} \\
&+ \left. 4\frac{\partial u}{\partial z}\frac{\partial^2 u}{\partial z^2}\right] + \alpha_2^*\left[\frac{2}{r}\frac{\partial u}{\partial r}\frac{\partial u}{\partial z} + \frac{2}{r}\frac{\partial u}{\partial r}\frac{\partial w}{\partial r} + \frac{2}{r}\frac{\partial u}{\partial z}\frac{\partial w}{\partial z}\right. \\
&+ \frac{2}{r}\frac{\partial w}{\partial r}\frac{\partial w}{\partial z} + 2\frac{\partial u}{\partial z}\frac{\partial^2 u}{\partial r^2} + 2\frac{\partial u}{\partial r}\frac{\partial^2 u}{\partial r\partial z} + 2\frac{\partial^2 u}{\partial r^2}\frac{\partial w}{\partial r} + 2\frac{\partial u}{\partial r}\frac{\partial^2 w}{\partial r^2} \\
&+ 4\frac{\partial u}{\partial z}\frac{\partial^2 w}{\partial r\partial z} + 2\frac{\partial w}{\partial z}\frac{\partial^2 u}{\partial r\partial z} + 2\frac{\partial w}{\partial r}\frac{\partial^2 w}{\partial r\partial z} + 2\frac{\partial w}{\partial z}\frac{\partial^2 w}{\partial r^2} + 8\frac{\partial w}{\partial z}\frac{\partial^2 w}{\partial z^2} \\
&+ \left. 2\frac{\partial u}{\partial z}\frac{\partial^2 u}{\partial z^2} + 2\frac{\partial w}{\partial r}\frac{\partial^2 u}{\partial z^2} + 2\frac{\partial w}{\partial r}\frac{\partial^2 w}{\partial r\partial z}\right] + \beta_3\left[\frac{4}{r}\frac{\partial u}{\partial z}\left(\frac{\partial u}{\partial r}\right)^2\right. \\
&+ \frac{4}{r}\frac{\partial w}{\partial r}\left(\frac{\partial u}{\partial r}\right)^2 + \frac{4u^2}{r^3}\frac{\partial u}{\partial z} + \frac{4u^2}{r^3}\frac{\partial w}{\partial r} + \frac{4}{r}\frac{\partial u}{\partial z}\left(\frac{\partial w}{\partial z}\right)^2 \\
&+ \frac{4}{r}\frac{\partial w}{\partial r}\left(\frac{\partial w}{\partial z}\right)^2 + \frac{2}{r}\left(\frac{\partial u}{\partial z}\right)^3 + \frac{2}{r}\left(\frac{\partial w}{\partial r}\right)^3 + \frac{6}{r}\left(\frac{\partial u}{\partial z}\right)^2\frac{\partial w}{\partial r} \\
&+ \frac{6}{r}\frac{\partial u}{\partial z}\left(\frac{\partial w}{\partial r}\right)^2 + 4\left(\frac{\partial u}{\partial r}\right)^2\frac{\partial^2 u}{\partial r\partial z} + 4\left(\frac{\partial u}{\partial r}\right)^2\frac{\partial^2 w}{\partial r^2} + 8\frac{\partial u}{\partial r}\frac{\partial u}{\partial z}\frac{\partial^2 u}{\partial r^2} \\
&+ 8\frac{\partial u}{\partial r}\frac{\partial w}{\partial r}\frac{\partial^2 u}{\partial r^2} + \frac{8u}{r^2}\frac{\partial u}{\partial r}\frac{\partial u}{\partial z} + \frac{8u}{r^2}\frac{\partial u}{\partial r}\frac{\partial w}{\partial r} + \frac{4u^2}{r^2}\frac{\partial^2 u}{\partial r\partial z} + \frac{4u^2}{r^2}\frac{\partial^2 w}{\partial r^2} \\
&+ 4\left(\frac{\partial w}{\partial z}\right)^2\frac{\partial^2 u}{\partial r\partial z} + 4\left(\frac{\partial w}{\partial z}\right)^2\frac{\partial^2 w}{\partial r^2} + 8\frac{\partial u}{\partial z}\frac{\partial w}{\partial z}\frac{\partial^2 w}{\partial r\partial z} + 8\frac{\partial w}{\partial r}\frac{\partial w}{\partial z}\frac{\partial^2 w}{\partial r\partial z} \\
&+ 6\left(\frac{\partial u}{\partial z}\right)^2\frac{\partial^2 u}{\partial r\partial z} + 6\left(\frac{\partial u}{\partial z}\right)^2\frac{\partial^2 w}{\partial r^2} + 6\left(\frac{\partial w}{\partial r}\right)^2\frac{\partial^2 u}{\partial r\partial z} + 6\left(\frac{\partial w}{\partial r}\right)^2\frac{\partial^2 w}{\partial r^2} \\
&+ 12\frac{\partial u}{\partial z}\frac{\partial w}{\partial r}\frac{\partial^2 u}{\partial r\partial z} + 12\frac{\partial u}{\partial z}\frac{\partial w}{\partial r}\frac{\partial^2 w}{\partial r^2} + 8\left(\frac{\partial u}{\partial r}\right)^2\frac{\partial^2 w}{\partial z^2} + 16\frac{\partial u}{\partial r}\frac{\partial w}{\partial z}\frac{\partial^2 u}{\partial r\partial z} \\
&+ \frac{8u^2}{r^2}\frac{\partial^2 w}{\partial z^2} + \frac{16u}{r^2}\frac{\partial u}{\partial z}\frac{\partial w}{\partial z} + 24\left(\frac{\partial w}{\partial z}\right)^2\frac{\partial^2 w}{\partial z^2} + 4\left(\frac{\partial u}{\partial z}\right)^2\frac{\partial^2 w}{\partial z^2} \\
&+ 4\left(\frac{\partial w}{\partial r}\right)^2\frac{\partial^2 w}{\partial z^2} + 8\frac{\partial u}{\partial z}\frac{\partial w}{\partial r}\frac{\partial^2 w}{\partial z^2} + 8\frac{\partial u}{\partial z}\frac{\partial w}{\partial z}\frac{\partial^2 u}{\partial z^2} + 8\frac{\partial u}{\partial z}\frac{\partial w}{\partial z}\frac{\partial^2 w}{\partial r\partial z} \\
&+ \left. 8\frac{\partial w}{\partial r} + 8\frac{\partial w}{\partial r}\frac{\partial w}{\partial z}\frac{\partial^2 w}{\partial r\partial z}\right]. \tag{1.42}
\end{aligned}
$$

Using boundary layer approximation, we have

$$
\begin{aligned}
u\frac{\partial u}{\partial r} + w\frac{\partial u}{\partial z} \;=\;& -\frac{1}{\rho}\frac{\partial p}{\partial r} + \nu\frac{\partial^2 u}{\partial z^2} + \frac{\alpha_1^*}{\rho}\left[\frac{\partial u}{\partial z}\frac{\partial^2 w}{\partial z^2} + 3\frac{\partial u}{\partial r}\frac{\partial^2 u}{\partial z^2} + w\frac{\partial^3 u}{\partial z^3} + u\frac{\partial^3 u}{\partial r\partial z^2}\right. \\
& \left. +2\frac{\partial w}{\partial z}\frac{\partial^2 u}{\partial z^2} + 4\frac{\partial u}{\partial z}\frac{\partial^2 u}{\partial r\partial z}\right] + \frac{\alpha_2^*}{\rho}\left[2\frac{\partial u}{\partial z}\frac{\partial^2 w}{\partial z^2} + 2\frac{\partial u}{\partial r}\frac{\partial^2 u}{\partial z^2}\right. \\
& \left. +\frac{1}{r}\left(\frac{\partial u}{\partial z}\right)^2 + 6\frac{\partial u}{\partial z}\frac{\partial^2 u}{\partial r\partial z} + 2\frac{\partial w}{\partial z}\frac{\partial^2 u}{\partial z^2}\right] + \frac{\beta_3^*}{\rho}\left[6\left(\frac{\partial u}{\partial z}\right)^2\frac{\partial^2 u}{\partial z^2}\right].
\end{aligned}
\tag{1.43}
$$

1.5 Solution methodology

Homotopy analysis technique was derived from the basic and fundamental topological concept characterized as homotopy. Two functions are said to be homotopic if one function can be continuously deformed into the other function. If q_1 and q_2 are two continuous functions which maps from a topological space U into topological space V then q_1 is homotopic to q_2 if there exists a continuous map Q

$$
Q:\; U \times [0,1] \to V,
\tag{1.44}
$$

such that for each $u \in U$

$$
Q\left(u,0\right) = q_1\left(u\right), \quad Q\left(u,1\right) = q_2\left(u\right).
\tag{1.45}
$$

Then map Q is called homotopic between q_1 and q_2. Homotopy analysis method is proposed by Liao [74] in 1992, which is used to solve the highly nonlinear equations. Homotopy is a continuous deformation or variation of a function/equation. It has several advantages over the other methods i.e., (i) it is independent of small or large parameters (ii) ensures the convergence of series solution (iii) provides great freedom to select the base function and linear operator. Such flexibility and freedom help us in solving the highly nonlinear problems. This technique is applied successfully for the construction of series solutions of various nonlinear problems [75-89].

Consider the nonlinear differential equation of the form

$$
\mathcal{N}\left[u\left(\eta\right)\right] = 0,
\tag{1.46}
$$

where $\mathcal{N}$ represents the nonlinear operator, u denotes an unknown dependent function and x denotes the independent variable. The homotopic equation [74] is

$$
\left(1 - q\right)\mathcal{L}\left[\hat{u}(\eta; q) - u_0(\eta)\right] = q\hbar\mathcal{N}\left[\hat{u}(\eta; q)\right],
\tag{1.47}
$$

in which the embedding parameter q, $0 \leq q \leq 1$, the auxiliary parameter $\hbar \neq 0$, auxiliary linear operator $\mathcal{L}$ and initial guess $u_0(\eta)$ satisfying the boundary conditions. It is also noted that the above equation is known as zeroth order deformation equation. When $q = 0$ and $q = 1$ then

$$
\hat{u}(\eta; 0) - u_0(\eta) = 0, \text{ and } \hat{u}(\eta; 1) - u(\eta) = 0,
\tag{1.48}
$$

respectively. Thus with the variation of q from 0 to 1, the solution $\hat{u}(\eta; q)$ starts from initial guess $u_0(\eta)$ and goes to the final solution $u(\eta)$. Writing $\hat{u}(\eta; q)$ in the Taylor series corresponding to the embedding parameter q we get

$$\hat{u}(\eta; q) = u_0(\eta) + \sum_{m=1}^{\infty} u_m(\eta)q^m, \quad u_m(\eta) = \frac{1}{m!} \left. \frac{\partial^m \hat{u}(\eta; q)}{\partial q^m} \right|_{q=0}. \tag{1.49}$$

The mth order equation is

$$L\left[u_m(\eta) - \chi_m u_{m-1}(\eta)\right] = \hbar \mathcal{R}_m\left(u_{m-1}\right), \tag{1.50}$$

with

$$R_m\left(u_{m-1}\right) = \frac{1}{(m-1)!} \left. \frac{\partial^{m-1} \hat{u}(\eta; q)}{\partial q^{m-1}} \right|_{q=0}, \tag{1.51}$$

$$\chi_m = \begin{cases} 0, & m \leq 1, \\ 1, & m > 1. \end{cases} \tag{1.52}$$

The solution of equation can be obtained using a suitable software like MATHEMATICA or MAPLE. If the auxiliary parameter, the initial guess and the auxiliary linear operator is chosen accurately, the series will converge at $q = 1$

$$\hat{u}(x) = u_0(\eta) + \sum_{m=1}^{\infty} u_m(\eta). \tag{1.53}$$

Chapter 2

Boundary-layer flow of Walters-B fluid with Newtonian heating

The flow of Walters-B fluid over a stretching surface with Newtonian heating is studied in this chapter. The governing partial differential equations are first simplified through boundary layer approximations and then reduced into ordinary differential equations by using the appropriate substitutions. The resulting problems have been solved for the series solutions by homotopic approach. Convergence analysis is performed and appropriate values are determined by plotting the so called $\hbar-$curves. Graphical results for the dimensionless velocity and temperature are presented and discussed for various physical parameters. In addition the expressions of skin friction coefficient and the local Nusselt number are presented. The dimensionless expressions of wall shear stress and wall mass flux are analyzed graphically and numerically.

2.1   Mathematical formulation

We consider the magnetohydrodynamic stagnation point flow of Walters-B fluid towards a stretching sheet along the x-axis. The flow is confined to $y \geq 0$. A uniform magnetic field of strength B_0 is applied perpendicular to the plane of stretching surface. The induced magnetic field is neglected through the assumption of small magnetic Reynolds number. The electric field is absent. Let $U_m(x) = cx$ be the velocity of stretching sheet while the velocity of external flow is $U_e(x) = ax$, where a and c are the positive constants. Using the velocity field $\mathbf{V} = [u\,(x,y)\,,v\,(x,y)\,,0]$ and temperature $\mathbf{T} = T\,(x,y)$ fields, the governing two-dimensional boundary layer equations are ([14], [15]):

$$\frac{\partial u}{\partial x} + \frac{\partial v}{\partial y} = 0, \tag{2.1}$$

$$
\begin{aligned}
u\frac{\partial u}{\partial x} + v\frac{\partial u}{\partial y} \;=\;& U_e\frac{dU_e}{dx} + \nu\frac{\partial^2 u}{\partial y^2} - \frac{k_0}{\rho}\left[u\frac{\partial^3 u}{\partial x\partial y^2} + v\frac{\partial^3 u}{\partial y^3} + \frac{\partial u}{\partial x}\frac{\partial^2 u}{\partial y^2}\right. \\
&\left. - \frac{\partial u}{\partial y}\frac{\partial^2 u}{\partial x\partial y}\right] - \frac{\sigma B_0^2}{\rho}\,(u - U_e)\,,
\end{aligned}
\tag{2.2}
$$

$$u\frac{\partial T}{\partial x} + v\frac{\partial T}{\partial y} = \frac{K}{\rho c_p}\frac{\partial^2 T}{\partial y^2} + \frac{\sigma B_0^2}{\rho c_p}(u - U_e)^2, \tag{2.3}$$

where u and v are the velocity components parallel to the $x-$ and $y-$ directions respectively, ρ the fluid density, σ the electrical conductivity of fluid, K the thermal conductivity, T the temperature and c_p the specific heat. The boundary conditions are given by

$$
\begin{aligned}
u(x,0) &= U_w(x) = cx, \ v(x,0) = v_w = 0, \ \left.\frac{\partial T}{\partial y}\right|_{y=0} = -h_s T, \\
u &\to U_e(x) = ax, \ T \to T_\infty \text{ as } y \to \infty.
\end{aligned}
\tag{2.4}
$$

It is noted that horizontal velocity $U_w(x)$ at $y = 0$, represents the stretching velocity which is produced by applying two forces equal in magnitude but opposite in direction such that origin is kept constant while $U_e(x)$ represents variable free stream velocity when y approaches infinity. Vertical velocity v_w at $y = 0$, represents that their is no suction/injection at the surface. It is also noted that h_s is the heat transfer coefficient (which measures the strength of Newtonian heating), c the stretching rate and T_∞ the ambient temperature. In Eq. (2.4) the condition of temperature at $y = 0$, is known as the Newtonian heating boundary condition which indicates that heat transfer rate from the bounding surface with finite heat capacity is proportional to the local surface temperature.

Introducing the following dimensionless variables

$$u(x,y) = cxf'(\eta), \ v(x,y) = -\sqrt{c\nu}f(\eta), \ \theta = \frac{T - T_\infty}{T_\infty}, \ \eta = \sqrt{\frac{c}{\nu}}y, \tag{2.5}$$

the governing transformed equations may be written as follows:

$$f''' + A^2 - (f')^2 + ff'' - We\left[2f'f''' - ff^{(iv)} - (f'')^2\right] - Ha^2(f' - A) = 0, \tag{2.6}$$

$$f'(0) = 1, \ f(0) = 0, \ f'(\infty) = A, \tag{2.7}$$

$$\theta'' + \Pr f \, \theta' + Ha^2 \Pr Ec \, (f' - A)^2 = 0, \tag{2.8}$$

$$\theta'(0) = -\gamma_1(1 + \theta(0)), \ \theta(\infty) = 0, \tag{2.9}$$

in which prime denotes differentiation with respect to η, Pr the Prandtl number, We the Weissenberg number, Ha the Hartman number, Ec the Eckert number and γ_1 the conjugate parameter for Newtonian heating. These parameters are defined as

$$
\begin{aligned}
Ha &= \sqrt{\frac{\sigma B_0^2}{\rho c}}, \quad A = \frac{a}{c}, \quad We = \frac{k_0 c}{\mu_0}, \\
\Pr &= \frac{\mu_0 c_p}{K}, \quad Ec = \frac{U_m^2}{c_p T_\infty}, \quad \gamma_1 = h_s\sqrt{\frac{\nu}{a}}.
\end{aligned}
\tag{2.10}
$$

The skin friction coefficient C_f and the local Nusselt number Nu_x are

$$C_f = \frac{\tau_w}{\rho U_m^2}, \qquad Nu_x = \frac{x q_w}{K(T - T_\infty)}, \tag{2.11}$$

in which the wall skin friction (τ_w) and the wall heat flux (q_w) are given by

$$\tau_w = \left[\mu_0 \frac{\partial u}{\partial y} - k_0 \left(u \frac{\partial^2 u}{\partial x \partial y} + v \frac{\partial^2 u}{\partial y^2} + 2 \frac{\partial u}{\partial x} \frac{\partial u}{\partial y} \right)^3 \right]_{y=0}, \quad q_w = -K \left(\frac{\partial T}{\partial y} \right)_{y=0}. \tag{2.12}$$

In dimensionless form, these quantities are expressed as follows:

$$(\mathrm{Re}_x)^{1/2} C_f = (1 - 3We) f''(0), \quad (\mathrm{Re}_x)^{-1/2} Nu_x = \gamma_1 \left(1 + \frac{1}{\theta(0)} \right), \tag{2.13}$$

where $\mathrm{Re}_x = cx^2/\nu$ denotes the local Reynolds number.

2.2 Mechanism of homotopy analysis

This method was proposed by Liao [108] in 1992, which is used to obtain the solutions of highly nonlinear problems. It has several advantages over the other methods i.e., (i) it is independent of small or large parameters (ii) ensures the convergence of series solution (iii) provides great freedom to select the base function and linear operator. Such flexibility and freedom help us in solving the highly nonlinear problems. It is also noted that linear part of the differential equation is selected as the linear operator for the homotopy analysis method. However in semi-infinite domain it is preferred in such a way that the solution appears in the form of exponential functions for rapid convergence analysis. For homotopy solutions, we define the velocity and temperature distributions by the following set of base functions.

$$\left\{ \eta^k \exp(-n\eta) \,|\, k \geq 0, n \geq 0 \right\}, \tag{2.14}$$

with

$$f_m(\eta) = \sum_{n=0}^{\infty} \sum_{k=0}^{\infty} a_{m,n}^k \eta^k \exp(-n\eta), \tag{2.15}$$

$$\theta_m(\eta) = \sum_{n=0}^{\infty} \sum_{k=0}^{\infty} b_{m,n}^k \eta^k \exp(-n\eta), \tag{2.16}$$

where $a_{m,n}^k$ and $b_{m,n}^k$ are the constants. We have chosen the following initial guesses $f_0(\eta)$, $\theta_0(\eta)$ and the auxiliary linear operators $\mathcal{L}_i \, (i = f, \theta)$:

$$f_0(\eta) = A\eta + (1 - A)(1 - \exp(-\eta)), \qquad \theta_0(\eta) = \frac{\gamma_1 \exp(-\eta)}{1 - \gamma_1}, \tag{2.17}$$

$$\mathcal{L}_f[f(\eta)] = \frac{d^3 f}{d\eta^3} - \frac{df}{d\eta}, \qquad \mathcal{L}_\theta[\theta(\eta)] = \frac{d^2 \theta}{d\eta^2} - \theta, \tag{2.18}$$

satisfying the following properties

$$\mathcal{L}_f \left[C_1 + C_2 \exp(\eta) + C_3 \exp(-\eta) \right] = 0, \tag{2.19}$$

$$\mathcal{L}_\theta \left[C_4 \exp(\eta) + C_5 \exp(-\eta) \right] = 0.$$

in which $C_i \, (i = 1 - 5)$ are constants.

2.2.1 Zeroth-order deformation problems

The zeroth order deformation problems are

$$(1 - q) \, \mathcal{L}_f \left[\hat{f}(\eta; q) - f_0(\eta) \right] = q \hbar_f \mathcal{N}_f \left[\hat{f}(\eta; q) \right], \tag{2.20}$$

$$(1 - q) \, \mathcal{L}_\theta \left[\hat{\theta}(\eta; q) - \theta_0(\eta) \right] = q \hbar_\theta \mathcal{N}_\theta \left[\hat{f}(\eta; q), \hat{\theta}(\eta; q) \right], \tag{2.21}$$

$$\hat{f}(0, q) = 0, \quad \left. \frac{\partial \hat{f}(\eta, q)}{\partial \eta} \right|_{\eta=0} = 1, \quad \left. \frac{\partial \hat{f}(\eta, q)}{\partial \eta} \right|_{\eta \to \infty} = A,$$

$$\left. \frac{\partial \hat{\theta}(\eta, q)}{\partial \eta} \right|_{\eta=0} = -\gamma_1 \left(1 + \hat{\theta}(\eta, q) \right) \Big|_{\eta=0}, \quad \hat{\theta}(\eta, q) \Big|_{\eta \to \infty} = 0. \tag{2.22}$$

In the above expressions $q \, \epsilon \, [0, 1]$ and $\hbar_f \neq 0$, $\hbar_\theta \neq 0$ are the embedding and auxiliary parameters respectively. The non-linear operators are given by

$$\begin{aligned}
\mathcal{N}_f[\hat{f}(\eta, q)] &= \frac{\partial^3 \hat{f}}{\partial \eta^3} + A^2 - \left(\frac{\partial \hat{f}}{\partial \eta} \right)^2 + f \frac{\partial^2 \hat{f}}{\partial \eta^2} - We \left[2 \frac{\partial \hat{f}}{\partial \eta} \frac{\partial^3 \hat{f}}{\partial \eta^3} - f \frac{\partial^4 \hat{f}}{\partial \eta^4} \right. \\
&\quad \left. - \left(\frac{\partial^2 \hat{f}}{\partial \eta^2} \right)^2 \right] - Ha^2 \left(\frac{\partial \hat{f}}{\partial \eta} - A \right),
\end{aligned} \tag{2.23}$$

$$\mathcal{N}_\theta[\hat{f}(\eta, q), \hat{\theta}(\eta, q)] = \frac{\partial^2 \hat{\theta}}{\partial \eta^2} + \Pr f \frac{\partial \hat{\theta}}{\partial \eta} + Ha^2 \Pr Ec \left(\frac{\partial \hat{f}}{\partial \eta} - A \right)^2, \tag{2.24}$$

where $\mathcal{N}_f$ and $\mathcal{N}_\theta$ are the nonlinear operators. For $q = 0$ and $q = 1$, we have

$$\hat{f}(\eta; 0) = f_0(\eta), \quad \hat{f}(\eta; 1) = f(\eta), \tag{2.25}$$

$$\hat{\theta}(\eta; 0) = \theta_0(\eta), \quad \hat{\theta}(\eta; 1) = \hat{\theta}(\eta), \tag{2.26}$$

and $\hat{f}(\eta, q)$ and $\hat{\theta}(\eta, q)$ vary from initial guesses $f_0(\eta)$, $\theta_0(\eta)$ to the final solutions $f(\eta)$ and $\theta(\eta)$ when q varies from 0 to 1. By Taylor's series expansion, we obtain

$$\hat{f}(\eta, q) = f_0(\eta) + \sum_{m=1}^{\infty} f_m(\eta) q^m, \quad f_m(\eta) = \frac{1}{m!} \left. \frac{\partial^m \hat{f}(\eta; q)}{\partial q^m} \right|_{q=0}, \tag{2.27}$$

21

$$\hat{\theta}(\eta, q) = \theta_0(\eta) + \sum_{m=1}^{\infty} \theta_m(\eta) q^m, \ \theta_m(\eta) = \frac{1}{m!} \left. \frac{\partial^m \hat{\theta}(\eta; q)}{\partial q^m} \right|_{q=0}, \tag{2.28}$$

where the convergence of above series strongly depend upon $\hbar_f$ and $\hbar_\theta$. Considering that $\hbar_f$ and $\hbar_\theta$ are selected properly so that Eqs. (2.27) and (2.28) converge at $q = 1$ and thus we have

$$\hat{f}(\eta) = f_0(\eta) + \sum_{m=1}^{\infty} f_m(\eta), \tag{2.29}$$

$$\hat{\theta}(\eta) = \theta_0(\eta) + \sum_{m=1}^{\infty} \theta_m(\eta). \tag{2.30}$$

2.2.2 mth-order deformation problems

Differentiate Eqs. (2.20-2.22) m-times with respect to q and then set $q = 0$ we get the mth order deformation equations for momentum and energy which are given below

$$\mathcal{L}_f \left[\hat{f}_m(\eta) - \chi_m \hat{f}_{m-1}(\eta) \right] = \hbar_f \mathcal{R}_m^f(\eta), \tag{2.31}$$

$$\hat{f}_m(0, q) = 0, \quad \left. \frac{\partial \hat{f}_m(\eta, q)}{\partial \eta} \right|_{\eta=0} = 0, \quad \left. \frac{\partial \hat{f}_m(\eta, q)}{\partial \eta} \right|_{\eta \to \infty} = 0, \tag{2.32}$$

$$\mathcal{L}_\theta \left[\hat{\theta}_m(\eta) - \chi_m \hat{\theta}_{m-1}(\eta) \right] = \hbar_\theta \mathcal{R}_m^\theta(\eta), \tag{2.33}$$

$$\left. \frac{\partial \hat{\theta}_m(\eta, q)}{\partial \eta} \right|_{\eta=0} + \gamma \left. \hat{\theta}_m(\eta, q) \right|_{\eta=0} = 0, \quad \left. \hat{\theta}_m(\eta, q) \right|_{\eta \to \infty} = 0. \tag{2.34}$$

Nonlinear operator for momentum equation is

$$\begin{aligned}
\mathcal{R}_m^f(\eta) = {} & f_{m-1}'''(\eta) + A^2(1 - \chi_m) - \sum_{k=0}^{m-1} f_{m-1-k}' f_k' + \sum_{k=0}^{m-1} f_{m-1-k} f_k'' \\
& - We \sum_{k=0}^{m-1} \left[2 f_{m-1-k}' f''' - f_{m-1-k} f_k^{(iv)} - f_{m-1-k}'' f_k'' \right] - Ha^2 f_{m-1}' \\
& + Ha^2 A(1 - \chi_m).
\end{aligned} \tag{2.35}$$

Nonlinear operator for energy equation is

$$\begin{aligned}
\mathcal{R}_m^\theta(\eta) = {} & \theta_{m-1}''(\eta) + \Pr \sum_{k=0}^{m-1} f_{m-1-k} \theta_k' + Ha^2 \Pr Ec \sum_{k=0}^{m-1} f_{m-1-k}' f_k' \\
& + Ha^2 \Pr Ec A^2(1 - \chi_m) - 2\, Ha^2 \Pr Ec\, A f_{m-1}'(\eta).
\end{aligned} \tag{2.36}$$

The general solutions of the mth order deformation problems are

$$f(\eta) = f^* + C_1 + C_2 \exp(\eta) + C_3 \exp(-\eta), \tag{2.37}$$

$$\theta(\eta) = \theta^* + C_4 \exp(\eta) + C_5 \exp(-\eta), \tag{2.38}$$

in which f^* and θ^* are the particular solutions.

2.3   Convergence of the homotopy solutions

The convergence of series solutions and the approximation rate strongly depend upon auxiliary parameters $\hbar_f$ and $\hbar_\theta$. The appropriate values of these parameters can be determined by plotting the so-called $\hbar-$curves. Here $\hbar_f-$ and $\hbar_\theta-$curves for various values of Weissenberg number We have been plotted in the Figs. 2.2 and 2.3. The admissible values of $\hbar_f$ and $\hbar_\theta$ lie along the line parallel to the $\hbar_f-$ and $\hbar_\theta-$axes. For example when $We = 0.5$ the series solutions are convergent for $\hbar_f \in [-1, -0.5]$ and $\hbar_\theta \in [-1, -0.5]$.

2.4   Results and discussion

Physical interpretation to the obtained results of velocity and temperature distributions for various parametric values is discussed in this section. Fig. 2.4 depicts the variations in the $x-$component of velocity with an increase in Weissenberg number We. When the velocity of stretching sheet is greater than the free stream velocity i.e. $A < 1$, the velocity decreases with an increase in We. However it enhances with an increase in We when $A > 1$. Irrespective of the values of A, the momentum boundary layer thins when We is increased. Physically increasing values of We enhance tensile stresses which oppose the momentum transport and hence boundary layer thickness decreases. When fluid is passing over the surface, a thin boundary layer in such situation exists within which the fluid adapts the velocity of the body because of friction/drag forces or it is the distance from the plate/sheet to the region where no changes occur in the velocity of the fluid. Effects of Hartman number on the horizontal component of velocity are presented in Fig. 2.5. Larger values of Hartman number correspond to a decrease in the velocity. In fact the applied transverse magnetic field in an electrically conducting fluid creates a resistive force like drag force known as the Lorentz force. This force has tendency to resist the fluid motion and due to this reason the momentum boundary layer thins with an increase in magnetic field strength. Fig. 2.6 elucidates that velocity field f' is an increasing function of ratio A. The boundary layer thickness increases with an increase in A when $A < 1$, whereas boundary layer becomes thinner when A is increased provided $A > 1$. Further the boundary layer is not formed for $A = 1$. Fig. 2.7 shows the influence of Weissenberg number on the temperature distribution. An increase in the Weissenberg number leads to an increase in the local fluids temperature and thicker thermal boundary layer. Fig. 2.8 perceives the behavior of Hartman number on the temperature $\theta(\eta)$. Increasing values of Ha indicates stronger Lorentz force which enhances resistance in the fluid motion and hence augments the local fluid temperature. Impact of ratio A on temperature can be seen from Fig. 2.9. We observed that both the temperature and the thermal boundary layer thickness increase by enhancing the free stream velocity. The behavior of conjugate parameter γ_1 characterizing the strength of Newtonian heating can be depicted from Fig. 2.10. It is obvious that stronger convective heating allows the thermal effect to penetrate deeper into the quiescent fluid. Due to this reason the thermal boundary layer thickness with an increase in γ_1

surface heat flux, being proportional to γ_1 is an increasing function of γ_1 (see in Fig. 2.6). Prandtl number being the ratio of momentum diffusivity to the thermal diffusivity reduces conduction but enhances pure convection (i.e. heat flow per unit area). Due to this reason thermal boundary layer thins and rate of heat transfer at the sheet increases when Pr is increased (see Fig. 2.11). Viscous dissipation is the heat generation within the flow caused by shear in the flow. Larger values of Ec heat up the fluid near the immediate vicinity of the bounding surface and hence thermal boundary layer thickness increases (Fig. 2.12). Effects of Weissenberg number We on the wall shear stress can be examined from Fig. 2.13. It is noticed that wall shear stress can be appreciably reduced by assuming larger Weissenberg number. On the other hand an opposite behavior is noted for the ratio parameter A verses Hartman number Ha on the skin friction coefficient (see Fig. 2.14). Local Nusselt number decreases with an increase in Ec but it increases for larger Prandtl number (see Figs. 2.15 and 2.16). Table 2.1 is prepared to analyze the convergence of series solutions for a specific case. Tables 2.2 and 2.3 provide the numerical values of skin friction coefficient and local Nusselt number for different values of involved parameters. The magnitude of skin friction coefficient is reduced when either We or A is increased. The magnitude of local Nusselt number enhances with the increase in Prandtl number Pr and A while it decreases for larger We, Ha and Ec. Table 2.4 is drawn to analyze a comparative study in the limiting case by taking $Ha = 0 = We$. This table shows a very good agreement.
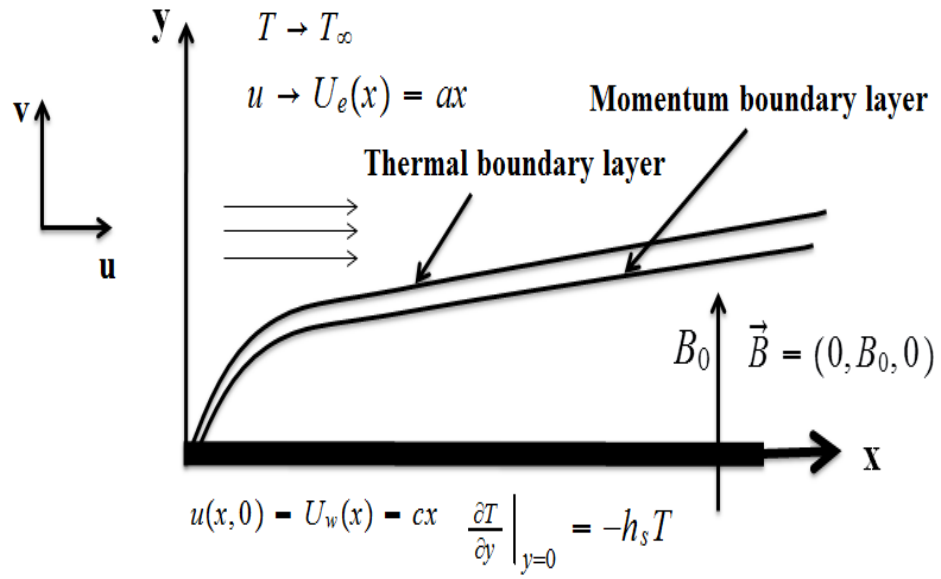
Fig. 2.1: Description of flow model.
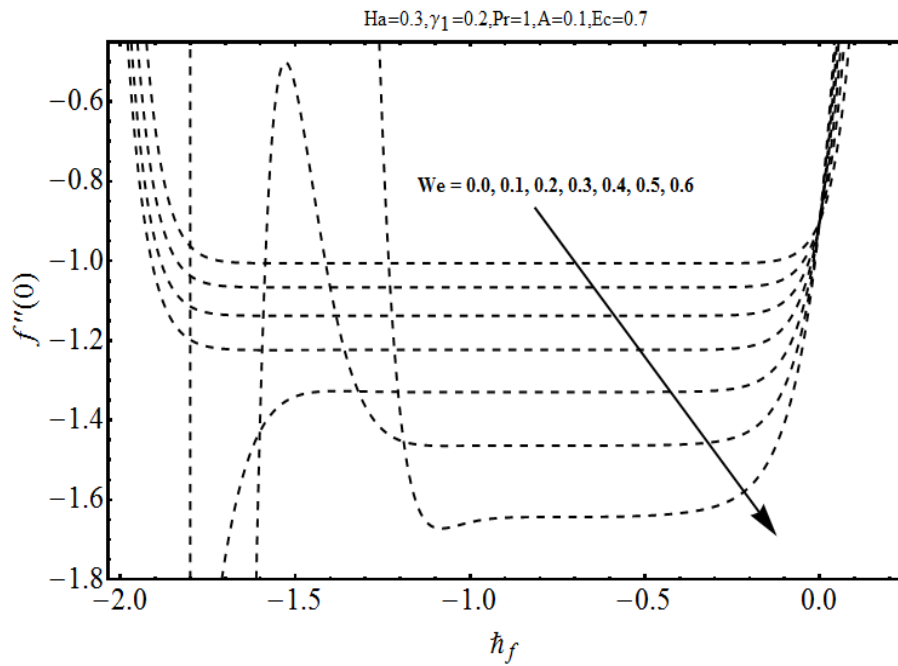
Fig. 2.2: $\hbar$−curves for the function $f\left(\eta\right).$
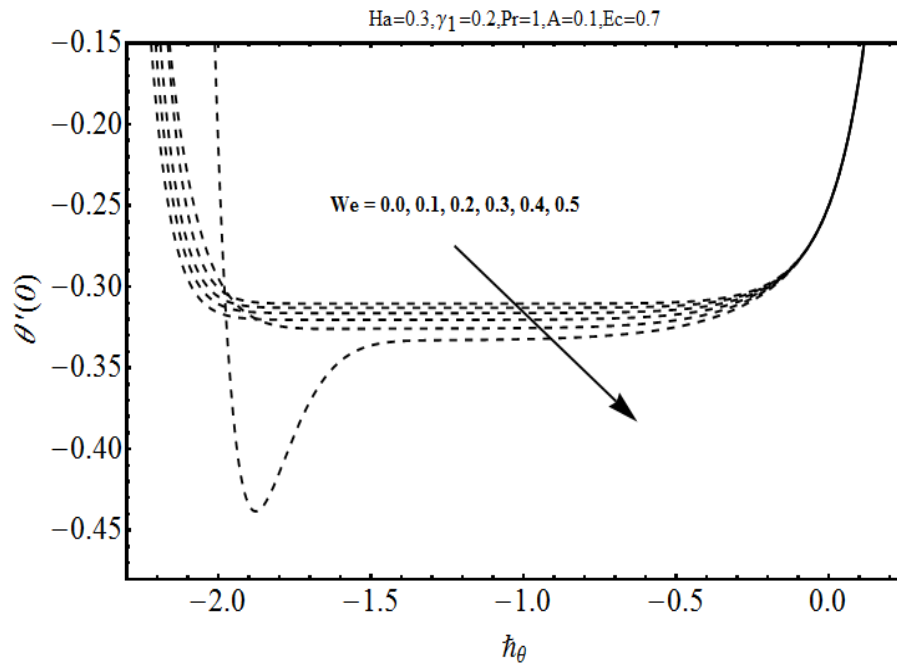
Fig. 2.3: $\hbar$−curves for the function $\theta\left(\eta\right)$.
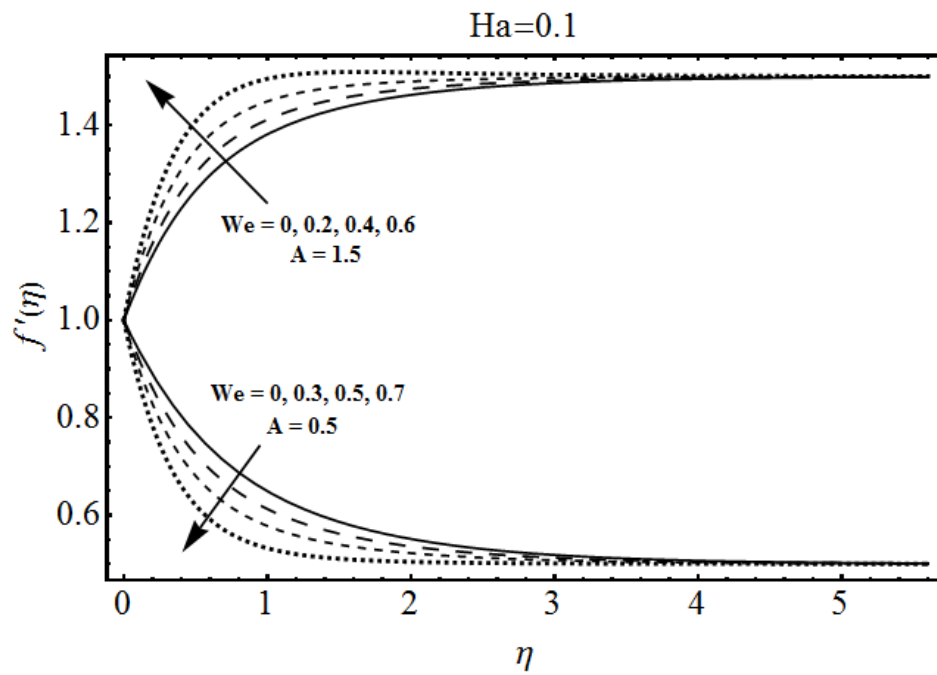
Fig. 2.4: Influence of We on $f'\left(\eta\right)$.
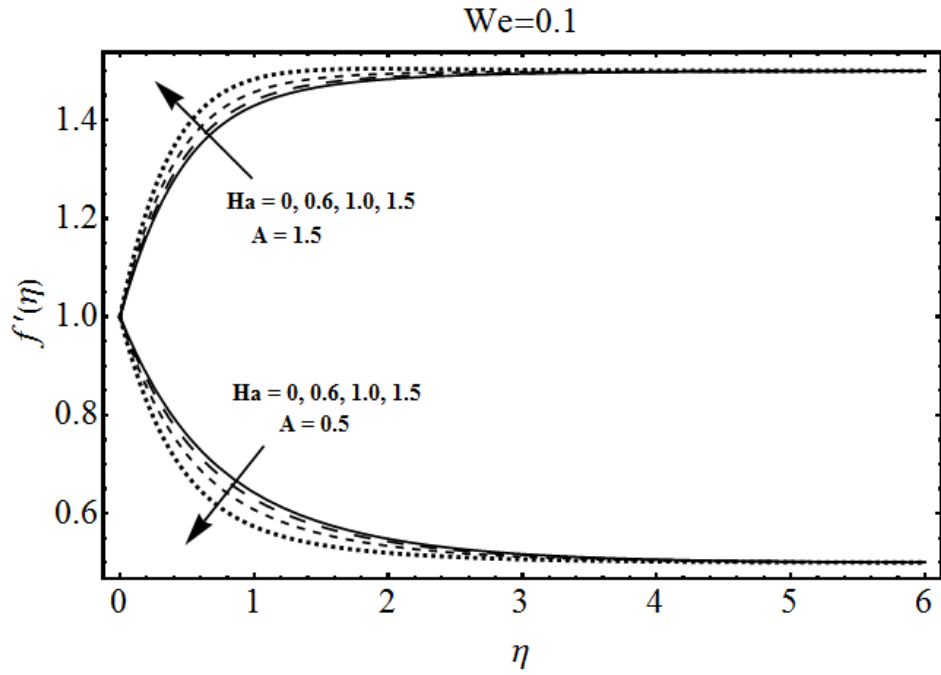
Fig. 2.5: Influence of Ha on $f'(\eta)$.
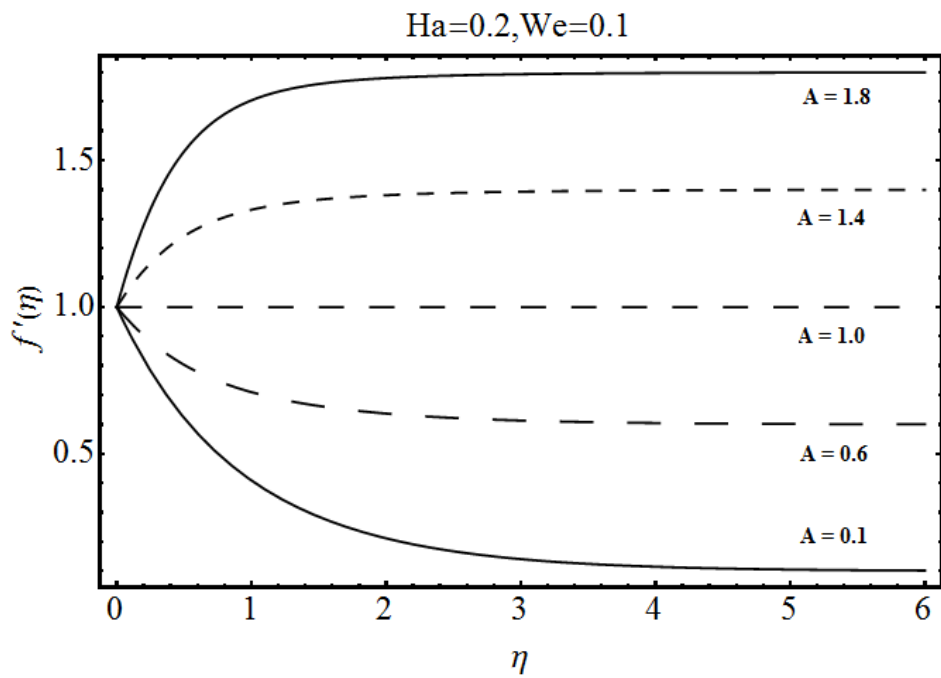
Fig. 2.6: Influence of A on $f'(\eta)$.
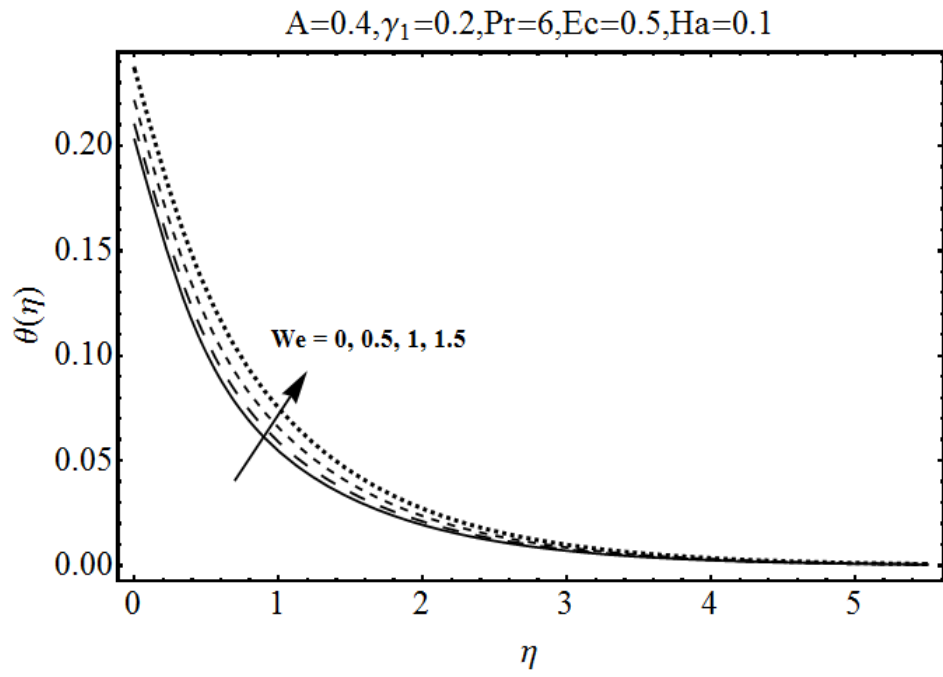
Fig. 2.7: Effect of We on $\theta\left(\eta\right)$.
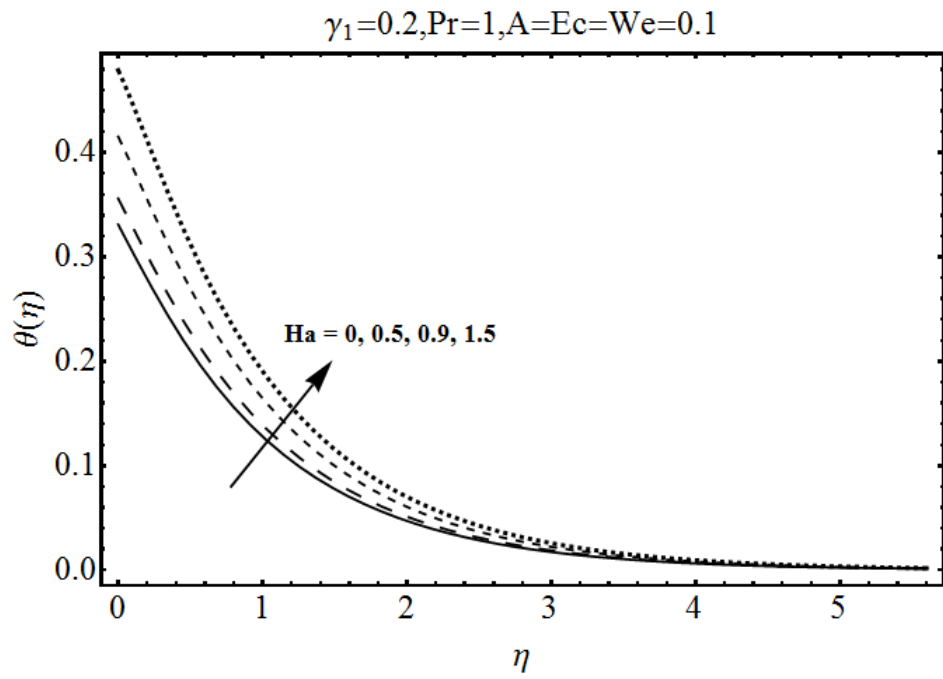
Fig. 2.8: Influence of Ha on $\theta\left(\eta\right)$.
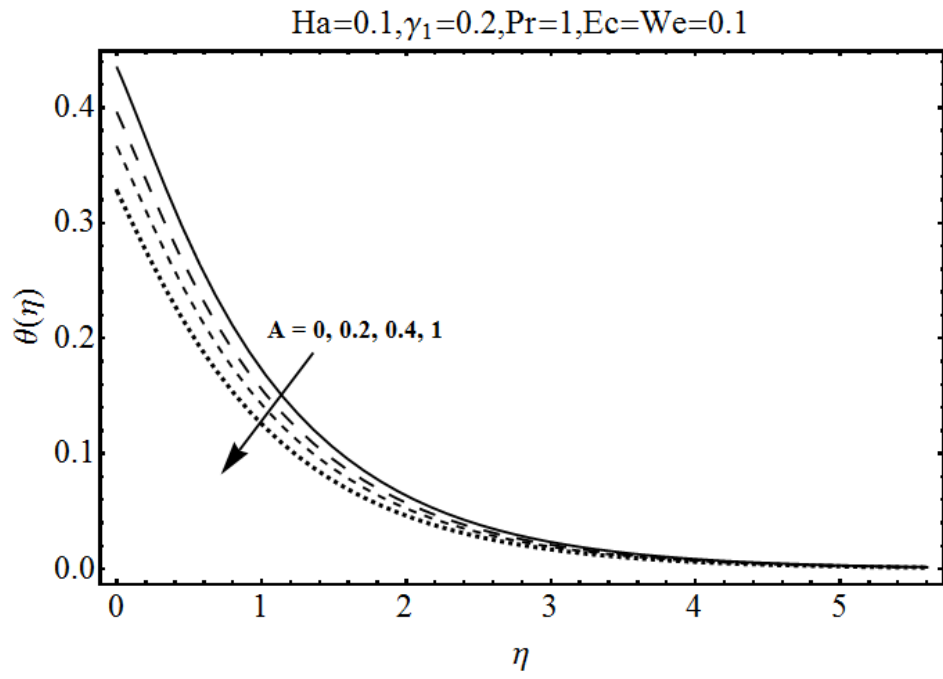
Fig. 2.9: Influence of A on $\theta(\eta)$.
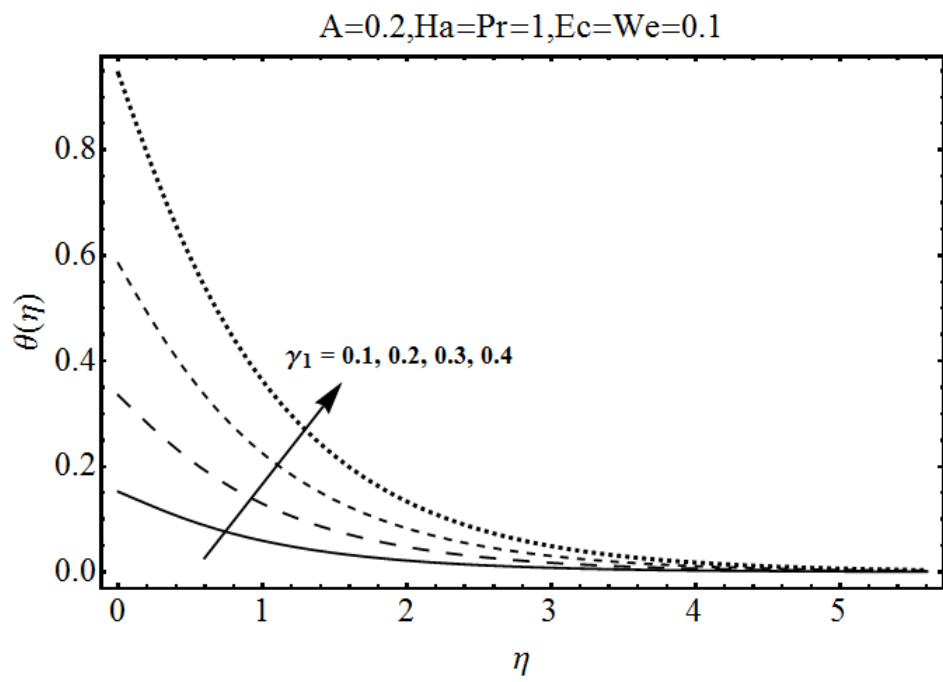
Fig. 2.10: Influence of γ_1 on $\theta(\eta)$.
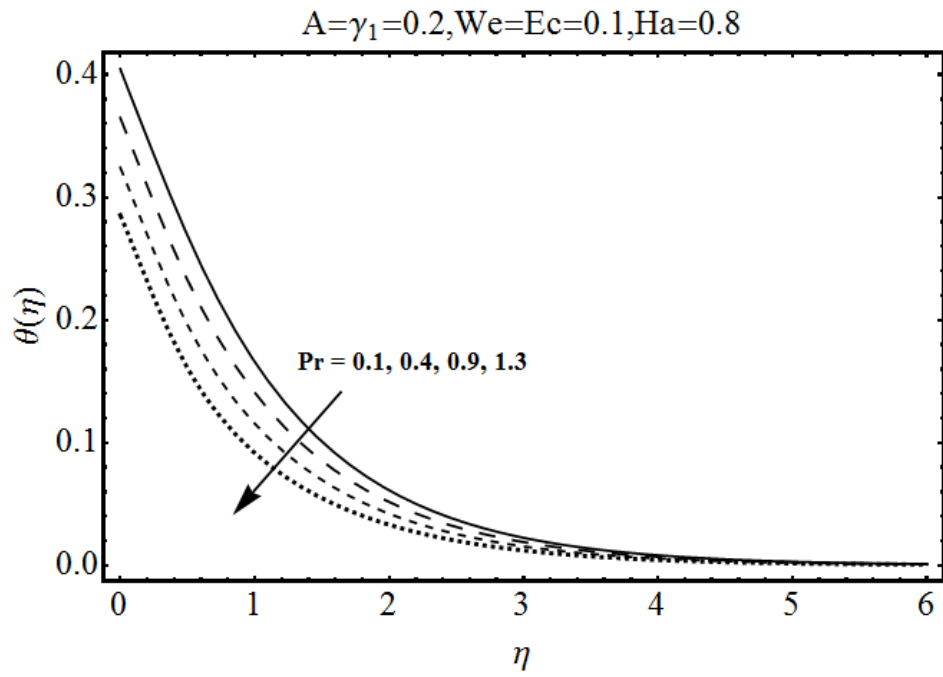
Fig. 2.11: Influence of Pr on $\theta(\eta)$.
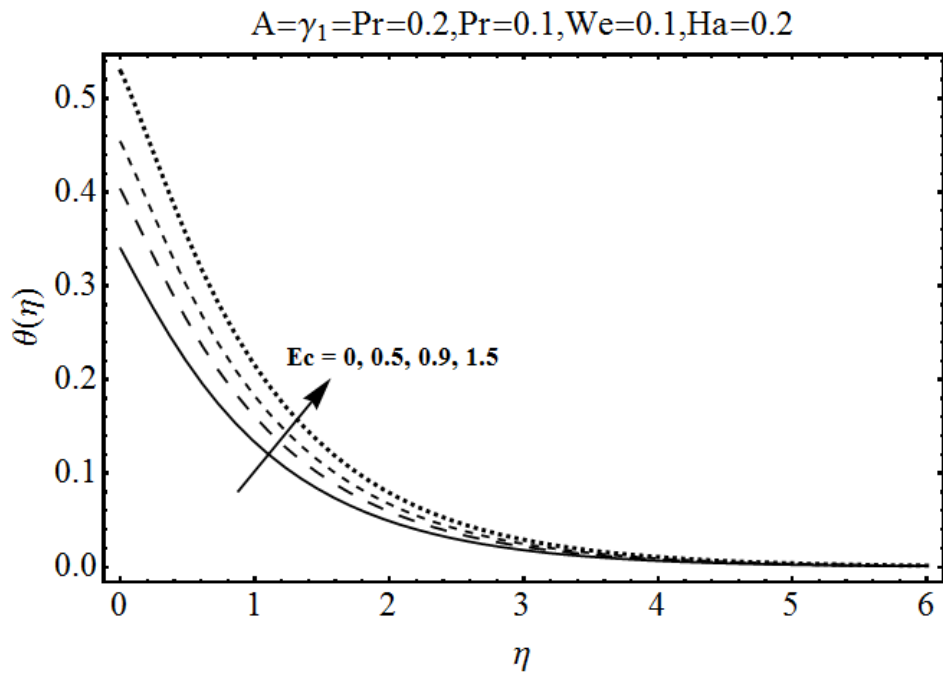
Fig. 2.12: Influence of Ec on $\theta(\eta)$.
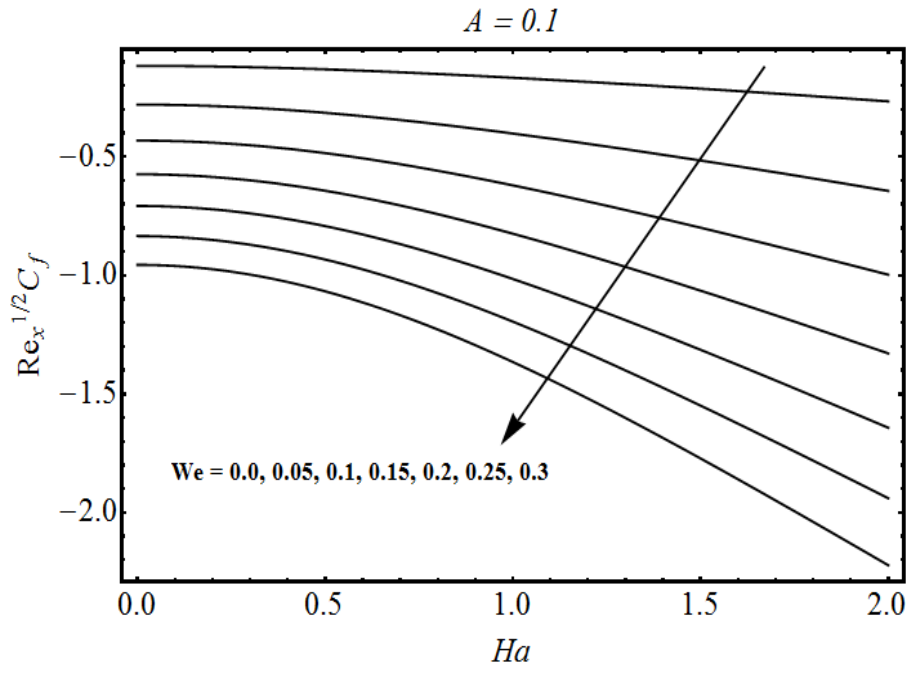
Fig. 2.13: Variation of skin friction for different values of We when $0 \le Ha \le 2$.
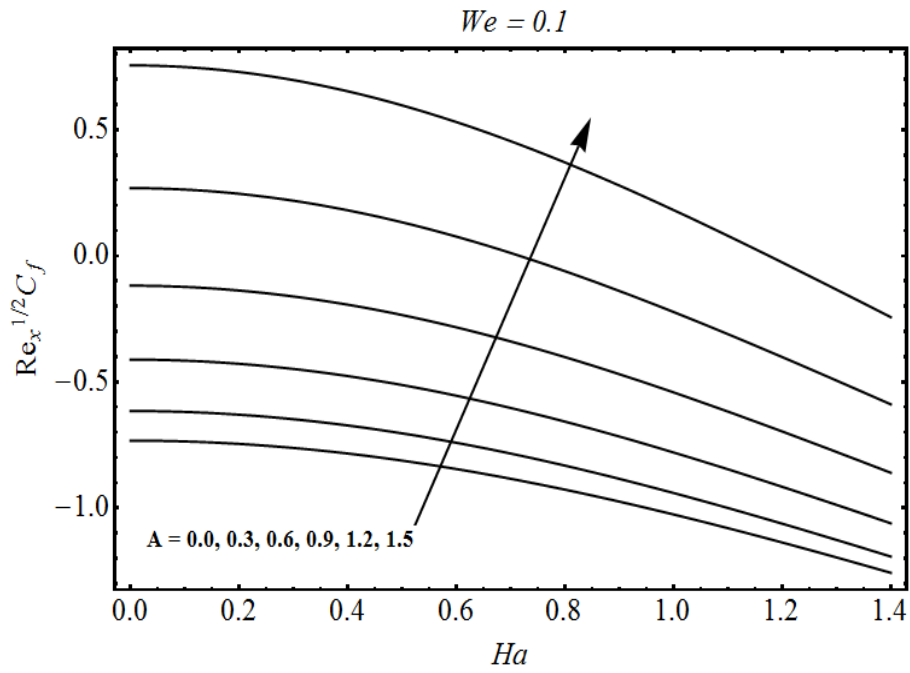
Fig. 2.14: Variation of skin friction for different values of A when $0 \le Ha \le 1.4$.
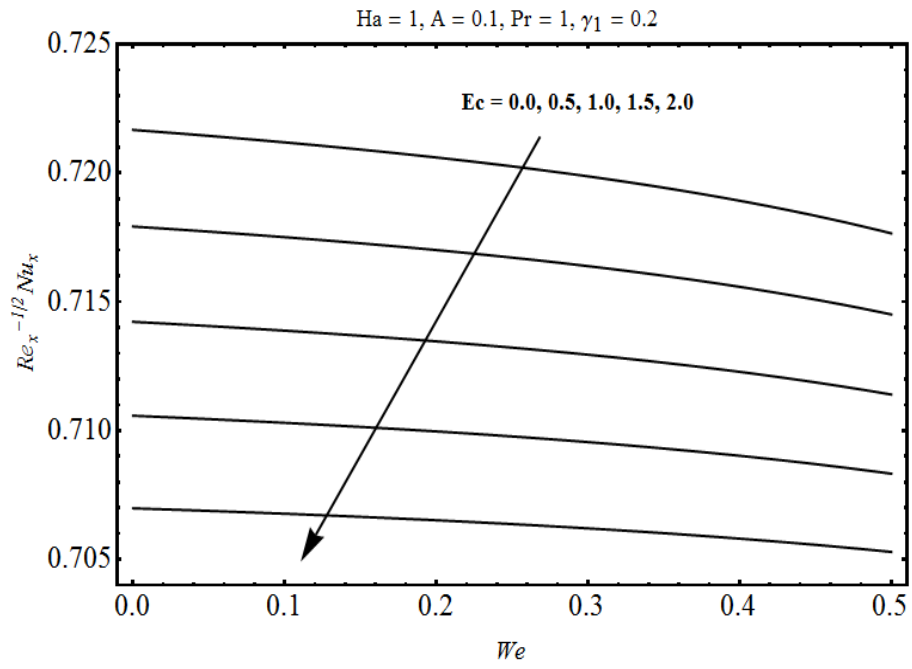
Fig. 2.15: Variation of Nusselt number for different values of Ec when
$0 \leq We \leq 0.5$.
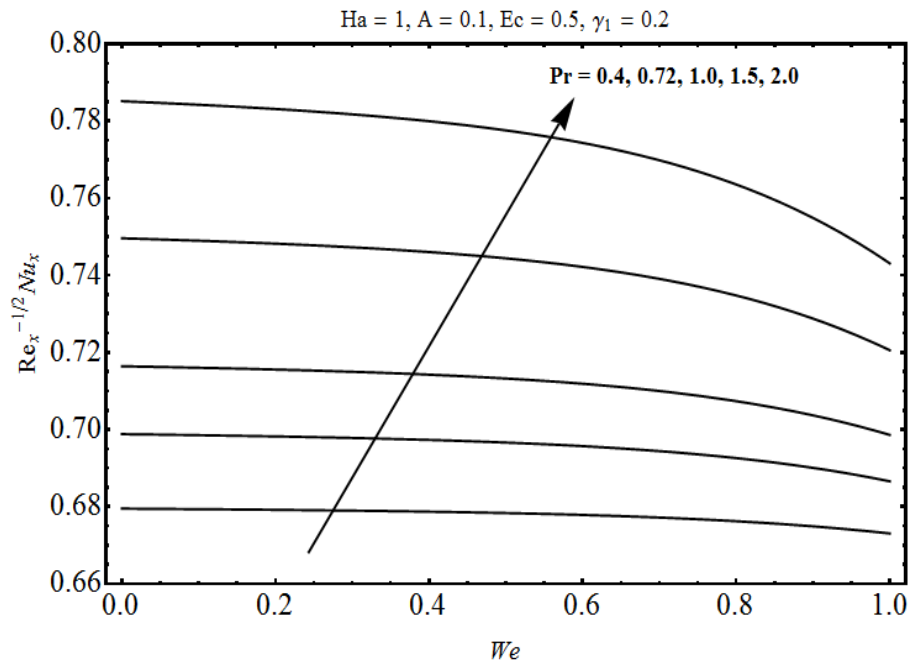
Fig. 2.16: Variation of Nusselt number for different values of Pr when
$0 \leq We \leq 1$.

Table 2.1: Convergence of homotopy solutions when $Ha = A = 0.1$, $\gamma_1 = We = 0.2$, $\Pr = 1$ and $Ec = 0.7$.

Order of approximation	$-f''(0)$	$-\theta'(0)$
1	1.0053	0.26247
5	1.0958	0.28885
10	1.1003	0.30049
12	1.1004	0.30260
34	1.1004	0.30662
38	1.1004	0.30662
45	1.1004	0.30662
60	1.1004	0.30662

Table 2.2: Numerical values of skin friction coefficient $Re_x^{1/2}C_f$ for different values of physical parameters.

We	Ha	A	$-\operatorname{Re}_x^{1/2}C_f$
0.1	1	0.1	1.0380
0.2			0.6294
0.3			0.1683
0.1	1.0	0.1	1.0380
	1.1		1.0920
	1.2		1.1480
0.1	1.0	0.1	1.0380
		0.2	1.0210
		0.3	0.9925

Table 2.3: Numerical values of local Nusselt number $Re_x^{-1/2}Nu_x$ for different values of physical parameters.

We	Ha	A	$\Pr$	Ec	$\operatorname{Re}_x^{-1/2}Nu_x$
0.1	1.0	0.1	1	0.5	0.3670
0.2					0.3621
0.3					0.3558
0.1	0.8	0.1	1	0.5	0.4091
	0.9				0.3860
	1.0				0.3670
0.1	1.0	0.2	1	0.5	0.3719
		0.3			0.3757
		0.4			0.3790

We	Ha	A	Pr	Ec	$\mathrm{Re}_x^{-1/2}\, Nu_x$
0.1	1.0	0.1	1.1	0.5	0.3802
			1.2		0.3919
			1.3		0.4022
0.1	1.0	0.1	1	0.5	0.3670
				0.6	0.3535
				0.7	0.3423

Table 2.4: Comparison of $f''(0)$ with Mahapatra and Gupta [90] and Hayat et al. [100] in the limiting cases when $We = Ha = 0$.

	$f''(0)$		
A	Mahapatra and Gupta [36]	Hayat et al. [37]	Present
0.1	-0.9694	-0.96802	-0.96803
0.2	-0.9181	-0.91692	-0.91690
0.5	-0.6673	-0.66722	-0.66721
2.0	2.0175	2.0175	2.0175
3.0	4.7293	4.7291	4.7292

2.5   Concluding remarks

Two-dimensional stagnation point flow of Walters-B fluid towards a surface subject to Newtonian heating is examined. The key points of this work are mentioned below.

- The horizontal velocity $f'(\eta)$ is decreasing function of Ha and We when $A < 1$ whereas it is increasing functions of Ha and We for $A > 1$.

- Increasing values of Ha and We correspond to a thinner momentum boundary layer.

- An increase in Prandtl number decreases the thermal boundary layer thickness and it enhances rate of heat transfer at the bounding surface.

- The temperature and surface heat transfer significantly increases when strength of Newtonian heating is enhanced.

Chapter 3

Analysis of melting heat transfer and mixed convection in the flow of Walter-B fluid

The work in this chapter focuses on melting heat transfer in the stagnation point flow of Walter-B fluid toward an impermeable stretching sheet. Flow analysis is explored with mixed convection, viscous dissipation and Joule heating. Suitable transformations are employed to achieve the systems of ordinary differential equations. Arising nonlinear problems are solved successfully for the convergent series solutions. Charateristics of various pertinent parameters on the velocity and temperature distributions, skin friction coefficient and Nusselt number are examined. It is found that velocity has opposite behavior for melting parameter and Weissenberg number.

3.1   Mathematical formulation

Let us consider the problem of steady mixed convection flow of Walter-B fluid towards a stretching surface. An incompressible fluid is electrically conducting in the presence of constant magnetic field of strength $(0, B_0, 0)$. Electric field effect is not included. Induced magnetic field for small magnetic Reynolds number is neglected. Effects of viscous dissipation and Joule heating are present. Heat transfer through melting process is taken into account. Here x and $y-$ axes are taken along and perpendicular to the sheet. The flow is confined to $y \geq 0$. The velocity of stretching sheet is $U_w(x) = cx$ and the stagnation velosity is $U_e(x) = ax$ (where a and c are positive constants). The governing two-dimensional boundary layer flow equations for present flow problem are employed as follows:

$$\frac{\partial u}{\partial x} + \frac{\partial v}{\partial y} = 0, \tag{3.1}$$

$$u\frac{\partial u}{\partial x} + v\frac{\partial u}{\partial y} = U_e\frac{dU_e}{dx} + \nu\frac{\partial^2 u}{\partial y^2} - \frac{k_0}{\rho}\left[u\frac{\partial^3 u}{\partial x\partial y^2} + v\frac{\partial^3 u}{\partial y^3} + \frac{\partial u}{\partial x}\frac{\partial^2 u}{\partial y^2}\right.$$

$$\left. - \frac{\partial u}{\partial y}\frac{\partial^2 u}{\partial x\partial y}\right] + g\beta_T(T - T_\infty) + \frac{\sigma B_0^2}{\rho}(U_e - u), \tag{3.2}$$

$$u\frac{\partial T}{\partial x} + v\frac{\partial T}{\partial y} = \frac{K}{\rho c_p}\frac{\partial^2 T}{\partial y^2} + \frac{\sigma B_0^2}{\rho c_p}u^2 + \frac{\mu_0}{\rho c_p}\left(\frac{\partial u}{\partial y}\right)^2$$

$$+ \frac{2k_0}{\rho c_p}\left[\frac{\partial u}{\partial x}\left(\frac{\partial u}{\partial y}\right)^2 - \frac{1}{2}u\frac{\partial u}{\partial y}\frac{\partial^2 u}{\partial x\partial y} - \frac{1}{2}v\frac{\partial u}{\partial y}\frac{\partial^2 u}{\partial y^2}\right.$$

$$\left. + \frac{\partial v}{\partial y}\left(\frac{\partial u}{\partial y}\right)^2\right], \tag{3.3}$$

where u and v are the velocity components along the horizontal and vertical directions respectively, ρ the fluid density, σ the electrical conductivity of fluid, K the thermal conductivity, T the temperature, k_0 the short memory coefficient and c_p the specific heat. The relevent boundary conditions for the velocity and temprature field are [23]:

$$u(x,0) = U_w(x) = cx, \ T(x,0) = T_m, \tag{3.4}$$

$$u \to U_e(x) = ax, \ T \to T_\infty \text{ as } y \to \infty, \tag{3.5}$$

$$K\left(\frac{\partial T}{\partial y}\right)_{y=0} = \rho\left[\lambda + c_s(T_m - T_0)\right]v(x,0), \tag{3.6}$$

in which λ is the latent heat of the fluid, c_s is the heat capacity of the solid surface, T_∞ the ambient temperature. The boundary condition (3.6) shows that the heat conducted by the melting surface is equal to the heat of melting along the heat required to raise T_0 the solid temperature to T_m its melting temperature.

Considering

$$u(x,y) = cxf'(\eta), \ v(x,y) = -\sqrt{c\nu}f(\eta), \ \theta = \frac{T - T_m}{T_\infty - T_m}, \ \eta = \sqrt{\frac{c}{\nu}}y, \tag{3.7}$$

the incompressibility condition is identically satiesfied, whereas Eqs. (3.2-3.6) give

$$f''' + A^2 - (f')^2 + ff'' - We\left[2f'f''' - ff^{(iv)} - (f'')^2\right] + (Ha)^2(A - f') + Gr\theta = 0, \tag{3.8}$$

$$\theta'' + \Pr f\,\theta' + \Pr Ec\,(f'')^2 - We\Pr Ec[f'(f'')^2 - ff''f'''] + (Ha - A)^2\Pr Ecf'^2 = 0, \tag{3.9}$$

$$f'(0) = 1, \quad \Pr f(0) + M\theta'(0) = 0, \ \theta(0) = 0,$$

$$f'(\infty) = A, \quad f''(\infty) = 0, \quad \theta(\infty) = 1. \tag{3.10}$$

In above equations Ha is the Hartman number, A is the ratio parameter, Gr is the Grashof number, We is

the Weissenberg number, Pr is the Prandtl number, Ec is the Eckert number and M is the dimensionless melting parameter (which is a combination of the Stefan numbers for the liquid $C_p(T_\infty - T_m)/\lambda$ and for the solid $c_s(T_m - T_0)/\lambda$ phases). The values of these parameters are given below:

$$
\begin{aligned}
(Ha)^2 &= \frac{\sigma B_0^2}{\rho c}, \ A = \frac{a}{c}, \ Gr = \frac{g\beta_T (T_\infty - T_m)}{c^2 x}, \ We = \frac{k_0 c}{\mu_0}, \\
\mathrm{Pr} &= \frac{\mu_0 c_p}{K}, \quad Ec = \frac{(cx)^2}{c_p (T_\infty - T_m)}, \quad M = \frac{C_p(T_\infty - T_m)}{\lambda + c_s(T_m - T_0)}.
\end{aligned}
\tag{3.11}
$$

Expressions of skin friction coefficient C_f and the local Nusselt number Nu_x can be written as follows:

$$
C_f = \frac{\tau_{xy}}{\rho\,(cx)^2}, \qquad Nu_x = \frac{r q_w}{K\,(T - T_\infty)},
\tag{3.12}
$$

in which shear stress (τ_{xy}) and heat flux (q_w) at the wall are

$$
\tau_{xy} = \left[\mu_0 \frac{\partial u}{\partial y} - k_0 \left(u \frac{\partial^2 u}{\partial x \partial y} + v \frac{\partial^2 u}{\partial y^2} + 2\frac{\partial u}{\partial x}\frac{\partial u}{\partial y} \right)^3 \right]_{y=0}, \ q_w = -K \left(\frac{\partial T}{\partial y} \right)_{y=0}.
\tag{3.13}
$$

Skin friction and local Nusselt number in dimensionless forms are

$$
(\mathrm{Re}_x)^{-1/2} C_f = \{1 - 3We\} f''(0),
\tag{3.14}
$$

$$
(\mathrm{Re}_x)^{-1/2} Nu_x = -\theta'(0).
\tag{3.15}
$$

3.2 Homotopic solutions

We define the velocity and temperature distribution by a set of base functions

$$
\left\{ \eta^k \exp(-n\eta) \,|k \ge 0, n \ge 0 \right\},
\tag{3.16}
$$

in term of following infinite series

$$
f_m(\eta) = \sum_{n=0}^{\infty} \sum_{k=0}^{\infty} a_{m,n}^k \eta^k \exp(-n\eta),
\tag{3.17}
$$

$$
\theta_m(\eta) = \sum_{n=0}^{\infty} \sum_{k=0}^{\infty} b_{m,n}^k \eta^k \exp(-n\eta),
\tag{3.18}
$$

where $a_{m,n}^k$ and $b_{m,n}^k$ are the constants. We have chosen the initial guesses $f_0(\eta)$ and $\theta_0(\eta)$ and the auxiliary linear operators $\mathcal{L}_f$ and $\mathcal{L}_\theta$ by the rule of solution expression and the boundary conditions

$$
f_0(\eta) = A\eta + (1 - A)(1 - \exp(-\eta)) - \frac{M}{\mathrm{Pr}}, \qquad \theta_0(\eta) = 1 - \exp(-\eta),
\tag{3.19}
$$

$$
\mathcal{L}_f[f(\eta)] = \frac{d^3 f}{d\eta^3} - \frac{df}{d\eta}, \qquad \mathcal{L}_\theta[\theta(\eta)] = \frac{d^2\theta}{d\eta^2} - \theta,
\tag{3.20}
$$

$$\mathcal{L}_f \left[C_6 + C_7 \exp(\eta) + C_8 \exp(-\eta) \right] = 0,$$

$$\mathcal{L}_\theta \left[C_9 \exp(\eta) + C_{10} \exp(-\eta) \right] = 0, \tag{3.21}$$

with $C_i \, (i = 6 - 10)$ as the constants.

3.2.1 Zeroth-order problem

The zeroth-order deformation problems are

$$(1-q)\,\mathcal{L}_f \left[\hat{f}(\eta, q) - f_0(\eta) \right] = q\hbar_f \mathcal{N}_f \left[\hat{f}(\eta, q) \right], \tag{3.22}$$

$$\left. \frac{\partial \hat{f}(\eta, q)}{\partial \eta} \right|_{\eta=0} = 1, \quad \Pr \hat{f}(\eta, q) \Big|_{\eta \to 0} + M \left. \frac{\partial \hat{\theta}(\eta, q)}{\partial \eta} \right|_{\eta=0} = 0, \quad \left. \frac{\partial \hat{f}(\eta, q)}{\partial \eta} \right|_{\eta \to \infty} = A, \tag{3.23}$$

$$(1-q)\,\mathcal{L}_\theta \left[\hat{\theta}(\eta, q) - \theta_0(\eta) \right] = q\hbar_\theta \mathcal{N}_\theta \left[\hat{f}(\eta, q), \hat{\theta}(\eta, q) \right], \tag{3.24}$$

$$\hat{\theta}(\eta, q) \Big|_{\eta \to 0} = 0, \qquad \hat{\theta}(\eta, q) \Big|_{\eta \to \infty} = 1. \tag{3.25}$$

Here $q \in [0,1]$ is embedding parmeter and $\hbar_f$ and $\hbar_\theta$ are non-zero auxiliary parameters. The non-linear operators are

$$\begin{aligned}
\mathcal{N}_f \left[\hat{f}(\eta, q) \right] = & \; \frac{\partial^3 \hat{f}}{\partial \eta^3} + A^2 - \left(\frac{\partial \hat{f}}{\partial \eta} \right)^2 + f \frac{\partial^2 \hat{f}}{\partial \eta^2} - We \left[2 \frac{\partial \hat{f}}{\partial \eta} \frac{\partial^3 \hat{f}}{\partial \eta^3} - f \frac{\partial^4 \hat{f}}{\partial \eta^4} \right. \\
& \left. - \left(\frac{\partial^2 \hat{f}}{\partial \eta^2} \right)^2 \right] + (Ha)^2 \left(A - \frac{\partial \hat{f}}{\partial \eta} \right) + Gr \, \theta,
\end{aligned} \tag{3.26}$$

$$\begin{aligned}
\mathcal{N}_\theta \left[\hat{\theta}(\eta, q), \hat{f}(\eta, q) \right] = & \; \frac{\partial^2 \hat{\theta}}{\partial \eta^2} + \Pr f \frac{\partial \hat{\theta}}{\partial \eta} + \Pr Ec \left(\frac{\partial^2 \hat{\theta}}{\partial \eta^2} \right)^2 \\
& - We \Pr Ec \left[3 \frac{\partial \hat{f}}{\partial \eta} \left(\frac{\partial^2 \hat{f}}{\partial \eta^2} \right)^2 - f \frac{\partial^2 \hat{f}}{\partial \eta^2} \frac{\partial^3 \hat{f}}{\partial \eta^3} \right] \\
& + (Ha)^2 \Pr Ec \left(\frac{\partial \hat{f}}{\partial \eta} \right)^2.
\end{aligned} \tag{3.27}$$

3.2.2 mth-order deformation problems

The mth order deformation problems are presented in the following forms:

$$\mathcal{L}_f \left[\hat{f}_m(\eta) - \chi_m \hat{f}_{m-1}(\eta) \right] = \hbar_f \mathcal{R}_m^f(\eta), \tag{3.28}$$

$$\left. \frac{\partial \hat{f}(\eta, q)}{\partial \eta} \right|_{\eta=0} = 0, \quad \Pr \hat{f}(\eta, q) \Big|_{\eta \to 0} + M \left. \frac{\partial \hat{\theta}(\eta, q)}{\partial \eta} \right|_{\eta=0} = 0, \quad \left. \frac{\partial \hat{f}(\eta, q)}{\partial \eta} \right|_{\eta \to \infty} = 0, \tag{3.29}$$

$$\mathcal{L}_\theta \left[\hat{\theta}_m(\eta) - \chi_m \hat{\theta}_{m-1}(\eta) \right] = \hbar_f \mathcal{R}_m^\theta(\eta), \tag{3.30}$$

$$\hat{\theta}\left(\eta,q\right)\Big|_{\eta\to0}=0,\qquad\hat{\theta}\left(\eta,q\right)\Big|_{\eta\to\infty}=0,\tag{3.31}$$

$$\begin{aligned}\mathcal{R}_m^f\left(\eta\right)&=f_{m-1}'''\left(\eta\right)+A^2\left(1-\chi_m\right)-\sum_{k=0}^{m-1}f_{m-1-k}'f_k'+\sum_{k=0}^{m-1}f_{m-1-k}f_k''\\&\quad-We\sum_{k=0}^{m-1}\left[2f_{m-1-k}'f'''-f_{m-1-k}f_k^{(iv)}-f_{m-1-k}''f_k''\right]\\&\quad+\left(Ha\right)^2A\left(1-\chi_m\right)-\left(Ha\right)^2f_{m-1}'+Gr\ \theta_{m-1},\end{aligned}\tag{3.32}$$

$$\begin{aligned}\mathcal{R}_m^\theta\left(\eta\right)&=\theta_{m-1}''\left(\eta\right)+\Pr\sum_{k=0}^{m-1}f_{m-1-k}\theta_k'+\Pr Ec\sum_{k=0}^{m-1}f_{m-1-k}''f_k''\\&\quad-We\Pr Ec\sum_{k=0}^{m-1}\left[3f_{m-1-k}'\sum_{l=0}^k f_{k-l}''f_l''-f_{m-1-k}\sum_{l=0k-l}^k f_{k-l}''f_l'''\right]\\&\quad+\left(Ha\right)^2\Pr Ec\sum_{k=0}^{m-1}f_{m-1-k}'f_k'.\end{aligned}\tag{3.33}$$

For $q=0$ and $q=1$, we can write

$$\hat{f}\left(\eta;0\right)=f_0\left(\eta\right),\quad\hat{f}\left(\eta;1\right)=f\left(\eta\right),\tag{3.34}$$

$$\hat{\theta}\left(\eta;0\right)=\theta_0\left(\eta\right),\quad\hat{\theta}\left(\eta;1\right)=\theta\left(\eta\right),\tag{3.35}$$

and with the variation of q from 0 to 1, $\hat{f}\left(\eta;q\right)$ and $\hat{\theta}\left(\eta;q\right)$ vary from the initial solutions $f_0\left(\eta\right)$ and $\theta_0(\eta)$ to the final solutions $f\left(\eta\right)$ and $\theta(\eta)$ respectively. By Taylor's series, we have

$$\hat{f}\left(\eta,q\right)=f_0\left(\eta\right)+\sum_{m=1}^\infty f_m\left(\eta\right)q^m,\quad f_m\left(\eta\right)=\frac{1}{m!}\frac{\partial^m\hat{f}\left(\eta,q\right)}{\partial q^m}\bigg|_{q=0},\tag{3.36}$$

$$\hat{\theta}\left(\eta,q\right)=\theta_0\left(\eta\right)+\sum_{m=1}^\infty\theta_m\left(\eta\right)q^m,\quad\theta_m\left(\eta\right)=\frac{1}{m!}\frac{\partial^m\hat{\theta}\left(\eta,q\right)}{\partial q^m}\bigg|_{q=0}.\tag{3.37}$$

The value of auxiliary parameter is chosen in such a way that the above series converge at $q=1$ i.e.

$$\hat{f}\left(\eta\right)=f_0\left(\eta\right)+\sum_{m=1}^\infty f_m\left(\eta\right),\tag{3.38}$$

$$\hat{\theta}\left(\eta\right)=\theta_0\left(\eta\right)+\sum_{m=1}^\infty\theta_m\left(\eta\right).\tag{3.39}$$

The general solutions (f_m,θ_m) of Eqs. $(3.28-3.31)$ in terms of special solutions (f_m^*,θ_m^*) are given by

$$f_m\left(\eta\right)=f_m^*+C_6+C_7\exp\left(\eta\right)+C_8\exp\left(-\eta\right),\tag{3.40}$$

$$\theta_m\left(\eta\right)=\theta_m^*+C_9\exp\left(\eta\right)+C_{10}\exp\left(-\eta\right).\tag{3.41}$$

3.3 Convergence of the homotopy solutions

The derived series solutions (3.36) and (3.37) contain auxiliary parameters $\hbar_f$ and $\hbar_\theta$. The convergence of the series solutions strongly depend upon these auxiliary parameters. In order to obtain the admissible values of auxiliary parameters, the $\hbar$-curves are sketched at 14th order of approximation for velocity and 15th order for temperature (see Fig. 3.1). It is found that range for admissible values of $\hbar_f$ and $\hbar_\theta$ are $-1 \le \hbar_f < -0.1$ and $-1.3 \le \hbar_\theta < -0.1$.

3.4 Results and discussion

This section enlightens the effects of various emerging parameters on the velocity, temperature, skin friction coefficient and local Nusselt number. Fig. 3.2 is displayed to examine the effect of melting parameter M on dimensionless velocity f'. Here $M = 0$ corresponds to the case when melting heat effects are negligible and $M \ne 0$ when melting effect is appreciable. It is noted from Fig. 3.2 that dimensionless velocity f' increases when melting parameter is increased. Such increase in velocity enhances momentum boundary layer. Fig. 3.3 illustrates the influence of Weissenberg number We on the dimensionless velocity f'. Clearly an increase in We shows a decrease in velocity f'. In fact due to liquid elasticity there is a restoring force by the fluid against deformation. Effect of ratio parameter A is presented in Fig. 3.4. By increasing ratio parameter A the velocity f' increases whereas momentum boundary layer thickness increases for $A > 1$ and it decreases for $A < 1$. Influence of external magnetic field on velocity f' is shown in Fig. 3.5. An increase in Hartman number Ha corresponds to an increase in applied magnetic field. Consequently the magnitude of Lorentz force (a drag force) increases. Since Lorentz force opposes the flow therefore fluid particles are slows down (see Fig. 3.5). Momentum boundary layer via Hartman number is decreased. Effect of buoyancy force is portrayed in Fig. 3.6. Here $Gr > 0$ is the case when buoyant force acts as favourable pressure gradient where $Gr < 0$ corresponds to adverse pressure gradient and buoyant force opposes the flow (see Fig. 3.6). Momentum boundary layer thickness increases for $Gr > 0$ and it decreases when $Gr < 0$. Comparison of Figs. 3.6 and 3.7 shows that Pr and Gr have opposite effects on velocity $f'(\eta)$. It is found from Fig. 3.8 that dimensionless temperature $\theta(\eta)$ decreases when melting parameter M is increased. Since melting causes a decrease in temperature of sheet and heat flows from hotter fluid to colder sheet. As expected the temperature of fluid decreases. Fig. 3.9 indicates that the temperature decreases with an increase in We. Fig. 3.10 is presented to see the influence of ratio parameter on temperature $\theta(\eta)$. Here temperature increases but the thermal boundary layer thickness reduces. Fig. 3.11 indicates that the temperature profile $\theta(\eta)$ is increasing function of Ha. However thermal boundary layer decreases. Figs. 3.12 and 3.13 have been potrayed to investigate the effects of Pr and Ec on the temperature $\theta(\eta)$. From Fig. 3.12 we observed that larger Pr corresponds to an increase in temperature and decay in thermal boundary layer thickness through lower thermal diffusitivity. Similar behavior is noted for Eckert number Ec on the temperature $\theta(\eta)$. Fig. 3.14 gives the variation of We on the local skin friction coefficient versus Ha $(1 \le Ha \le 2)$. There is an enhancement in the skin friction coefficients when Weisenberg number We increases. Fig. 3.15 represents

the effects of ratio A on the local skin friction coefficient $\mathrm{Re}_x^{1/2} C_f$ versus M when $0 \leq M \leq 1$. Skin friction coefficient is increased by increasing A. Figs. 3.16 and 3.17 display the effect of Pr on skin friction coefficient when Gr $(0.6 \leq Gr \leq 2)$ and Ec $(0 \leq Ec \leq 1)$. It is observed that Pr have opposit behavior with respect to Gr and Ec. Fig. 3.18 indicates that the effect of We on Nusselt number is a decreasing function when $1 \leq Ha \leq 2$. Nusselt number is increased for ratio parameter A when $0 \leq M \leq 1$ (see Fig. 3.19). Effect of Pr on $\mathrm{Re}_x^{-1/2} Nu_x$ corresponding to Gr and Ec is given in the Figs. 3.20 and 3.21. These Figs. elucidate that both have the same increasing behavior.
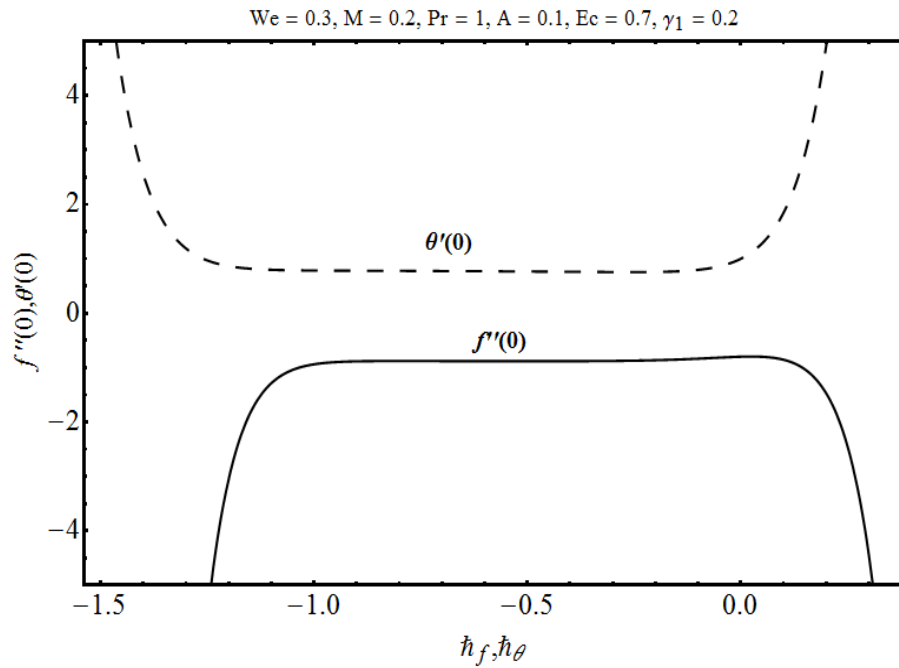
Fig. 3.1: $\hbar-$curves for the functions $f\left(\eta\right)$ and $\theta\left(\eta\right).$
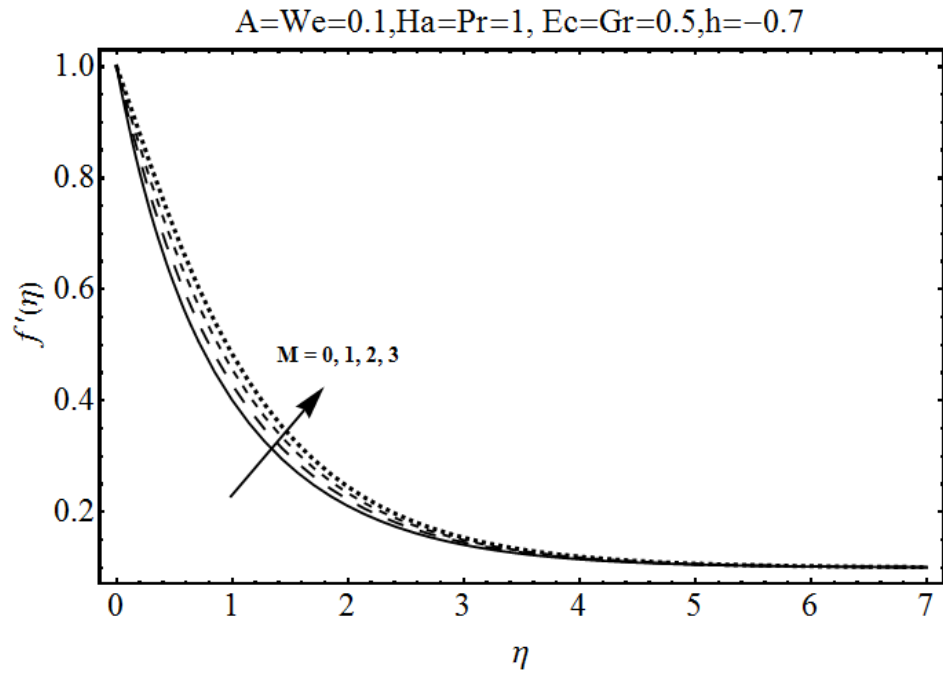
Fig. 3.2: Influence of M on $f'(\eta)$.
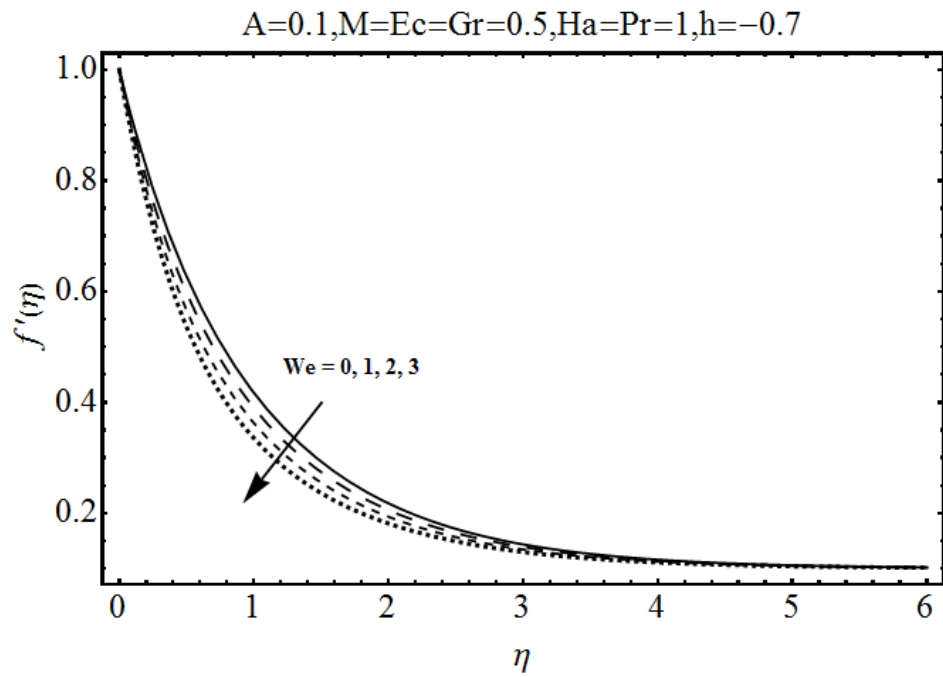
Fig. 3.3: Influence of We on $f'(\eta)$.

We=0.1,M=Ec=Gr0.5,Ha=Pr=1,h=−0.7
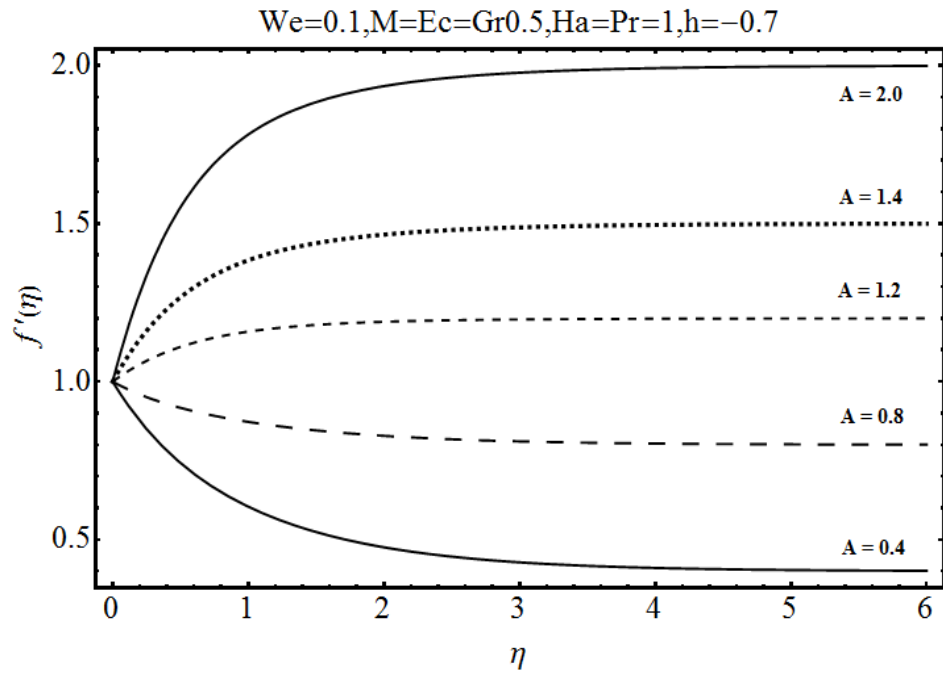
Fig. 3.4: Influence of A on $f'(\eta)$.

A=We=0.1,M=Ec=Gr=0.5,Pr=1,h=−0.7
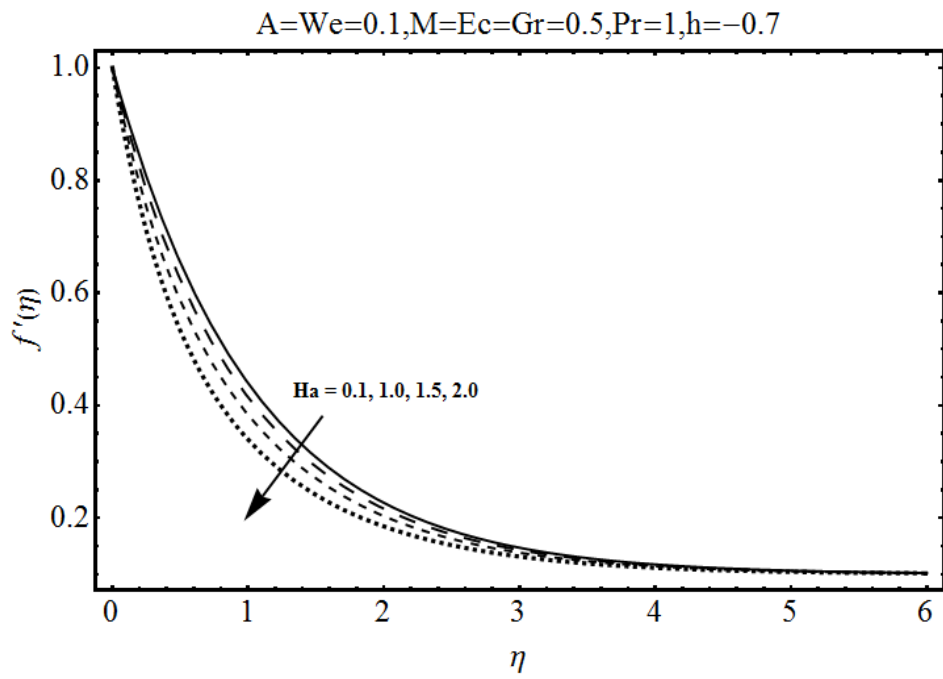
Fig. 3.5: Influence of Ha on $f'(\eta)$.
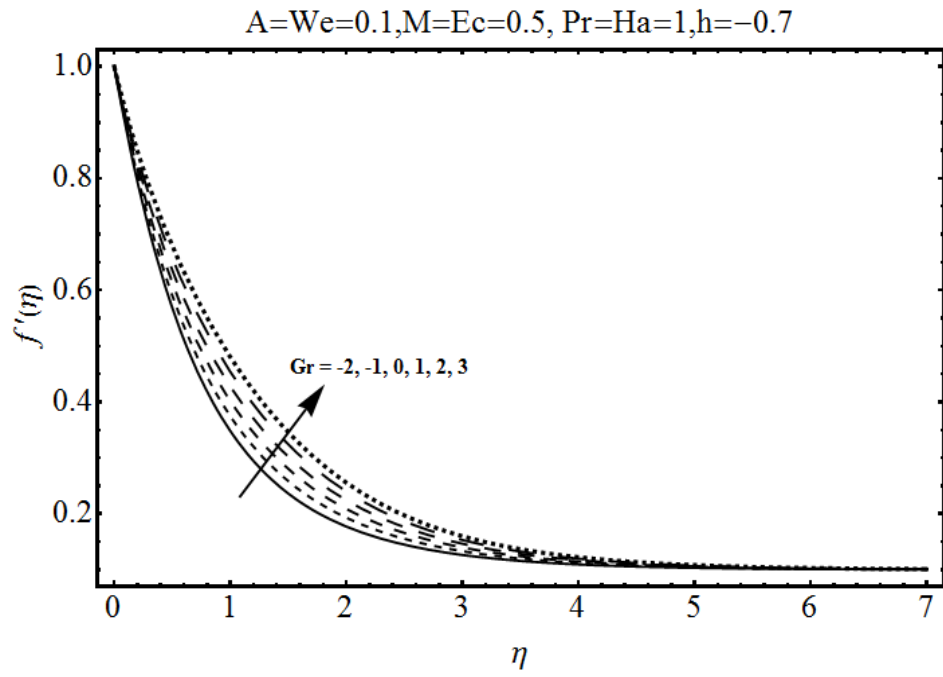
Fig. 3.6: Influence of Gr on $f'(\eta)$.
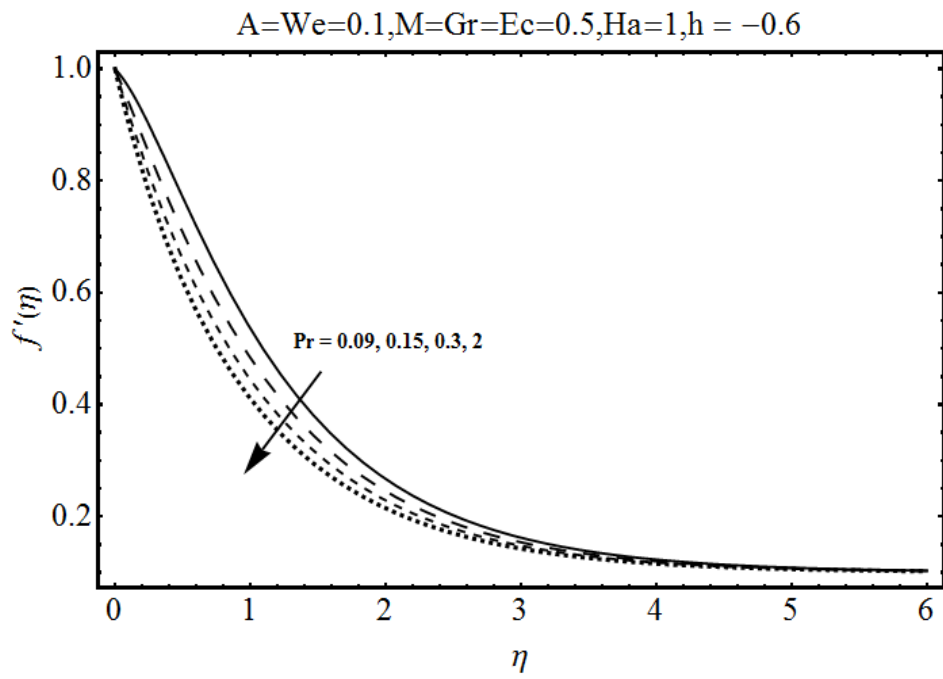
Fig. 3.7: Influence of Pr on $f'(\eta)$.
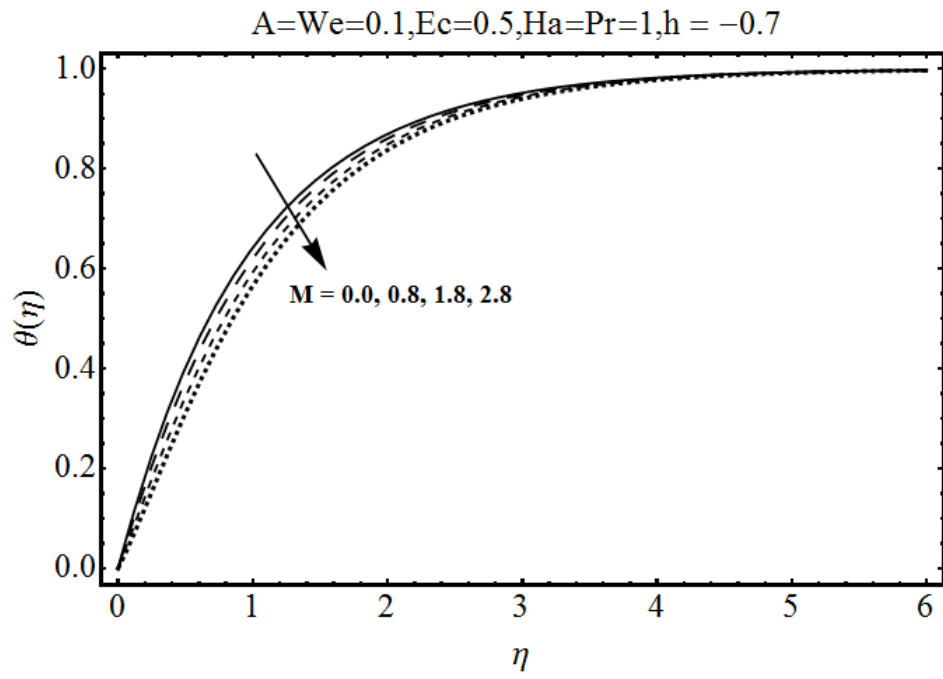
Fig. 3.8: Influence of M on $\theta(\eta)$.
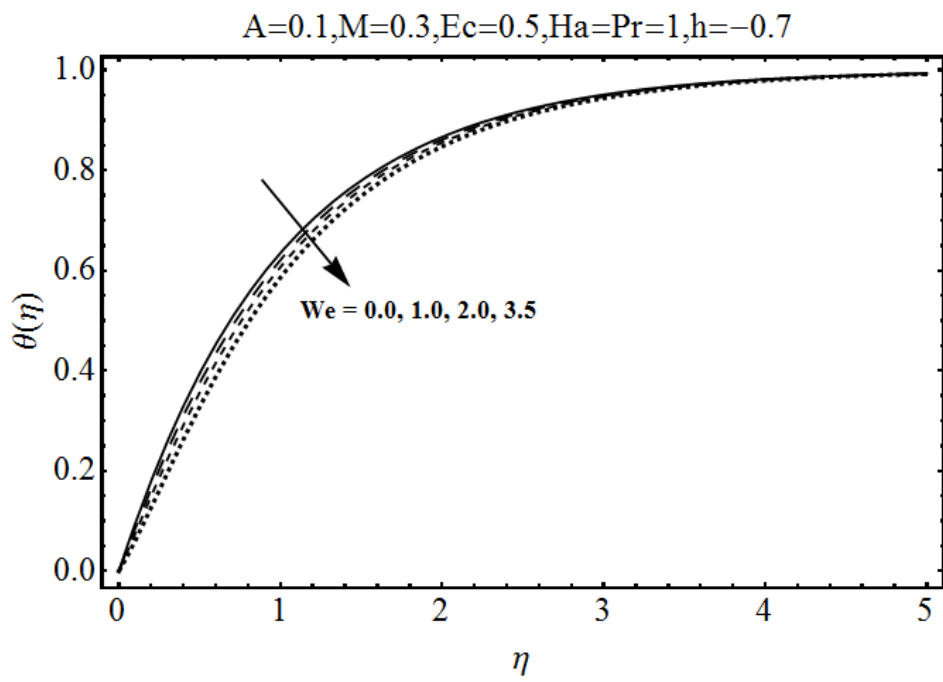
Fig. 3.9: Influence of We on $\theta(\eta)$.
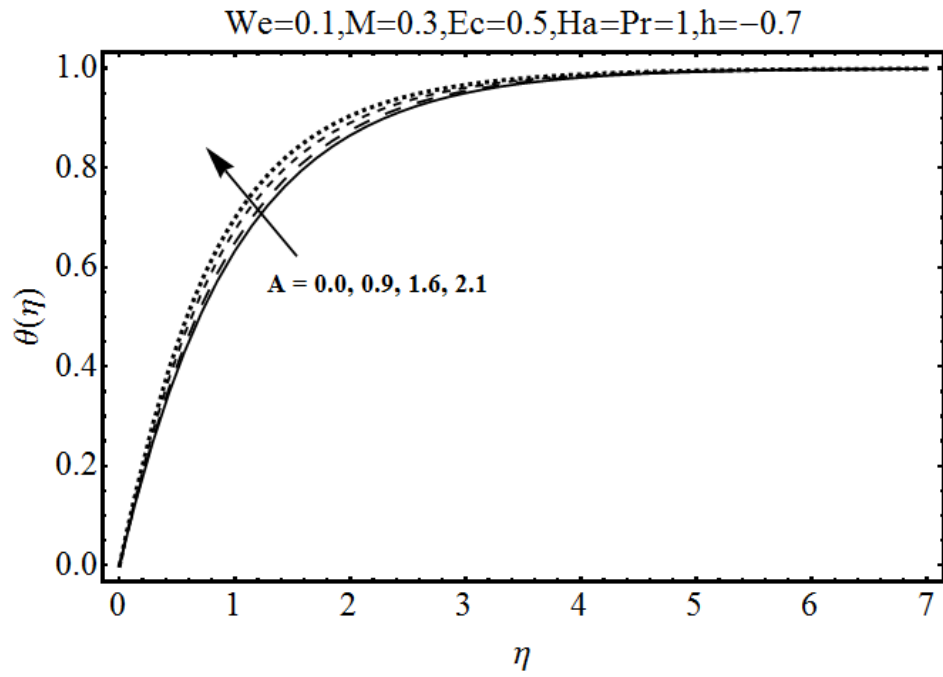
Fig. 3.10: Influence of A on $\theta(\eta)$.
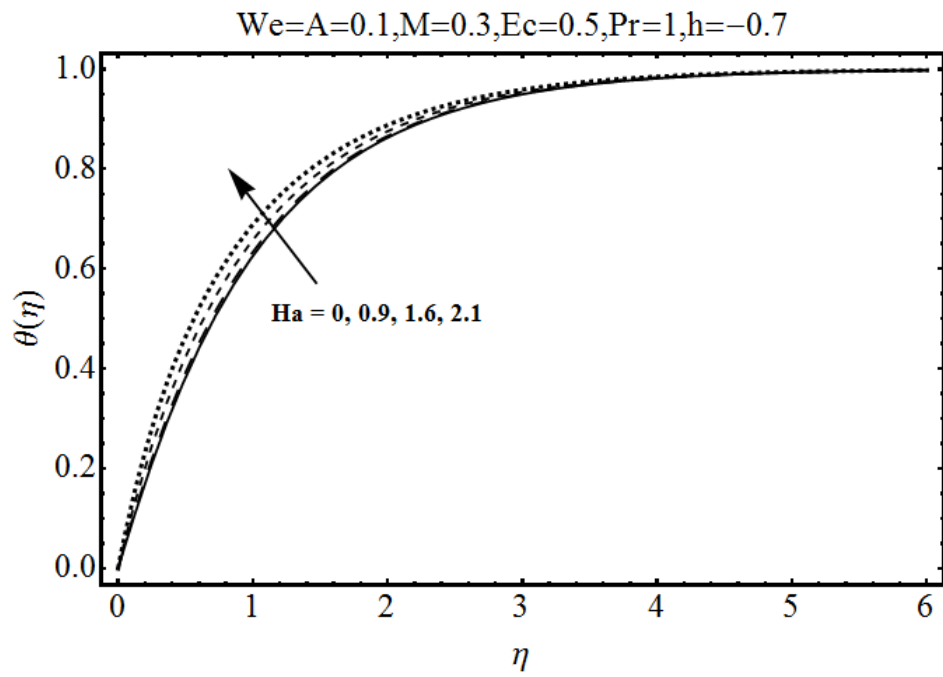
Fig. 3.11: Influence of Ha on $\theta(\eta)$.

We=A=0.1,M=0.3,Ec=0.5,Ha=1,h=−0.7
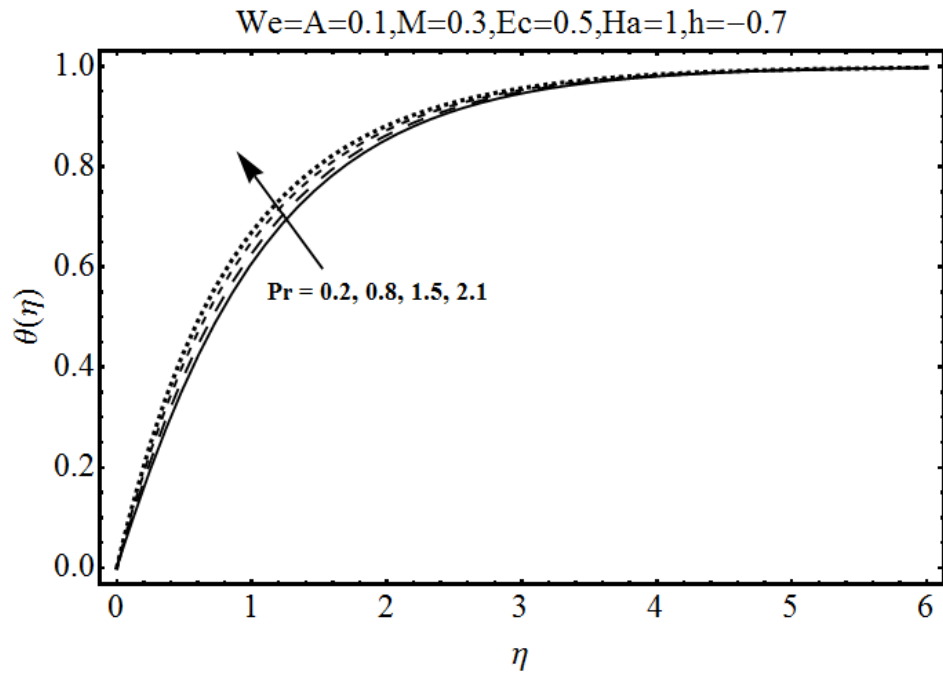
Fig. 3.12: Influence of Pr on $\theta(\eta)$.

We=A=0.1,M=0.3,Pr=Ha=1,h=−0.7
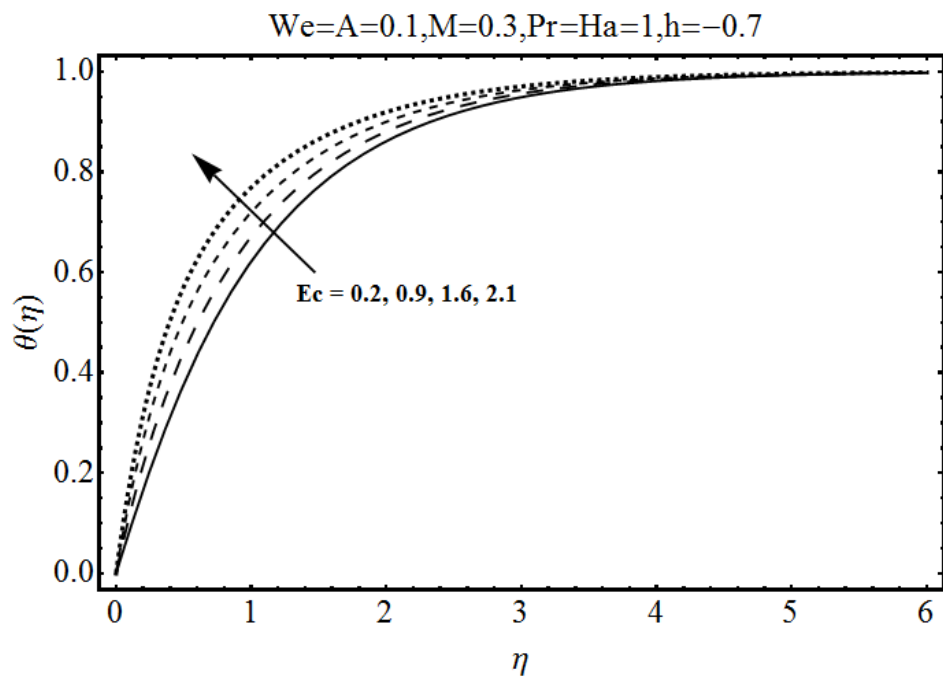
Fig. 3.13: Influence of Ec on $\theta(\eta)$.
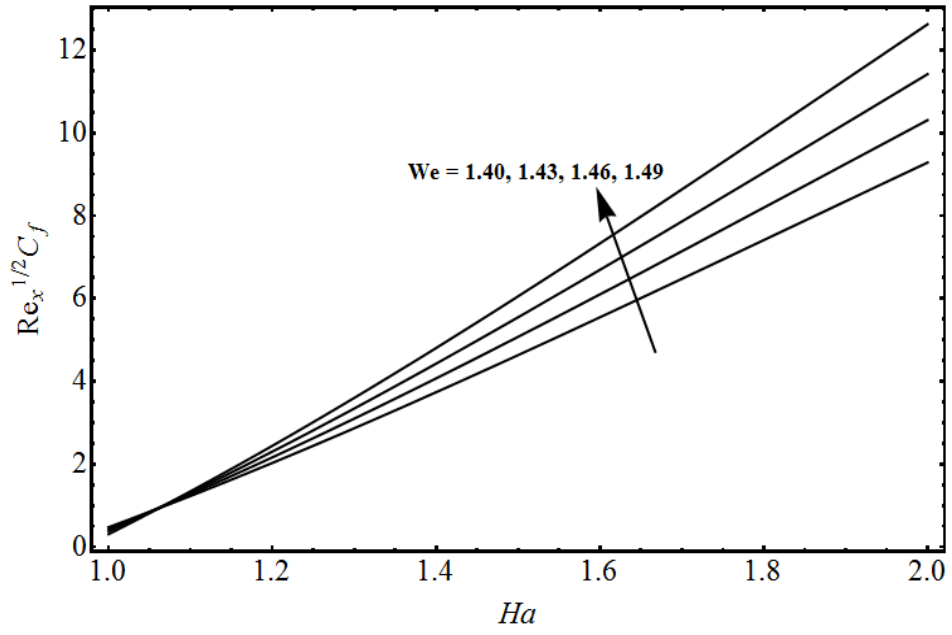
Fig. 3.14: Influence of We on $\mathrm{Re}_x^{1/2} C_f$ when $1 \le Ha \le 2$.
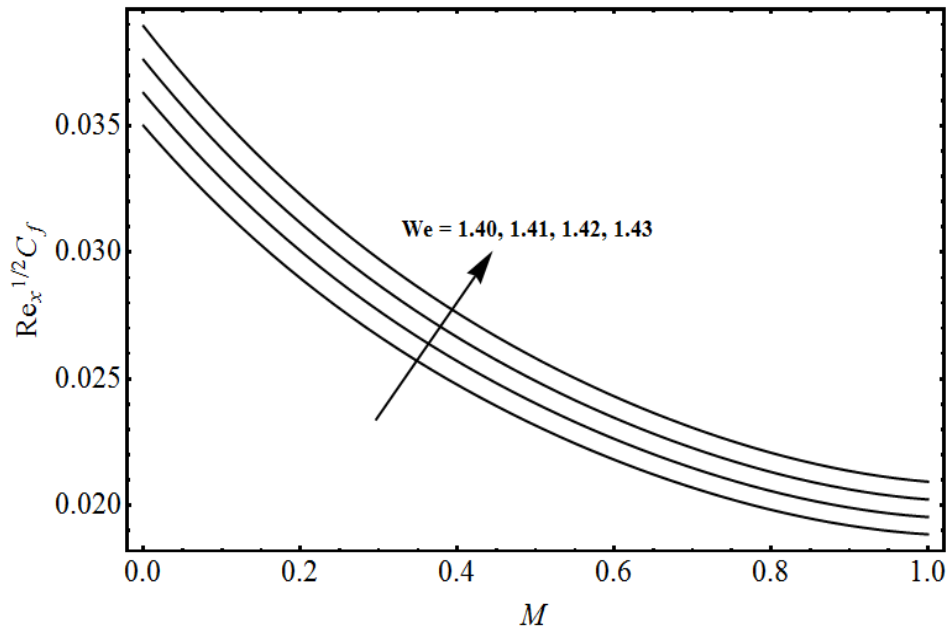
Fig. 3.15: Influence of We on $\mathrm{Re}_x^{1/2} C_f$ when $0 \le M \le 1$.
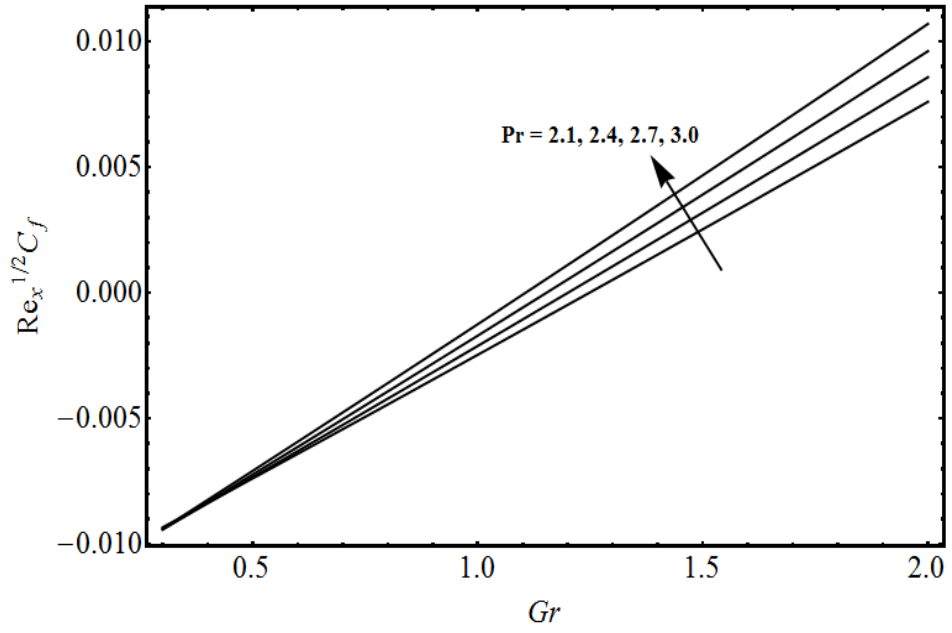
Fig. 3.16: Influence of Pr on $\mathrm{Re}_x^{1/2} C_f$ when $0.45 \leq Gr \leq 2$.
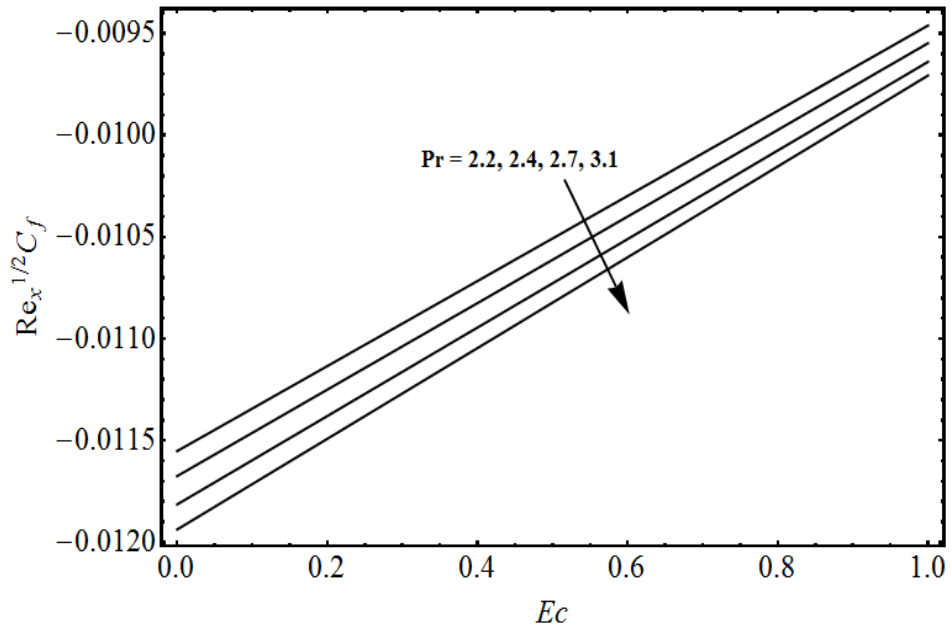
Fig. 3.17: Influence of Pr on $\mathrm{Re}_x^{1/2} C_f$ when $0.0 \leq Ec \leq 1$.
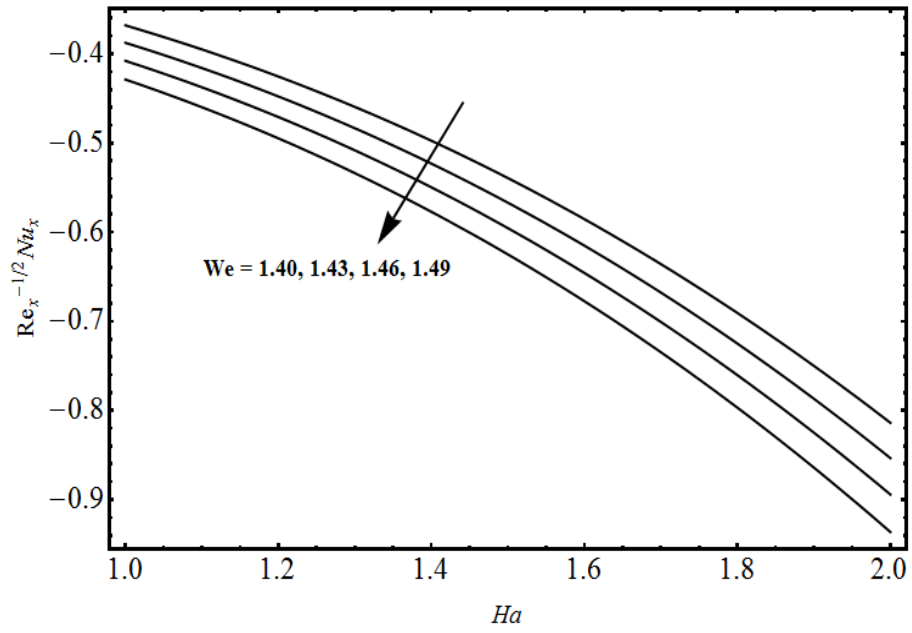
Fig. 3.18: Influence of Pr on $\mathrm{Re}_x^{-1/2}\, Nu_x$ when $1 \leq Ha \leq 2$.
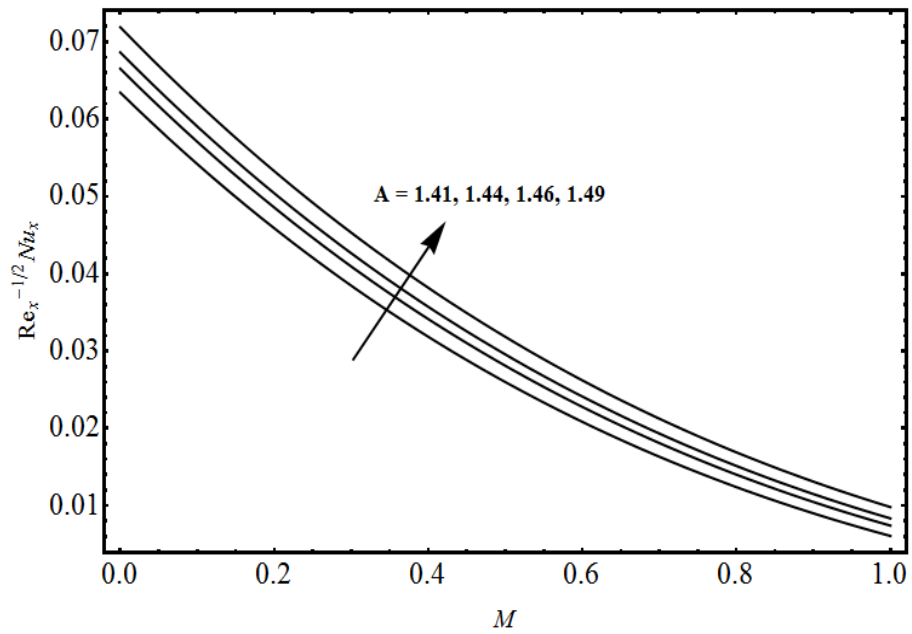
Fig. 3.19: Influence of A on $\mathrm{Re}_x^{-1/2}\, Nu_x$ when $0 \leq M \leq 1$.
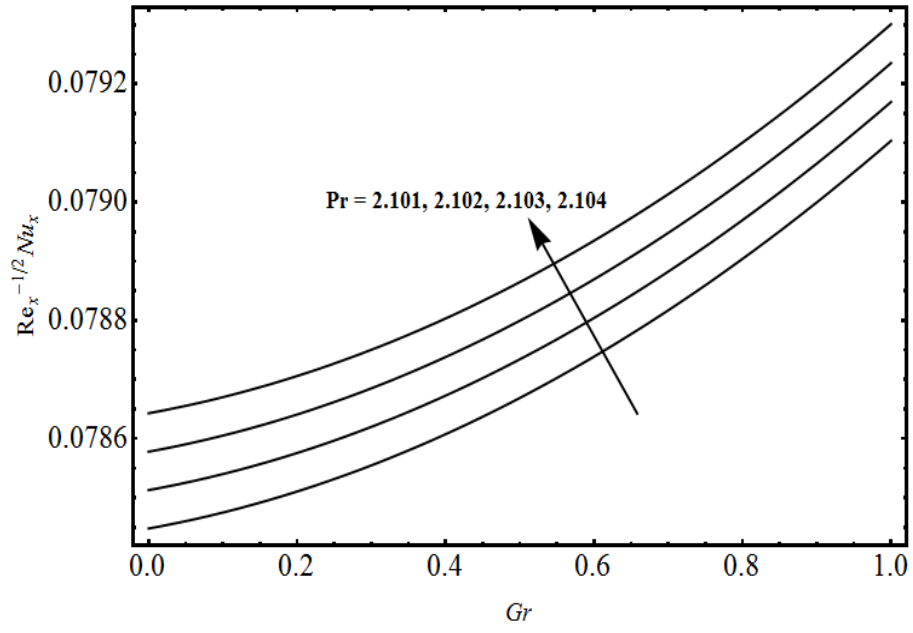
Fig. 3.20: Influence of Pr on $\mathrm{Re}_x^{-1/2} Nu_x$ when $0 \leq Gr \leq 1$.
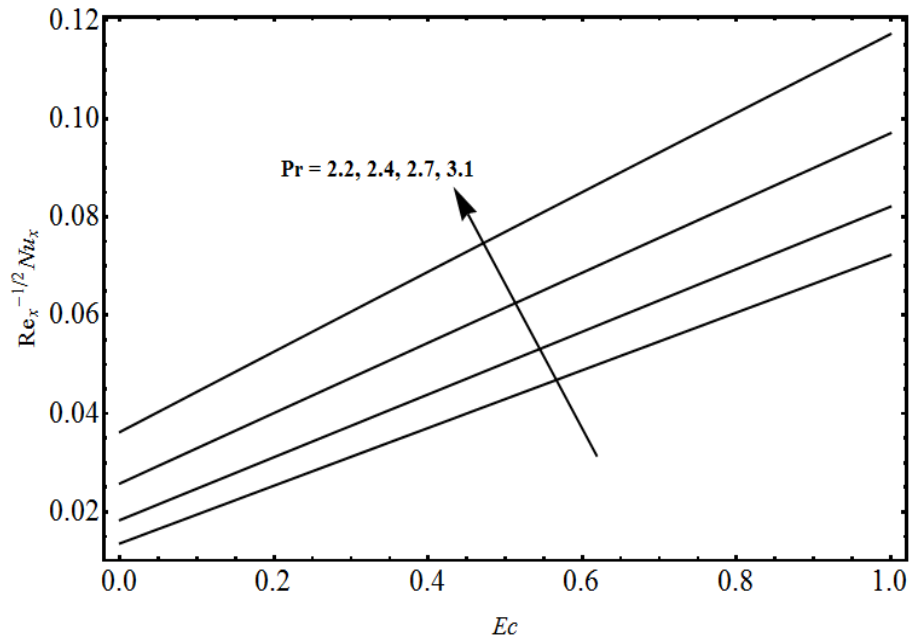
Fig. 3.21: Influence of Pr on $\mathrm{Re}_x^{-1/2} Nu_x$ when $0 \leq Ec \leq 1$.

Table 3.1: Convergence of homotopy solutions when $We = 0.2$, $Ha = 0.1$, $M = 0.1$, $A = 0.2$, $Gr = 0.1$, $\Pr = 1$ and $Ec = 0.7$.

Order of approximation	$-f''(0)$	$\theta'(0)$
1	0.8483	0.9481
2	0.8891	0.9141
5	0.9767	0.8693
10	1.0500	0.8602
19	1.0690	0.8752
28	1.0690	0.8858
30	1.0690	0.8858
35	1.0690	0.8858

3.5 Concluding remarks

The main observations of the presented analysis are listed below.

- Effects of melting parameter M and Weissenberg number We on the velocity are opposite.

- Effect of ratio A is to increase both the velocity and temperature fields significantly.

- Effects of We, Ha and $\Pr$ on velocity profile f' are similar in a qualitative sense.

- Behaviors of We and $\Pr$ on the temperature θ are opposite.

- Temperature field is increased via Eckert number Ec.

- Nusselt number for $\Pr$ versus both Gr and Ec are opposite when $0.6 \leq Gr \leq 2$ and $0 \leq Ec \leq 1$.

- Skin friction coefficient for A and $\Pr$ are similar when $0 \leq M \leq 1$ and $0 \leq Ec \leq 1$.

Chapter 4

Impact of melting phenomenon in the Falkner-Skan wedge flow of second grade nanofluid: A revised model

This chapter investigates the magnetohydrodynamic (MHD) Falkner-Skan flow of second grade nanofluid. The flow is caused by a stretching wedge with melting heat transfer and heat generation/absorption. A system of ordinary differential equations is obtained by using suitable transformations. Convergent series solutions are derived. Influence of various pertinent parameters on the velocity, temperature and concentration is evaluated. Analysis of the obtained results shows that fluid flow enhances with the increase of wedge and second grade fluid parameters. Also thermophoresis and Brownian motion parameters have reverse behavior on the temperature and concentration fields.

4.1 Mathematical formulation

Consider the steady two-dimensional Falkner-Skan flow of an incompressible second grade nanofluid. Fluid flow is induced by a stretched wedge with the velocity $U_w(x) = bx^n$. The free stream velocity is $U_e(x) = ax^n$ where b, a and n are positive constants with $0 \leq n \leq 1$. We have chosen $T_\infty > T_m$ where T_m is the temperature of the melting surface and T_∞ the ambient temperature. The flux of the nanoparticle volume fraction at $y = 0$, is taken to be zero. A uniform magnetic field of strength B_0 is applied at an angle ψ. Electric and induced magnetic fields are neglected. Effects of Brownian motion and thermophoresis are presented. Under these assumptions, the boundary layer equations governing the flow can be expressed as follows:

$$\frac{\partial u}{\partial x} + \frac{\partial v}{\partial y} = 0, \tag{4.1}$$

$$
\begin{aligned}
u\frac{\partial u}{\partial x} + v\frac{\partial u}{\partial y} &= \nu\frac{\partial^2 u}{\partial y^2} + \frac{\alpha_1^*}{\rho}\left[\frac{\partial u}{\partial x}\frac{\partial^2 u}{\partial y^2} + u\frac{\partial^3 u}{\partial y^2 \partial x} - \frac{\partial u}{\partial y}\frac{\partial^2 v}{\partial y^2} + v\frac{\partial^3 u}{\partial y^3}\right] \\
&\quad + U_e\frac{dU_e}{dx} - \frac{\sigma B_0^2}{\rho}\sin^2\psi\,(u - U_e),
\end{aligned}
\tag{4.2}
$$

$$u\frac{\partial T}{\partial x} + v\frac{\partial T}{\partial y} = \frac{k}{\rho c_p}\frac{\partial^2 T}{\partial y^2} + \tau\left[D_B\frac{\partial T}{\partial y}\frac{\partial C}{\partial y} + \frac{D_T}{T_\infty}\left(\frac{\partial T}{\partial y}\right)^2\right] + \frac{Q_0}{\rho c_p}(T - T_m), \tag{4.3}$$

$$u\frac{\partial C}{\partial x} + v\frac{\partial C}{\partial y} = D_B\frac{\partial^2 C}{\partial y^2} + \frac{D_T}{T_\infty}\frac{\partial^2 T}{\partial y^2}. \tag{4.4}$$

The corresponding boundary conditions are

$$u = U_w(x) = bx^n,\ T = T_m,\ D_B\frac{\partial C}{\partial y} + \frac{D_T}{T_\infty}\frac{\partial T}{\partial y} = 0\ \ \text{at}\ \ y = 0,$$

$$u \to U_e(x) = ax^n,\ T \to T_\infty,\ C \to C_\infty\ \ \text{as}\ y \to \infty, \tag{4.5}$$

and

$$k\left(\frac{\partial T}{\partial y}\right)_{y=0} = \rho\left[\lambda + c_s(T_m - T_0)\right]v(x,0), \tag{4.6}$$

where u represents velocity along $x-$ direction and v the velocity along $y-$ direction, ν the kinematic viscosity, α_1^* the material fluid parameter, ρ the fluid density, σ the electrical conductivity of the fluid, T the temperature, k the fluid thermal conductivity, D_B the Brownian diffusion coefficient, D_T the thermophoresis diffusion coefficient, Q_0 the dimensional heat generation/absorption coefficient, c_p the specific heat, C the concentration, C_∞ the ambient fluid concentration, λ the fluid latent heat and c_s the surface heat capacity. The boundary condition (4.6) shows that the heat conducted to the melting surface is equal to the melting heat plus the sensible heat required to raise the solid temperature T_0 to its melting temperature T_m (see Epstein and Cho [19]).

We employ the following transformations

$$\eta = \left(\frac{(n+1)U_e}{2\nu x}\right)^{\frac{1}{2}}y,\ \Psi = \left(\frac{2\nu x U_e}{n+1}\right)^{\frac{1}{2}}f(\eta),\ \theta(\eta) = \frac{T - T_m}{T_\infty - T_m},\ \phi(\eta) = \frac{C - C_m}{C_\infty - C_m}, \tag{4.7}$$

where C_m is melting surface concentration and Ψ is the stream function defined through the relationship $u = \partial\Psi/\partial y,\ v = -\partial\Psi/\partial x$. Here the continuity equation is satisfied automatically and Eqs. $(4.2 - 4.6)$ take the following forms:

$$f''' + \left(\frac{2n}{n+1}\right)(1 - f'^2) + ff'' + \alpha_1\left[(3n-1)f'f''' + \left(\frac{3n-1}{2}\right)f''^2\right.$$
$$\left. + (n-1)\eta f''f''' - \left(\frac{n+1}{2}\right)ff^{iv}\right] - (Ha)^2\sin^2\psi(f'-1) = 0, \tag{4.8}$$

$$\frac{1}{\Pr}\theta'' + f\theta' + Nb\theta'\phi' + Nt\theta'^2 + \alpha\theta = 0, \tag{4.9}$$

$$\frac{1}{Sc}\phi'' + f\phi' + \frac{Nt}{Nb}\theta'' = 0, \tag{4.10}$$

$$f'(\eta) = A,\ \Pr f(\eta) + M\theta'(\eta) = 0,\ \theta(\eta) = 0,\ Nb\phi'(\eta) + Nt\theta'(\eta) = 0\ \ \text{at}\ \eta = 0,$$

$$f'(\eta) \to 1,\ \theta(\eta) \to 1,\ \phi(\eta) \to 1\ \ \text{as}\ \eta \to \infty. \tag{4.11}$$

Here $\alpha_1 = \alpha_1^* ax^{n-1}/\mu$ the second grade fluid parameter, $(Ha)^2 = \sigma B_0^2/\rho ax^{n-1}$ the Hartman number,

Pr $= \mu c_p/k$ the Prandtl number, $Nb = \tau D_B(C_\infty - C_m)/\nu$ the Brownian motion parameter, $Nt = \tau D_T(T_\infty - T_m)/\nu T_\infty$ the thermophoresis parameter, $\alpha = Q_0 S/\rho c_p a x^{n-1}$ the heat generation/absorption parameter, $Sc = \nu/D_B$ the Schmidt number, $A = b/a$ the ratio of rates and $M = C_p(T_\infty - T_m)/(\lambda + c_s(T_m - T_0))$ the melting parameter.

Skin friction coefficient is defined by

$$C_f = \frac{2\tau_{xy}}{\rho U_w^2}, \ \ \tau_{xy} = \mu \left.\frac{\partial u}{\partial y}\right|_{y=0} + \alpha_1^* \left(u\frac{\partial^2 u}{\partial y \partial x} + v\frac{\partial^2 u}{\partial y^2} + 2\frac{\partial u}{\partial x}\frac{\partial u}{\partial y} \right)_{y=0}. \tag{4.12}$$

In dimensionless form, the above equation can be written below:

$$(\mathrm{Re}_x)^{1/2} C_f = f''(0) - \alpha_1 \left(\frac{n+2}{2}A + \frac{n+1}{2}f(0) \right) f''(0). \tag{4.13}$$

Nusselt number with heat transfer q_w is defined as

$$Nu_x = \frac{xq_w}{k(T_\infty - T_m)}, \ \ q_w = -k \left.\frac{\partial T}{\partial y}\right|_{y=0}. \tag{4.14}$$

In dimensionless form, the above equation becomes

$$(\mathrm{Re}_x)^{-1/2} Nu_x = -\theta'(0). \tag{4.15}$$

4.2 Homotopic solutions

Initial guesses $(f_0(\eta), \theta_0(\eta), \phi_0(\eta))$ and linear operators $(\mathcal{L}_f, \mathcal{L}_\theta, \mathcal{L}_\phi)$ are taken in the forms:

$$f_0(\eta) = A\left(1 - e^{-\eta}\right) - \frac{M}{\mathrm{Pr}}, \ \ \theta_0(\eta) = 1 - e^{-\eta}, \ \ \phi_0(\eta) = 1 + e^{-\frac{Nt}{Nb}\eta}, \tag{4.16}$$

$$\mathcal{L}_f = f''' - f', \ \ \mathcal{L}_\theta = \theta'' - \theta, \ \ \mathcal{L}_\phi = \phi'' - \phi, \tag{4.17}$$

with

$$\mathcal{L}_f(C_{11} + C_{12}e^\eta + C_{13}e^{-\eta}) = 0, \ \ \mathcal{L}_\theta(C_{14}e^\eta + C_{15}e^{-\eta}) = 0, \ \ \mathcal{L}_\phi(C_{16}e^\eta + C_{17}e^{-\eta}) = 0, \tag{4.18}$$

where $C_{11} - C_{17}$ are the arbitrary constants.

4.2.1 Zeroth−order deformation equations

The zeroth order deformation problems are constructed as follows:

$$(1-q)\mathcal{L}_f\left[\hat{f}(\eta,q) - f_0(\eta)\right] = q\hbar_f\mathcal{N}_f[\hat{f}(\eta,q)], \tag{4.19}$$

$$(1-q)\mathcal{L}_\theta\left[\hat{\theta}(\eta,q) - \theta_0(\eta)\right] = q\hbar_\theta\mathcal{N}_\theta[\hat{\theta}(\eta,q), \hat{f}(\eta,q), \hat{\phi}(\eta,q)], \tag{4.20}$$

$$(1 - q)\mathcal{L}_\phi \left[\hat{\phi}(\eta, q) - \phi_0(\eta) \right] = q\hbar_\phi \mathcal{N}_\phi[\hat{\phi}(\eta, q), \hat{f}(\eta, q), \hat{\theta}(\eta, q)], \tag{4.21}$$

where $q \in [0, 1]$ is the embedding parameter, $\hbar_f$, $\hbar_\theta$ and $\hbar_\phi$ are the non-zero auxiliary parameters and $\mathcal{N}_f$, $\mathcal{N}_\theta$ and $\mathcal{N}_\phi$ are the nonlinear operators given by

$$\begin{aligned}
\mathcal{N}_f \left[\hat{f}(\eta, q) \right] &= \frac{\partial^3 \hat{f}(\eta, q)}{\partial \eta^3} + \left(\frac{2n}{n+1} \right) \left[1 - \left(\frac{\partial \hat{f}(\eta, q)}{\partial \eta} \right)^2 \right] + \hat{f}(\eta, q) \frac{\partial^2 \hat{f}(\eta, q)}{\partial \eta^2} \\
&\quad + \alpha_1 \left[(3n-1) \frac{\partial \hat{f}(\eta, q)}{\partial \eta} \frac{\partial^3 \hat{f}(\eta, q)}{\partial \eta^3} + \left(\frac{3n-1}{2} \right) \left(\frac{\partial^2 \hat{f}(\eta, q)}{\partial \eta^2} \right)^2 \right. \\
&\quad \left. + (n-1)\eta \frac{\partial^2 \hat{f}(\eta, q)}{\partial \eta^2} \frac{\partial^3 \hat{f}(\eta, q)}{\partial \eta^3} - \left(\frac{n+1}{2} \right) \hat{f}(\eta, q) \frac{\partial^4 \hat{f}(\eta, q)}{\partial \eta^4} \right] \\
&\quad - (Ha)^2 \sin^2 \psi \left(\frac{\partial \hat{f}(\eta, q)}{\partial \eta} - 1 \right), \tag{4.22}
\end{aligned}$$

$$\begin{aligned}
\mathcal{N}_\theta \left[\hat{\theta}(\eta, q), \hat{f}(\eta, q), \hat{\phi}(\eta, q) \right] &= \frac{1}{\Pr} \frac{\partial^2 \hat{\theta}(\eta, q)}{\partial \eta^2} + \hat{f}(\eta, q) \frac{\partial \hat{\theta}(\eta, q)}{\partial \eta} + Nb \frac{\partial \hat{\theta}(\eta, q)}{\partial \eta} \frac{\partial \hat{\phi}(\eta, q)}{\partial \eta} \\
&\quad + Nt \left(\frac{\partial \hat{\theta}(\eta, q)}{\partial \eta} \right)^2 + \alpha \hat{\theta}(\eta, q), \tag{4.23}
\end{aligned}$$

$$\mathcal{N}_\phi[\hat{\phi}(\eta, q), \hat{f}(\eta, q), \hat{\theta}(\eta, q)] = \frac{1}{Sc} \frac{\partial^2 \hat{\phi}(\eta, q)}{\partial \eta^2} + \hat{f}(\eta, q) \frac{\partial \hat{\phi}(\eta, q)}{\partial \eta} + \frac{Nt}{Nb} \frac{\partial^2 \hat{\theta}(\eta, q)}{\partial \eta^2}. \tag{4.24}$$

The boundary conditions are

$$\hat{f}'(0, q) = A, \ \Pr \hat{f}(0, q) + M\hat{\theta}'(0, q) = 0, \ \hat{f}'(\infty, q) = 1,$$

$$\hat{\theta}(0, q) = 0, \ \hat{\theta}(\infty, q) = 1,$$

$$Nb\hat{\phi}'(0, q) + Nt\hat{\theta}'(0, q) = 0, \ \hat{\phi}(\infty, q) = 1. \tag{4.25}$$

4.2.2 mth−order deformation equations

The mth-order deformation equations can be written in the forms

$$\mathcal{L}_f \left[f_m(\eta) - \chi_m f_{m-1}(\eta) \right] = \hbar_f \mathcal{R}_f^m(\eta), \tag{4.26}$$

$$\mathcal{L}_\theta \left[\theta_m(\eta) - \chi_m \theta_{m-1}(\eta) \right] = \hbar_\theta \mathcal{R}_\theta^m(\eta), \tag{4.27}$$

$$\mathcal{L}_\phi \left[\phi_m(\eta) - \chi_m \phi_{m-1}(\eta) \right] = \hbar_\phi \mathcal{R}_\phi^m(\eta), \tag{4.28}$$

$$\mathcal{R}_f^m(\eta) = f'''_{m-1} + \left(\frac{2n}{n+1} \right) \left[1 - \sum_{k=0}^{m-1} f'_{m-1-k} f'_k \right] + \sum_{k=0}^{m-1} f_{m-1-k} f''_k + \alpha_1 \left[(3n-1) \sum_{k=0}^{m-1} f'_{m-1-k} f'''_k \right.$$

$$+ \left(\frac{3n-1}{2} \right) \sum_{k=0}^{m-1} f''_{m-1-k} f''_k + (n-1)\eta \sum_{k=0}^{m-1} f''_{m-1-k} f'''_k - \left(\frac{n+1}{2} \right) \sum_{k=0}^{m-1} f_{m-1-k} f_k^{iv} \Big]$$
$$- (Ha)^2 \sin^2 \psi \left(f'_{m-1} - 1 \right), \tag{4.29}$$

$$\mathcal{R}_\theta^m(\eta) = \frac{1}{\Pr} \theta''_{m-1} + \sum_{k=0}^{m-1} \left[\theta'_{m-1-l} f_l + Nb \phi'_{l-j} \theta'_j + Nt \theta'_{l-j} \theta'_j \right] + \alpha \theta_{m-1}, \tag{4.30}$$

$$\mathcal{R}_\phi^m(\eta) = \frac{1}{Sc} \phi''_{m-1} + \sum_{k=0}^{m-1} \phi'_{m-1-l} f_l + \frac{Nt}{Nb} \theta''_{m-1}, \tag{4.31}$$

with boundary conditions

$$f'_m(0) = \Pr f_m(0) + M\theta'_m(0) = f'_m(\infty) = \theta_m(0) = 0,$$
$$\theta_m(\infty) = Nb\phi'_m(0) + Nt\theta'_m(0) = \phi_m(\infty) = 0. \tag{4.32}$$

The general solutions (f_m, θ_m, ϕ_m) comprising the special solutions $(f_m^*, \theta_m^*, \phi_m^*)$ are given by

$$f_m(\eta) = f_m^*(\eta) + C_{11} + C_{12} e^\eta + C_{13} e^{-\eta},$$

$$\theta_m(\eta) = \theta_m^*(\eta) + C_{14} e^\eta + C_{15} e^{-\eta},$$

$$\phi_m(\eta) = \phi_m^*(\eta) + C_{16} e^\eta + C_{17} e^{-\eta}, \tag{4.33}$$

where the constants C_i $(i = 11, 12, ..., 17)$ through the boundary conditions (4.32) have the values

$$C_{12} = C_{14} = C_{16} = 0, \ C_{11} = -C_{13} - f_m^*(0) - \frac{M}{\Pr} \left(\theta_m^*(0) + \frac{\partial \theta_m^*(\eta)}{\partial \eta} \Big|_{\eta=0} \right),$$
$$C_{15} = -\theta_m^*(0), \ C_{17} = \frac{\partial \phi_m^*(\eta)}{\partial \eta} \Big|_{\eta=0} + \frac{Nt}{Nb} \left(\theta_m^*(0) + \frac{\partial \theta_m^*(\eta)}{\partial \eta} \Big|_{\eta=0} \right). \tag{4.34}$$

4.3 Convergence of the homotopy solutions

A homotopy analysis technique provides us great freedom and an easy way to adjust and control the convergence region of the series solutions. The auxiliary parameters $\hbar_f$, $\hbar_\theta$ and $\hbar_\phi$ play an important role for the convergence of the series solutions. Therefore we have sketched the $\hbar$−curves at 10th−order of approximations (see Fig. 4.1(a, b)). The admissible ranges of the auxiliary parameters are $-1.5 \leq \hbar_f \leq -0.6$, $-1.35 \leq \hbar_\theta \leq -0.65$ and $-1.2 \leq \hbar_\phi \leq -0.65$. Table 4.1 shows the convergence of series solutions of momentum, temperature and concentration equations. It is noted that 15th order of approximation is sufficient for the convergence of $f''(0)$ and 30th order of approximations are enough for the convergence of $\theta'(0)$ and $\phi'(0)$.

4.4 Results and discussion

Influence of various involved parameters on the velocity, temperature and concentration profiles is sketched in this section (see Figs. $(4.2 - 4.14)$).

4.4.1 Dimensionless velocity profile

Effect of wedge parameter n on the velocity profile $f'(\eta)$ is analyzed in Fig. 4.2. There is an increase in velocity when n is increased. In Fig. 4.3, the velocity profile is plotted for different values of angle of inclination ψ. An increase in the angle of inclination α leads to a decrease in the velocity and momentum boundary layer thickness. It is also noted that for $\psi = 0$ the magnetic field has no effect on the velocity profile. Fig. 4.4 illustrates the variation of second grade fluid parameter α_1 on the velocity profile $f'(\eta)$. It is observed that the velocity profile $f'(\eta)$ and boundary layer thickness are increasing functions of α_1. Behavior of Hartman number Ha on velocity profile $f'(\eta)$ is displayed in Fig. 4.5. The applied magnetic field has the tendency to slow down the movement of the fluid which decreases the velocity profile.

4.4.2 Dimensionless temperature profile

Effect of thermophoresis parameter Nt on the temperature profile $\theta(\eta)$ is depicted in Fig. 4.6. Substantial increase in temperature is observed by increasing thermophoresis parameter Nt. Significant rise in fluid temperature is observed when Brownian motion parameter Nb is enhanced (see Fig. 4.7). Fig. 4.8 displays the influence of Prandtl number Pr on the temperature $\theta(\eta)$. Here the temperature profile increases in the presence of melting parameter by increasing Pr but thermal boundary layer thickness decreases. In fact with an increase of Pr, heat is transferred towards the plate during the melting process and consequently the temperature profile increases. It can be seen from Fig. 4.9 that the heat generation and absorption parameter α has opposite effect on the temperature field $\theta(\eta)$. It is observed that temperature distribution is increasing function of heat generation parameter while it is decreasing function of heat absorption parameter. Because heat generation process produces more heat so temperature profile enhances. Temperature field increases for larger values of angle of inclination ψ (see Fig. 4.10). Since increasing values of angle ψ corresponds to stronger magnetic field which opposes the fluid motion. Hence temperature profile increases. Fig. 4.11 shows the variations of melting parameter M on temperature profile. It is noted that temperature profile decreases for larger values of melting parameter due to the fact that temperature difference increases between ambient and melting surface which reduces the temperature of the fluid. Further the thermal boundary layer thickness increases when melting parameter is increased.

4.4.3 Dimensionless concentration profile

Concentration profiles $\phi(\eta)$ for different values of thermophoresis parameter Nt, Brownian motion parameter Nb and Schmidt number Sc are plotted in the Figs. (4.12-4.14). Effect of thermophoresis parameter Nt on the concentration profile is shown in Fig. 4.12. There is a decrease in concentration

when Nt is increased. Fig. 4.13 elucidates the variations in the concentration field ϕ for increasing values of Brownian motion parameter Nb. Here concentration profile increases with an increase in Nb. Effect of Schmidt number Sc on concentration profile is shown in Fig. 4.14. Decreasing behavior of concentration profile is noted for larger Schmidt number. In fact Schmidt number is the ratio of momentum diffusivity to mass diffusivity. Hence higher values of Schmidt number correspond to small mass diffusivity and the concentration profile decreases.

4.4.4 Local skin friction coefficient and Nusselt number

In Table 4.2 some numerical values of local skin friction coefficient and Nusselt number are given. Tabular values show that skin friction coefficient decreases by increasing n, Nt and Nb while it increases for larger values of α_1, Ha, ψ and M. It is also noted that Nusselt number decreases by increasing n, α_1, M and Nb and it increases for larger values of Ha, ψ and Nt. Table 4.3 represents the comparison of present study with Kuo [36] and White [37] when $n = \alpha_1 = Ha = \psi = 0$. It is worth mentioning that the comparison is in good agreement.
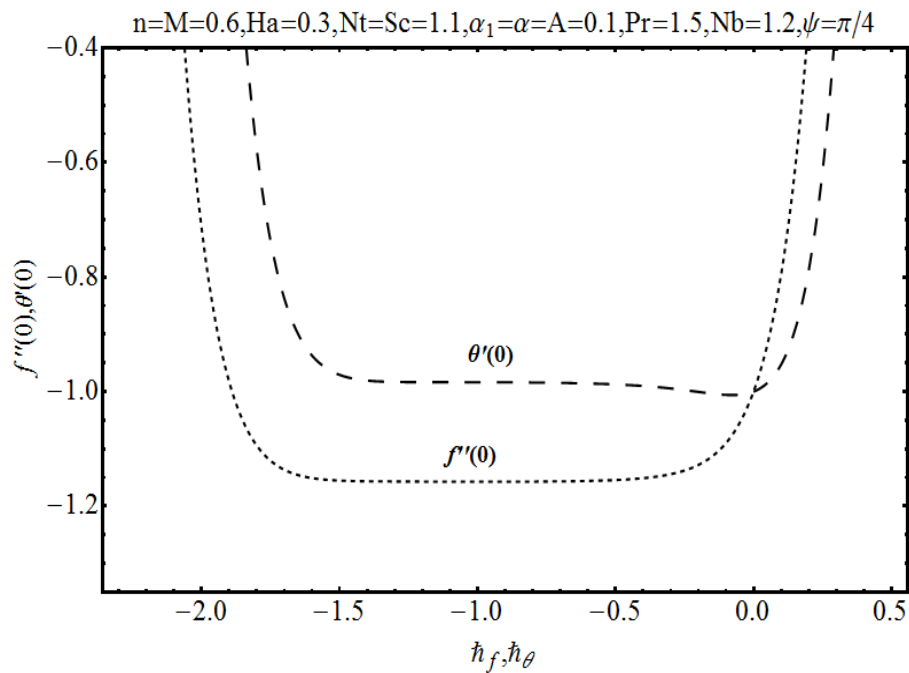
Fig. 4.1(a): $\hbar$−curves for $f''(0)$ and $\theta'(0)$.
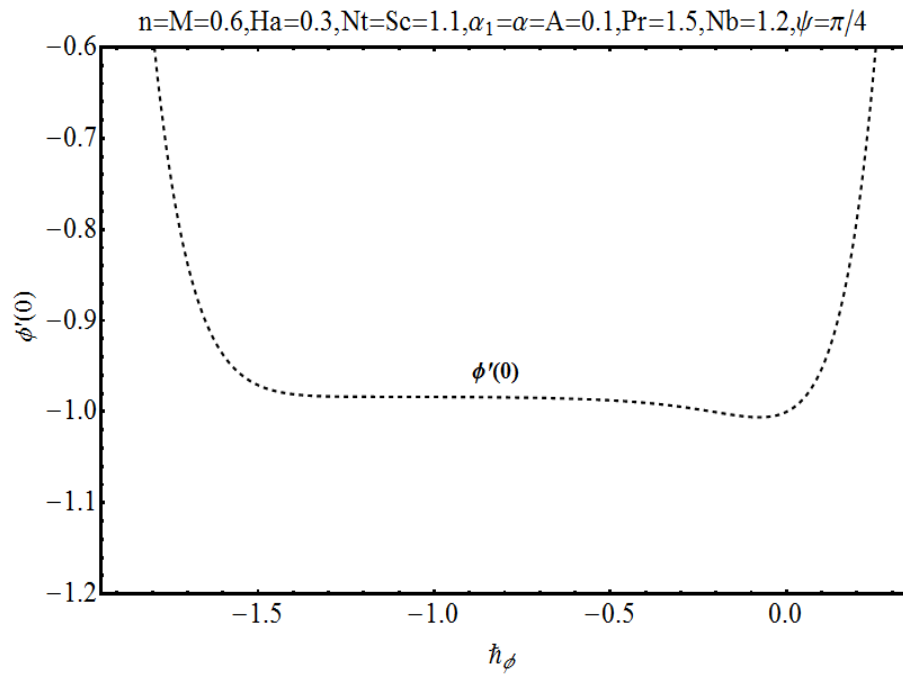
Fig. 4.1(b): $\hbar-$curve for $\phi'(0)$.
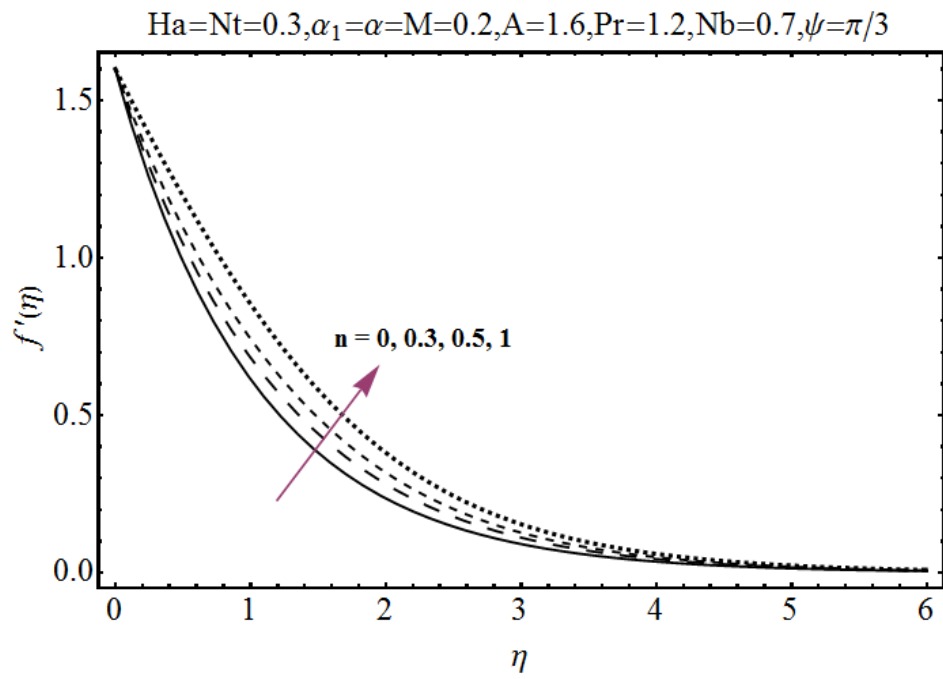
Fig. 4.2: Effect of n on $f'(\eta)$.
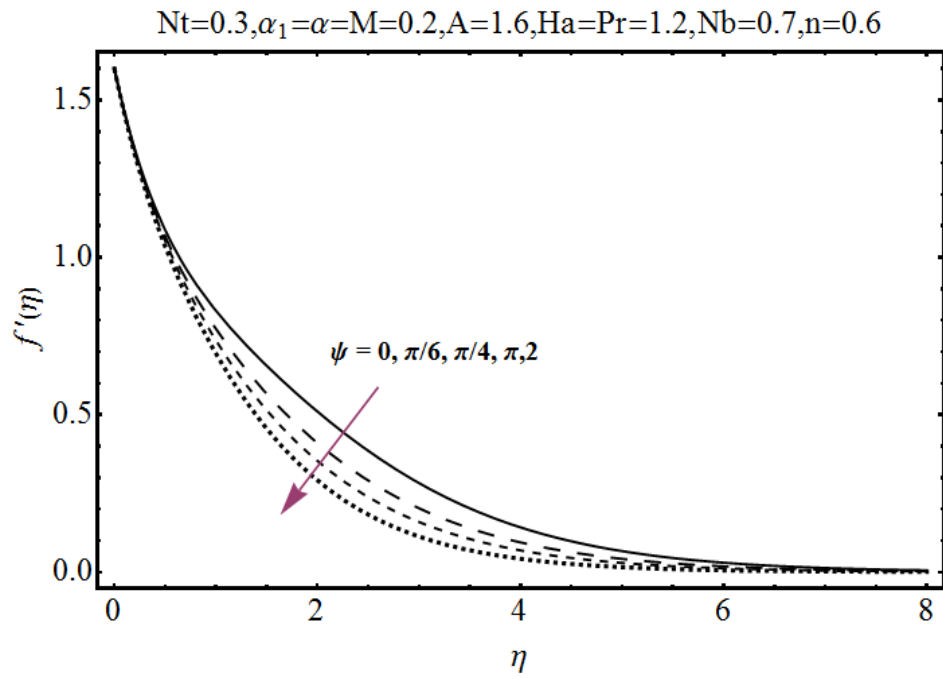
Fig. 4.3: Effect of ψ on $f'(\eta)$.
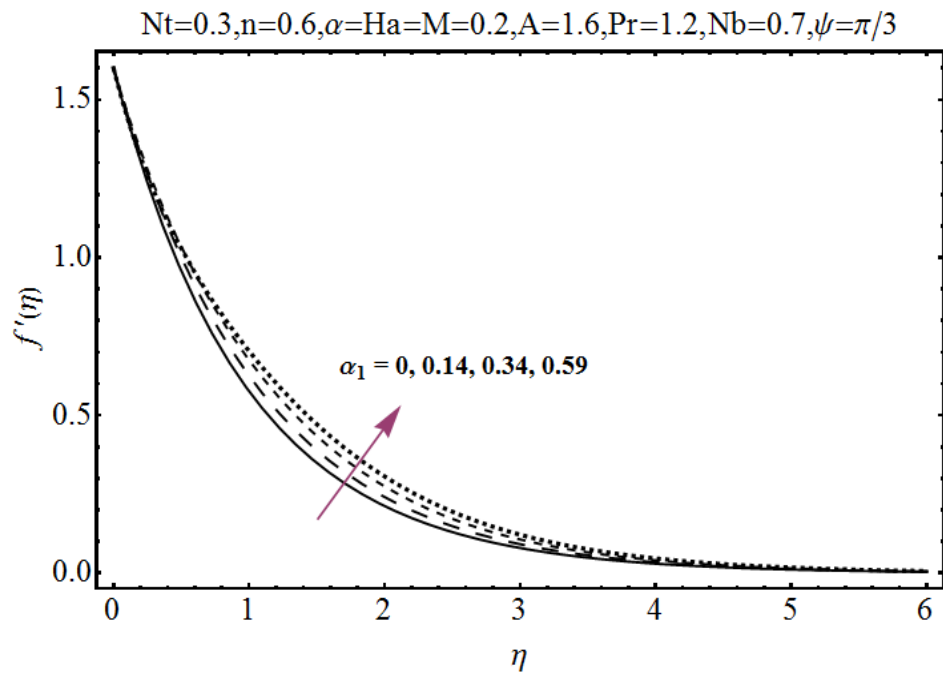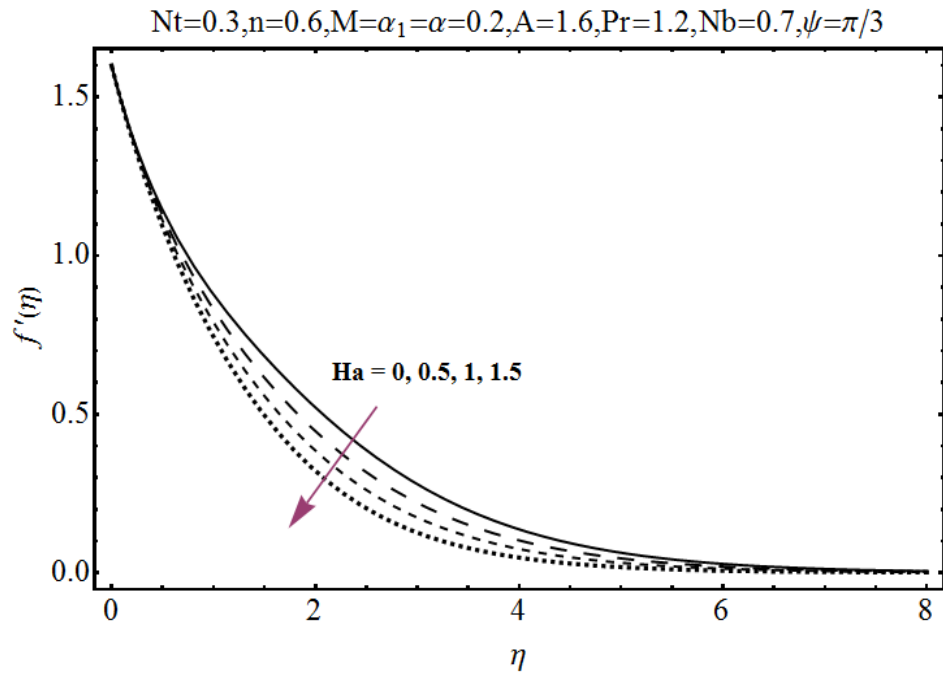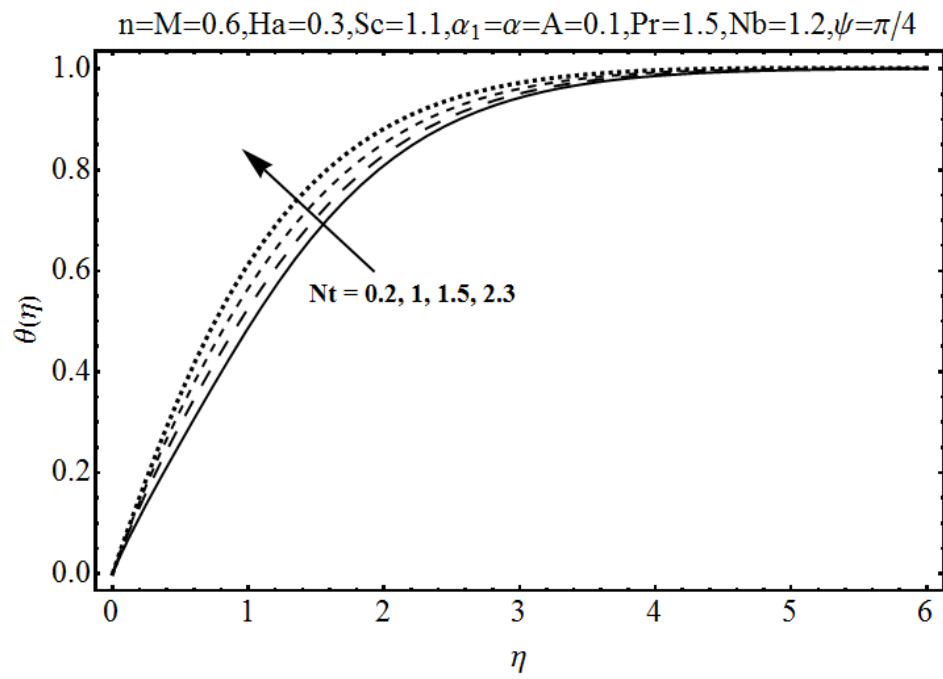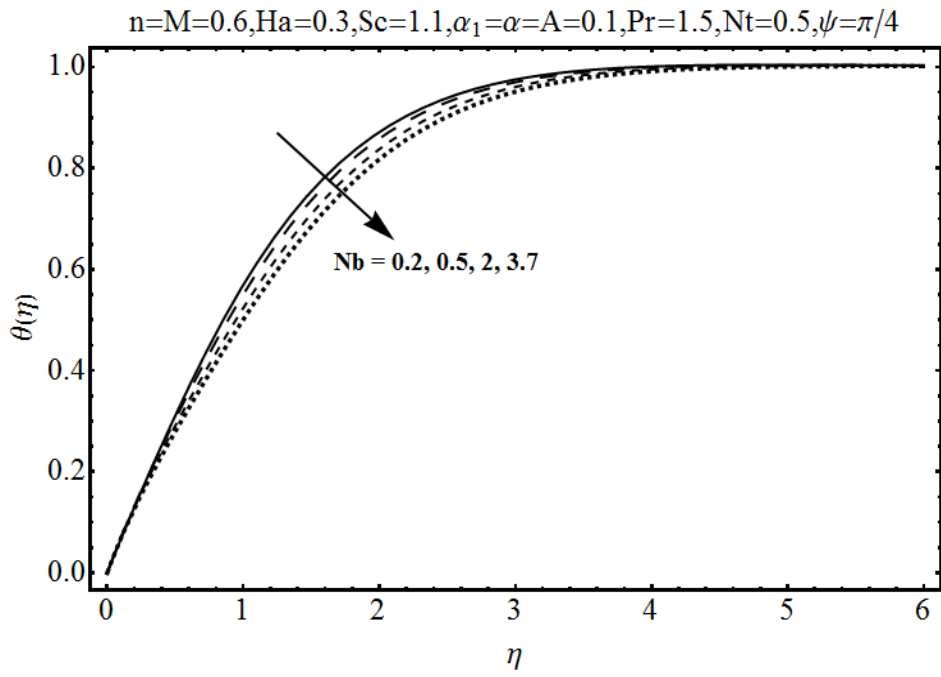
Plot title: Nt=0.3,α_1=α=M=0.2,A=1.6,Ha=Pr=1.2,Nb=0.7,n=0.6

$\psi = 0, \pi/6, \pi/4, \pi, 2$

Fig. 4.4: Effect of α_1 on $f'(\eta)$.

Plot title: Nt=0.3,n=0.6,α=Ha=M=0.2,A=1.6,Pr=1.2,Nb=0.7,ψ=$\pi/3$

$\alpha_1 = 0, 0.14, 0.34, 0.59$

Nt=0.3,n=0.6,M=α_1=α=0.2,A=1.6,Pr=1.2,Nb=0.7,ψ=$\pi/3$

Ha = 0, 0.5, 1, 1.5

Fig. 4.5: Effect of Ha on $f'(\eta)$.

n=M=0.6,Ha=0.3,Sc=1.1,α_1=α=A=0.1,Pr=1.5,Nb=1.2,ψ=$\pi/4$

Nt = 0.2, 1, 1.5, 2.3

Fig. 4.6: Effect of Nt on $\theta(\eta)$.

n=M=0.6,Ha=0.3,Sc=1.1,$\alpha_1=\alpha=A=0.1$,Pr=1.5,Nt=0.5,$\psi=\pi/4$

Nb = 0.2, 0.5, 2, 3.7

Fig. 4.7: Effect of Nb on $\theta(\eta)$.

n=M=Nt=0.6,Ha=0.3,Sc=1.1,$\alpha_1=\alpha=A=0.1$,Nb=1.2,$\psi=\pi/4$

Pr = 0.1, 0.5, 1, 1.5

Fig. 4.8: Effect of Pr on $\theta(\eta)$.

n=M=Nt=0.6,Ha=0.3,Sc=1.1,α_1=A=0.1,Pr=1.5,Nb=1.2,ψ=π/4

α = -0.24, -0.16, 0, 0.15, 0.25, 0.35

Fig. 4.9: Effect of α on $\theta(\eta)$.

n=M=Nt=0.6,Ha=0.3,Sc=1.1,α_1=α=A=0.1,Pr=1.5,Nb=1.2

ψ = 0, π/6, π/4, π/2

Fig. 4.10: Effect of ψ on $\theta(\eta)$.

n=M=Nt=0.6,Ha=0.3,Sc=1.1,$\alpha_1=\alpha=A=0.1$,Pr=1.5,Nb=1.2,$\psi=\pi/4$

Fig. 4.11: Effect of M on $\theta(\eta)$.

n=0.6,Ha=0.3,Sc=1.1,$\alpha_1=\alpha=A=0.1$,Pr=Nb=1.2,M=0.2,$\psi=\pi/4$
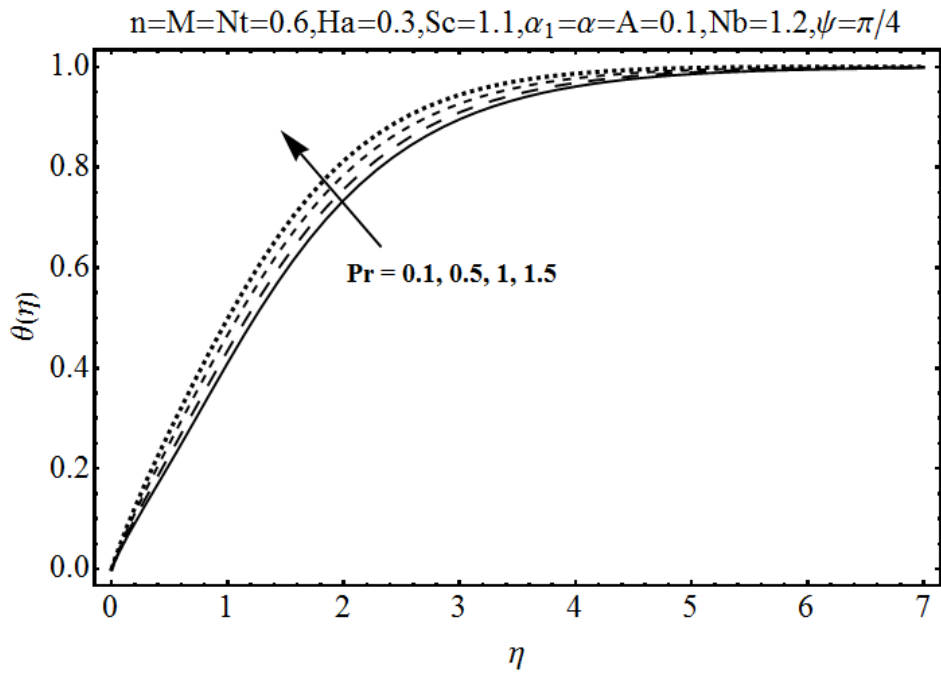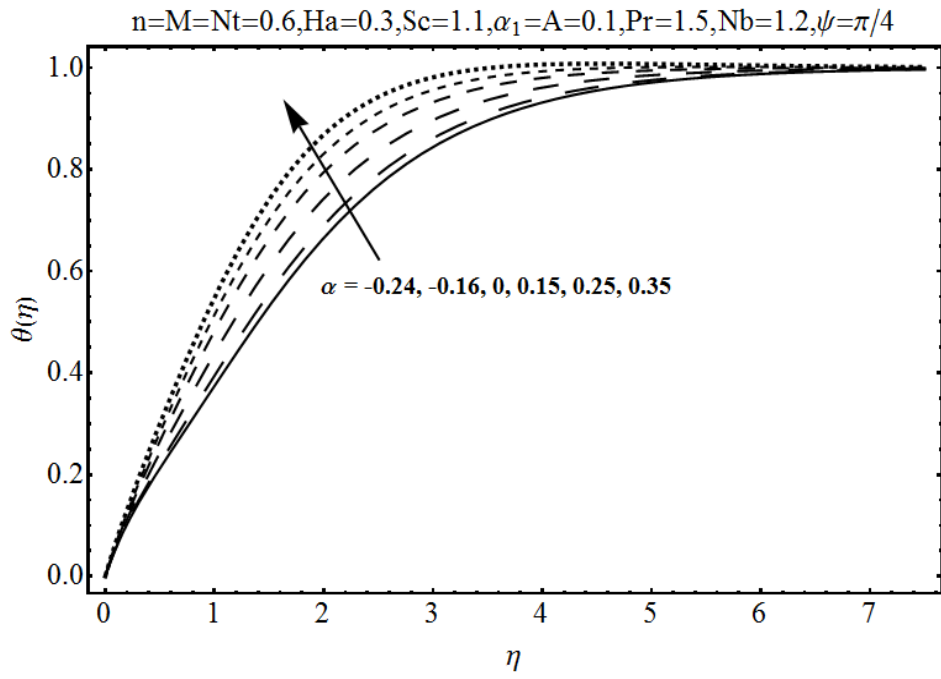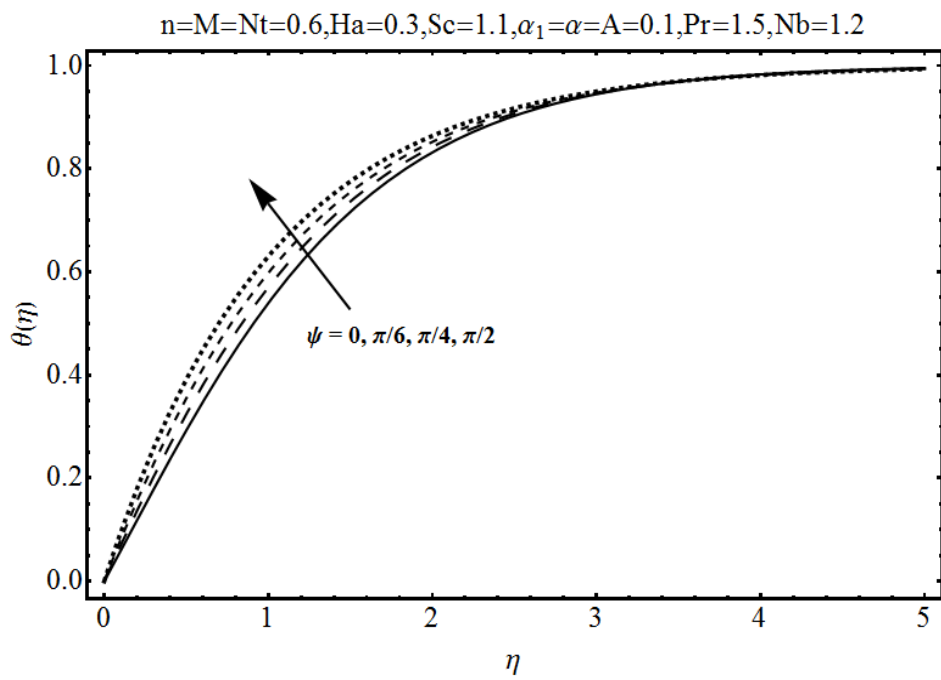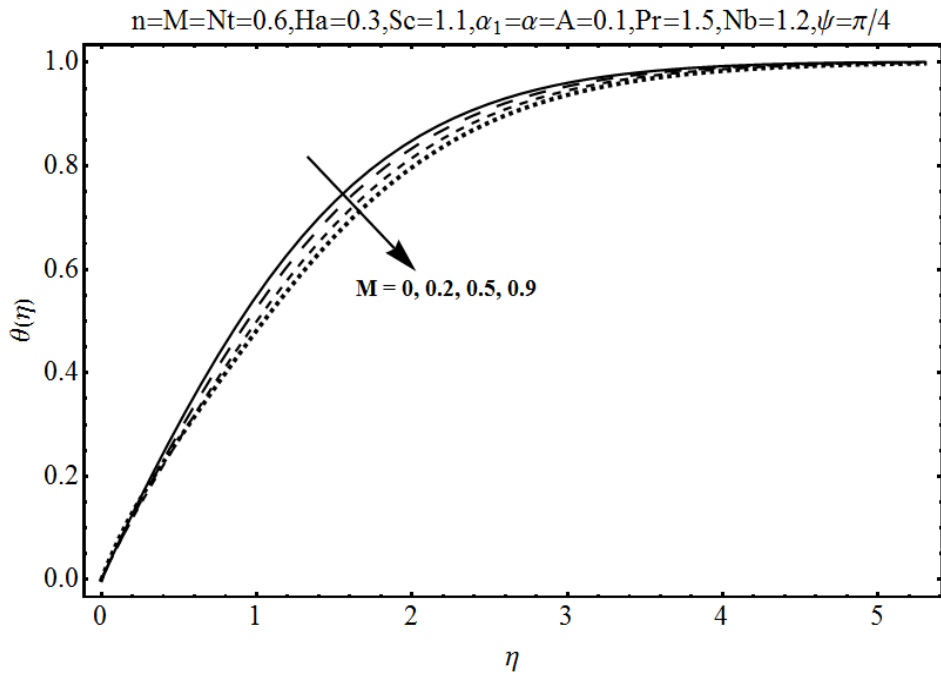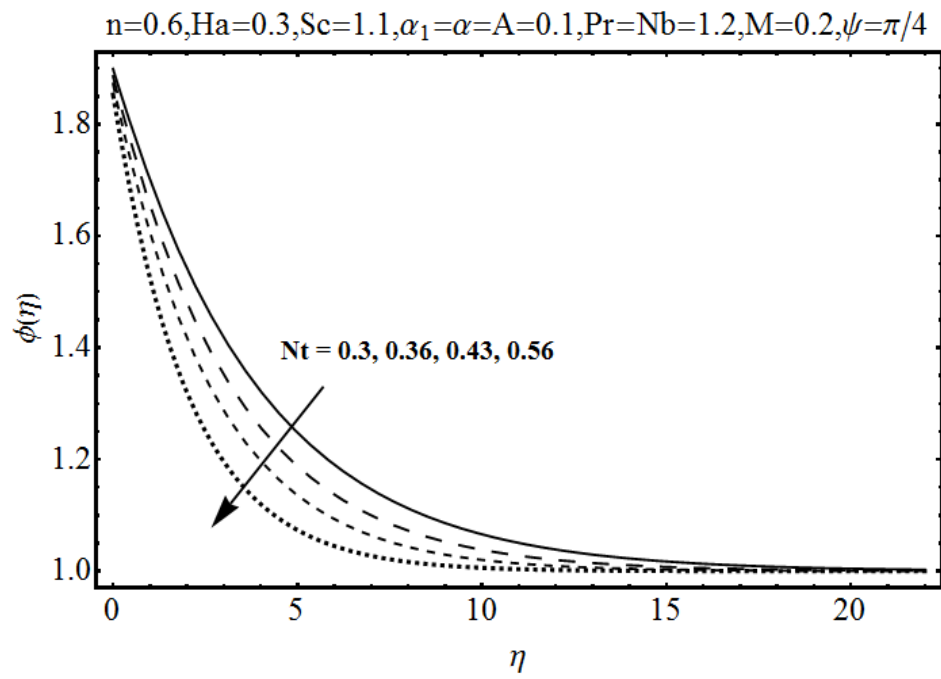
Fig. 4.12: Effect of Nt on $\phi(\eta)$.
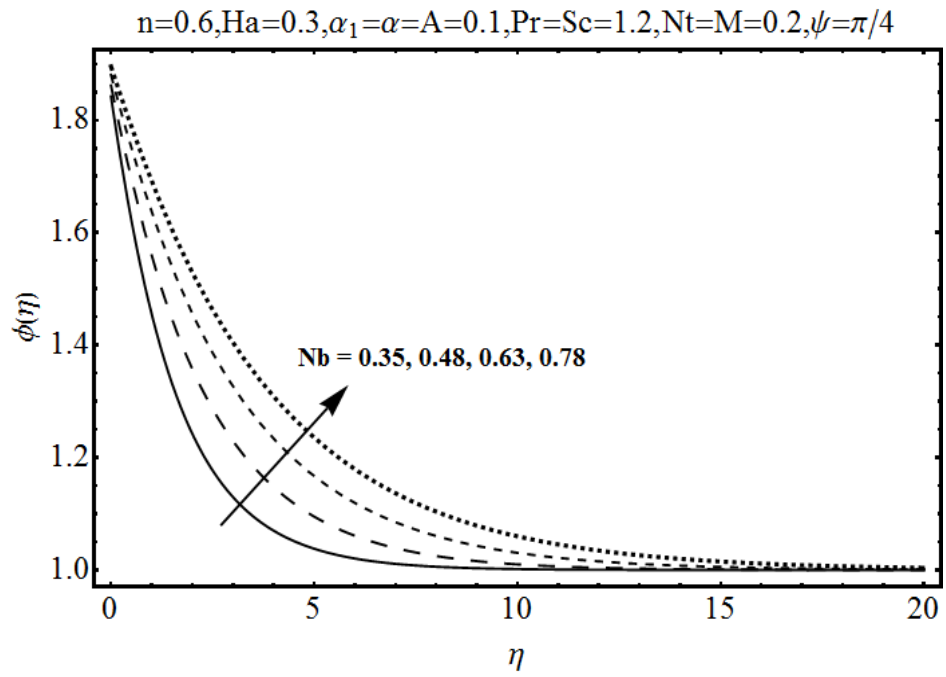
Fig. 4.13: Effect of Nb on $\phi(\eta)$.
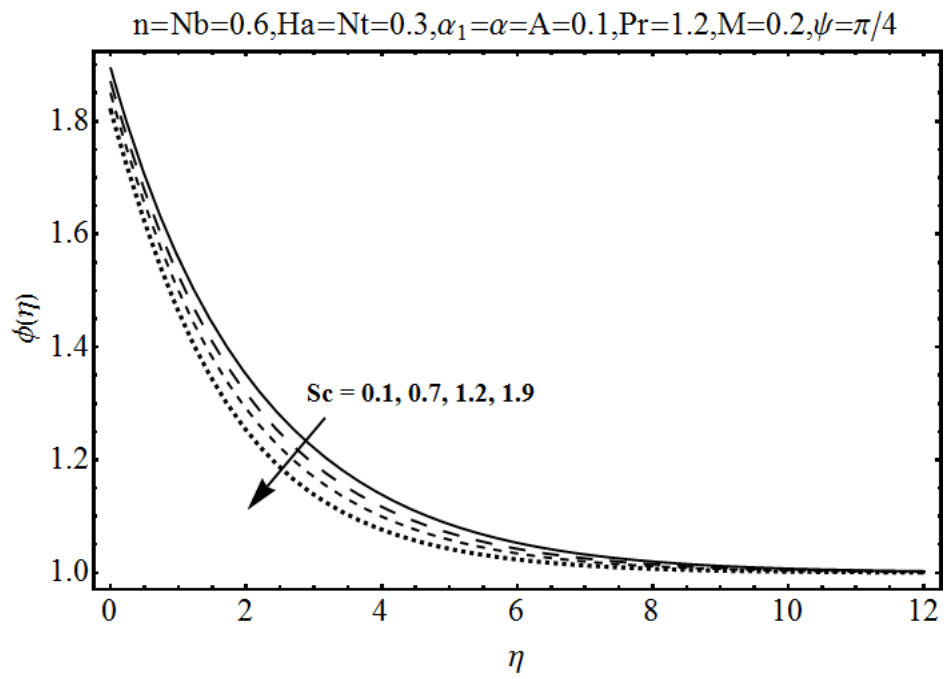
Fig. 4.14: Effect of Sc on $\phi(\eta)$.

Table 4.1: Convergence of HAM solutions for different order of approximations when $n = 0.6$, $Ha = 0.3$, $M = \alpha = 0.2$, $\psi = \pi/4$, $\alpha_1 = Nt = 0.1$, $Nb = 0.5$ and $\Pr = Sc = 1.2$.

Order of approximation	$-f''(0)$	$\theta'(0)$	$-\phi'(0)$
1	0.7938	0.9655	0.1931
5	0.7222	0.8641	0.1728
10	0.7182	0.7851	0.1570
15	0.7188	0.7375	0.1475
30	0.7188	0.7085	0.1417
35	0.7188	0.7085	0.1417
50	0.7188	0.7085	0.1417

Table 4.2: Numerical values of local skin friction coefficient and Nusselt number when $A = \alpha = 0.1$, $\Pr = 1.2$ and $Sc = 1.3$.

n	α_1	Ha	ψ	M	Nt	Nb	$(\mathrm{Re}_x)^{1/2} C_f$	$-\mathrm{Re}_x^{-1/2} Nu_x$
0.0	0.1	0.5	$\pi/3$	0.3	0.1	0.5	0.3870	0.5799
0.1							0.3158	0.5127
0.2							0.2853	0.4853
0.2	0.0	0.5	$\pi/3$	0.3	0.1	0.5	0.2825	0.5239
	0.1						0.2853	0.4853
	0.2						0.2863	0.4709
0.2	0.1	0.4	$\pi/3$	0.3	0.1	0.5	0.2112	0.4617
		0.5					0.2853	0.4853
		0.6					0.3636	0.5065
0.2	0.1	0.5	$\pi/5$	0.3	0.1	0.5	0.1595	0.4662
			$\pi/3$				0.2853	0.4853
			$\pi/2$				0.3452	0.5238
0.2	0.1	0.5	$\pi/3$	0.3	0.1	0.5	0.2853	0.4853
				0.4			0.2871	0.4632
				0.5			0.2909	0.4450
0.2	0.1	0.5	$\pi/3$	0.3	0.1	0.5	0.2853	0.4853
					0.3		0.2830	0.5598
					0.5		0.2801	0.5737
0.2	0.1	0.5	$\pi/3$	0.3	0.1	0.3	0.2874	0.5231
						0.4	0.2867	0.5038
						0.5	0.2853	0.4853

Table 4.3: Comparison of $f(\eta)$ and $f'(\eta)$ with the numerical solutions by Kuo [36] and White [37] when $n = \alpha_1 = Ha = \psi = 0$.

η	$f(\eta)$			$f'(\eta)$		
	Present	Kuo [36]	White [37]	Present	Kuo [36]	White [37]
0.0	0.000000	0.000000	0.000000	0.000000	0.000000	0.000000
0.1	0.002346	0.002348	0.00235	0.046956	0.046959	0.04696
0.2	0.009390	0.009391	0.00939	0.093906	0.093905	0.09391
0.3	0.021127	0.021128	0.02113	0.140807	0.140806	0.14081
0.4	0.037547	0.037549	0.03755	0.187606	0.187605	0.18761
0.5	0.058641	0.058643	0.05864	0.234227	0.234228	0.23423
0.6	0.084384	0.084386	0.08439	0.280578	0.280575	0.28058
0.7	0.114749	0.114745	0.11474	0.326534	0.326532	0.32653
0.8	0.149676	0.149674	0.14967	0.371965	0.371963	0.37196
0.9	0.189113	0.189115	0.18911	0.416716	0.416718	0.41672
1.0	0.232994	0.232990	0.23299	0.460632	0.460633	0.46063
1.1	0.281205	0.281208	0.28121	0.503536	0.503535	0.50354
1.2	0.333654	0.333657	0.33366	0.545248	0.545246	0.54525
1.3	0.390213	0.390211	0.39021	0.585587	0.585589	0.58559
1.4	0.450726	0.450724	0.45072	0.624385	0.624386	0.62439
1.5	0.515032	0.515031	0.51503	0.661472	0.661474	0.66147
2.0	0.886795	0.886797	0.88680	0.816696	0.816695	0.81669
2.2	1.054943	1.054947	1.05495	0.863302	0.863304	0.86330
2.6	1.414826	1.414824	1.41482	0.930602	0.930601	0.93060
3.0	1.795565	1.795568	1.79557	0.969053	0.969055	0.96905

4.5   Concluding remarks

Characteristics of melting heat transfer in Falkner-Skan wedge flow of second grade nanofluid is studied. Effects of heat generation/absorption are also taken into account. The key points are summarized as follows:

- Fluid flow enhances with the increase of wedge and second grade fluid parameters.

- Angle of inclination has opposite effect on the velocity and temperature.

- Increasing values of Prandtl number correspond to high temperature.

- Thermophoresis and Brownian motion parameters have reverse behavior on the temperature and concentration fields.

- Increasing values of Schmidt number decrease the concentration field.

- Wall shear stress and heat transfer rate increase by increasing Hartman number and angle of inclination.

- Present analysis is in good agreement with previous published results in limiting sense.

Chapter 5

MHD axisymmetric flow of third grade fluid between stretching sheets with heat transfer

This chapter looks at the heat transfer effects in magnetohydrodynamic (MHD) axisymmetric flow of third-grade fluid between the stretching sheets. Viscous and Joule heating effects are given due attention. The resulting nonlinear problem is computed for velocity and temperature fields. Expressions of skin friction coefficient and local Nusselt number are calculated. Dimensionless results of velocity and temperature fields are examined for various parameters of interest. Numerical values of skin friction coefficient and Nusselt number are obtained and analyzed.

5.1   Mathematical formulation

Let us consider the heat transfer characteristics in the flow of an electrically conducting third grade fluid between the radial stretching sheets. Constant magnetic field of strength $\mathbf{B}_0$ is applied perpendicular to planes of sheet (i.e. along z-direction). There is no external electric field and induced magnetic field is neglected under the assumption of small magnetic Reynolds number. Both sheets are maintained at constant temperature T_w. In addition Joule heating and viscous dissipation are present. Conservation laws of mass, momentum and energy equations are given below:

$$\frac{\partial u}{\partial r} + \frac{u}{r} + \frac{\partial w}{\partial z} = 0, \tag{5.1}$$

$$
\begin{aligned}
\rho\left(u\frac{\partial u}{\partial r} + w\frac{\partial u}{\partial z}\right) =\ & -\frac{\partial p}{\partial r} + \mu\left(\frac{\partial^2 u}{\partial r^2} + \frac{\partial^2 u}{\partial z^2} + \frac{1}{r}\frac{\partial u}{\partial r} - \frac{u}{r^2}\right) \\
& + \alpha_1^*\left[-\frac{2u^2}{r^3} - 2\frac{w}{r^2}\frac{\partial u}{\partial z} + \frac{4}{r}\left(\frac{\partial u}{\partial r}\right)^2 + \frac{\partial u}{\partial z}\frac{\partial^2 w}{\partial z^2} + w\frac{\partial^3 u}{\partial z^3} - 2\frac{u}{r^2}\frac{\partial u}{\partial r}\right. \\
& \left. + 3\frac{\partial u}{\partial r}\frac{\partial^2 u}{\partial z^2} + 3\frac{\partial w}{\partial r}\frac{\partial^2 w}{\partial z^2} + \frac{2}{r}\left(\frac{\partial w}{\partial r}\right)^2 + \frac{2w}{r}\frac{\partial^2 u}{\partial r\partial z} + 5\frac{\partial w}{\partial r}\frac{\partial^2 u}{\partial r\partial z}\right.
\end{aligned}
$$

$$+4\frac{\partial w}{\partial z}\frac{\partial^2 w}{\partial r\partial z}+\frac{\partial u}{\partial r}\frac{\partial^2 w}{\partial r\partial z}+u\frac{\partial^3 u}{\partial r\partial z^2}+w\frac{\partial^3 w}{\partial r\partial z^2}+\frac{2u}{r}\frac{\partial^2 u}{\partial r^2}$$

$$+10\frac{\partial u}{\partial r}\frac{\partial^2 u}{\partial r^2}+3\frac{\partial u}{\partial z}\frac{\partial^2 w}{\partial r^2}+4\frac{\partial w}{\partial r}\frac{\partial^2 w}{\partial r^2}+2w\frac{\partial^3 u}{\partial r^2\partial z}+u\frac{\partial^3 w}{\partial r^2\partial z}+2u\frac{\partial^3 u}{\partial r^3}$$

$$+\frac{2}{r}\frac{\partial u}{\partial z}\frac{\partial w}{\partial r}+2\frac{\partial w}{\partial z}\frac{\partial^2 u}{\partial z^2}+4\frac{\partial u}{\partial z}\frac{\partial^2 u}{\partial r\partial z}\Big]+\alpha_2^*\left[-\frac{4u^2}{r^3}+\frac{4}{r}\left(\frac{\partial u}{\partial r}\right)^2+2\frac{\partial u}{\partial z}\frac{\partial^2 w}{\partial z^2}\right.$$

$$+2\frac{\partial u}{\partial r}\frac{\partial^2 u}{\partial z^2}+2\frac{\partial w}{\partial r}\frac{\partial^2 w}{\partial z^2}+4\frac{\partial w}{\partial r}\frac{\partial^2 u}{\partial r\partial z}+\frac{1}{r}\left(\frac{\partial w}{\partial r}\right)^2+\frac{1}{r}\left(\frac{\partial u}{\partial z}\right)^2+2\frac{\partial u}{\partial r}\frac{\partial^2 w}{\partial r\partial z}$$

$$+2\frac{\partial w}{\partial z}+2\frac{\partial u}{\partial z}\frac{\partial^2 u}{\partial r\partial z}+8\frac{\partial u}{\partial r}\frac{\partial^2 u}{\partial r^2}+2\frac{\partial u}{\partial z}\frac{\partial^2 w}{\partial r^2}+2\frac{\partial w}{\partial r}\frac{\partial^2 w}{\partial r^2}$$

$$+\frac{2}{r}\frac{\partial u}{\partial z}\frac{\partial w}{\partial r}+2\frac{\partial w}{\partial z}\frac{\partial^2 u}{\partial z^2}+4\frac{\partial u}{\partial z}\frac{\partial^2 u}{\partial r\partial z}\Big]+\beta_3\left[-\frac{8u^3}{r^4}+\frac{8}{r}\left(\frac{\partial u}{\partial r}\right)^3-\frac{8u^2}{r^3}\frac{\partial u}{\partial r}\right.$$

$$+\frac{8}{r}\frac{\partial u}{\partial r}\left(\frac{\partial w}{\partial z}\right)^2+\frac{4}{r}\frac{\partial u}{\partial r}\left(\frac{\partial u}{\partial z}\right)^2+\frac{4}{r}\frac{\partial u}{\partial r}\left(\frac{\partial w}{\partial r}\right)^2+\frac{8}{r}\frac{\partial u}{\partial r}\frac{\partial u}{\partial z}\frac{\partial w}{\partial r}$$

$$+24\left(\frac{\partial u}{\partial r}\right)^2\frac{\partial^2 u}{\partial r^2}+\frac{8u^2}{r^2}\frac{\partial^2 u}{\partial r^2}+\frac{16u}{r^2}\frac{\partial u}{\partial r}+8\left(\frac{\partial w}{\partial z}\right)^2\frac{\partial^2 u}{\partial r^2}+16\frac{\partial u}{\partial r}\frac{\partial w}{\partial z}\frac{\partial^2 w}{\partial r\partial z}$$

$$+4\frac{\partial u}{\partial z}\frac{\partial^2 u}{\partial r^2}+4\frac{\partial w}{\partial r}\frac{\partial^2 u}{\partial r^2}+16\frac{\partial u}{\partial r}\frac{\partial u}{\partial z}\frac{\partial^2 u}{\partial r\partial z}+8\frac{\partial u}{\partial r}\frac{\partial u}{\partial z}\frac{\partial^2 w}{\partial r^2}$$

$$+16\frac{\partial u}{\partial r}\frac{\partial w}{\partial r}\frac{\partial^2 u}{\partial r\partial z}+8\frac{\partial u}{\partial r}\frac{\partial w}{\partial r}\frac{\partial^2 w}{\partial r^2}+4\left(\frac{\partial u}{\partial r}\right)^2\frac{\partial^2 u}{\partial z^2}+4\left(\frac{\partial u}{\partial r}\right)^2\frac{\partial^2 w}{\partial r\partial z}+\frac{4u^2}{r^2}\frac{\partial^2 u}{\partial z^2}$$

$$+\frac{4u^2}{r^2}\frac{\partial^2 w}{\partial r\partial z}+\frac{4u}{r^2}\left(\frac{\partial u}{\partial z}\right)^2+8\frac{\partial u}{\partial z}\frac{\partial w}{\partial z}\frac{\partial^2 w}{\partial z^2}+8\frac{\partial w}{\partial r}\frac{\partial w}{\partial z}\frac{\partial^2 w}{\partial z^2}+4\left(\frac{\partial w}{\partial z}\right)^2\frac{\partial^2 u}{\partial z^2}$$

$$+4\left(\frac{\partial w}{\partial z}\right)^2\frac{\partial^2 w}{\partial r\partial z}+6\left(\frac{\partial u}{\partial z}\right)^2\frac{\partial^2 u}{\partial z^2}+6\left(\frac{\partial w}{\partial r}\right)^2\frac{\partial^2 u}{\partial z^2}+12\frac{\partial u}{\partial z}\frac{\partial w}{\partial r}\frac{\partial^2 w}{\partial r\partial z}$$

$$+12\frac{\partial u}{\partial z}\frac{\partial w}{\partial r}\frac{\partial^2 u}{\partial z^2}-\frac{8u}{r^2}\left(\frac{\partial u}{\partial r}\right)^2-\frac{8u}{r^2}\left(\frac{\partial w}{\partial z}\right)^2-\frac{4u}{r^2}\left(\frac{\partial w}{\partial r}\right)^2$$

$$+6\left(\frac{\partial u}{\partial z}\right)^2\frac{\partial^2 w}{\partial r\partial z}+6\left(\frac{\partial w}{\partial r}\right)^2\frac{\partial^2 w}{\partial r\partial z}\Big]-\sigma B_0^2 u, \tag{5.2}$$

$$\rho\left(u\frac{\partial w}{\partial r}+w\frac{\partial w}{\partial z}\right)=-\frac{\partial p}{\partial z}+\mu\left[\frac{1}{r}\frac{\partial w}{\partial r}+\frac{\partial^2 w}{\partial r^2}+\frac{\partial^2 w}{\partial z^2}\right]$$

$$+\alpha_1^*\left[\frac{u}{r}\frac{\partial^2 w}{\partial r^2}+\frac{w}{r}\frac{\partial^2 u}{\partial z^2}+\frac{u}{r}\frac{\partial^2 u}{\partial r\partial z}+\frac{w}{r}\frac{\partial^2 w}{\partial r\partial z}+\frac{3}{r}\frac{\partial u}{\partial r}\frac{\partial u}{\partial z}\right.$$

$$+\frac{3}{r}\frac{\partial w}{\partial r}\frac{\partial w}{\partial z}+\frac{1}{r}\frac{\partial u}{\partial z}\frac{\partial w}{\partial z}+\frac{1}{r}\frac{\partial u}{\partial r}\frac{\partial w}{\partial r}+2\frac{\partial u}{\partial r}\frac{\partial^2 w}{\partial r^2}+u\frac{\partial^3 w}{\partial r^3}$$

$$+3\frac{\partial w}{\partial r}\frac{\partial^2 u}{\partial z^2}+w\frac{\partial^3 u}{\partial r\partial z^2}+4\frac{\partial u}{\partial r}\frac{\partial^2 u}{\partial r\partial z}+u\frac{\partial^3 u}{\partial r^2\partial z}+4\frac{\partial w}{\partial r}\frac{\partial^2 w}{\partial r\partial z}$$

$$+w\frac{\partial^3 w}{\partial r^2\partial z}+3\frac{\partial u}{\partial z}\frac{\partial^2 u}{\partial r^2}+3\frac{\partial w}{\partial z}\frac{\partial^2 w}{\partial r^2}+5\frac{\partial u}{\partial z}\frac{\partial^2 w}{\partial r\partial z}+\frac{\partial w}{\partial z}\frac{\partial^2 u}{\partial r\partial z}$$

$$+\frac{\partial w}{\partial r}\frac{\partial^2 u}{\partial r^2}+2u\frac{\partial^3 w}{\partial r\partial z^2}+2\frac{\partial w}{\partial z}\frac{\partial^2 w}{\partial z^2}+2w\frac{\partial^3 w}{\partial z^3}+8\frac{\partial w}{\partial z}\frac{\partial^2 w}{\partial z^2}$$

$$+4\frac{\partial u}{\partial z}\frac{\partial^2 u}{\partial z^2}\Big]+\alpha_2^*\left[\frac{2}{r}\frac{\partial u}{\partial r}\frac{\partial u}{\partial z}+\frac{2}{r}\frac{\partial u}{\partial r}\frac{\partial w}{\partial r}+\frac{2}{r}\frac{\partial u}{\partial z}\frac{\partial w}{\partial z}\right.$$

$$+\frac{2}{r}\frac{\partial w}{\partial r}\frac{\partial w}{\partial z}+2\frac{\partial u}{\partial z}\frac{\partial^2 u}{\partial r^2}+2\frac{\partial u}{\partial r}\frac{\partial^2 u}{\partial r\partial z}+2\frac{\partial^2 u}{\partial r^2}\frac{\partial w}{\partial r}+2\frac{\partial u}{\partial r}\frac{\partial^2 w}{\partial r^2}$$

$$+4\frac{\partial u}{\partial z}\frac{\partial^2 w}{\partial r\partial z}+2\frac{\partial w}{\partial z}\frac{\partial^2 u}{\partial r\partial z}+2\frac{\partial w}{\partial r}\frac{\partial^2 w}{\partial r\partial z}+2\frac{\partial w}{\partial z}\frac{\partial^2 w}{\partial r^2}+8\frac{\partial w}{\partial z}\frac{\partial^2 w}{\partial z^2}$$

$$
\begin{aligned}
&+2\frac{\partial u}{\partial z}\frac{\partial^2 u}{\partial z^2} + 2\frac{\partial w}{\partial r}\frac{\partial^2 u}{\partial z^2} + 2\frac{\partial w}{\partial r}\frac{\partial^2 w}{\partial r\partial z}\Bigg] + \beta_3\Bigg[\frac{4}{r}\frac{\partial u}{\partial z}\left(\frac{\partial u}{\partial r}\right)^2 \\
&+\frac{4}{r}\frac{\partial w}{\partial r}\left(\frac{\partial u}{\partial r}\right)^2 + \frac{4u^2}{r^3}\frac{\partial u}{\partial z} + \frac{4u^2}{r^3}\frac{\partial w}{\partial r} + \frac{4}{r}\frac{\partial u}{\partial z}\left(\frac{\partial w}{\partial z}\right)^2 \\
&+\frac{4}{r}\frac{\partial w}{\partial r}\left(\frac{\partial w}{\partial z}\right)^2 + \frac{2}{r}\left(\frac{\partial u}{\partial z}\right)^3 + \frac{2}{r}\left(\frac{\partial w}{\partial r}\right)^3 + \frac{6}{r}\left(\frac{\partial u}{\partial z}\right)^2\frac{\partial w}{\partial r} \\
&+\frac{6}{r}\frac{\partial u}{\partial z}\left(\frac{\partial w}{\partial r}\right)^2 + 4\left(\frac{\partial u}{\partial r}\right)^2\frac{\partial^2 u}{\partial r\partial z} + 4\left(\frac{\partial u}{\partial r}\right)^2\frac{\partial^2 w}{\partial r^2} + 8\frac{\partial u}{\partial r}\frac{\partial u}{\partial z}\frac{\partial^2 u}{\partial r^2} \\
&+8\frac{\partial u}{\partial r}\frac{\partial w}{\partial r}\frac{\partial^2 u}{\partial r^2} + \frac{8u}{r^2}\frac{\partial u}{\partial r}\frac{\partial u}{\partial z} + \frac{8u}{r^2}\frac{\partial u}{\partial r}\frac{\partial w}{\partial r} + \frac{4u^2}{r^2}\frac{\partial^2 u}{\partial r\partial z} + \frac{4u^2}{r^2}\frac{\partial^2 w}{\partial r^2} \\
&+4\left(\frac{\partial w}{\partial z}\right)^2\frac{\partial^2 u}{\partial r\partial z} + 4\left(\frac{\partial w}{\partial z}\right)^2\frac{\partial^2 w}{\partial r^2} + 8\frac{\partial u}{\partial z}\frac{\partial w}{\partial z}\frac{\partial^2 w}{\partial r\partial z} + 8\frac{\partial w}{\partial r}\frac{\partial w}{\partial z}\frac{\partial^2 w}{\partial r\partial z} \\
&+6\left(\frac{\partial u}{\partial z}\right)^2\frac{\partial^2 u}{\partial r\partial z} + 6\left(\frac{\partial u}{\partial z}\right)^2\frac{\partial^2 w}{\partial r^2} + 6\left(\frac{\partial w}{\partial r}\right)^2\frac{\partial^2 u}{\partial r\partial z} + 6\left(\frac{\partial w}{\partial r}\right)^2\frac{\partial^2 w}{\partial r^2} \\
&+12\frac{\partial u}{\partial z}\frac{\partial w}{\partial r}\frac{\partial^2 u}{\partial r\partial z} + 12\frac{\partial u}{\partial z}\frac{\partial w}{\partial r}\frac{\partial^2 w}{\partial r^2} + 8\left(\frac{\partial u}{\partial r}\right)^2\frac{\partial^2 w}{\partial z^2} + 16\frac{\partial u}{\partial r}\frac{\partial w}{\partial z}\frac{\partial^2 u}{\partial r\partial z} \\
&+\frac{8u^2}{r^2}\frac{\partial^2 w}{\partial z^2} + \frac{16u}{r^2}\frac{\partial u}{\partial z}\frac{\partial w}{\partial z} + 24\left(\frac{\partial w}{\partial z}\right)^2\frac{\partial^2 w}{\partial z^2} + 4\left(\frac{\partial u}{\partial z}\right)^2\frac{\partial^2 w}{\partial z^2} \\
&+4\left(\frac{\partial w}{\partial r}\right)^2\frac{\partial^2 w}{\partial z^2} + 8\frac{\partial u}{\partial z}\frac{\partial w}{\partial r}\frac{\partial^2 w}{\partial z^2} + 8\frac{\partial u}{\partial z}\frac{\partial w}{\partial z}\frac{\partial^2 u}{\partial z^2} + 8\frac{\partial u}{\partial z}\frac{\partial w}{\partial z}\frac{\partial^2 w}{\partial r\partial z} \\
&+8\frac{\partial w}{\partial r} + 8\frac{\partial w}{\partial r}\frac{\partial w}{\partial z}\frac{\partial^2 w}{\partial r\partial z}\Bigg],
\end{aligned} \tag{5.3}
$$

$$
\begin{aligned}
\rho c_p\left(u\frac{\partial T}{\partial r} + w\frac{\partial T}{\partial z}\right) =\ & K\left(\frac{\partial^2 T}{\partial r^2} + \frac{1}{r}\frac{\partial T}{\partial r} + \frac{\partial^2 T}{\partial z^2}\right) + \sigma B_0^2 u^2 \\
&+\mu\left[2\frac{u^2}{r^2} + 2\left(\frac{\partial u}{\partial r}\right)^2 + \left(\frac{\partial u}{\partial z}\right)^2 + 2\frac{\partial u}{\partial z}\frac{\partial w}{\partial r} + \left(\frac{\partial w}{\partial r}\right)^2 + 2\left(\frac{\partial w}{\partial z}\right)^2\right] \\
&+\alpha_1^*\left[2\frac{u^3}{r^3} + 2\frac{u^2}{r^2}\frac{\partial u}{\partial r} + 4\left(\frac{\partial u}{\partial r}\right)^3 + 2u\frac{\partial u}{\partial r}\frac{\partial^2 u}{\partial r^2} + 2w\frac{\partial u}{\partial r}\frac{\partial^2 u}{\partial r\partial z} + 2\frac{uw}{r^2}\frac{\partial u}{\partial z}\right. \\
&+u\frac{\partial u}{\partial z}\frac{\partial^2 u}{\partial r\partial z} + 3\frac{\partial u}{\partial r}\left(\frac{\partial u}{\partial z}\right)^2 + w\frac{\partial u}{\partial z}\frac{\partial^2 u}{\partial z^2} + u\frac{\partial w}{\partial r}\frac{\partial^2 u}{\partial r\partial z} + 6\frac{\partial u}{\partial r}\frac{\partial u}{\partial z}\frac{\partial w}{\partial r} \\
&+w\frac{\partial w}{\partial r}\frac{\partial^2 u}{\partial z^2} + 3\frac{\partial u}{\partial r}\left(\frac{\partial w}{\partial r}\right)^2 + u\frac{\partial u}{\partial z}\frac{\partial^2 w}{\partial r^2} + u\frac{\partial w}{\partial r}\frac{\partial^2 w}{\partial r^2} + w\frac{\partial w}{\partial z}\frac{\partial^2 w}{\partial r\partial z} \\
&+w\frac{\partial w}{\partial r}\frac{\partial^2 w}{\partial r\partial z} + 3\left(\frac{\partial u}{\partial z}\right)^2\frac{\partial w}{\partial z} + 4\left(\frac{\partial w}{\partial z}\right)^3 + 6\frac{\partial u}{\partial z}\frac{\partial w}{\partial r}\frac{\partial w}{\partial z} + 3\left(\frac{\partial w}{\partial r}\right)^2\frac{\partial w}{\partial z} \\
&\left.+2u\frac{\partial w}{\partial z}\frac{\partial^2 w}{\partial r\partial z} + 2w\frac{\partial w}{\partial z}\frac{\partial^2 w}{\partial z^2}\right] + \alpha_2^*\left[4\frac{u^3}{r^3} + 4\left(\frac{\partial u}{\partial r}\right)^3 + 3\frac{\partial u}{\partial r}\left(\frac{\partial u}{\partial z}\right)^2\right. \\
&+6\frac{\partial u}{\partial r}\frac{\partial u}{\partial z}\frac{\partial w}{\partial r} + 4\left(\frac{\partial w}{\partial z}\right)^3 + 3\frac{\partial u}{\partial r}\left(\frac{\partial w}{\partial r}\right)^2 + 3\left(\frac{\partial u}{\partial z}\right)^2\frac{\partial w}{\partial z} + 6\frac{\partial u}{\partial z}\frac{\partial w}{\partial r}\frac{\partial w}{\partial z} \\
&\left.+3\left(\frac{\partial w}{\partial r}\right)^2\frac{\partial w}{\partial z}\right] + \beta_3\left[8\frac{u^4}{r^4} + 8\left(\frac{\partial u}{\partial r}\right)^4 + 16\frac{u^2}{r^2}\left(\frac{\partial u}{\partial r}\right)^2 + 8\frac{u^2}{r^2}\left(\frac{\partial u}{\partial z}\right)^2\right. \\
&+8\left(\frac{\partial u}{\partial r}\right)^2\left(\frac{\partial u}{\partial z}\right)^2 + 2\left(\frac{\partial u}{\partial z}\right)^4 + 16\frac{u^2}{r^2}\frac{\partial u}{\partial z}\frac{\partial w}{\partial r} + 8\left(\frac{\partial w}{\partial z}\right)^4 \\
&+16\left(\frac{\partial u}{\partial r}\right)^2\frac{\partial u}{\partial z}\frac{\partial w}{\partial r} + 8\left(\frac{\partial u}{\partial z}\right)^3\frac{\partial w}{\partial r} + 8\frac{u^2}{r^2}\left(\frac{\partial w}{\partial r}\right)^2 + 8\left(\frac{\partial u}{\partial r}\right)^2\left(\frac{\partial w}{\partial r}\right)^2
\end{aligned}
$$

$$+12\left(\frac{\partial u}{\partial z}\right)^2\left(\frac{\partial w}{\partial r}\right)^2+8\frac{\partial u}{\partial z}\left(\frac{\partial w}{\partial r}\right)^3+2\left(\frac{\partial w}{\partial r}\right)^4+16\frac{u^2}{r^2}\left(\frac{\partial w}{\partial z}\right)^2$$

$$+16\left(\frac{\partial u}{\partial r}\right)^2\left(\frac{\partial w}{\partial z}\right)^2+8\left(\frac{\partial u}{\partial z}\right)^2\left(\frac{\partial w}{\partial z}\right)^2+16\frac{\partial u}{\partial z}\frac{\partial w}{\partial r}\left(\frac{\partial w}{\partial z}\right)^2$$

$$+8\left(\frac{\partial w}{\partial r}\right)^2\left(\frac{\partial w}{\partial z}\right)^2\Bigg].\tag{5.4}$$

The boundary conditions are

$$u\left(r,H\right)=ar,\;\;\frac{\partial u\left(r,0\right)}{\partial z}=0,\;T(r,H)=T_w,\tag{5.5}$$

$$w\left(r,H\right)=0,\;w\left(r,0\right)=0,\;T(r,0)=T_w,\tag{5.6}$$

where a is the stretching rate.

Setting

$$u\left(r,z\right)=arf'\left(\eta\right),\;w\left(r,z\right)=-2aHf\left(\eta\right),\;\theta=\frac{T}{T_w},\;\eta=\frac{z}{H},\tag{5.7}$$

incompressible condition is automatically satisfied and Eqs. $(4.11)-(4.15)$ after eliminating the pressure terms give

$$f^{(iv)}+2\operatorname{Re}ff'''-2\alpha_1\left[2f''f'''+f'f^{(iv)}+ff^{(v)}\right]-2\alpha_2\left[2f''f'''+f'f^{(iv)}\right]$$

$$+\beta\left[56f'''^3+192f'f''f'''+24f'^2f^{(iv)}+12\delta^2f''f'''^2+6\delta^2f''^2f^{(iv)}\right]$$

$$-\operatorname{Re}Ha^2f'=0,\tag{5.8}$$

$$\theta''+2\Pr\operatorname{Re}f\theta'+Ec\Pr\left[12f'^2+\delta^2f''^2-\alpha_1\left\{24f'^3+24ff'f''+2\delta^2f'f''^2+2\delta^2ff''f'''\right\}\right.$$

$$\left.-\alpha_2\left\{24f'^3+3\delta^2f'f''^2\right\}+\beta\left\{288f'^4+48\delta^2f'^2f''^2+2\delta^4f''^4\right\}+\operatorname{Re}Ha^2f'^2\right]=0,\tag{5.9}$$

$$f'\left(1\right)=1,\;\;\;f''\left(0\right)=0\;\;\;f\left(1\right)=0,\;\;\;f\left(0\right)=0,\tag{5.10}$$

$$\theta(1)=1,\;\theta(0)=0,\tag{5.11}$$

where the dimensionless parameters are

$$\operatorname{Re}=\frac{aH^2}{\nu},\;Ha^2=\frac{\sigma B_0^2H}{\rho ar},\;\nu=\frac{\mu}{\rho},\;\alpha_1=\frac{\alpha_1^*a}{\mu},\;\delta=\frac{r}{H},$$

$$\alpha_2=\frac{\alpha_2^*a}{\mu},\;\beta=\frac{\beta_3a^2}{\mu},\;\Pr=\frac{\mu c_p}{K},\;Ec=\frac{a^2H^2}{c_pT_w}.\tag{5.12}$$

Here Re denotes the Reynolds number, Pr the Prandtl number, Ec the Eckert number, Ha the Hartman number, $(\alpha_1,\alpha_2,\beta)$ third-grade parameters and δ the dimensionless radial distance.

Local skin friction coefficient is defined by

$$C_f = \frac{\tau_w}{\frac{1}{2}\rho\,(ar)^2} = \frac{\tau_{rz}|_{z=H}}{\frac{1}{2}\rho\,(ar)^2},$$

$$C_f = \mathrm{Re}_r^{-1/2}\left[2f''\,(1) + 4\alpha_1 f'''\,(1) - 4\alpha_2 f'''\,(1) + 48\beta f'''\,(1) + 4\beta\delta^2 f''^3\,(1)\right]. \tag{5.13}$$

The other physical quantity of interest is Nusselt number. It is defined as follows:

$$Nu_1 = \frac{Hq_w}{KT_w} = -\frac{HK\frac{\partial T}{\partial z}\big|_{z=H}}{KT_w} = -\theta'(1), \tag{5.14}$$

in which $\mathrm{Re}_r = arH/\nu$ is the local Reynolds number.

5.2 Homotopic solutions

Here we choose the base functions

$$\left\{\eta^{2n+1}; n \geqslant 0\right\}, \tag{5.15}$$

$$\left\{\eta^{2n}; n \geqslant 0\right\}, \tag{5.16}$$

and write

$$f\,(\eta) = \sum_{n=0}^{\infty} a_n \eta^{2n+1}, \tag{5.17}$$

$$\theta(\eta) = \sum_{n=0}^{\infty} b_n \eta^{2n}, \tag{5.18}$$

where a_n and b_n are the coefficients to be dertermined. The initial guesses and auxiliary linear operators are

$$f_0\,(\eta) = \frac{3}{2}\eta^3 - \frac{1}{2}\eta, \tag{5.19}$$

$$\theta_0\,(\eta) = 1, \tag{5.20}$$

$$\mathcal{L}_f\,[f\,(\eta)] = \frac{d^4 f}{d\eta^4}, \tag{5.21}$$

$$\mathcal{L}_\theta\,[\theta\,(\eta)] = \frac{d^2 f}{d\eta^2}. \tag{5.22}$$

The above linear operators have the following properties

$$\mathcal{L}_f\left[\frac{C_{18}}{6}\eta^3 + \frac{C_{19}}{2}\eta^2 + C_{20}\eta + C_{21}\right] = 0, \tag{5.23}$$

$$\mathcal{L}_\theta\,[C_{22} + C_{23}\eta] = 0, \tag{5.24}$$

where $C_i\,(i = 18 - 23)$ are the constants.

5.2.1 Zeroth-order deformation problem

Zeroth-order deformation problems are given by

$$(1-q)\mathcal{L}_f\left[\hat{f}(\eta,q)-f_0(\eta)\right]=q\hbar_f\mathcal{N}_f\left[\hat{f}(\eta,q)\right], \tag{5.25}$$

$$\hat{f}'(1,q)=1,\quad \hat{f}''(0,q)=0,\quad \hat{f}(1,q)=0,\quad \hat{f}(0,q)=0, \tag{5.26}$$

$$(1-q)\mathcal{L}_\theta\left[\hat{\theta}(\eta,q)-\theta_0(\eta)\right]=q\hbar_\theta\mathcal{N}_\theta\left[\hat{\theta}(\eta,q)\right], \tag{5.27}$$

$$\hat{\theta}(1,q)=1,\quad \hat{\theta}(0,q)=0, \tag{5.28}$$

where $\hbar_f\neq0$, $\hbar_\theta\neq0$ and $q\in[0,1]$ are respectively the auxiliary and embedding parameters. When q varies from 0 to 1, then $\hat{f}(\eta,q)$ varies from initial guess $f_0(\eta)$ to final solution $f(\eta)$ and $\hat{\theta}(\eta,q)$ varies from initial guess $\theta_0(\eta)$ to final solution $\theta(\eta)$. The non-linear operators are

$$\begin{aligned}
\mathcal{N}_f\left[f(\eta,q)\right] &= \frac{\partial^4\hat{f}}{\partial\eta^4}+2\operatorname{Re}\hat{f}\frac{\partial^3\hat{f}}{\partial\eta^3}-2\alpha_1\left[2\frac{\partial^2\hat{f}}{\partial\eta^2}\frac{\partial^3\hat{f}}{\partial\eta^3}+\frac{\partial\hat{f}}{\partial\eta}\frac{\partial^4\hat{f}}{\partial\eta^4}+\hat{f}\frac{\partial^5\hat{f}}{\partial\eta^5}\right]-2\alpha_2\left[2\frac{\partial^2\hat{f}}{\partial\eta^2}\frac{\partial^3\hat{f}}{\partial\eta^3}+\frac{\partial\hat{f}}{\partial\eta}\frac{\partial^4\hat{f}}{\partial\eta^4}\right]\\
&\quad+\beta\left[56\left(\frac{\partial^2\hat{f}}{\partial\eta^2}\right)^3+192\frac{\partial\hat{f}}{\partial\eta}\frac{\partial^2\hat{f}}{\partial\eta^2}\frac{\partial^3\hat{f}}{\partial\eta^3}+24\left(\frac{\partial\hat{f}}{\partial\eta}\right)^2\frac{\partial^4\hat{f}}{\partial\eta^4}+12\delta^2\frac{\partial^2\hat{f}}{\partial\eta^2}\left(\frac{\partial^3\hat{f}}{\partial\eta^3}\right)^2\right.\\
&\quad\left.+6\delta^2\left(\frac{\partial^2\hat{f}}{\partial\eta^2}\right)^2\frac{\partial^4\hat{f}}{\partial\eta^4}\right]-\operatorname{Re}Ha^2\frac{\partial\hat{f}}{\partial\eta},
\end{aligned} \tag{5.29}$$

$$\begin{aligned}
\mathcal{N}_\theta\left[\theta(\eta,q),f(\eta,q)\right] &= \frac{\partial^2\hat{\theta}}{\partial\eta^2}+2\operatorname{Pr}\operatorname{Re}\hat{f}\frac{\partial\hat{\theta}}{\partial\eta}+\operatorname{Pr}Ec\left[12\left(\frac{\partial\hat{f}}{\partial\eta}\right)^2+\delta^2\left(\frac{\partial^2\hat{f}}{\partial\eta^2}\right)^2-\alpha_1\left\{24\left(\frac{\partial\hat{f}}{\partial\eta}\right)^3\right.\right.\\
&\quad+24\hat{f}\frac{\partial\hat{f}}{\partial\eta}\frac{\partial^2\hat{f}}{\partial\eta^2}+2\delta^2\frac{\partial\hat{f}}{\partial\eta}\left(\frac{\partial^2\hat{f}}{\partial\eta^2}\right)^2+2\delta^2\hat{f}\frac{\partial^2\hat{f}}{\partial\eta^2}\frac{\partial^3\hat{f}}{\partial\eta^3}\Bigg\}-\alpha_2\left\{24\left(\frac{\partial\hat{f}}{\partial\eta}\right)^3\right.\\
&\quad\left.+3\delta^2\frac{\partial\hat{f}}{\partial\eta}\left(\frac{\partial^2\hat{f}}{\partial\eta^2}\right)^2\right\}+\beta\left\{288\left(\frac{\partial\hat{f}}{\partial\eta}\right)^4+48\delta^2\left(\frac{\partial\hat{f}}{\partial\eta}\right)^2\left(\frac{\partial^2\hat{f}}{\partial\eta^2}\right)^2\right.\\
&\quad\left.\left.+2\delta^4\left(\frac{\partial^2\hat{f}}{\partial\eta^2}\right)^4\right\}+\operatorname{Re}Ha^2\left(\frac{\partial\hat{f}}{\partial\eta}\right)^2\right].
\end{aligned} \tag{5.30}$$

In view of Taylor series expansion, we write

$$\hat{f}_m(\eta)=\frac{1}{m!}\frac{\partial^m f(\eta,q)}{\partial q^m}\bigg|_{q=0}, \tag{5.31}$$

$$\hat{f}(\eta,q)=f_0(\eta)+\sum_{m=1}^{\infty}f_m(\eta)q^m, \tag{5.32}$$

$$\hat{\theta}_m(\eta)=\frac{1}{m!}\frac{\partial^m\theta(\eta,q)}{\partial q^m}\bigg|_{q=0}, \tag{5.33}$$

$$\hat{\theta}(\eta, q) = \theta_0(\eta) + \sum_{m=1}^{\infty} \theta_m(\eta) q^m. \tag{5.34}$$

The above expressions for $q = 1$ reduce to

$$\hat{f}(\eta) = f_0(\eta) + \sum_{m=1}^{\infty} f_m(\eta), \tag{5.35}$$

$$\hat{\theta}(\eta) = \theta_0(\eta) + \sum_{m=1}^{\infty} \theta_m(\eta). \tag{5.36}$$

5.2.2 mth-order deformation problems

Differentiating m-times the zeroth-order deformation problems in Eqs. $(5.25) - (5.28)$ with respect to q and then dividing by $m!$ and setting $q = 0$ one has

$$\mathcal{L}_f \left[\hat{f}_m(\eta) - \chi_m \hat{f}_{m-1}(\eta) \right] = \hbar_f \mathcal{R}_m^f(\eta), \tag{5.37}$$

$$\left. \frac{\partial \hat{f}_m(\eta, q)}{\partial \eta} \right|_{\eta=1} = 0, \quad \left. \frac{\partial^2 \hat{f}_m(\eta, q)}{\partial \eta^2} \right|_{\eta=0} = 0, \quad \hat{f}_m(1, q) = 0 \quad \hat{f}_m(0, q) = 0, \tag{5.38}$$

$$\mathcal{L}_\theta \left[\hat{\theta}_m(\eta) - \chi_m \hat{\theta}_{m-1}(\eta) \right] = \hbar_\theta \mathcal{R}_m^\theta(\eta), \tag{5.39}$$

$$\hat{\theta}_m(1, q) = 0. \quad \hat{\theta}(0, q) = 0, \tag{5.40}$$

$$
\begin{aligned}
\mathcal{R}_m^f(\eta) &= f_{m-1}^{(iv)}(\eta) + \sum_{k=0}^{m-1} \left[2 \operatorname{Re} f_{m-1-k} f_k''' - 2\alpha_1 \left(2 f_{m-1-k}'' f_k''' + f_{m-1-k}' f_k^{(iv)} + f_{m-1-k} f_k^{(v)} \right) \right. \\
&\quad - 2\alpha_2 \left(2 f_{m-1-k}'' f_k''' + f_{m-1-k}' f_k^{(iv)} \right) + \beta \sum_{l=0}^{k} \left\{ 56 f_{m-1-k}'' f_{k-l}'' f_l'' + 192 f_{m-1-k}' f_{k-l}'' f_l''' \right. \\
&\quad \left. \left. + 24 f_{m-1-k}' f_{k-l}' f_l^{(iv)} + 12\delta^2 f_{m-1-k}'' f_{k-l}''' f_l'' + 6\delta^2 f_{m-1-k}'' f_{k-l}'' f_l^{(iv)} \right\} \right] \\
&\quad - \operatorname{Re} Ha^2 f_{m-1}'',
\end{aligned} \tag{5.41}
$$

$$
\begin{aligned}
\mathcal{R}_m^\theta(\eta) &= \theta_{m-1}''(\eta) + 2 \operatorname{Pr} \operatorname{Re} \sum_{k=0}^{m-1} f_{m-1-k} \theta_k' + Ec \operatorname{Pr} \sum_{k=0}^{m-1} \left[12 f_{m-1-k}' f_k' + \delta^2 f_{m-1-k}'' f_k'' \right. \\
&\quad - \alpha_1 \sum_{l=0}^{k} \left\{ 24 f_{m-1-k}' f_{k-l}' f_l' + 24 f_{m-1-k} f_{k-l}' f_l'' + 2\delta^2 f_{m-1-k}' f_{k-l}'' f_l'' \right. \\
&\quad \left. + 2\delta^2 f_{m-1-k} f_{k-l}'' f_l''' \right\} - \alpha_2 \sum_{l=0}^{k} \left\{ 24 f_{m-1-k}' f_{k-l}' f_l' + 3\delta^2 f_{m-1-k}' f_{k-l}'' f_l'' \right\} \\
&\quad + \beta \sum_{l=0}^{k} \left\{ 288 f_{m-1-k}' f_{k-l}' \sum_{j=0}^{l} f_{l-j}' f_j' + 48\delta^2 f_{m-1-k}' f_{k-l}' \sum_{j=0}^{l} f_{l-j}'' f_j'' \right. \\
&\quad \left. + 2\delta^4 f_{m-1-k}'' f_{k-l}'' \sum_{j=0}^{l} f_{l-j}'' f_j'' \right\} + \operatorname{Re} Ha^2 f_{m-1-k}'' f_k' \right].
\end{aligned} \tag{5.42}
$$

The general solutions of the problems given by Eqs. $(5.37) - (5.40)$ are

$$f(\eta) = f^* + \frac{1}{6}C_{18}\eta^3 + \frac{1}{2}C_{19}\eta^2 + C_{20}\eta + C_{21}, \qquad (5.43)$$

$$\theta(\eta) = \theta^* + C_{22} + C_{23}\eta, \qquad (5.44)$$

in which f^* and θ^* are the particular solutions.

5.3 Convergence of the homotopy solutions

The Eqs. (5.8)-(5.11) have been solved using homotopy analysis method (HAM). The series solutions strongly depends upon the auxiliary parameters $\hbar_f$ and $\hbar_\theta$. In order to get the suitable range of these parameters the so-called $\hbar-$curves are plotted in the Figs. 5.1 and 5.2. These Figs. show that suitable ranges for $\hbar_f$ and $\hbar_\theta$ are $-0.5 \leq (\hbar_f, \hbar_\theta) < -0.1$. Furthermore, convergence of series solution is checked and shown in Table. 5.1. It is obvious that series solutions converge at 26th order of approximation up to 6 decimal places.

5.4 Results and discussion

This section includes the salient features of various parameters on velocity field f' and temperature field θ. Hence the Figs. 5.3-5.11 are sketched. Figs. 5.3 and 5.4 are displayed for the behavior of third grade parameter β on the radial and axial velocities. It is seen that both radial and axial velocities are increasing functions of third grade parameter β. Figs. 5.5 and 5.6 depict the variations of second grade parameter α_1 and Prandtl number Pr on temperature profile θ. It is found from these Figs. that the dimensionless temperature field decreases with an increase in α_1. However an increase in Pr yields an increase in the temperature field. Fig. 5.7 shows the effect of Ec number on the temperature field. Since the Eckert number Ec is the ratio of kinetic energy to enthalpy. Thus an increase in Ec gives an increase in kinetic energy of fluid particles. Therefore an increase in temperature of fluid is observed when Ec increases. Fig. 5.8 describes the influence of third grade parameter β on dimensionless temperature $\theta(\eta)$. It can be seen that the temperature field is increasing function of β. The behavior of second grade parameter on the temperature field is illustrated in Fig. 5.9. The temperature field decreases when the second-grade parameter increases. Effect of Reynolds number Re is plotted in Fig. 5.10. Here the temperature field θ increases for Re. Fig. 5.11 illustrates that the temperature field θ is increasing function of Hartman number Ha. Table 5.2 is prepared to examine the influence of dimensionless parameter on skin friction coefficient $\mathrm{Re}_r^{1/2} C_f$. This table shows that $\mathrm{Re}_r^{1/2} C_f$ is an increasing function of α_1, Re and Ha whereas it decreases when α_2 and β are increased. It is also noted that shear stress at the surface of sheet increases by increasing the strength of applied magnetic field. Table 5.3 represents the variation of dimensionless parameters on Nusselt numbers $\mathrm{Re}_x^{-1/2} Nu_1$ and $\mathrm{Re}_x^{-1/2} Nu_2$. Clearly $\mathrm{Re}_r^{-1/2} Nu_1$ and $\mathrm{Re}_r^{-1/2} Nu_2$ are increasing functions of β, Re, Ha, Pr and Ec whereas $\mathrm{Re}_r^{-1/2} Nu_1$ and $\mathrm{Re}_r^{-1/2} Nu_2$

decrease when dimensionless parameters α_1 and α_2 are increased.

$\alpha_1=0.01, \alpha_2=0.2, \delta=\beta=0.1, Ha=1, Re=2$
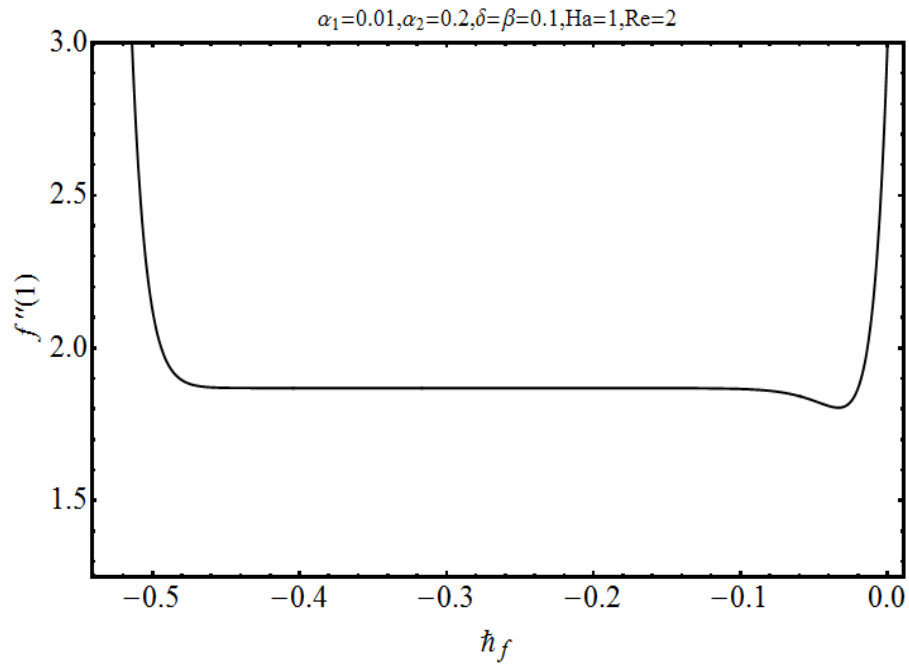
Fig. 5.1: $\hbar_f$−curve of $f''(1)$ at 28th order of approximation.

$\alpha_1=0.01, \alpha_2=0.2, Pr=\delta=\beta=Ha=0.1, Re=2, Ec=0.2$
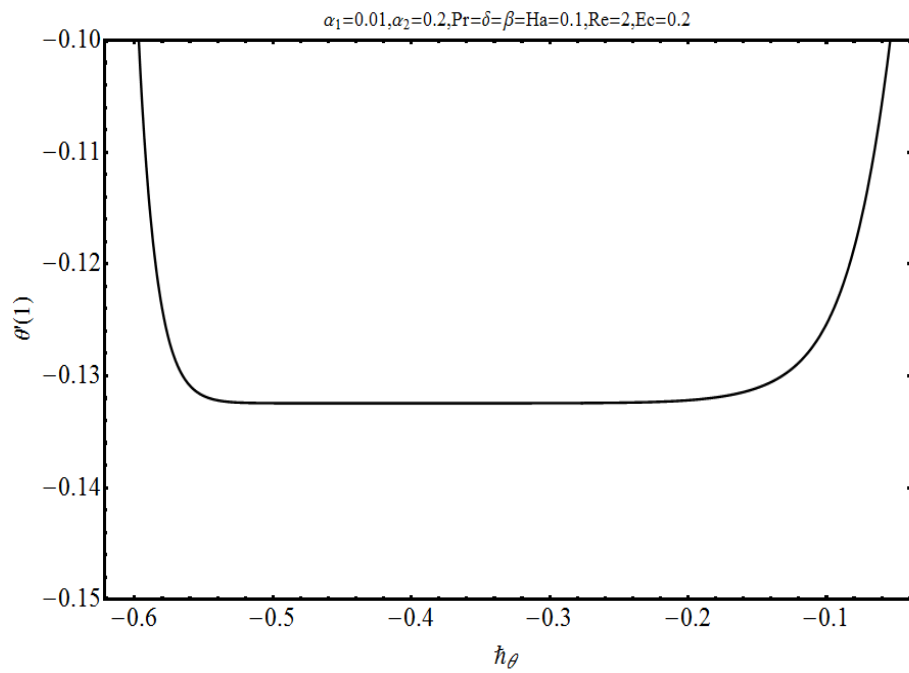
Fig. 5.2: $\hbar_\theta$−curve of $\theta'(1)$ at 27th order of approximation.
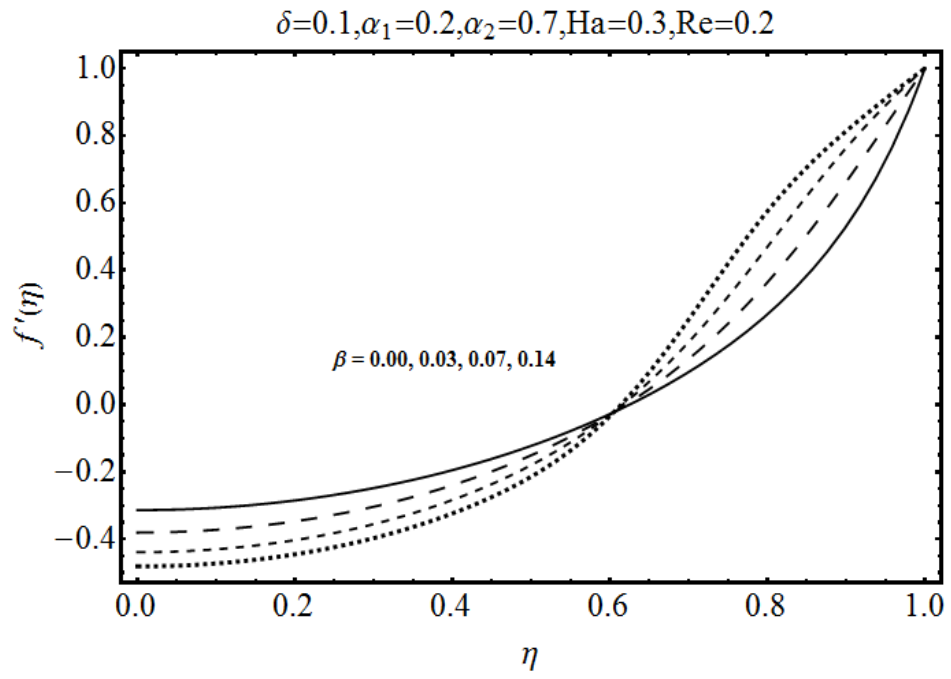
Fig. 5.3 : Influence of β on $f'(\eta)$.
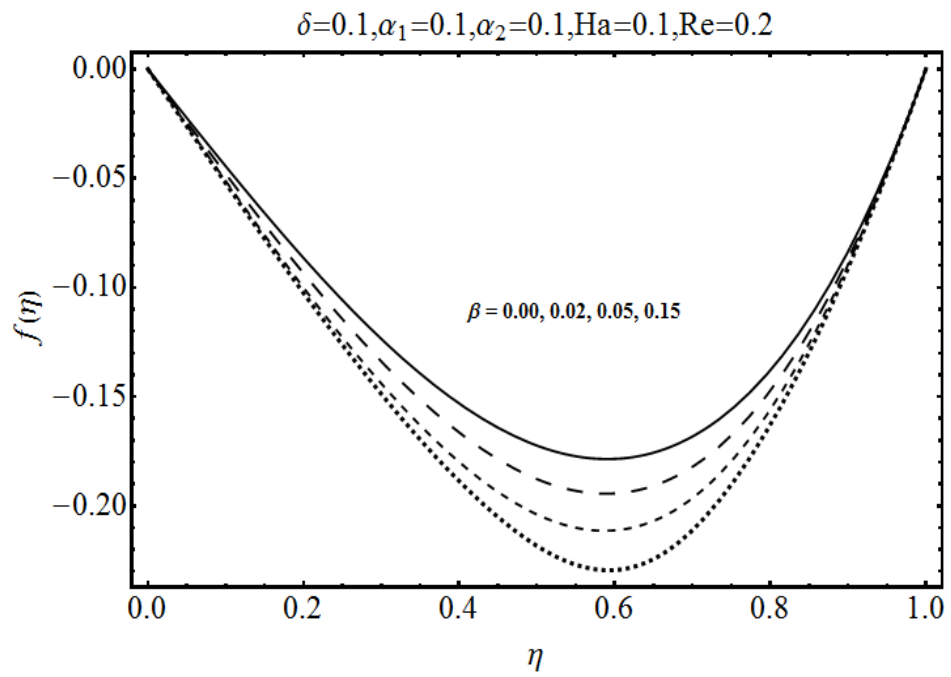
Fig. 5.4 : Influence of β on $f(\eta)$.

$$\delta=0.3, \alpha_2=0.4, \text{Ha}=1, \text{Re}=0.3, \beta=\text{Ec}=\text{Pr}=0.1$$

$\alpha_1 = 0, 0.3, 0.6, 0.9$

Fig. 5.5: Influence of α_1 on $\theta(\eta)$.

$$\delta=0.3, \alpha_1=0.1, \alpha_2=0.4, \text{Ha}=1, \text{Re}=0.3, \beta=\text{Ec}=0.1$$

Pr = 0.10, 0.11, 0.12, 0.13

Fig. 5.6: Influence of Pr on $\theta(\eta)$.

$$\delta=0.3, \alpha_1=0.1, \alpha_2=0.4, \mathrm{Ha}=1, \mathrm{Re}=0.3, \beta=\mathrm{Pr}=0.1$$

Ec = 0.10, 0.11, 0.12, 0.13

Fig. 5.7: Influence of Ec on $\theta(\eta)$.

$$\delta=0.3, \alpha_1=0.1, \alpha_2=0.4, \mathrm{Ha}=1, \mathrm{Re}=0.3, \mathrm{Ec}=\mathrm{Pr}=0.1$$

β = 0.00, 0.01, 0.02, 0.03
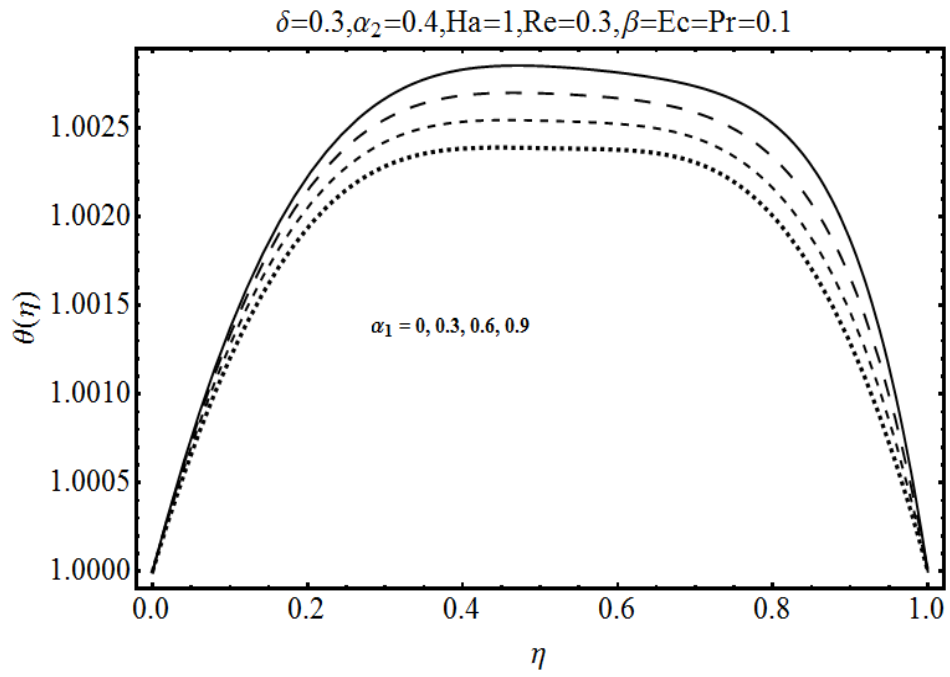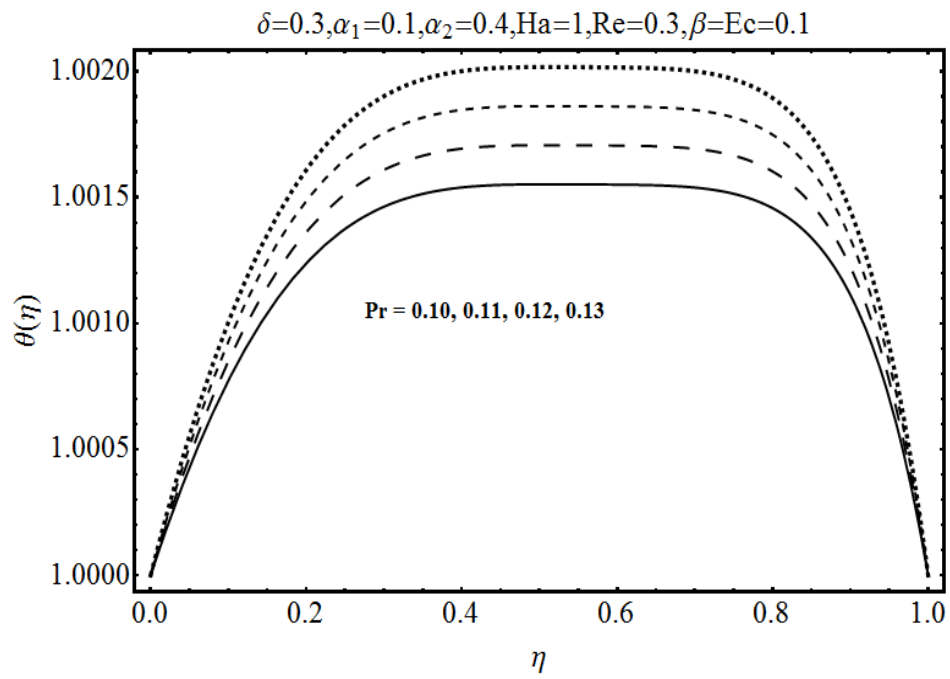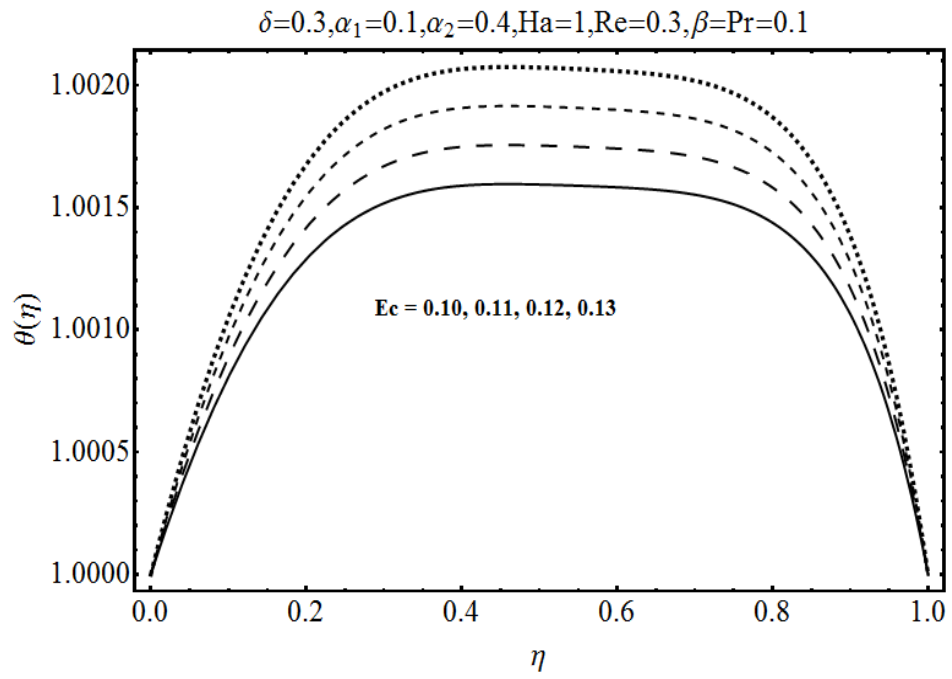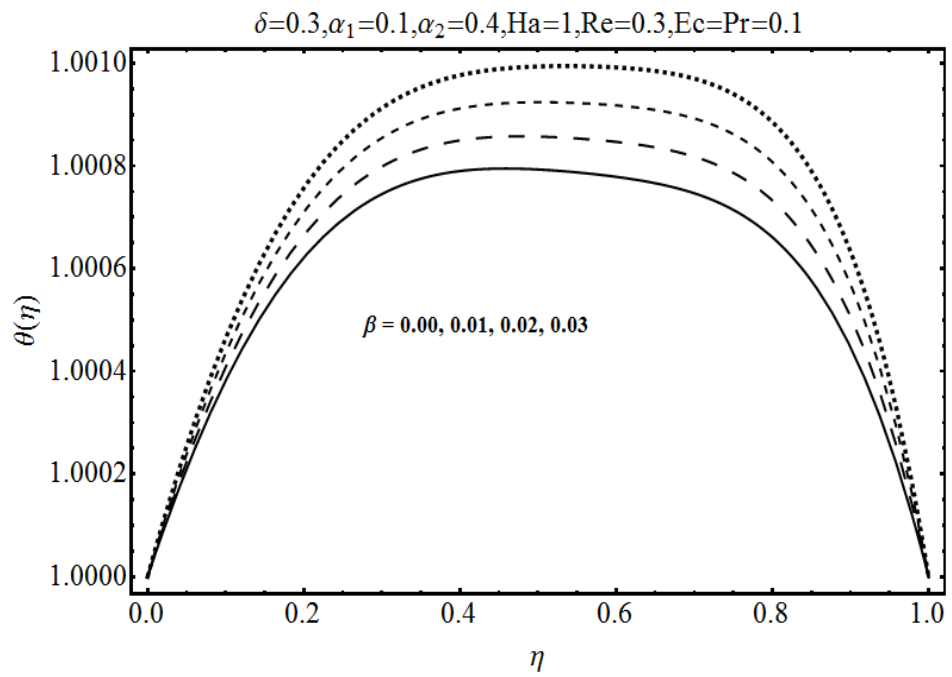
Fig. 5.8: Influence of β on $\theta(\eta)$.
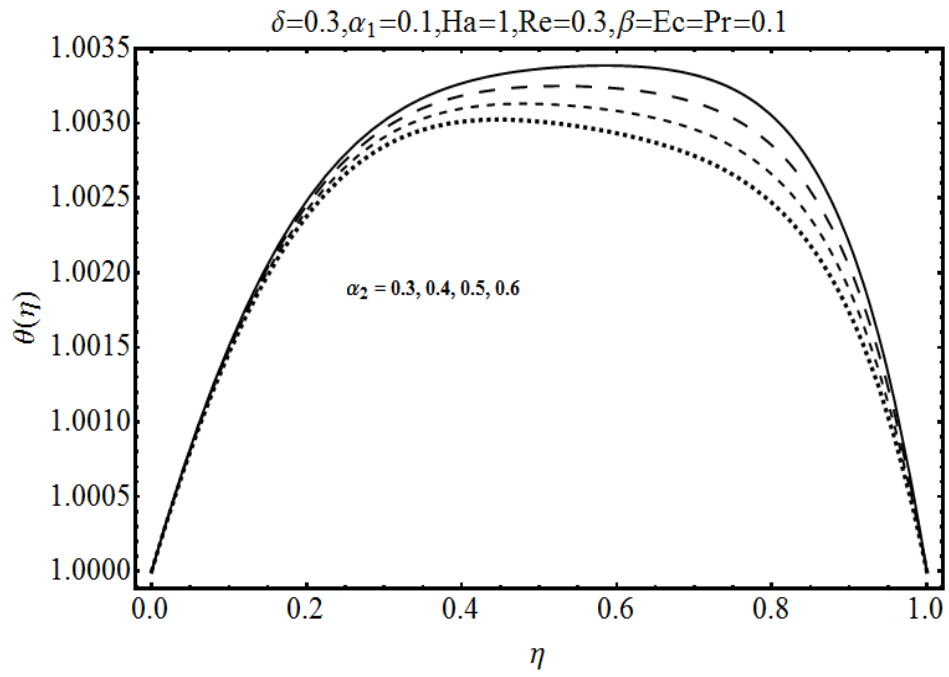
Fig. 5.9: Influence of α_2 on $\theta(\eta)$.

Fig. 5.10: Influence of Re on $\theta(\eta)$.

$$\delta=0.3, \alpha_1=0.1, \alpha_2=0.4, Re=0.3, \beta=Ec=Pr=0.1$$

Ha = 0.0, 2.5, 3.5, 4.5
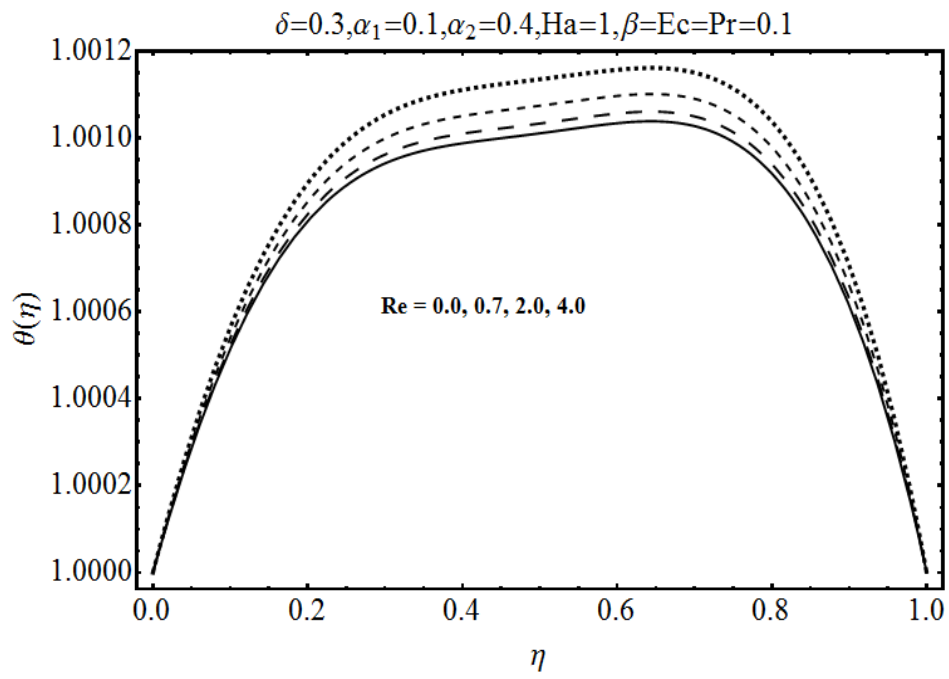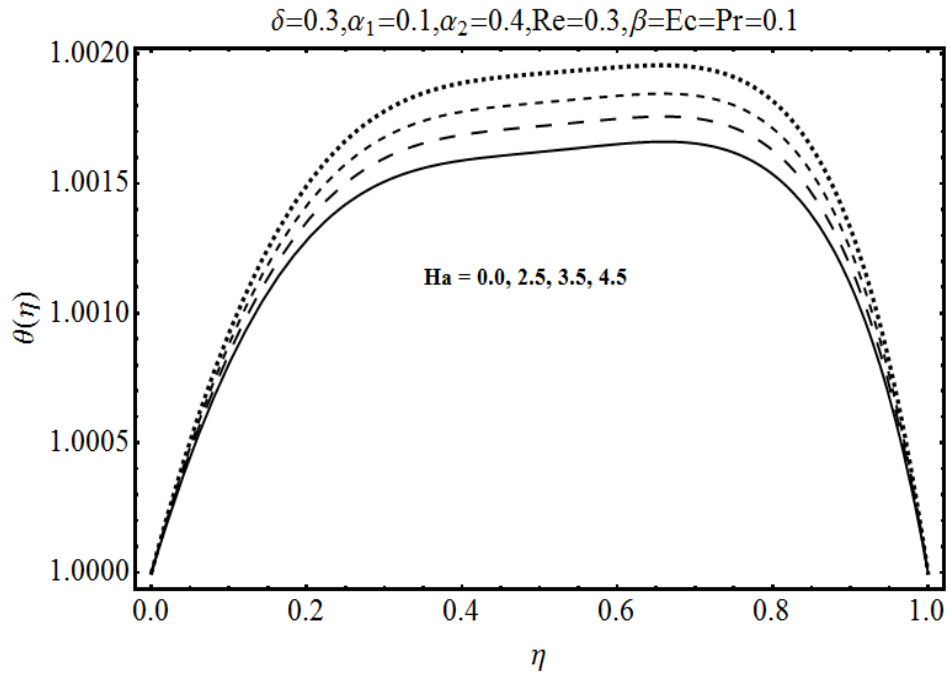
Fig. 5.11: Influence of Ha on $\theta(\eta)$.

Table 5.1: Convergence of homotopy solutions when $\alpha_1 = 0.01$, $\beta = 0.1$, $\alpha_2 = 0.1$, $\delta = 0.3$, $Ha = 0.1$, $Re = 2$, $Pr = 0.71$, $Ec = 0.1$ and $\hbar_f = \hbar_\theta = -0.4$.

Order of approximation	$f''(1)$	$-\theta'(1)$
1	1.01239	0.0372775
2	2.03212	0.0722032
5	1.84750	0.115979
10	1.86945	0.123692
26	1.86848	0.124370
30	1.86848	0.124370
40	1.86848	0.124370

Table 5.2: Numerical values of skin friction coefficients $Re_r^{1/2} C_f$ for different values of physical parameters.

α_1	α_2	β	Re	Ha	$Re_r^{1/2} C_f$
0.00	0.01	0.1	2	0.1	6.07234
0.01					6.84608
0.02					7.74272
0.03					8.83994
0.01	0.00	0.01	0.1	0.1	6.85566
	0.01				6.84609
	0.02				6.82144
	0.03				6.78433

α_1	α_2	β	Re	Ha	$\mathrm{Re}_r^{1/2}\,C_f$
0.01	0.1	0.0	0.1	0.1	6.84608
		0.1			5.13500
		0.2			4.57691
		0.3			4.22002
0.01	0.01	0.01	0.0	0.2	6.80888
			0.1		6.84828
			0.2		6.88793
			0.3		6.92783
0.01	0.01	0.01	0.1	0.0	6.84535
				0.1	6.84609
				0.2	6.84828
				0.3	6.85193

Table 5.3: Numerical values of Nusselt number Nu for different values of physical parameters.

α_1	α_2	β	Re	Ha	Pr	Ec	$\mathrm{Re}_r^{-1/2}\,Nu_1$	$-\,\mathrm{Re}_r^{-1/2}\,Nu_2$
0.0	0.2	0.01	0.2	0.1	0.71	0.1	0.168744	0.168744
0.1							0.152786	0.152786
0.2							0.138297	0.138297
0.25							0.131467	0.131467
0.01	0.0	0.01	2	0.1	0.71	0.2	0.447318	0.447318
	0.1						0.389180	0.389180
	0.2						0.334372	0.334372
	0.3						0.281762	0.281762
0.01	0.2	0.0	0.2	0.1	0.71	0.2	0.252642	0.252642
		0.1					0.616315	0.616315
		0.11					0.662727	0.662727
		0.12					0.705145	0.705145
0.01	0.2	0.01	0.0	0.1	0.71	0.2	0.333765	0.333765
			0.1				0.333961	0.333961
			0.2				0.334153	0.334153
			0.3				0.334342	0.334342
0.01	0.2	0.01	2	0.0	0.71	0.2	0.336810	0.336810
				0.1			0.337080	0.337080
				0.2			0.337889	0.337889
				0.3			0.339237	0.339237

α_1	α_2	β	Re	Ha	Pr	Ec	$\mathrm{Re}_r^{-1/2}\, Nu_1$	$-\,\mathrm{Re}_r^{-1/2}\, Nu_2$
0.01	0.2	0.01	2	0.1	0.71	0.2	0.337080	0.337080
					0.72		0.341904	0.341904
					0.73		0.346729	0.346729
					0.74		0.351557	0.351557
0.01	0.3	0.01	2	0.1	0.71	0.1	0.143037	0.143037
						0.2	0.286075	0.286075
						0.3	0.429112	0.429112
						0.4	0.460342	0.460342

5.5   Concluding remarks

We have explored the heat transfer characteristics in the axisymmetric flow of an electrically conducting third grade fluid between the radial stretching sheets. The main points of the present investigation are as follows:

- Temperature field increases for large values of Ha.

- Higher values of Eckert number Ec increase the temperature profile.

- Higher values of second grade parameter α_1 reduce the temperature profile and associated boundary layer thickness.

- Rate of heat transfer increases when β, Ha, Ec, Re and Pr are increased. However it decreases by increasing α_1 and α_2.

Chapter 6

Effect of Joule heating in flow of third grade fluid over radiative surface

The boundary layer flow of third grade fluid over an unsteady permeable stretching sheet with heat transfer is adressed in this chapter. The magnetic and electric fields in the momentum equations are considered. Thermal boundary layer equation includes both viscous and Ohmic dissipations. The related nonlinear partial differential system is reduced first into ordinary differential system and then solved for the series solutions. The dependence of velocity and temperature profiles on the various parameters are shown and discussed by sketching graphs. Expressions of skin friction coefficient and local Nusselt number are calculated and analyzed. Numerical values of skin friction coefficient and Nusselt number are tabulated and examined. It is observed that both velocity and temperature increase in presence of electric field. Further the temperature is increased due to the radiation parameter. Thermal boundary layer thickness increases by increasing Eckert number.

6.1   Mathematical formulation

We examine the two-dimensional boundary layer flow of magnetohydrodynamic (MHD) third grade fluid over a porous stretching surface. Here the fluid is electrically conducting in the presence of applied magnetic $\vec{B} = (0, B_0, 0)$ and electric $\vec{E} = (0, 0, -E_0)$ fields. The flow is because of stretching of sheet from a slit through two equal and opposite forces. The sheet velocity is taken linear parallel to the flow direction. The electric and magnetic fields obey the Ohm's law $\tilde{\mathbf{J}} = \sigma \left(\vec{E} + \vec{V} \times \vec{B} \right)$. Here $\tilde{\mathbf{J}}$ is the Joule current, σ is the electrical conductivity and $\vec{V}$ is the fluid velocity. The induced magnetic field and Hall current effects are ignored subject to small magnetic Reynolds number. Both the electric and magnetic fields contribute into the momentum and thermal boundary layer equations. The relevant equations in the aforestated conditions can be expressed as follows:

$$\frac{\partial u}{\partial x} + \frac{\partial v}{\partial y} = 0, \tag{6.1}$$

$$\frac{\partial u}{\partial t} + u\frac{\partial u}{\partial x} + v\frac{\partial u}{\partial y} = \nu\frac{\partial^2 u}{\partial y^2} + \frac{\alpha_1^*}{\rho}\left[\frac{\partial^3 u}{\partial t\partial y^2} + u\frac{\partial^3 u}{\partial x\partial y^2} + v\frac{\partial^3 u}{\partial y^3} + \frac{\partial u}{\partial x}\frac{\partial^2 u}{\partial y^2} + 3\frac{\partial u}{\partial y}\frac{\partial^2 u}{\partial x\partial y}\right]$$
$$+ 2\frac{\alpha_2^*}{\rho}\frac{\partial u}{\partial y}\frac{\partial^2 u}{\partial x\partial y} + 6\frac{\beta_3}{\rho}\left(\frac{\partial u}{\partial y}\right)^2\frac{\partial^2 u}{\partial y^2} + \frac{\sigma}{\rho}\left(E_0 B_0 - B_0^2 u\right), \tag{6.2}$$

$$\rho c_p\left(\frac{\partial T}{\partial t} + u\frac{\partial T}{\partial x} + v\frac{\partial T}{\partial y}\right) = K\frac{\partial^2 T}{\partial y^2} + \mu\left(\frac{\partial u}{\partial y}\right)^2 + \alpha_1^*\left[\frac{\partial u}{\partial y}\frac{\partial^2 u}{\partial t\partial y} + u\frac{\partial u}{\partial y}\frac{\partial^2 u}{\partial x\partial y} + v\frac{\partial u}{\partial y}\frac{\partial^2 u}{\partial y^2}\right]$$
$$+ 2\beta_3\left(\frac{\partial u}{\partial y}\right)^4 + \sigma\left(uB_0 - E_0\right)^2 - \frac{\partial q_r}{\partial y}. \tag{6.3}$$

In above equations u and v denote the velocity components in the x and y directions, α_1^*, α_2^* and β_3 are the fluid parameters, ν is the kinematic viscosity, ρ is the density of fluid, T is the fluid temperature, K is the thermal conductivity of fluid, c_p is the specific heat at constant pressure and the radiative heat flux q_r is [41, 42]:

$$q_r = -\frac{4\sigma^*}{3k_1}\frac{\partial T^4}{\partial y}, \tag{6.4}$$

where σ^* is the Stefan-Boltzmann constant and k_1 is the mean absorption coefficient. Through expansion of $T^4 \cong 4T_\infty^3 T - 3T_\infty^4$ and Eq. (6.3) becomes

$$\rho c_p\left(\frac{\partial T}{\partial t} + u\frac{\partial T}{\partial x} + v\frac{\partial T}{\partial y}\right) = \left(\frac{16\sigma^* T_\infty^3}{3k_1} + K\right)\frac{\partial^2 T}{\partial y^2} + \mu\left(\frac{\partial u}{\partial y}\right)^2$$
$$+ \alpha_1^*\left[\frac{\partial u}{\partial y}\frac{\partial^2 u}{\partial t\partial y} + u\frac{\partial u}{\partial y}\frac{\partial^2 u}{\partial x\partial y} + v\frac{\partial u}{\partial y}\frac{\partial^2 u}{\partial y^2}\right]$$
$$+ 2\beta_3\left(\frac{\partial u}{\partial y}\right)^4 + \sigma\left(uB_0 - E_0\right)^2. \tag{6.5}$$

The subjected conditions can be mentioned as follows:

$$u(x,0) = U_w, \ v(x,0) = V_w, \ T(x,0) = T_w,$$

$$u \to 0, \quad T \to T_\infty, \quad \text{as} \quad y \to \infty, \tag{6.6}$$

with V_w defined by

$$V_w = -\frac{\nu_0}{(1 - ct)^{1/2}}. \tag{6.7}$$

Here the mass transfer at surface with $V_w < 0$ is for injection and $V_w > 0$ for suction. Also the stretching velocity $U_w(x,t)$ and the surface temperature $T_w(x,t)$ are taken in the forms:

$$U_w(x,t) = \frac{ax}{1 - ct}, \ T_w(x,t) = T_\infty + T_0\frac{ax}{2\nu(1 - ct)^2}, \tag{6.8}$$

where a and c are the constants with $a > 0$ and $c \geq 0$ (i.e. $ct < 1$).

If ψ is the stream function then defining

$$\eta = \sqrt{\frac{U_w}{x\nu}}y, \ \psi = \sqrt{\nu x U_w}f(\eta), \ \theta = \frac{T - T_\infty}{T_w - T_\infty}, \tag{6.9}$$

$$u = \frac{\partial \psi}{\partial y}, \quad v = -\frac{\partial \psi}{\partial x}, \tag{6.10}$$

the incompressibility condition is identically satisfied and the resulting problems for f and θ are reduced into the following forms

$$f''' + f f'' - f'^2 - S\left\{ f' + \frac{1}{2}\eta f'' \right\} + \alpha_1 \left[2f' f''' - f f^{(iv)} + 3f''^2 \right.$$
$$\left. + S\left\{ 2f''' + \frac{1}{2}\eta f^{(iv)} \right\} \right] + 2\alpha_2 f''^2 + 6\beta \operatorname{Re} f''^2 f''' + Ha^2 \left\{ E_1 - f' \right\} = 0 , \tag{6.11}$$

$$\left(1 + \frac{4}{3}R_d \right) \theta'' - \Pr\left[f' \, \theta - f \, \theta' + \frac{S}{2}\left\{ \eta\theta' + 4\theta \right\} \right] + \Pr Ec \, f''^2 + \alpha_1 \Pr Ec \left[f' f''^2 \right.$$
$$\left. + \frac{S}{2}\left\{ 3f''^2 + \eta f'' f''' \right\} - f f'' f''' \right] + 2\beta \Pr Ec \operatorname{Re} f''^4 + Ha^2 \Pr Ec \left[f' - E_1 \right]^2 = 0, \tag{6.12}$$

$$f(0) = A, \quad f'(0) = 1, \quad f'(\infty) \to 0, \quad f''(\infty) \to 0, \quad \theta(0) = 1, \quad \theta(\infty) \to 0, \tag{6.13}$$

with

$$\begin{aligned}
\operatorname{Re} &= \frac{ax^2}{\nu(1-ct)}, \quad Ha^2 = \frac{\sigma B_0^2(1-ct)}{\rho a}, \quad E_1 = \frac{E_0(1-ct)}{B_0 ax}, \\
\alpha_1 &= \frac{\alpha_1^* a}{\mu(1-ct)}, \quad \alpha_2 = \frac{\alpha_2^* a}{\mu(1-ct)}, \quad \beta = \frac{\beta_3 a^2}{\mu(1-ct)^2}, \quad A = \frac{\nu_0}{\sqrt{a\nu}}, \\
S &= \frac{c}{a}, \quad R_d = \frac{4\sigma^* T_\infty^3}{k^* K}, \quad \Pr = \frac{\mu c_p}{K}, \quad Ec = \frac{U_w^2}{c_p(T_w - T_\infty)}.
\end{aligned} \tag{6.14}$$

Here Re denotes the Reynolds number, Ha the magnetic parameter, E_1 the electric parameter, α_1 and α_2 and β the fluid parameters, A the suction parameter, S the unsteadiness parameter, R_d the radiation parameter, Pr the Prandtl number and Ec the Eckert number.

The local skin friction coefficient is defined by

$$C_f = \frac{\tau_w}{\rho U_w^2} = \frac{\tau_{xy}|_{y=0}}{\rho U_w^2}, \tag{6.15}$$

$$\operatorname{Re}_x^{1/2} C_f = \left[f''(0) + \alpha_1 \left\{ 3\frac{S}{2}f''(0) + 3f''(0) - Sf'''(0) \right\} + 2\beta \operatorname{Re} f''^3(0) \right]. \tag{6.16}$$

The Nusselt number is given by

$$Nu_x = \frac{xq_w}{K(T_w - T_\infty)} = -\frac{x\left(K + \frac{16\sigma^* T_\infty^3}{3k_1} \right) \frac{\partial T}{\partial y}\big|_{y=0}}{K(T_w - T_\infty)}, \tag{6.17}$$

$$\operatorname{Re}_x^{-1/2} Nu_x = -\left(1 + \frac{4}{3}R_d \right)\theta'(0), \tag{6.18}$$

in which $\operatorname{Re}_x = \frac{ax^2}{\nu(1-ct)}$ is the local Reynolds number.

6.2 Homotopic solutions

The velocity and temperature in the set of base functions

$$\left\{ \eta^k \exp\left(-n\eta\right) \middle| k \geq 0, \ n \geq 0 \right\}, \tag{6.19}$$

can be expressed as follows

$$f\left(\eta\right) = a_{0,0}^0 + \sum_{n=0}^{\infty} \sum_{k=0}^{\infty} a_{m,n}^k \eta^k \exp\left(-n\eta\right), \tag{6.20}$$

$$\theta\left(\eta\right) = \sum_{n=0}^{\infty} \sum_{k=0}^{\infty} b_{m,n}^k \eta^k \exp\left(-n\eta\right), \tag{6.21}$$

where $a_{m,n}^k$ and $b_{m,n}^k$ are the coefficients.

The initial guesses f_0 and θ_0 in homotopy solutions are taken through the expressions

$$f_0(\eta) = A + 1 - \exp\left(-\eta\right), \tag{6.22}$$

$$\theta_0(\eta) = \exp\left(-\eta\right). \tag{6.23}$$

The auxiliary linear operators and their associated properties are

$$\mathcal{L}_f\left(f\right) = \frac{d^3 f}{d\eta^3} - \frac{df}{d\eta}, \quad \mathcal{L}_\theta\left(\theta\right) = \frac{d^2 \theta}{d\eta^2} - \theta, \tag{6.24}$$

$$\mathcal{L}_f\left[C_{24} + C_{25}\exp\left(\eta\right) + C_{26}\exp\left(-\eta\right)\right] = 0, \tag{6.25}$$

$$\mathcal{L}_\theta\left[C_{27}\exp\left(\eta\right) + C_{28}\exp\left(-\eta\right)\right] = 0, \tag{6.26}$$

where $C_i (i = 24 - 28)$ depict the arbitrary constants.

6.2.1 Zeroth-order problem

The zeroth order problems are

$$(1-p)\mathcal{L}_f[\hat{f}(\eta, q) - f_0(\eta)] = p\hbar_f \mathcal{N}_f\left[\hat{f}(\eta, q)\right], \tag{6.27}$$

$$\hat{f}(\eta; q)\Big|_{\eta = 0} = A, \quad \frac{\partial \hat{f}(\eta; q)}{\partial \eta}\Big|_{\eta = 0} = 1, \quad \frac{\partial \hat{f}(\eta; q)}{\partial \eta}\Big|_{\eta \to \infty} = 0, \tag{6.28}$$

$$(1-q)\mathcal{L}_\theta[\hat{\theta}(\eta, q) - \theta_0(\eta)] = q\hbar_\theta \mathcal{N}_\theta\left[\hat{f}(\eta, q), \hat{\theta}(\eta, q)\right], \tag{6.29}$$

$$\hat{\theta}(\eta; q)\Big|_{\eta = 0} = 1, \quad \hat{\theta}(\eta; q)\Big|_{\eta \to \infty} = 0, \tag{6.30}$$

with non-linear operators $\mathcal{N}_f\left[\hat{f}(\eta,q)\right]$ and $\mathcal{N}_\theta\left[\hat{f}(\eta,q),\hat{\theta}(\eta,q)\right]$ defined by

$$
\begin{aligned}
\mathcal{N}_f\left[\hat{f}(\eta;q)\right] =\ & \frac{\partial^3 \hat{f}(\eta,q)}{\partial\eta^3} + \hat{f}(\eta,q)\frac{\partial^2 \hat{f}(\eta,q)}{\partial\eta^2} - \left(\frac{\partial \hat{f}(\eta,q)}{\partial\eta}\right)^2 \\
& -S\left\{\frac{\partial \hat{f}(\eta,q)}{\partial\eta} + \frac{1}{2}\eta\frac{\partial^2 \hat{f}(\eta;q)}{\partial\eta^2}\right\} + \alpha_1\left\{2\frac{\partial \hat{f}(\eta,q)}{\partial\eta}\frac{\partial^3 \hat{f}(\eta;q)}{\partial\eta^3}\right. \\
& -\hat{f}(\eta,q)\frac{\partial^4 \hat{f}(\eta,q)}{\partial\eta^4} + S\left\{2\frac{\partial^3 \hat{f}(\eta;q)}{\partial\eta^3} + \frac{1}{2}\eta\frac{\partial^4 \hat{f}(\eta,q)}{\partial\eta^4}\right\} + 3\left.\left(\frac{\partial^2 \hat{f}(\eta,q)}{\partial\eta^2}\right)^2\right\} \\
& +2\alpha_2\left(\frac{\partial^2 \hat{f}(\eta,q)}{\partial\eta^2}\right)^2 + 6\beta\operatorname{Re}\left(\frac{\partial^2 \hat{f}(\eta,q)}{\partial\eta^2}\right)^2\frac{\partial^3 \hat{f}(\eta;q)}{\partial\eta^3} + Ha^2\left\{E_1 - \frac{\partial \hat{f}(\eta,q)}{\partial\eta}\right\},
\end{aligned}
\tag{6.31}
$$

$$
\begin{aligned}
\mathcal{N}_\theta\left[\hat{f}(\eta;q),\hat{\theta}(\eta;q)\right] =\ & \left(1 + \frac{4}{3}R_d\right)\frac{\partial^2\hat{\theta}(\eta;q)}{\partial\eta^2} + \Pr Ec\left(\frac{\partial^2 \hat{f}(\eta,q)}{\partial\eta^2}\right)^2 \\
& -\Pr\left[\frac{S}{2}\left\{4\theta + \eta\frac{\partial\hat{\theta}(\eta;q)}{\partial\eta}\right\} + \frac{\partial \hat{f}(\eta;q)}{\partial\eta}\hat{\theta}(\eta;q) - \hat{f}(\eta,q)\frac{\partial\hat{\theta}(\eta;q)}{\partial\eta}\right] \\
& +\alpha_1\Pr Ec\left[\frac{S}{2}\left\{3\left(\frac{\partial^2 \hat{f}(\eta,q)}{\partial\eta^2}\right)^2 + \eta\frac{\partial^2 \hat{f}(\eta,q)}{\partial\eta^2}\frac{\partial^3 \hat{f}(\eta;q)}{\partial\eta^3}\right\}\right. \\
& \left.+\frac{\partial \hat{f}(\eta;q)}{\partial\eta}\left(\frac{\partial^2 \hat{f}(\eta,q)}{\partial\eta^2}\right)^2 - \hat{f}(\eta,q)\frac{\partial^2 \hat{f}(\eta,q)}{\partial\eta^2}\frac{\partial^3 \hat{f}(\eta;q)}{\partial\eta^3}\right] \\
& +2\beta\Pr Ec\operatorname{Re}\left(\frac{\partial^2 \hat{f}(\eta;q)}{\partial\eta^2}\right)^4 + Ha^2\Pr Ec\left[\frac{\partial \hat{f}(\eta;q)}{\partial\eta} - E_1\right]^2,
\end{aligned}
\tag{6.32}
$$

in which $q \in [0,1]$ indicates the embedding parameter and $\hbar_f$ and $\hbar_\theta$ the nonzero auxiliary parameters.

Setting $q = 0$ and $q = 1$, we have

$$
\hat{f}(\eta;0) = f_0(\eta), \qquad \hat{f}(\eta;1) = f(\eta), \tag{6.33}
$$

$$
\hat{\theta}(\eta;0) = \theta_0(\eta), \qquad \hat{\theta}(\eta;1) = \theta(\eta). \tag{6.34}
$$

When q increases from 0 to 1, $\hat{f}(\eta;q)$ and $\hat{\theta}(\eta;q)$ deform from the initial solutions $f_0(\eta)$ and $\theta_0(\eta)$ to the final solutions $f(\eta)$ and $\theta(\eta)$ respectively. Taylor series of $\hat{f}(\eta;q)$ and $\hat{\theta}(\eta;q)$ gives

$$
\hat{f}(\eta;q) = f_0(\eta) + \sum_{m=1}^{\infty} f_m(\eta)q^m, \qquad f_m(\eta) = \frac{1}{m!}\left.\frac{\partial^m \hat{f}(\eta;q)}{\partial q^m}\right|_{p=0}, \tag{6.35}
$$

$$
\hat{\theta}(\eta;q) = \theta_0(\eta) + \sum_{m=1}^{\infty} \theta_m(\eta)q^m, \qquad \theta_m(\eta) = \frac{1}{m!}\left.\frac{\partial^m \hat{\theta}(\eta;q)}{\partial q^m}\right|_{p=0}. \tag{6.36}
$$

The auxiliary parameters are properly chosen such that the series solutions converge at $q = 1$. Therefore

$$f(\eta) = f_0(\eta) + \sum_{m=1}^{\infty} f_m(\eta), \tag{6.37}$$

$$\theta(\eta) = \theta_0(\eta) + \sum_{m=1}^{\infty} \theta_m(\eta). \tag{6.38}$$

6.2.2 mth-order deformation problems

The mth-order deformation problems are

$$\mathcal{L}_f \left[f_m(\eta) - \chi_m f_{m-1}(\eta) \right] = \hbar_f \mathcal{R}_m^f(\eta), \tag{6.39}$$

$$\hat{f}_m(\eta; p) \Big|_{\eta = 0} = 0, \quad \left. \frac{\partial \hat{f}_m'(\eta; p)}{\partial \eta} \right|_{\eta = 0} = 0, \quad \left. \frac{\partial \hat{f}_m'(\eta; p)}{\partial \eta} \right|_{\eta \to \infty} = 0, \tag{6.40}$$

$$\mathcal{L}_\theta \left[\theta_m(\eta) - \chi_m \theta_{m-1}(\eta) \right] = \hbar_\theta \mathcal{R}_m^\theta(\eta), \tag{6.41}$$

$$\hat{\theta}_m(\eta; p) \Big|_{\eta = 0} = 0, \quad \hat{\theta}_m(\eta; p) \Big|_{\eta \to \infty} = 0, \tag{6.42}$$

$$
\begin{aligned}
\mathcal{R}_m^f(\eta) \;=\; & f_{m-1}'''(\eta) + \sum_{k=0}^{m-1} \left(f_{m-1-k} f_k'' - f_{m-1-k}' f_k' \right) - S \left(f_{m-1}' + \frac{1}{2} \eta f_{m-1}'' \right) \\
& + \sum_{k=0}^{m-1} \alpha_1 \left[2 f_{m-1-k}' f_k''' - f_{m-1-k} f_k^{(iv)} + 3 f_{m-1-k}'' f_k'' \right] + \alpha_1 S \left\{ 2 f_{m-1}''' + \frac{1}{2} \eta f_{m-1}^{(iv)} \right\} \\
& + 2\alpha_2 \sum_{k=0}^{m-1} f_{m-1-k}'' f_k'' + 6\beta \operatorname{Re} \sum_{k=0}^{m-1} f_{m-1-k}'' \sum_{l=0}^{k} f_{k-l}'' f_l''' + Ha^2 \left[E_1 (1 - \chi_m) - f_{m-1}' \right],
\end{aligned}
\tag{6.43}
$$

$$
\begin{aligned}
\mathcal{R}_m^\theta(\eta) \;=\; & \left(1 + \frac{4}{3} R_d \right) \theta_{m-1}'' - \Pr \left[\sum_{k=0}^{m-1} f_{m-1-k}' \theta_k - \sum_{k=0}^{m-1} f_{m-1-k} \theta_k' + \frac{S}{2} \left\{ \eta \theta_{m-1}' + 4\theta_{m-1} \right\} \right] \\
& + \Pr Ec \sum_{k=0}^{m-1} f_{m-1-k}'' f_k'' + \alpha_1 \Pr Ec \left[\sum_{k=0}^{m-1} f_{m-1-k}' \sum_{l=0}^{k} f_{k-l}'' f_l'' \right. \\
& + \frac{S}{2} \sum_{k=0}^{m-1} \left\{ 3 f_{m-1-k}'' f_k'' + \eta f_{m-1-k}'' f_k''' \right\} - \sum_{k=0}^{m-1} f_{m-1-k} \sum_{l=0}^{k} f_{k-l}'' f_l''' \right] \\
& + 2\beta \Pr Ec \operatorname{Re} \sum_{k=0}^{m-1} f_{m-1-k}'' \sum_{l=0}^{k} f_{k-l}'' \sum_{s=0}^{l} f_{l-s}'' f_s'' + Ha^2 \Pr Ec \left[f_{m-1}' - E_1 (1 - \chi_m) \right]^2.
\end{aligned}
\tag{6.44}
$$

The general solutions of the Eqs. (6.35)-(6.37) are

$$f_m(\eta) = f_m^*(\eta) + C_{24} + C_{25} \exp(\eta) + C_{26} \exp(-\eta), \tag{6.45}$$

$$\theta_m(\eta) = \theta_m^*(\eta) + C_{27} \exp(\eta) + C_{28} \exp(-\eta). \qquad (6.46)$$

6.3 Convergence of the homotopy solutions

We note that the series solutions (6.33) and (6.34) contain the non-zero auxiliary parameters $\hbar_f$ and $\hbar_\theta$. These parameters are useful in adjusting and controlling the convergence. The $\hbar_f$ and $\hbar_\theta-$curves are plotted for 10th order of approximation in Fig. 6.1 for the suitable ranges of the auxiliary parameters. Here the suitable values for $\hbar_f$ and $\hbar_\theta$ are $-1.5 \leq \hbar_f < -0.53$ $-1.35 \leq \hbar_\theta < -0.4$. Furthermore, convergence of series solutions is checked and shown in Table 6.1. Note that the series solutions converge at 26th order of approximation up to 6 decimal places.

6.4 Results and discussion

This section illustrates the impact of physical parameters. The results are displayed graphically in the Figs. 6.2-6.20. The conclusions for flow field and other physical quantities of interest are drawn. The numerical values of the skin friction coefficient and local Nusselt number are presented in the Tables 6.2 and 6.3 for various values of α_1, α_2, β, S, Ha, E_1, Re, R_d, Pr and Ec. Fig. 6.2 displays the effect of Hartman number Ha on velocity profile by keeping other physical parameters fixed. It is of interest to note that the velocity profile decreases with an increase in Ha whereas the boundary layer thickness reduces. Clearly by increasing magnetic force, the Lorentz force increases which causes resistance in the fluid flow and consequently the velocity profile decreases. Fig. 6.3 shows the influence of third grade parameter β on the velocity profile $f'(\eta)$. Here we noticed that the velocity increases near the wall with an increased β whereas it vanishes away from the wall. Figs. 6.4 and 6.5 illustrate the variation of second grade parameters α_1 and α_2 on the velocity profile $f'(\eta)$ respectively. It is observed that the velocity profile $f'(\eta)$ is an increasing function of α_1. The velocity profile also increases when α_2 is increased. Fig. 6.6 is plotted for the effects of the suction parameter A on the velocity profile $f'(\eta)$. The velocity profile decreases by increasing parameter A. Further the boundary layer is also decreasing function of A. Fig. 6.7 is sketched for the influence of unsteadiness parameter S on the velocity profile. The velocity profile and the thermal boundary layer decrease for larger values of S. The behavior of Reynolds number Re on velocity profile is shown in Fig. 6.8. It is observed that the velocity profile decreases with an increase in Reynolds number. The influence of electric parameter E_1 is shown in Fig. 6.9. This Fig explains that as electric parameter increases, the velocity boundary layer increases near the plate with small rate but it increases away from the stretching plate more rapidly. In fact the Lorentz force (arising due to the electric field acts like an accelerating force) reduces the frictional resistance which causes to shift the stream line away from the stretching sheet. Fig. 6.10 portrays the effects of magnetic parameter Ha on the temperature profile $\theta(\eta)$. It is depicted that temperature profile and thermal boundary layer thickness increase with an increase in magnetic parameter. Fig. 6.11 is the plot of temperature profile $\theta(\eta)$ for various values of third grade parameter β. The effect of third grade parameter β on $\theta(\eta)$ shows a decrease near the wall. The boundary layer thickness also decreases. Figs. 6.12 and 6.13 describe

the effects of second grade parameters α_1 and α_2 on temperature profile $\theta(\eta)$. Fig. 6.12 depicts that the effect of second grade parameter α_1 is to reduce the temperature distribution in the boundary layer which results in thinning of the boundary layer thickness. Same behavior is shown in Fig. 6.13 for various values of α_2. The influence of suction parameter A and unsteadiness parameter S are analyzed in the Figs. 6.14 and 6.15. Here the temperature profile decreases with the increase of unsteadiness parameter S and the suction parameter A. Further the thermal boundary layer also decreases by increasing both the unsteadiness parameter S and the suction parameter A. Fig. 6.16 shows that the temperature profile and thermal boundary layer is decreasing function of Reynold number Re. The effects of thermal radiation parameter R_d on temperature is shown in Fig. 6.17. It is revealed that the radiation parameter R_d causes increase in the fluid temperature $\theta(\eta)$. On the other hand the thermal boundary layer thickness also increases. In Fig. 6.18 the influence of electric parameter E_1 on temperature profile is given. This Fig. depicts that the temperature profile and the boundary layer thickness increase with an increase of electric parameter E_1. Fig. 6.19 illustrates the effects of Prandtl number Pr on the temperature profile $\theta(\eta)$. Both the temperature and thermal boundary layer thickness are decreased by increasing Pr. We displayed the temperature field for various values of Eckert number Ec in Fig. 6.20. Effect of Eckert number is to increase the thermal boundary layer thickness due to the frictional heating. Fig. 6.21 shows the effects of Hartman number Ha on velocity $f'(\eta)$ and shear stress $f''(\eta)$. With the increase in Ha, the velocity field $f'(\eta)$ decreases near the wall and it vanishes far away from the wall while shear stress $f''(\eta)$ has same behavior for larger values of Hartman number Ha. An opposite behavior is noted when $0 \leq \eta \leq 0.6$. Fig. 6.22 demonstrates the effects of electric parameter E_1 on velocity $f'(\eta)$ and shear stress $f''(\eta)$. It is worthmentioning to point out that velocity is increasing function of electric parameter E_1 near the wall whereas opposite behavior for shear stress is observed for $0 \leq \eta \leq 1$.

The numerical values of skin friction coefficient for various physical parameters are shown in Table 6.2. Here the magnitude of skin friction coefficient increases for larger second grade parameters (α_1, α_2), third grade parameter β, unsteadiness parameter S, Hartman number Ha and Reynold number Re whereas it decreases with an increase in electric parameter E_1. Table 6.3 shows the effect of physical parameters on heat transfer characteristics at the wall $-\theta'(0)$. From this table we observe that for large values of second grade parameters (α_1, α_2), third grade parameter β, unsteadiness parameter S, radiation parameter R_d and Prandtl number Pr the heat transfer coefficient at the wall $-\theta'(0)$ increases while it decreases for Hartman number Ha, Reynold number Re, electric parameter E_1 and Eckert number Ec.
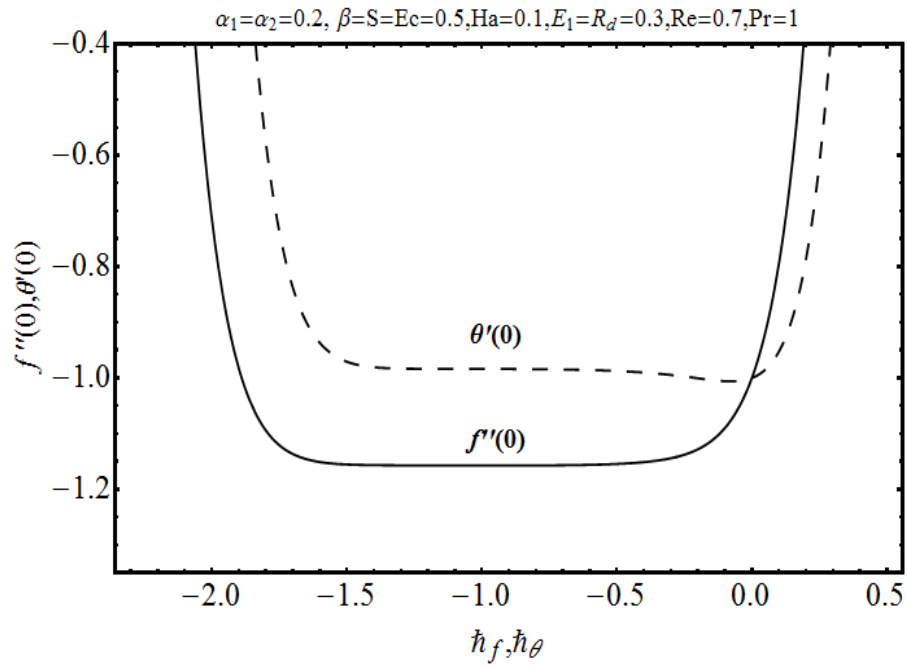
Fig. 6.1: $\hbar$-curves for the functions $f(\eta)$ and $\theta(\eta)$ at 10th order of approximation.

Fig. 6.2: Influence of Ha on $f'(\eta)$.

$E_1{=}0.1,\text{Ha}{=}2.4,\alpha_1{=}\alpha_2{=}0.2,\text{A}{=}1,\text{S}{=}0.4,\text{Re}{=}0.5$

$\beta = 0.0, 3.0, 0.5, 0.7$

Fig. 6.3: Influence of β on $f'(\eta)$.

$E_1{=}\alpha_2{=}\text{Ha}{=}0.2,\beta{=}0.1,\text{S}{=}0.4,\text{A}{=}\text{Re}{=}0.5$

$\alpha_1 = 0, 0.2, 0.3, 0.4$
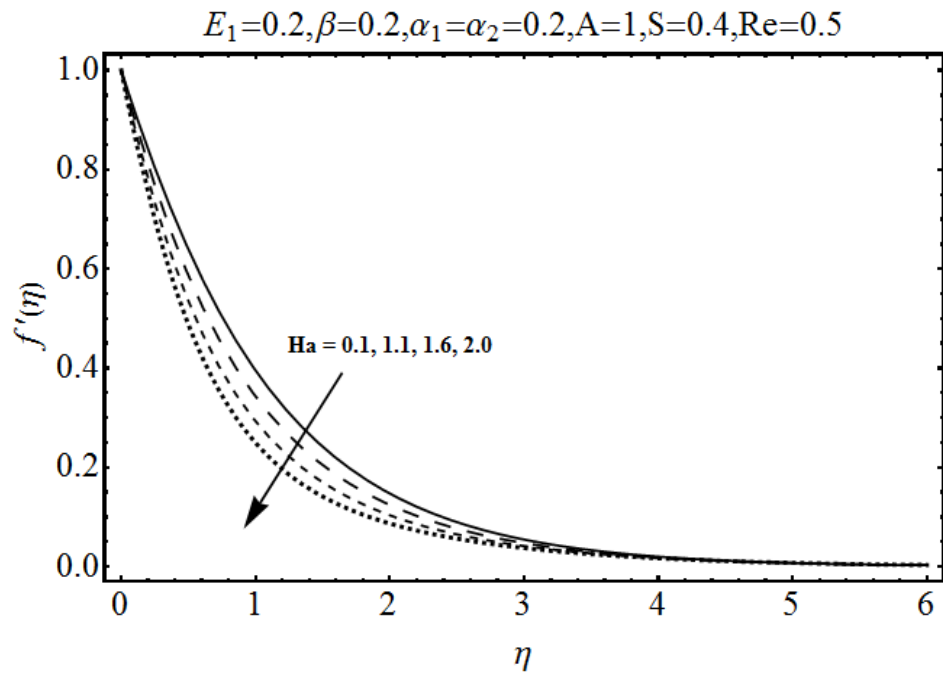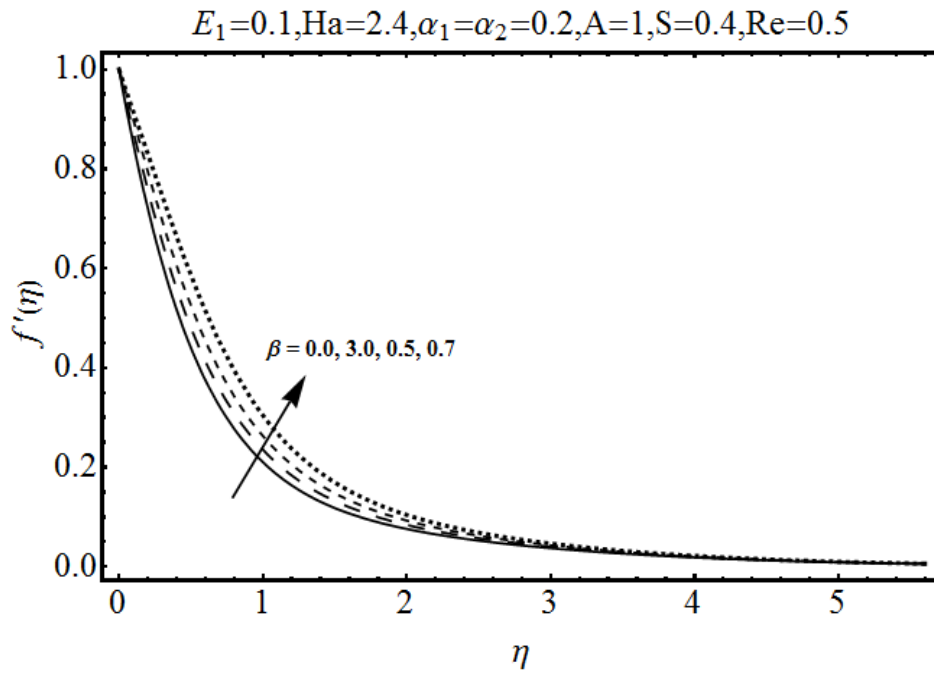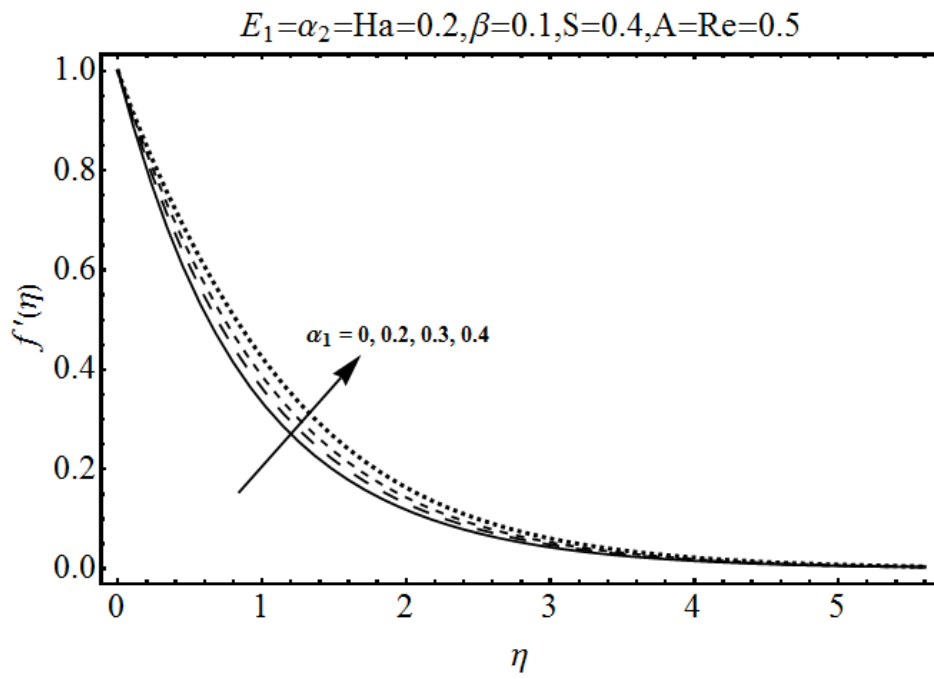
Fig. 6.4: Influence of α_1 on $f'(\eta)$.
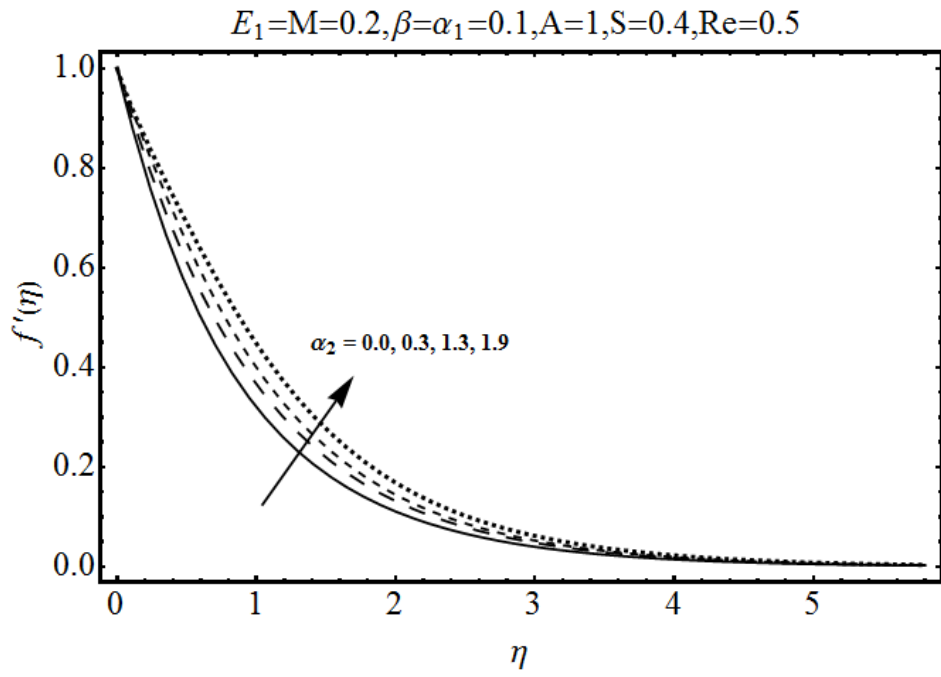
Fig. 6.5: Influence of α_2 on $f'(\eta)$.
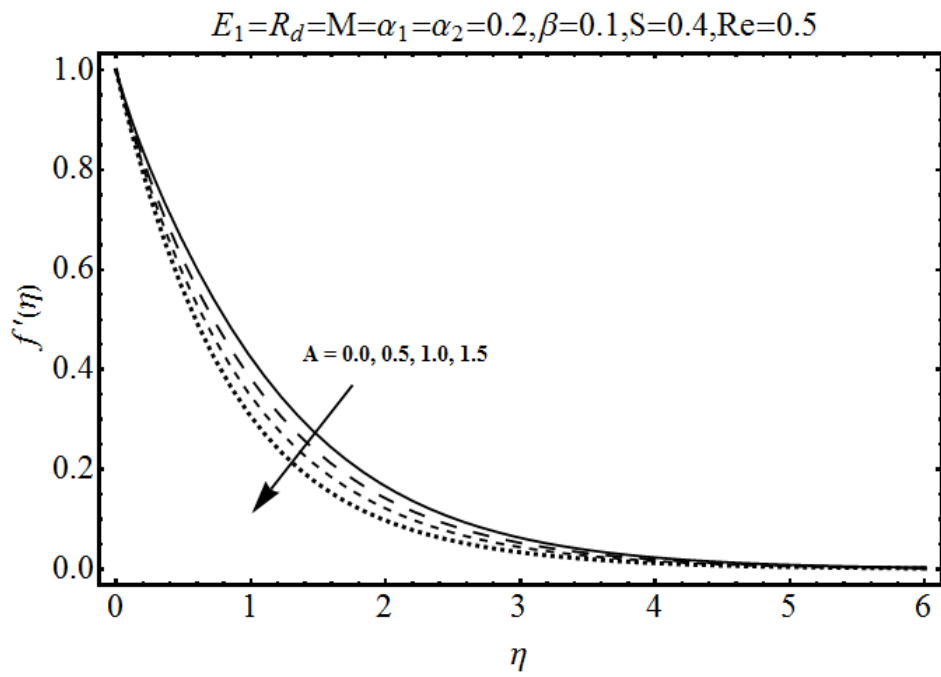
Fig. 6.6: Influence of A on $f'(\eta)$.
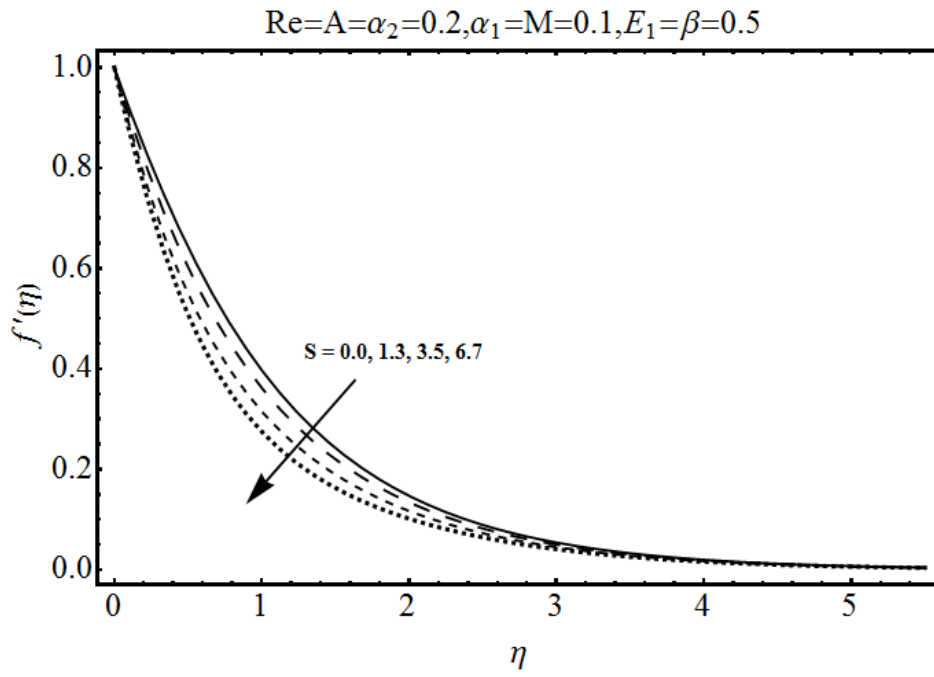
Fig. 6.7: Influence of S on $f'(\eta)$.
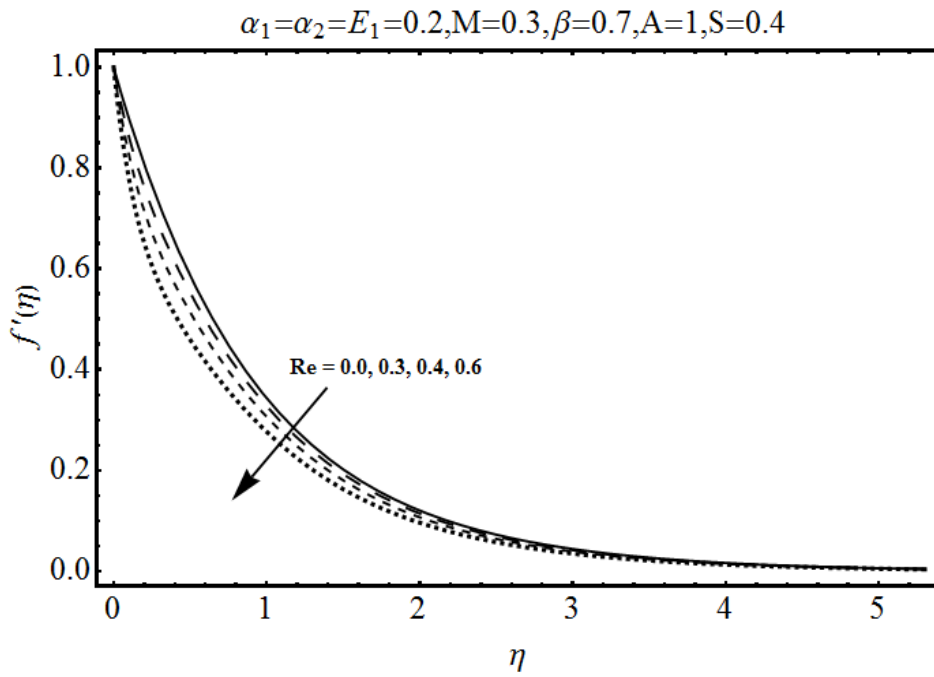
Fig. 6.8: Influence of Re on $f'(\eta)$.
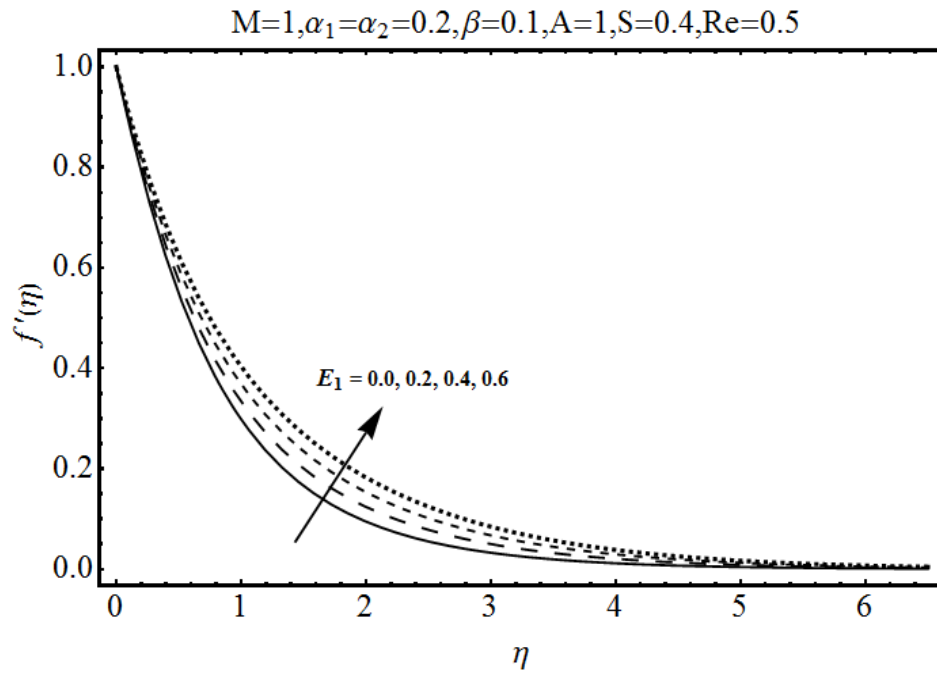
Fig. 6.9: Influence of E_1 on $f'(\eta)$.
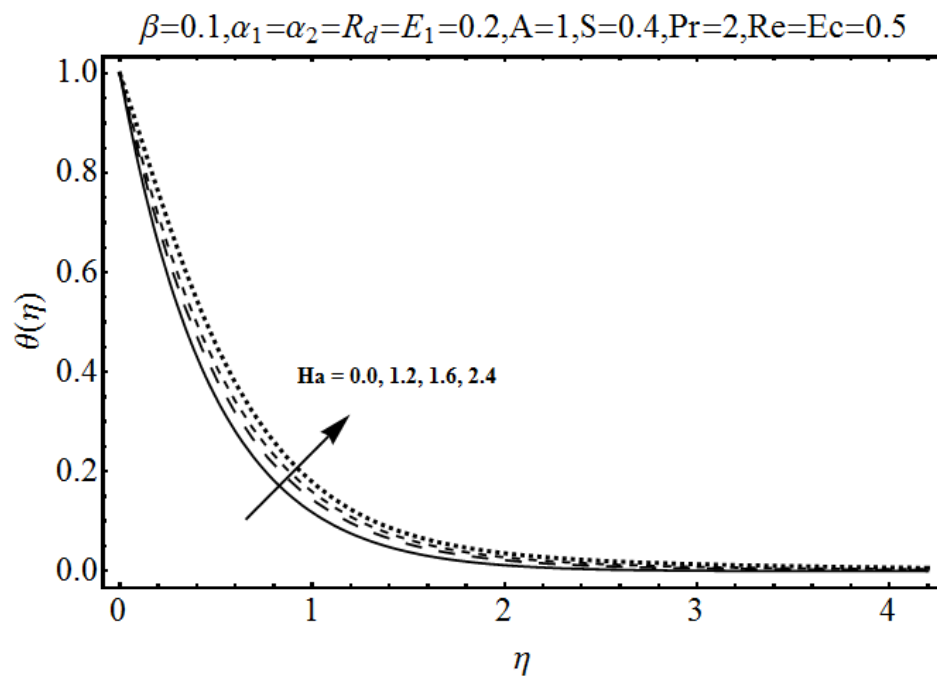
Fig. 6.10: Influence of Ha on $\theta(\eta)$.
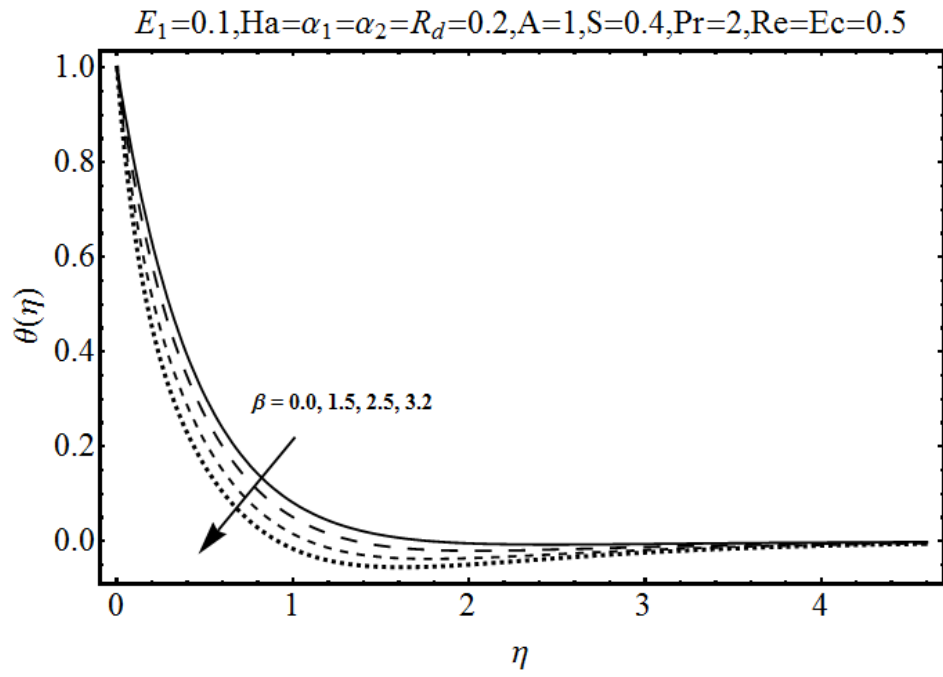
Fig. 6.11: Influence of β on $\theta(\eta)$.
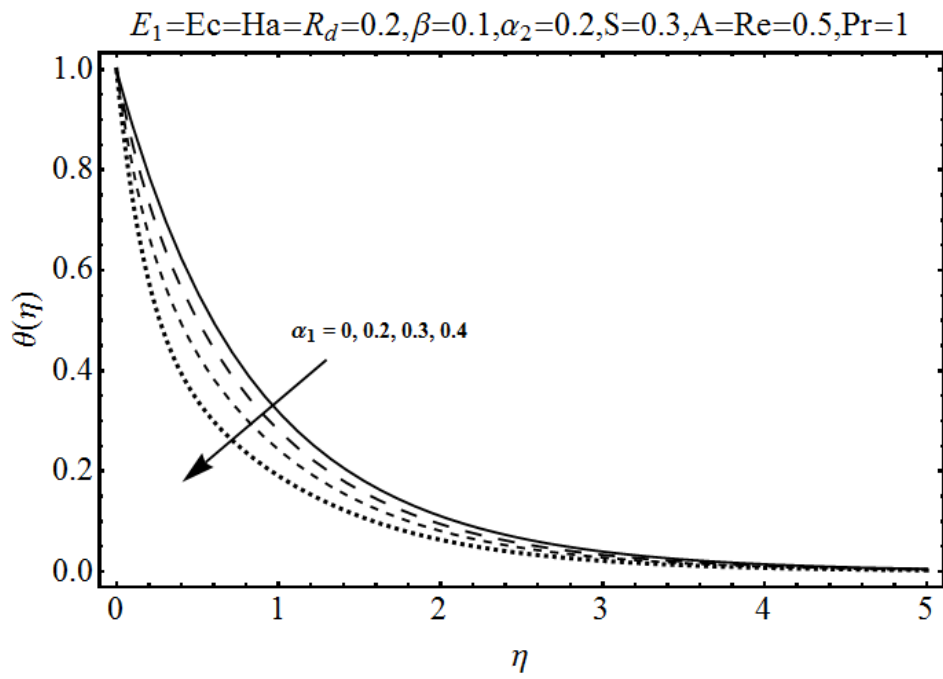
Fig. 6.12: Influence of α_1 on $\theta(\eta)$.
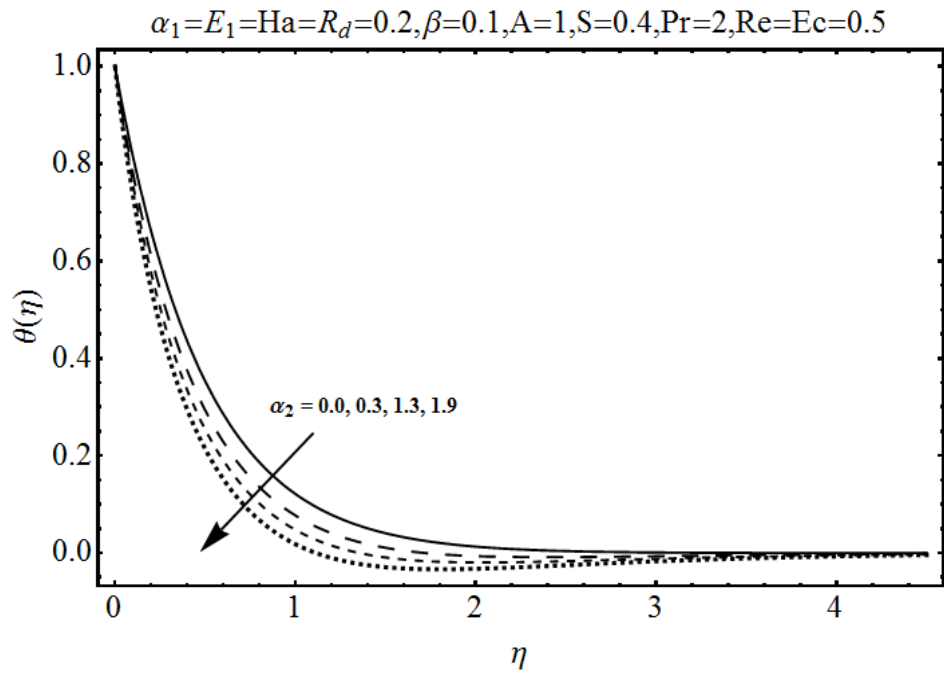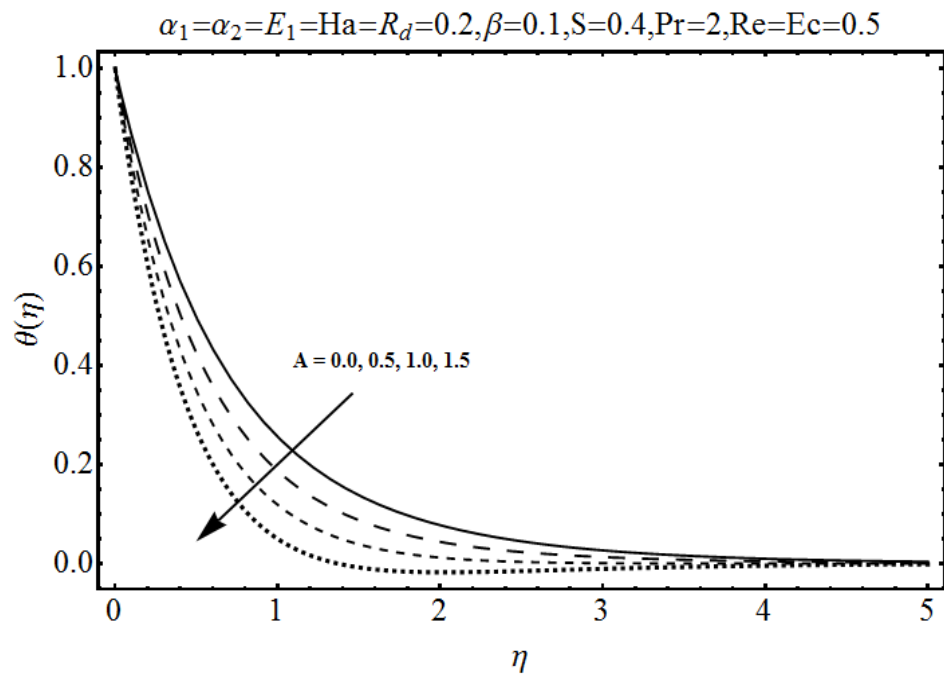
$\alpha_1 = E_1 = Ha = R_d = 0.2, \beta = 0.1, A = 1, S = 0.4, Pr = 2, Re = Ec = 0.5$

$\alpha_2 = 0.0, 0.3, 1.3, 1.9$

Fig. 6.13: Influence of α_2 on $\theta(\eta)$.

$\alpha_1 = \alpha_2 = E_1 = Ha = R_d = 0.2, \beta = 0.1, S = 0.4, Pr = 2, Re = Ec = 0.5$

$A = 0.0, 0.5, 1.0, 1.5$

Fig. 6.14: Influence of A on $\theta(\eta)$.

$$\alpha_1 = \alpha_2 = E_1 = \mathrm{Ha} = R_d = 0.2, \beta = 0.1, A = 1, \mathrm{Pr} = 2, \mathrm{Re} = \mathrm{Ec} = 0.5$$

$S = 0.0, 0.3, 0.6, 1.2$

Fig. 6.15: Influence of S on $\theta\left(\eta\right)$.

$$\alpha_1 = \alpha_2 = E_1 = \mathrm{Ha} = R_d = 0.2, \beta = A = 1, \mathrm{Pr} = 0.7, S = 0.4, \mathrm{Ec} = 0.5$$

$\mathrm{Re} = 0.0, 0.3, 0.7, 0.9$

Fig. 6.16: Influence of Re on $\theta\left(\eta\right)$.

$$\alpha_1=\alpha_2=E_1=\text{Ha}=0.2, \beta=0.1, A=1, S=0.4, \text{Pr}=2, \text{Re}=\text{Ec}=0.5$$

$R_d = 0.0, 0.5, 1.0, 1.5$
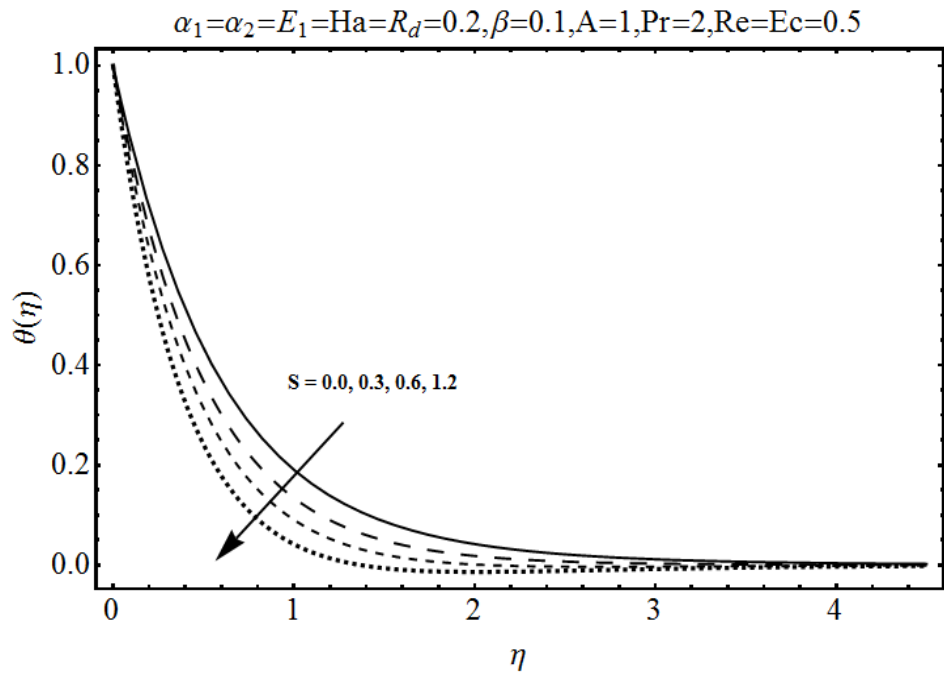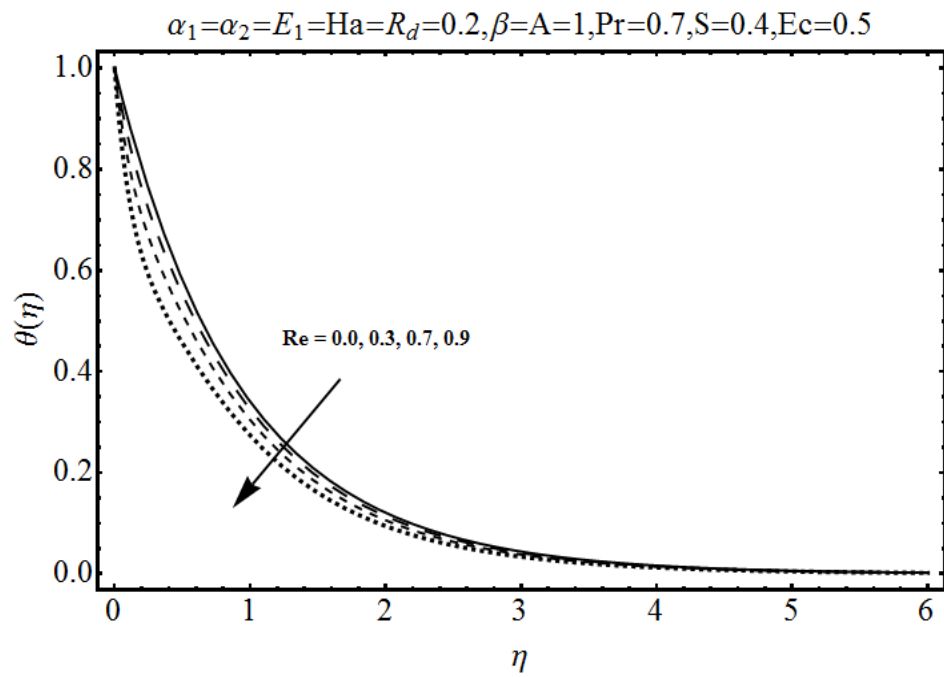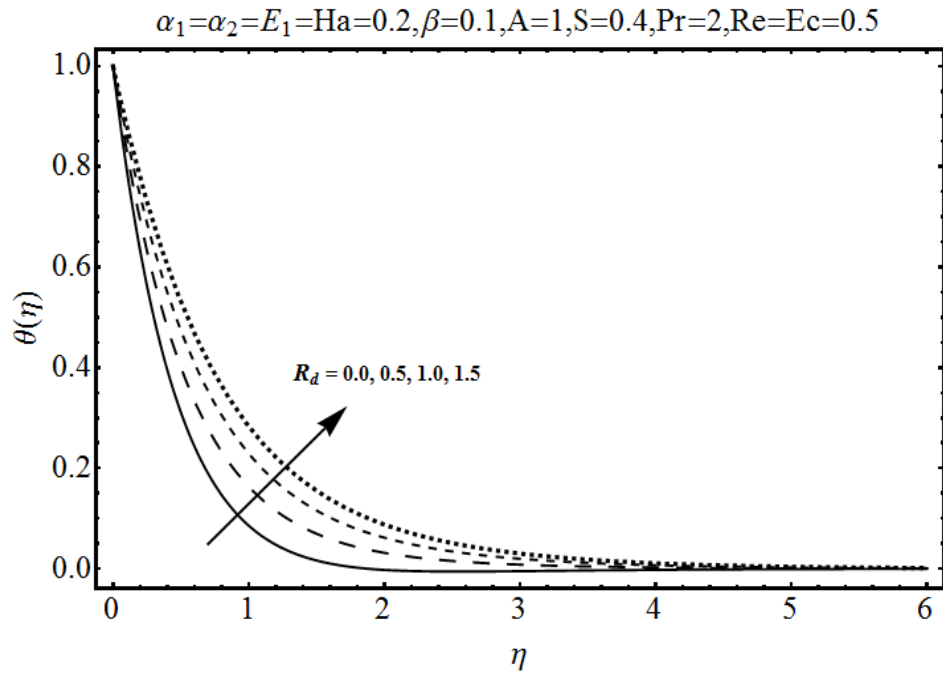
Fig. 6.17: Influence of R_d on $\theta(\eta)$.

$$\alpha_1=\alpha_2=R_d=\text{Ha}=0.2, \beta=0.1, A=1, S=0.4, \text{Pr}=1, \text{Re}=\text{Ec}=0.5$$

$E_1 = 0.0, 0.2, 0.4, 0.6$
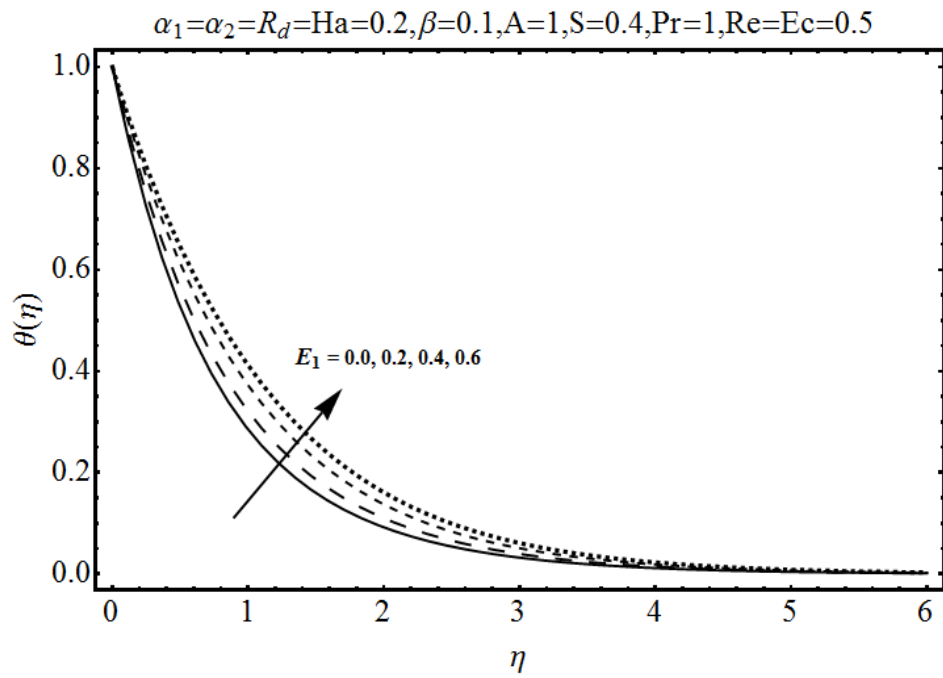
Fig. 6.18: Influence of E_1 on $\theta(\eta)$.

$$\alpha_1 = \alpha_2 = E_1 = R_d = \text{Ha} = 0.2, \beta = 0.1, A = 1, S = 0.4, \text{Re} = \text{Ec} = 0.5$$

Pr = 0.1, 0.4, 0.9, 1.5
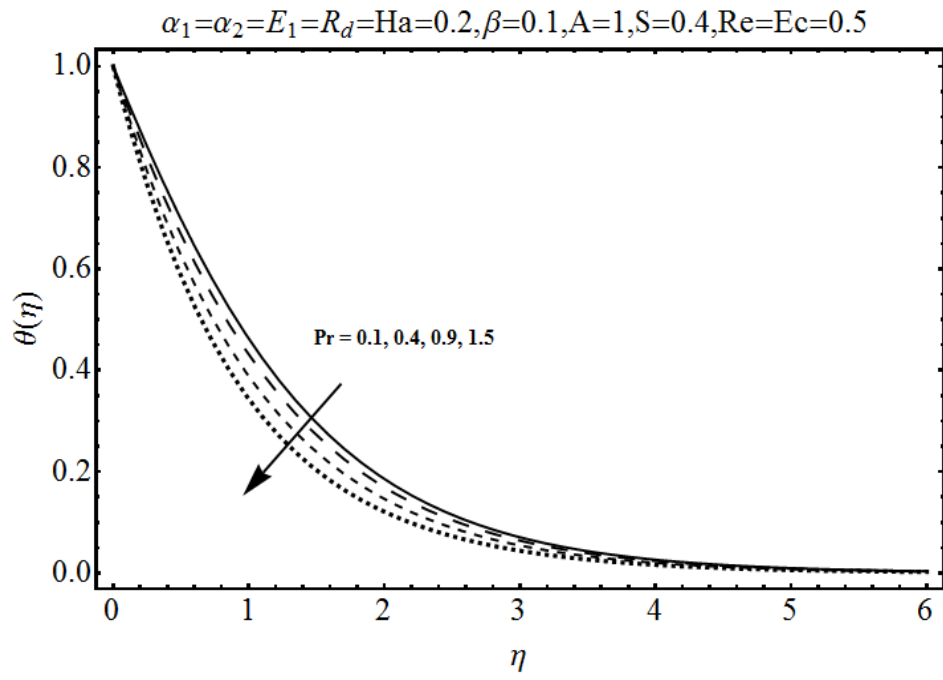
Fig. 6.19: Influence of Pr on $\theta(\eta)$.

$$\alpha_1 = \alpha_2 = E_1 = R_d = \text{Ha} = 0.2, \beta = 0.1, A = 1, S = 0.4, \text{Re} = 0.5, \text{Pr} = 1$$

Ec = 0, 0.5, 1, 1.5
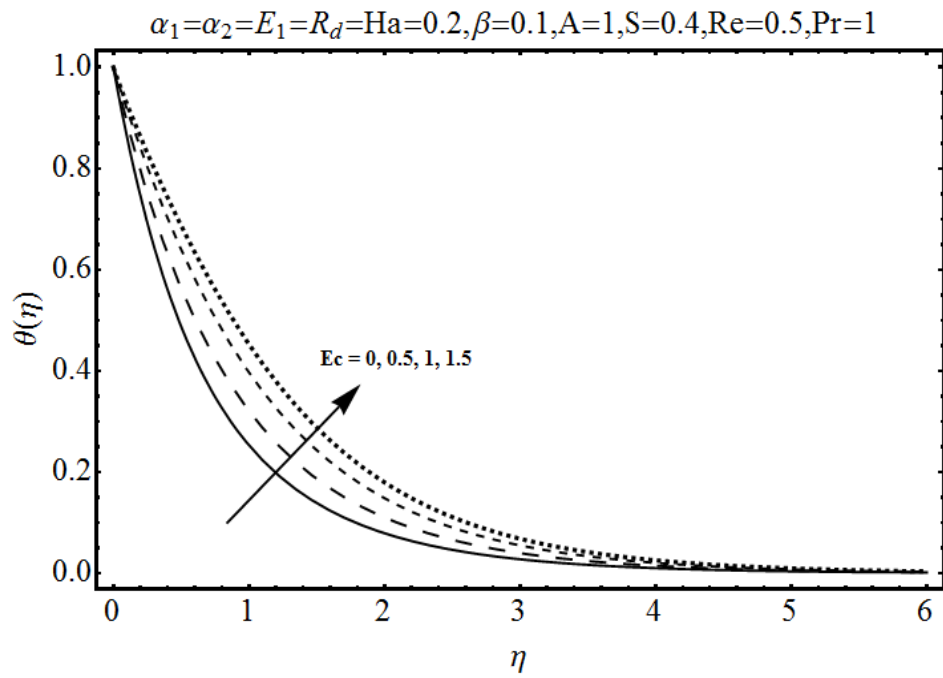
Fig. 6.20: Influence of Ec on $\theta(\eta)$.
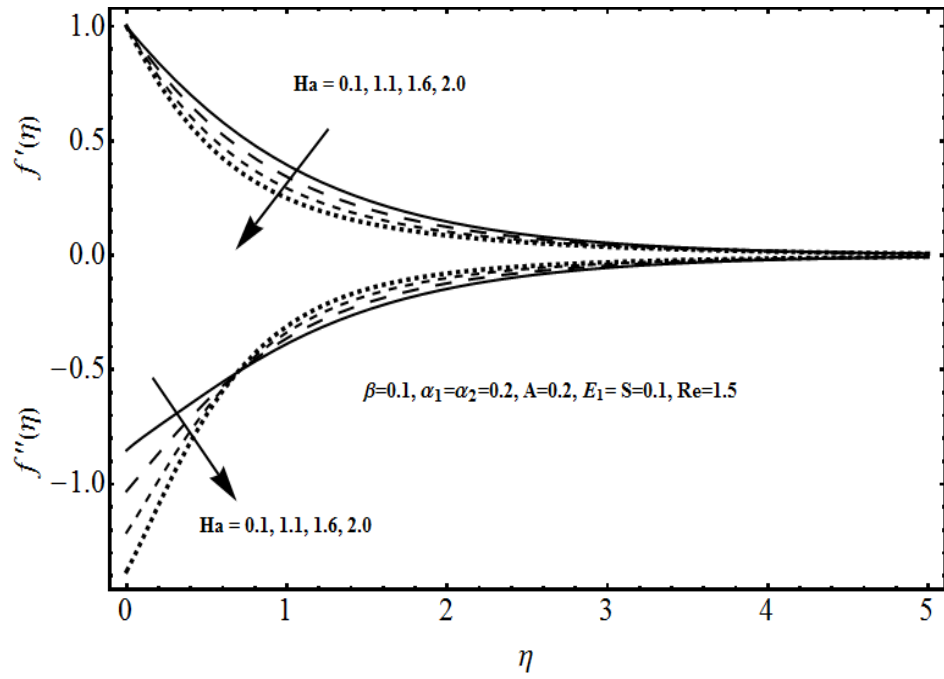
Fig. 6.21: Variations of $f'(\eta)$ and $f''(\eta)$ with η for several values of Hartman number Ha.
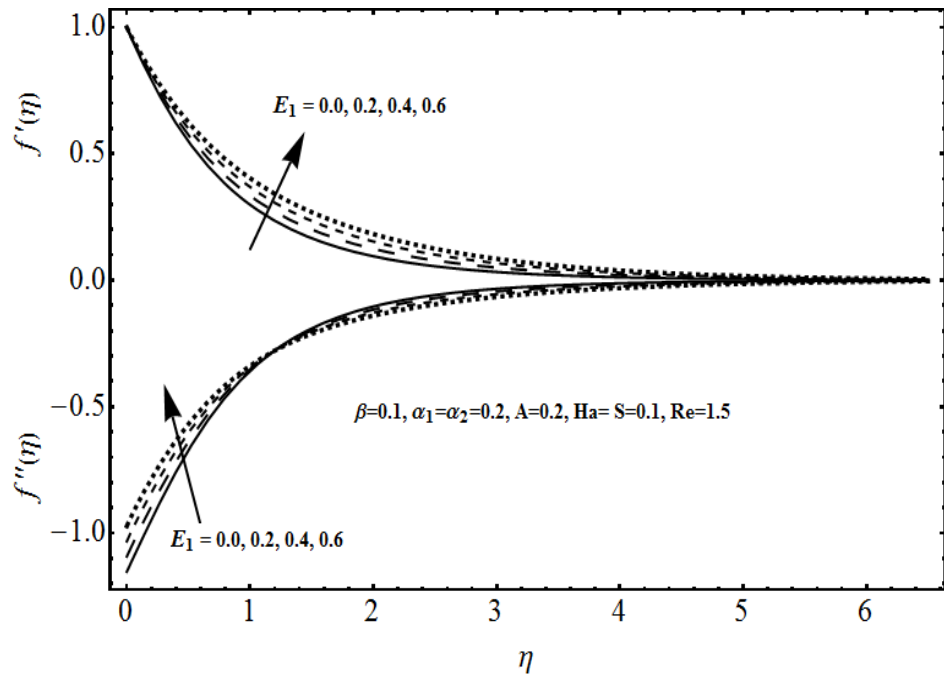
Fig. 6.22: Variations of $f'(\eta)$ and $f''(\eta)$ with η for several values of electric parameter E_1.

Table 6.1: Convergence of homotopy solutions when $\alpha_1 = 0.2$, $\beta = 0.5$, $\alpha_2 = 0.2$, $S = 0.2$, $A = 0.5$, $E_1 = 0.3$, $\mathrm{Re} = 0.7$, $R_1 = 0.3$, $Ha = 0.1$, $\mathrm{Pr} = 1$, $Ec = 0.5$.

Order of approximation	$-f''(0)$	$-\theta'(0)$
1	1.0419	1.0059
2	1.0720	1.0079
5	1.1210	1.0041
10	1.1442	0.99450
12	1.1458	0.99211
14	1.1458	0.99051
40	1.1458	0.99051

Table 6.2: Numerical values of skin friction coefficients $Re_x^{1/2}C_f$ for different values of physical parameters.

α_1	α_2	β	S	Ha	E_1	Re	$-Re_x^{1/2}C_f$
0.00	0.1	0.2	0.5	0.1	0.3	0.7	1.453
0.10							1.532
0.14							1.567
0.1	0.0	0.2	0.5	0.1	0.3	0.7	1.600
	0.1						1.632
	0.2						1.668
0.1	0.1	0.0	0.5	0.1	0.3	0.7	1.433
		0.1					1.489
		0.2					1.532
0.1	0.1	0.2	0.5	0.1	0.3	0.7	1.532
			0.6				1.592
			0.7				1.670
0.1	0.1	0.2	0.5	0.1	0.3	0.7	1.532
				0.2			1.536
				0.3			1.545
0.01	0.01	0.2	0.5	0.1	0.5	0.7	1.492
					0.6		1.487
					0.7		1.482
0.1	0.1	0.2	0.5	0.1	0.3	0.7	1.532
						0.8	1.542
						0.9	1.551

Table 6.3: Numerical values of Nusselt number $\mathrm{Re}_x^{-1/2} Nu_x$ for different values of physical parameters

α_1	α_2	β	S	Ha	E_1	Re	R_d	Pr	Ec	$\mathrm{Re}_x^{-1/2} Nu_x$
0.0	0.2	0.2	0.5	0.1	0.3	0.7	0.3	1.0	0.5	1.668
0.1										1.689
0.2										1.706
0.1	0.0	0.2	0.5	0.1	0.3	0.7	0.3	1.0	0.5	1.660
	0.1									1.674
	0.2									1.689
0.1	0.2	0.0	0.5	0.1	0.3	0.7	0.3	1.0	0.5	1.683
		0.3								1.691
		0.4								1.731
0.1	0.2	0.2	0.5	0.1	0.3	0.7	0.3	1.0	0.5	1.689
			0.6							1.805
			0.7							1.920
0.1	0.2	0.2	0.5	0.1	0.3	0.7	0.3	1.0	0.5	1.689
				0.5						1.669
				0.8						1.638
0.1	0.2	0.2	0.5	0.5	1.0	0.7	0.3	1.0	0.5	1.938
					1.5					1.889
					2.0					1.780
0.1	0.2	0.2	0.5	0.1	0.3	0.7	0.3	1.0	0.5	1.689
						1.0				1.668
						1.5				1.652
0.1	0.2	0.2	0.7	0.1	0.5	0.5	0.3	1.0	0.5	1.920
							0.4			1.991
							0.5			2.060

6.5 Concluding remarks

Here the flow of third grade fluid and heat transfer in the presence of thermal radiation and Ohmic dissipation are examined. The graphs are prepared to study the influence of the pertinent flow parameters including the second grade parameter (α_1, α_2), third grade parameter β, unsteadiness parameter S, magnetic parameter Ha, electric field parameter E_1, Reynolds number Re, radiation parameter R_d, Prandtl number Pr and Eckert number Ec. The following observations hold:

- Effect of third grade parameter β is to increase the boundary layer thickness.

- Maximum velocity is attained for higher values of electric parameter E_1.

- Effect of suction parameter, unsteadiness parameter and Reynolds number on boundary layer thickness is similar in a qualitative sense.

- Effects of E_1 and Pr on temperature profile are quite opposite.

- The velocity field $f'(\eta)$ is decreasing function of Hartman number Ha.

- Magnitude of skin friction coefficient $\mathrm{Re}_x^{1/2} C_f$ is increasing function of α_1, α_2, β, S, Ha and Re.

- Electric parameter E_1 decreases the magnitude of skin friction coefficient.

Chapter 7

Mixed convection flow of third grade fluid with variable thermal conductivity

Present chapter concentrates on the analysis of mixed convective boundary layer flow of third-grade fluid with variable thermal conductivity. Thermal conductivity is taken temperature dependent. The flow is caused by an exponential stretching surface. The partial differential equations governing the flow and heat transfer have been reduced into the ordinary differential equations by the appropriate transformations. Convergent series solutions for the velocity and temperature are constructed. The variations of different parameters on the velocity and temperature fields are discussed. Numerical values of local skin friction coefficient and local Nusselt number are examined through tabular values.

7.1 Mathematical formulation

We investigated the two-dimensional mixed convection flow of an incompressible third-grade fluid past an exponentially stretching surface.Thermal conductivity of the fluid is taken variable. Thermal radiation and viscous dissipation effects are negligible. The flow and temperature are governed by the following expressions:

$$\frac{\partial u}{\partial x} + \frac{\partial v}{\partial y} = 0, \tag{7.1}$$

$$
\begin{aligned}
u\frac{\partial u}{\partial x} + v\frac{\partial u}{\partial y} &= \nu\frac{\partial^2 u}{\partial y^2} + \frac{\alpha_1^*}{\rho}\left[u\frac{\partial^3 u}{\partial x\partial y^2} + \frac{\partial u}{\partial x}\frac{\partial^2 u}{\partial y^2} + 3\frac{\partial u}{\partial y}\frac{\partial^2 v}{\partial y^2} + v\frac{\partial^3 u}{\partial y^3}\right] \\
&\quad + 2\frac{\alpha_2^*}{\rho}\frac{\partial u}{\partial y}\frac{\partial^2 v}{\partial y^2} + 6\frac{\beta_3}{\rho}\left(\frac{\partial u}{\partial y}\right)^2\frac{\partial^2 u}{\partial y^2} + g\beta_T\left(T - T_\infty\right),
\end{aligned}
\tag{7.2}
$$

$$u\frac{\partial T}{\partial x} + v\frac{\partial T}{\partial y} = \frac{1}{\rho c_p}\frac{\partial}{\partial y}\left[k(T)\frac{\partial T}{\partial y}\right], \tag{7.3}$$

with the boundary conditions

$$
\begin{aligned}
u\left(x,0\right) &= U_w(x) = U_0\exp\left(\frac{x}{l}\right),\ v(x,0) = 0,\ T(x,0) = T_w = T_\infty + T_0\exp\left(\frac{x}{l}\right), \\
u &\to 0, \quad T \to T_\infty \quad \text{as} \quad y \to \infty.
\end{aligned}
\tag{7.4}
$$

In the above expressions u and v are the velocity components in the $x-$ and $y-$ directions respectively, α_1^*, α_2^* and β_3 are the material parameters of fluid, ρ is the fluid density, σ is the electric charge density, K is the thermal conductivity which depends upon temperature, c_p is the specific heat, T_0 is the reference temperature and T_∞ is the ambient temperature. The temperature dependent thermal conductivity can be expressed as follows:

$$K\left(T\right) = k_\infty \left(1 + \epsilon \frac{T - T_\infty}{\Delta T}\right), \tag{7.5}$$

where k_∞ is the thermal conductivity far away from the plate and ϵ measures the thermal conductivity with temperature. Using Eq. (7.5), Eq. (7.3) reduces to

$$u\frac{\partial T}{\partial x} + v\frac{\partial T}{\partial y} = \frac{1}{\rho c_p}\frac{\partial}{\partial y}\left[k_\infty \left(1 + \epsilon \frac{T - T_\infty}{\Delta T}\right)\frac{\partial T}{\partial y}\right]. \tag{7.6}$$

The transformations can be put into the forms

$$\begin{aligned}
\eta &= \sqrt{\frac{U_0}{2\nu l}}\exp\left(\frac{x}{2l}\right)y, \ \psi = \sqrt{2\nu l U_0}f\left(\eta\right)\exp\left(\frac{x}{2l}\right), \\
u\left(x,y\right) &= U_0 \exp\left(\frac{x}{l}\right)f'\left(\eta\right), \ v\left(x,y\right) = -\sqrt{\frac{\nu U_0}{2l}}\exp\left(\frac{x}{2l}\right)\left[f\left(\eta\right) + \eta f'\left(\eta\right)\right], \\
\theta &= \frac{T - T_\infty}{T_0}, \ \eta = \sqrt{\frac{c}{\nu}}y,
\end{aligned} \tag{7.7}$$

where ν is the kinematic viscosity, U_0 the reference velocity and ψ the stream function. Using these transformations, Eq. (7.1) is identically satisfied and the other governing transformed equations become

$$\begin{aligned}
&f''' - 2\left(f'\right)^2 + ff'' + \alpha_1\left\{3f'f''' - ff^{(iv)} - 2\eta f''f''' - 9\left(f''\right)^2\right\} \\
&-\alpha_2\left\{3\left(f''\right)^2 + \eta f''f'''\right\} + 3\beta \operatorname{Re}\left(f''\right)^2 f''' + \lambda\theta = 0,
\end{aligned}$$

$$f'\left(0\right) = 1, \ f\left(0\right) = 0, \ f'\left(\infty\right) = 0, \tag{7.8}$$

$$\left(1 + \epsilon\,\theta\right)\theta'' + \epsilon\left(\theta'\right)^2 + \Pr\left(f\,\theta' - f'\,\theta\right) = 0, \tag{7.9}$$

$$\theta(0) = 1, \ \theta(\infty) = 0. \tag{7.10}$$

Here Pr denotes the Prandtl number, Re_x is the Reynolds number and λ is the mixed convection parameter. We define

$$\begin{aligned}
\alpha_1 &= \frac{U_0\alpha_1^*\exp\left(\frac{x}{l}\right)}{\mu l}, \ \alpha_2 = \frac{U_0\alpha_2^*\exp\left(\frac{x}{l}\right)}{\mu l}, \ \beta = \frac{U_0^2\beta_3\exp\left(\frac{2x}{l}\right)}{\mu l^2}, \\
\Pr &= \frac{\mu_0 c_p}{K}, \ \lambda = \frac{Gr}{\operatorname{Re}_x^2}, \ \operatorname{Re}_x = \frac{U_w l}{\nu}.
\end{aligned} \tag{7.11}$$

The expressions of skin friction coefficient C_f and the local Nusselt number Nu_x are

$$C_f = \frac{\tau_{xy}}{\rho\left(cx\right)^2}, \qquad Nu_x = \frac{xq_w}{K\left(T - T_\infty\right)}, \tag{7.12}$$

in which the wall skin friction (τ_{xy}) and the wall heat flux (q_w) are

$$\tau_{xy} = \left[\mu_0 \frac{\partial u}{\partial y} + \frac{\alpha_1^*}{\rho}\left(2\frac{\partial u}{\partial x}\frac{\partial u}{\partial y} + v\frac{\partial^2 u}{\partial y^2} + u\frac{\partial^2 u}{\partial x \partial y}\right) + 2\frac{\beta_3}{\rho}\left(\frac{\partial u}{\partial y}\right)^3\right]_{y=0}, \tag{7.13}$$

$$q_w = -K\left(\frac{\partial T}{\partial y}\right)_{y=0}. \tag{7.14}$$

Dimensionless expressions of skin friction coefficient and local Nusselt number are

$$(\text{Re}_x)^{1/2}\, C_f = \sqrt{2}\left[f'' + \alpha_1(\frac{7}{2}f'f'' - \frac{1}{2}ff''') + \beta f''^3\right]_{\eta=0}, \tag{7.15}$$

$$(\text{Re}_x)^{-1/2}\, Nu_x = -\sqrt{\frac{X}{2}}\,\theta'(0), \tag{7.16}$$

where $X = x/l$.

7.2   Homotopic solutions

The definitions of initial guess $f_0(\eta)$ and $\theta_0(\eta)$ and auxiliary linear operators $\mathcal{L}_f$ and $\mathcal{L}_\theta$ are

$$f_0(\eta) = 1 - \exp(-\eta), \qquad \theta_0(\eta) = \exp(-\eta), \tag{7.17}$$

$$\mathcal{L}_f\left[f(\eta)\right] = \frac{d^3 f}{d\eta^3} - \frac{df}{d\eta}, \qquad \mathcal{L}_\theta\left[\theta(\eta)\right] = \frac{d^2\theta}{d\eta^2} - \theta, \tag{7.18}$$

with

$$\mathcal{L}_f\left[C_{29} + C_{30}\exp(\eta) + C_{31}\exp(-\eta)\right] = 0, \tag{7.19}$$

$$\mathcal{L}_\theta\left[C_{32}\exp(\eta) + C_{33}\exp(-\eta)\right] = 0, \tag{7.20}$$

where $C_i\,(i = 29 - 33)$ are the constants.

7.2.1   Zeroth-order deformation problems

The zeroth-order deformation problems can be defined as follows:

$$(1-q)\,\mathcal{L}_f\left[\hat{f}(\eta, q) - f_0(\eta)\right] = q\hbar_f \mathcal{N}_f\left[\hat{f}(\eta, q)\right], \tag{7.21}$$

$$\hat{f}(0, q) = 0, \qquad \left.\frac{\partial \hat{f}(\eta, q)}{\partial \eta}\right|_{\eta=0} = 1, \qquad \left.\frac{\partial \hat{f}(\eta, q)}{\partial \eta}\right|_{\eta\to\infty} = 0, \tag{7.22}$$

$$(1-q)\,\mathcal{L}_\theta\left[\hat{\theta}(\eta, q) - \theta_0(\eta)\right] = q\hbar_\theta \mathcal{N}_\theta\left[\hat{\theta}(\eta, q), \hat{f}(\eta, q)\right], \tag{7.23}$$

$$\left.\hat{\theta}(\eta, q)\right|_{\eta=0} = 1, \qquad \left.\hat{\theta}(\eta, q)\right|_{\eta\to\infty} = 0, \tag{7.24}$$

in which $q \in [0, 1]$ and $\hbar_f \neq 0$, $\hbar_\theta \neq 0$ are the embedding and auxiliary parameters respectively. The non-linear operators $\mathcal{N}_f$ and $\mathcal{N}_\theta$ can be expressed in the forms:

$$
\mathcal{N}_f\left[f\left(\eta, q\right)\right] = \frac{\partial^3 \hat{f}}{\partial \eta^3} - 2\left(\frac{\partial \hat{f}}{\partial \eta}\right)^2 + f\frac{\partial^2 \hat{f}}{\partial \eta^2} + \alpha_1\left[3\frac{\partial \hat{f}}{\partial \eta}\frac{\partial^3 \hat{f}}{\partial \eta^3} - f\frac{\partial^4 \hat{f}}{\partial \eta^4} - 2\eta\frac{\partial^2 \hat{f}}{\partial \eta^2}\frac{\partial^3 \hat{f}}{\partial \eta^3} - 9\left(\frac{\partial^2 \hat{f}}{\partial \eta^2}\right)^2\right]
$$

$$
-\alpha_2\left[3\left(\frac{\partial^2 \hat{f}}{\partial \eta^2}\right)^2 + \eta\frac{\partial^2 \hat{f}}{\partial \eta^2}\frac{\partial^3 \hat{f}}{\partial \eta^3}\right] + 3\beta\left(\frac{\partial^2 \hat{f}}{\partial \eta^2}\right)^2\frac{\partial^3 \hat{f}}{\partial \eta^3} + \lambda\theta, \tag{7.25}
$$

$$
\mathcal{N}_\theta\left[\theta\left(\eta, q\right), f\left(\eta, q\right)\right] = \left(1 + \epsilon\,\theta\right)\frac{\partial^2 \hat{\theta}}{\partial \eta^2} + \epsilon\left(\frac{\partial \hat{\theta}}{\partial \eta}\right)^2 + \Pr\left(f\frac{\partial \hat{\theta}}{\partial \eta} - \theta\frac{\partial \hat{f}}{\partial \eta}\right). \tag{7.26}
$$

By Taylor series we arrive at

$$
\hat{f}\left(\eta, q\right) = f_0\left(\eta\right) + \sum_{m=1}^{\infty} f_m\left(\eta\right)q^m, \quad \hat{f}_m\left(\eta\right) = \frac{1}{m!}\frac{\partial^m f\left(\eta, q\right)}{\partial q^m}\bigg|_{q=0}, \tag{7.27}
$$

$$
\hat{\theta}\left(\eta, q\right) = \theta_0\left(\eta\right) + \sum_{m=1}^{\infty} \theta_m\left(\eta\right)q^m, \quad \hat{\theta}_m\left(\eta\right) = \frac{1}{m!}\frac{\partial^m \theta\left(\eta, q\right)}{\partial q^m}\bigg|_{q=0}. \tag{7.28}
$$

The convergence of the series (7.27) and (7.28) strictly based upon $\hbar_f$ and $\hbar_\theta$. The value of $\hbar_f$ and $\hbar_\theta$ are chosen in such a way that the series (7.27) and (7.28) are convergent at $q = 1$ and hence

$$
\hat{f}\left(\eta\right) = f_0\left(\eta\right) + \sum_{m=1}^{\infty} f_m\left(\eta\right), \tag{7.29}
$$

$$
\hat{\theta}\left(\eta\right) = \theta_0\left(\eta\right) + \sum_{m=1}^{\infty} \theta_m\left(\eta\right). \tag{7.30}
$$

7.2.2   mth-order deformation problems

The mth order deformation problems are given by the following relations

$$
\mathcal{L}_f\left[\hat{f}_m\left(\eta\right) - \chi_m\hat{f}_{m-1}\left(\eta\right)\right] = \hbar_f\mathcal{R}_m^f\left(\eta\right), \tag{7.31}
$$

$$
\hat{f}_m\left(0, q\right) = 0, \quad \frac{\partial \hat{f}_m\left(\eta, q\right)}{\partial \eta}\bigg|_{\eta=0} = 0, \quad \frac{\partial \hat{f}_m\left(\eta, q\right)}{\partial \eta}\bigg|_{\eta\to\infty} = 0, \tag{7.32}
$$

$$
\mathcal{L}_\theta\left[\hat{\theta}_m\left(\eta\right) - \chi_m\hat{\theta}_{m-1}\left(\eta\right)\right] = \hbar_\theta\mathcal{R}_m^\theta\left(\eta\right), \tag{7.33}
$$

$$
\hat{\theta}_m\left(\eta, q\right)\bigg|_{\eta=0} = 0, \quad \hat{\theta}_m\left(\eta, q\right)\bigg|_{\eta\to\infty} = 0, \tag{7.34}
$$

$$
\mathcal{R}_m^f\left(\eta\right) = f_{m-1}'''\left(\eta\right) - 2\sum_{k=0}^{m-1} f_{m-1-k}'f_k' + \sum_{k=0}^{m-1} f_{m-1-k}f_k'' + \alpha_1\sum_{k=0}^{m-1}\left[3f_{m-1-k}'f_m''' - f_{m-1-k}f_k^{(iv)}\right.
$$

$$
\left. -2\eta f_{m-1-k}''f_k''' - 9f_{m-1-k}''f_k''\right] + \alpha_2\sum_{k=0}^{m-1}\left[3f_{m-1-k}''f_k'' + \eta f_{m-1-k}''f_k'''\right]
$$

$$+3\beta \operatorname{Re} \sum_{k=0}^{m-1} f''_{m-1-k} \sum_{l=0}^{k} f''_{k-l} f'''_{l} + \lambda \theta_{m-1}, \tag{7.35}$$

$$\mathcal{R}^{\theta}_m(\eta) = \theta''_{m-1}(\eta) + \epsilon \sum_{k=0}^{m-1} \theta_{m-1-k} \theta''_k + \epsilon \sum_{k=0}^{m-1} \theta'_{m-1-k} \theta'_k + \operatorname{Pr} \sum_{k=0}^{m-1} \left(f_{m-1-k} \theta'_k - \theta_{m-1-k} f'_k \right). \tag{7.36}$$

The general solutions (f_m, θ_m) of the mth order in terms of special solutions (f^*_m, θ^*_m) are

$$f_m(\eta) = f^*_m + C_{29} + C_{30} \exp(\eta) + C_{31} \exp(-\eta), \tag{7.37}$$

$$\theta_m(\eta) = \theta^*_m + C_{32} \exp(\eta) + C_{33} \exp(-\eta), \tag{7.38}$$

where the arbitrary constants can be determined through the boundary conditions (7.32) and (7.34). The values of such arbitrary constants are

$$\begin{aligned} C_{31} &= C_{32} = 0, \qquad C_{30} = \left. \frac{\partial f^*_m(\eta)}{\partial \eta} \right|_{\eta=0}, \qquad C_{29} = -C_{30} - f^*_m(0), \\ C_{33} &= -\theta^*_m(0). \end{aligned} \tag{7.39}$$

7.3 Convergence of the homotopy solutions

The convergence of series solutions (7.27) and (7.28) depends upon the auxiliary parameters $\hbar_f$ and $\hbar_\theta$ which are used to control the convergence of the series solutions. We have plotted the $\hbar$-curves to select the admissible value of auxiliary parameters $\hbar_f$ and $\hbar_\theta$ (see Fig. 7.1). The $\hbar$-curves are sketched at 18th order of approximation for velocity and temperature field in Fig. 7.1. It is found that the suitable ranges of $\hbar_f$ and $\hbar_\theta$ are $-1.43 \leq \hbar_f < -0.3$ and $-1.3 \leq \hbar_\theta < -0.3$.

7.4 Results and discussion

In order to have an insight for the effects of all the physical parameters on the velocity and temperature profiles, we have prepared the Figs. 7.2-7.19. Table 7.2 presents the variation of skin friction coefficient $\operatorname{Re}_x^{1/2} C_f$ and the local Nusselt number $\operatorname{Re}_x^{-1/2} Nu_x$ for various considered parameters. Figs. 7.2 and 7.3 are plotted to see the influences of velocity profile $f'(\eta)$ and temperature profile $\theta(\eta)$ for various values of third grade parameter β respectively. Fig. 7.2 shows that an increase in third grade parameter β enhances the velocity $f'(\eta)$ and associated boundary layer thickness. Temperature field $\theta(\eta)$ and the thermal boundary layer decrease for third grade parameter β in Fig. 7.3. The behavior of second grade parameter α_1 on the velocity and temperature profiles are presented in the Figs. 7.4 and 7.5. It is noted that the velocity and temperature profiles increase with the increase of second grade parameter α_1. Further the momentum and thermal boundary layers are increased for increasing values of α_1. Fig. 7.6 illustrates the behavior of second grade parameter α_2 on the velocity profile $f'(\eta)$. An increase in α_2 enhances the velocity profile $f'(\eta)$. Similar behavior is shown in Fig. 7.7 for temperature profile $\theta(\eta)$. Influence of mixed convection parameter λ on velocity profile $f'(\eta)$ is plotted in Fig. 7.8. It is

clearly seen that larger values of λ increase the velocity and the boundary layer thickness. Larger mixed convection parameter λ corresponds to the stronger effects of the buoyancy forces. Thus it yields an increase in flow velocity. Fig. 7.9 shows the effects of mixed convection parameter λ on the temperature field $\theta(\eta)$. It is observed that both temperature and thermal boundary layer decrease by increasing λ. It is evident from Fig. 7.10 that the velocity enhances through increase in small parameter of thermal conductivity ϵ. When ϵ increases then thermal conductivity of fluid increases. Hence the velocity of the particles increases which enhances the fluid velocity. Same trend is seen for the temperature profile which increases with increasing ϵ (see Fig. 7.11). Thermal conductivity increases with the increase of ϵ (so heat is transferred more rapidly through the fluid molecules). Thus temperature profile increases. Fig. 7.12 draws the velocity profile for various values of Prandtl number. Effect of increasing Prandtl number Pr is to decrease the velocity at a point in the flow field. There is thinning of the boundary layer. Fig. 7.13 represents the graph of the temperature profile for different values of Prandtl number Pr. This Fig. depicts that the effects of increasing Prandtl number Pr is to decrease the temperature throughout the boundary layer which results in decrease of the thermal boundary layer thickness. The Prandtl number is the ratio of momentum diffusivity to thermal diffusivity. Thus with the increase of Prandtl number, thermal diffusivity decreases, that is heat diffuses with slow rate. Therefore temperature profile decreases. Fig. 7.14 illustrates the effect of Reynolds number Re on the velocity profile $f'(\eta)$. An increase in Re enhances the velocity profile $f'(\eta)$. Opposite behavior is noted in Fig. 7.15 for temperature profile $\theta(\eta)$. Fig. 7.16 displays the effects of third grade parameter β on the velocity and shear stress. Here velocity profile is increasing function of β whereas the shear stress increases near the wall and away from the wall it decreases. Variations of velocity $f'(\eta)$ and $f''(\eta)$ for several values of mixed convection parameter λ are shown in Fig. 7.17. With increasing the values of λ, the horizontal velocity is found to increase the favorable flow. It is noted that λ greatly effects the solutions. The $f''(\eta)$ increases for $0 \leq \eta \leq 1$ otherwise it shows opposite behavior. The variations of temperature $\theta(\eta)$ and temperature gradient $\theta'(\eta)$ for various values of third grade parameter β are shown in Fig. 7.18. It is noted that the temperature profile decreases for an increase in third grade parameter β. However the temperature gradient decreases near the wall for $0 \leq \eta \leq 1$ while it increases for β. Fig. 7.19 demonstrates the effect of mixed convection parameter λ on the temperature and temperature gradient. We observe that the temperature profile is decreased. The temperature gradient away from the wall is increasing while it decreases near the wall.

Table 7.1 shows the convergence of the series solutions for velocity and temperature. It is noted that 15th order of approximations are sufficient for the convergence of the required equations. Table 7.2 represents the numerical values of skin friction coefficient $\mathrm{Re}_x^{1/2} C_f$ and the local Nusselt number $\mathrm{Re}_x^{-1/2} Nu_x$ respectively. From Table 7.2, it can be seen that the values of $\mathrm{Re}_x^{1/2} C_f$ decrease for third grade parameter β and mixed convection parameter λ. The opposite phenomenon is observed for $\mathrm{Re}_x^{-1/2} Nu_x$ (as can be seen from Table 7.2). Increasing the values of second grade parameters α_1, α_2 and the Prandtl number Pr increased $\mathrm{Re}_x^{1/2} C_f$ and the opposite trend is observed for second grade parameter α_1, α_2 on $\mathrm{Re}_x^{-1/2} Nu_x$. From Table 7.2 it is also concluded that the absolute values of $\mathrm{Re}_x^{1/2} C_f$ decrease as the thermal conductivity parameter ϵ increases. Similar phenomenon is noted for $\mathrm{Re}_x^{-1/2} Nu_x$.

$\alpha_1=0.1, \alpha_2=0.2,\ \beta=0.1, \epsilon=0.5, \lambda=0.2, Re=0.1, Pr=2$
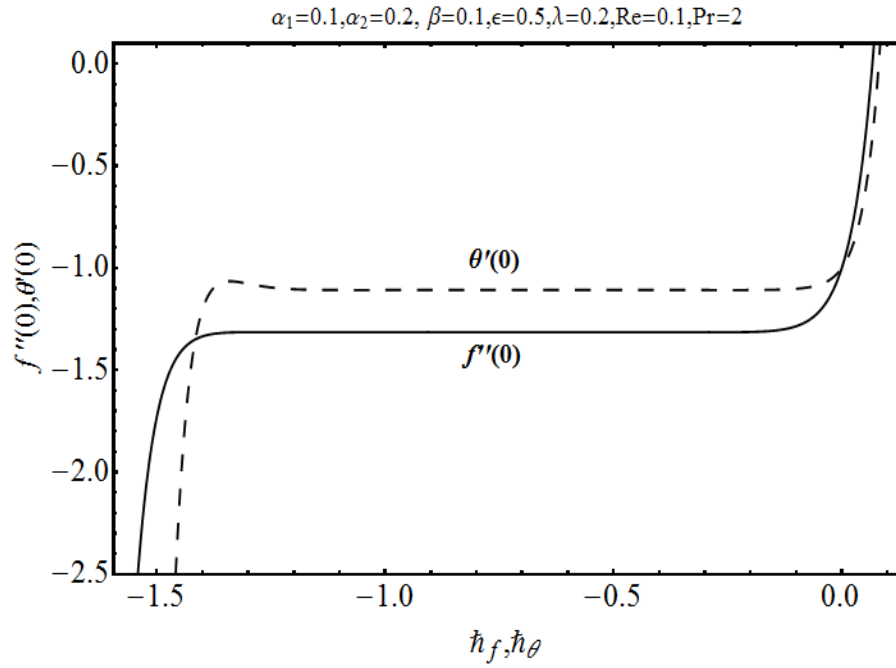
Fig. 7.1: $\hbar-$curves for the functions of $f(\eta)$ and $\theta(\eta)$ at 18th order of approximation.

$\alpha_1=0.3, \alpha_2=\epsilon=0.2, Pr=1, Re=1.2, \lambda=0.1$
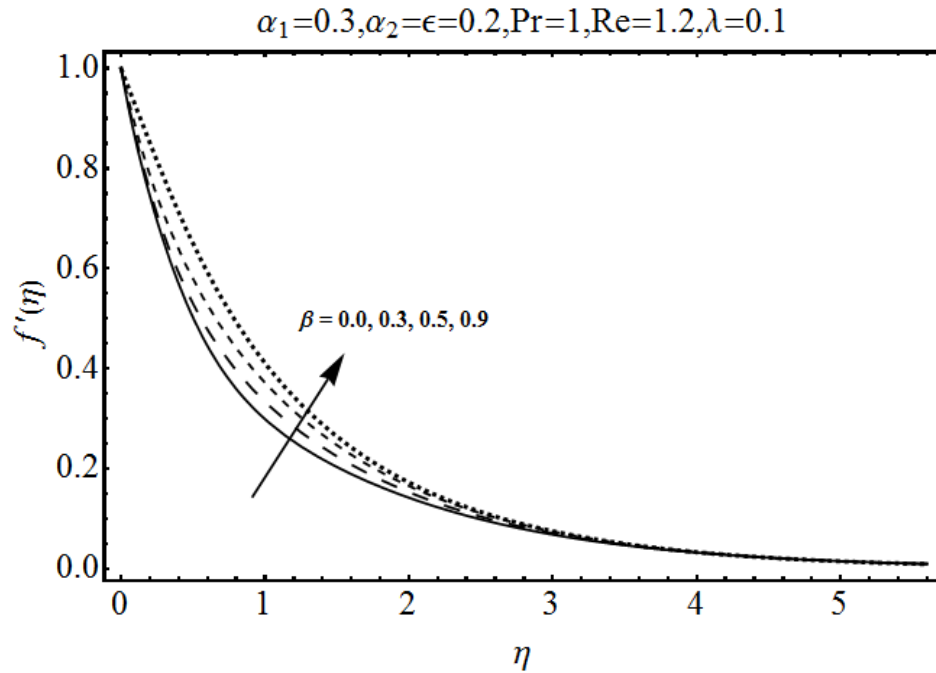
Fig. 7.2: Variation of velocity component $f'(\eta)$ for various values of third grade parameter β.
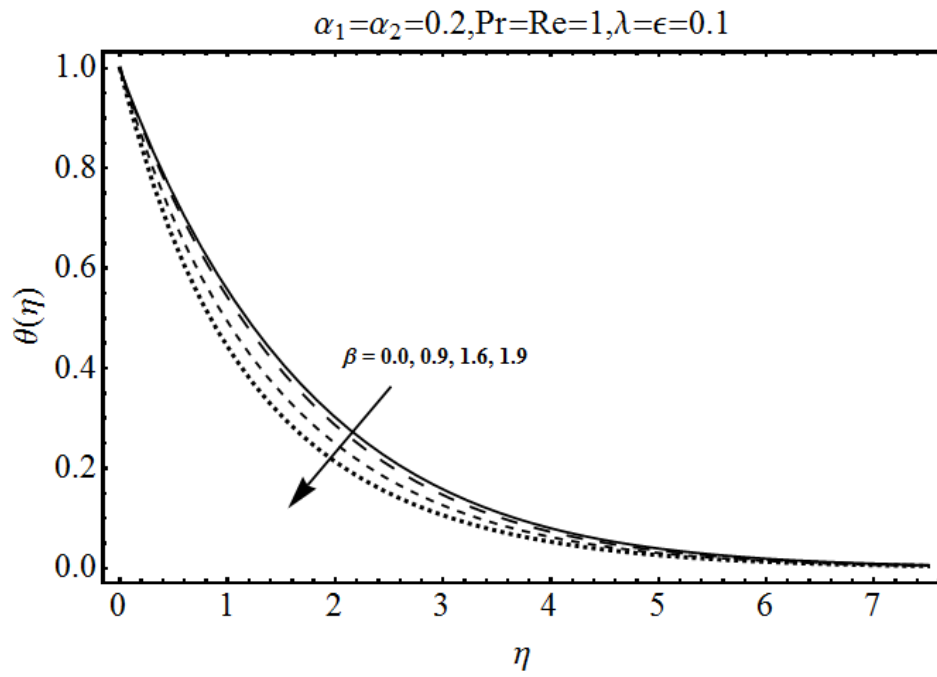
Fig. 7.3: Variation of temperature profile $\theta(\eta)$ for various values of third grade parameter β.
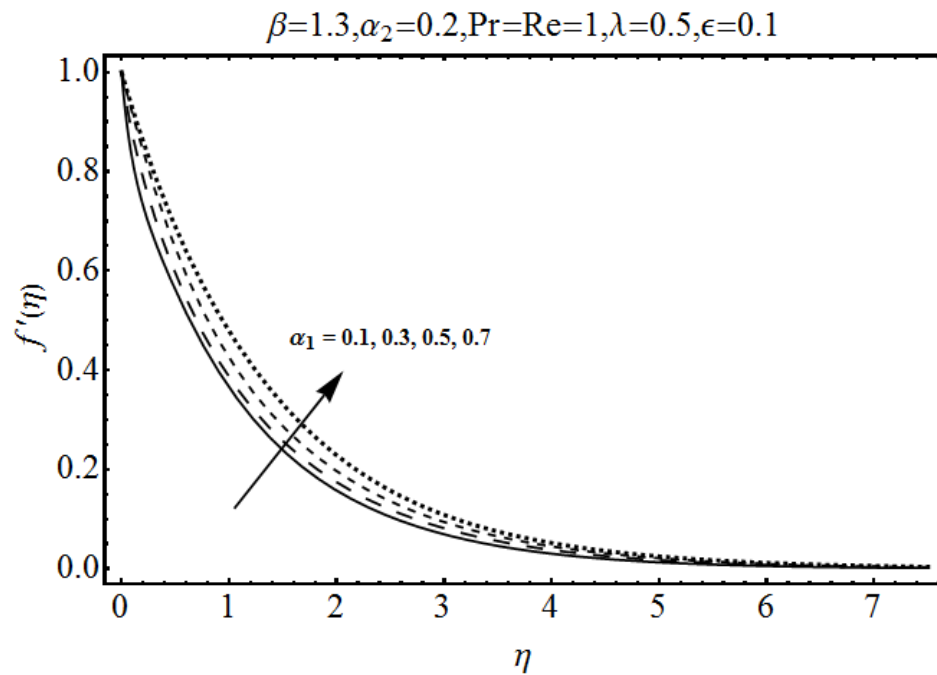
Fig. 7.4: Variation of velocity component $f'(\eta)$ for various values of second grade parameter α_1.
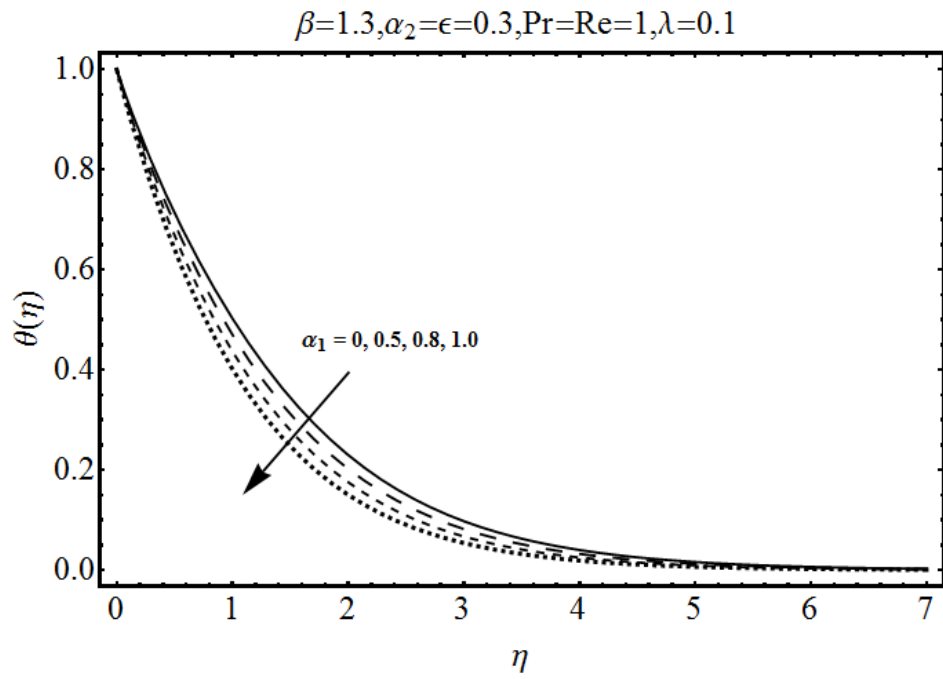
Fig. 7.5: Variation of temperature profile $\theta(\eta)$ for various values of second grade parameter α_1.
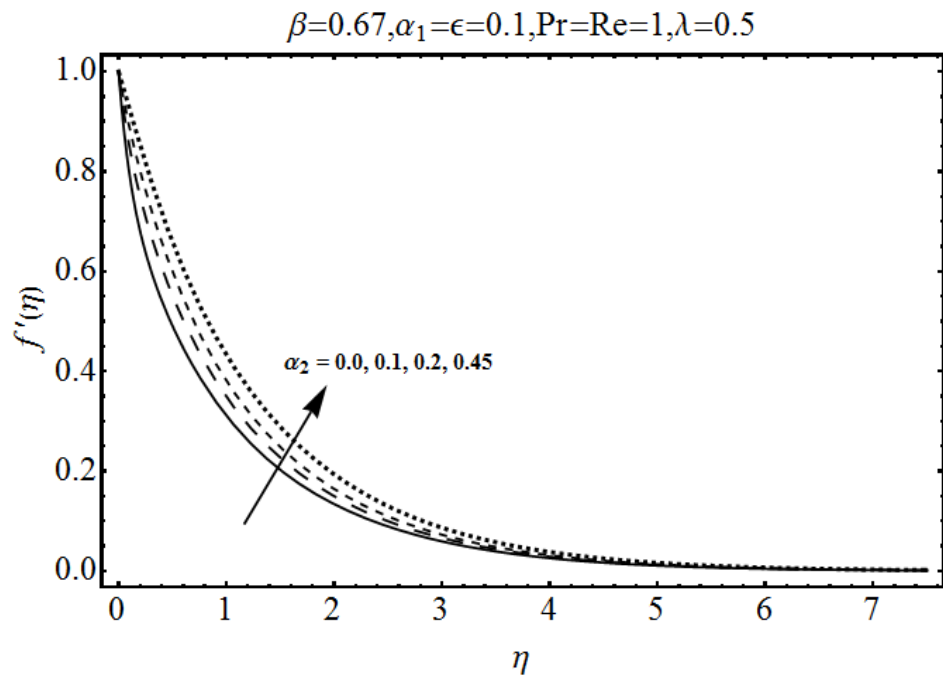
Fig. 7.6: Variation of velocity component $f'(\eta)$ for various values of second grade parameter α_2.
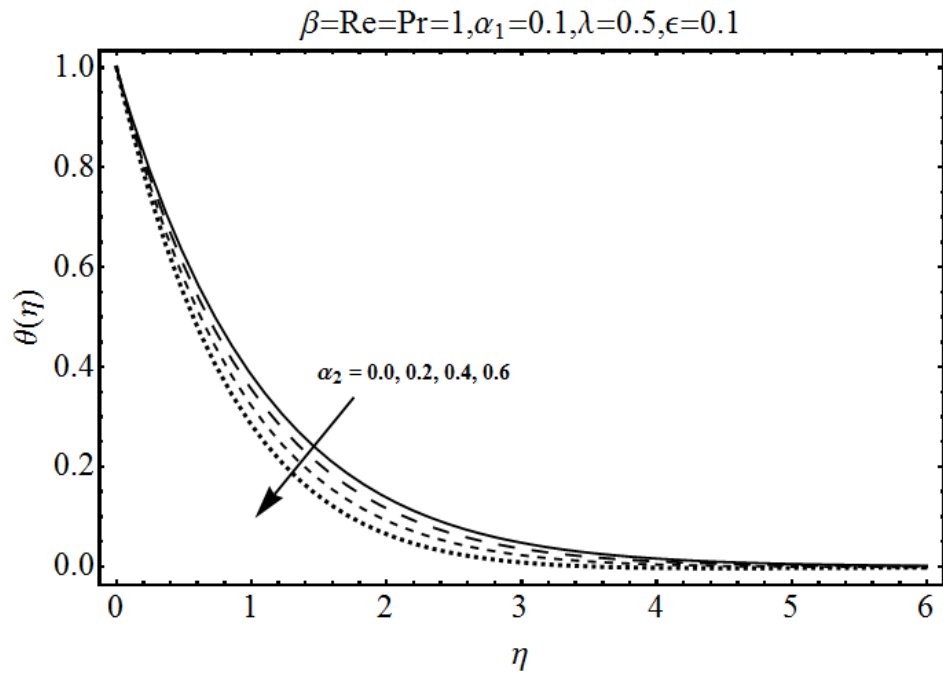
Fig. 7.7: Variation of temperature profile $\theta(\eta)$ for various values of second grade parameter α_2.
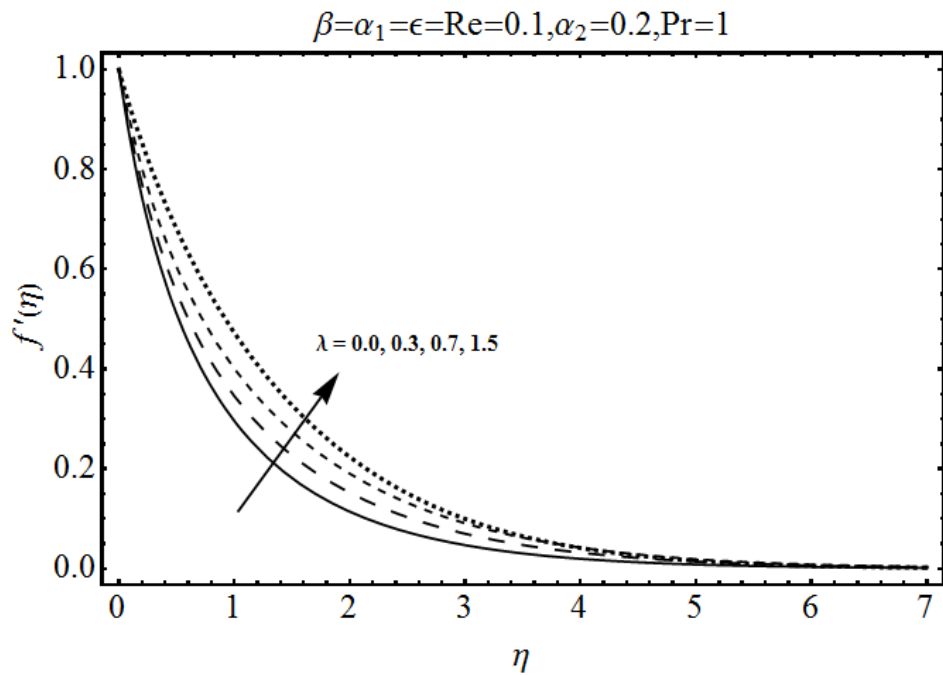
Fig. 7.8: Variation of velocity component $f'(\eta)$ for various values of mixed convection parameter λ.
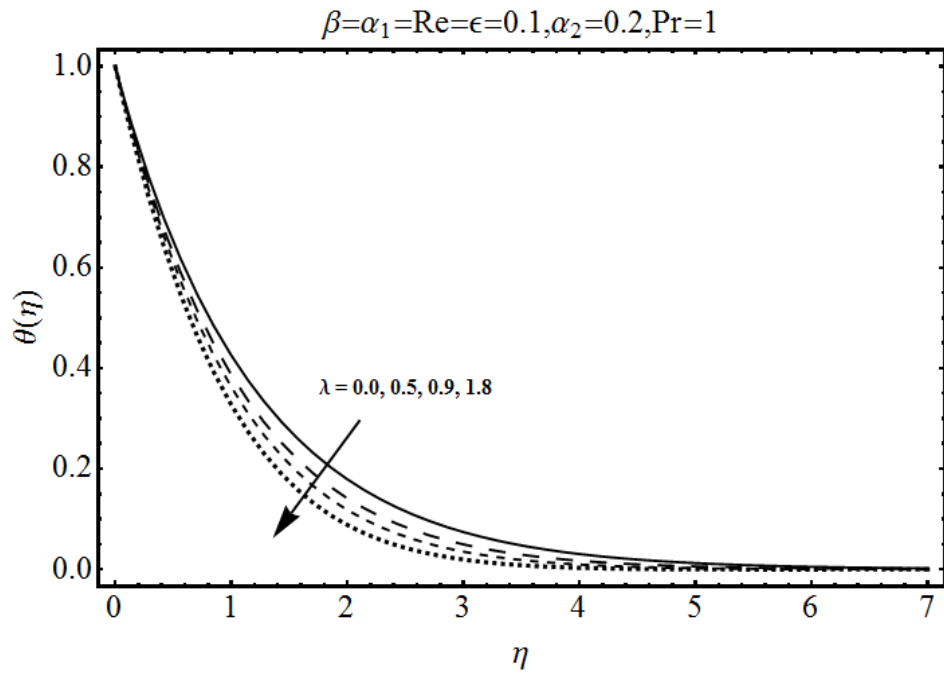
Fig. 7.9: Variation of temperature profile $\theta\left(\eta\right)$ for various values of mixed convection parameter λ.
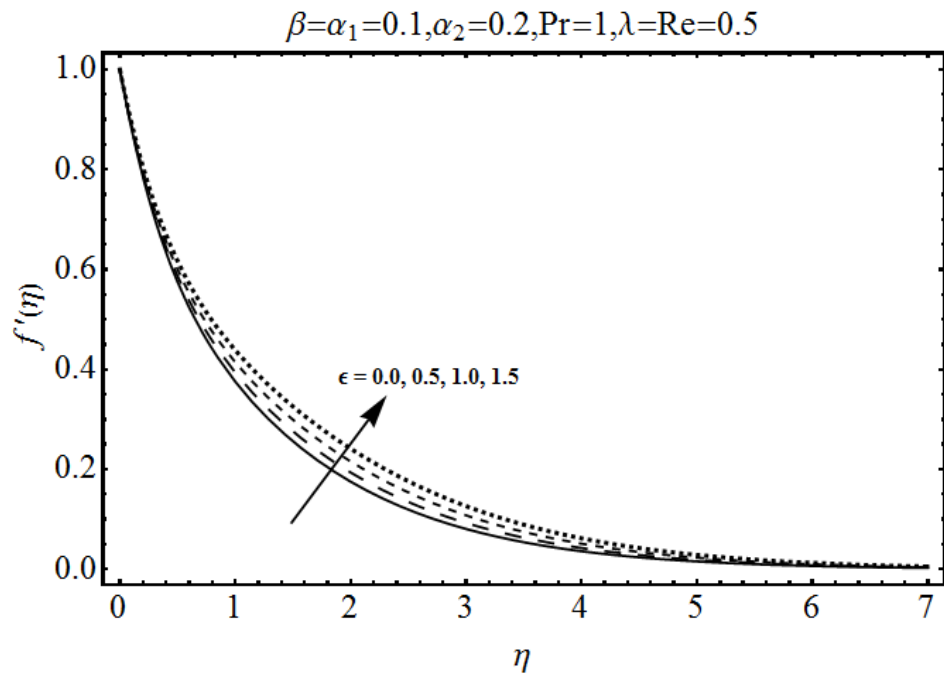
Fig. 7.10: Variation of velocity component $f'\left(\eta\right)$ for various values of small parameter ϵ.
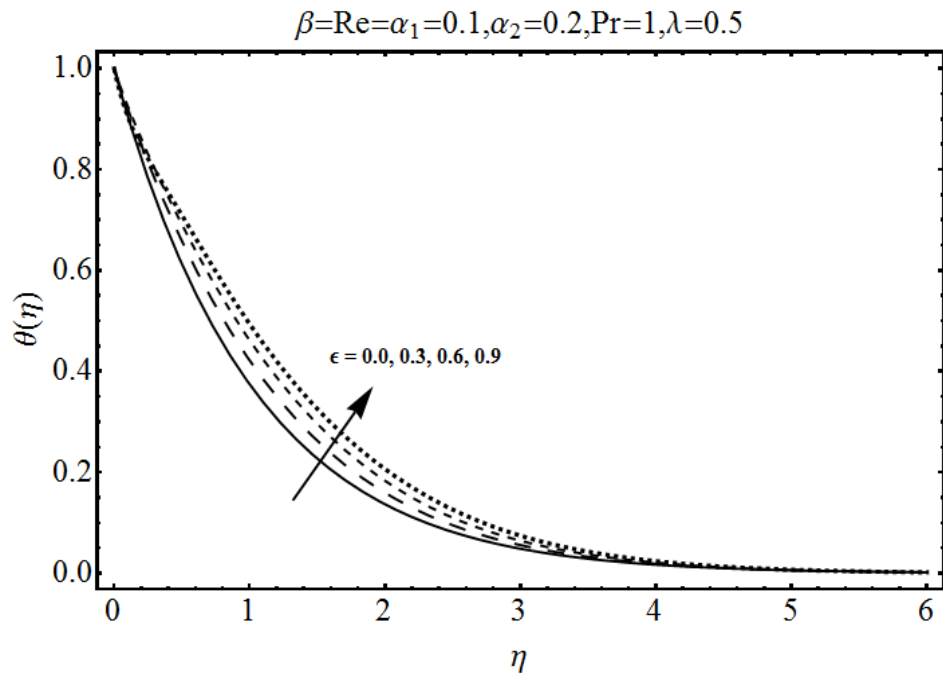
Fig. 7.11: Variation of temperature profile $\theta\left(\eta\right)$ for various values of small parameter ϵ.
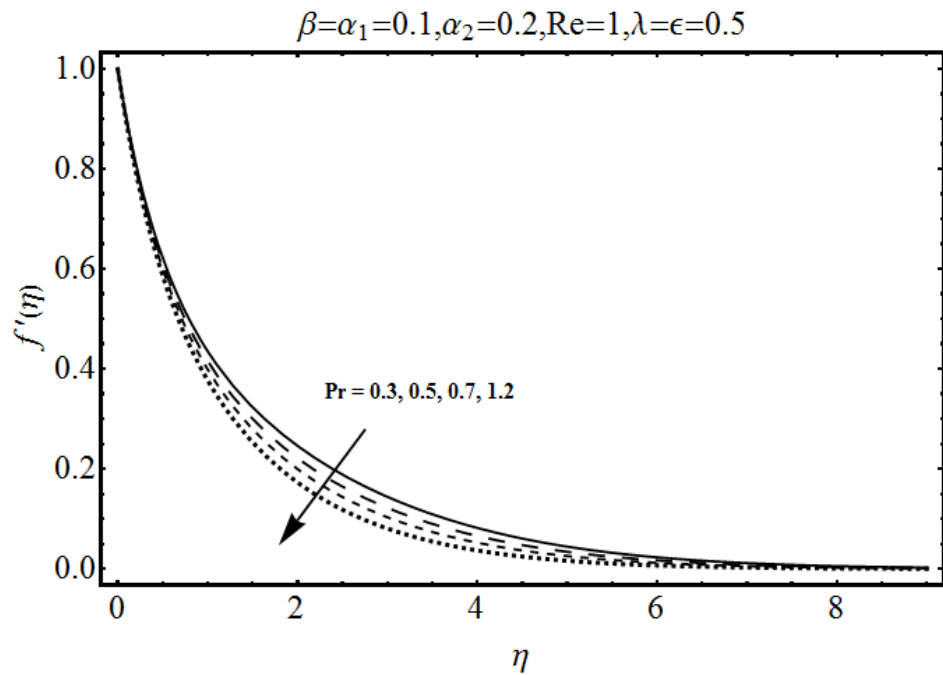
Fig. 7.12: Variation of velocity component $f'\left(\eta\right)$ for various values of Prandtl number Pr.
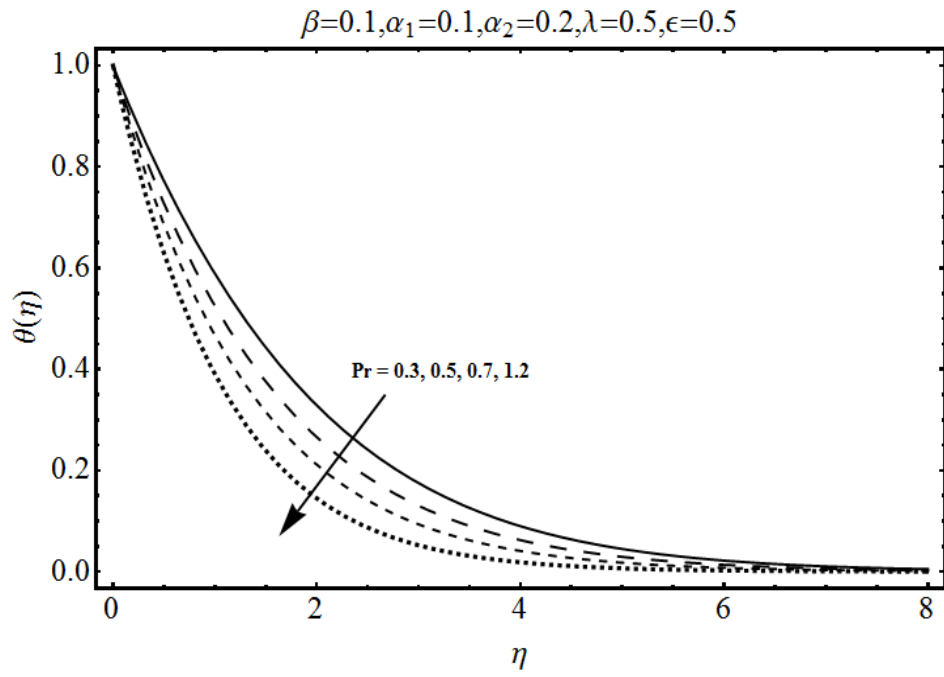
Fig. 7.13: Variation of temperature profile $\theta(\eta)$ for various values of
Prandtl number Pr.
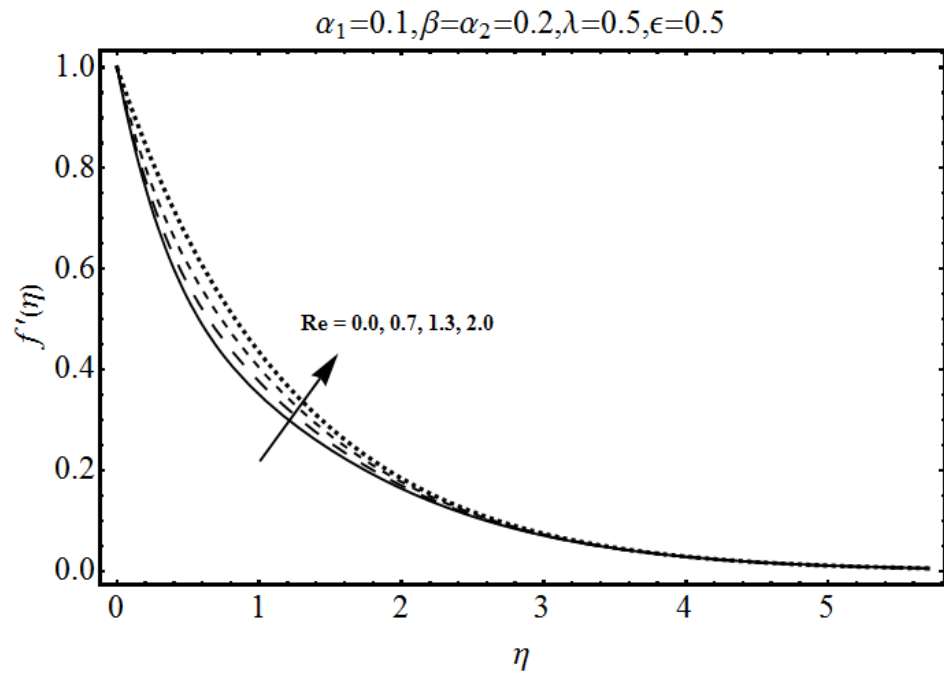
Fig. 7.14: Variation of velocity component $f'(\eta)$ for various values of
Reynold number Re.
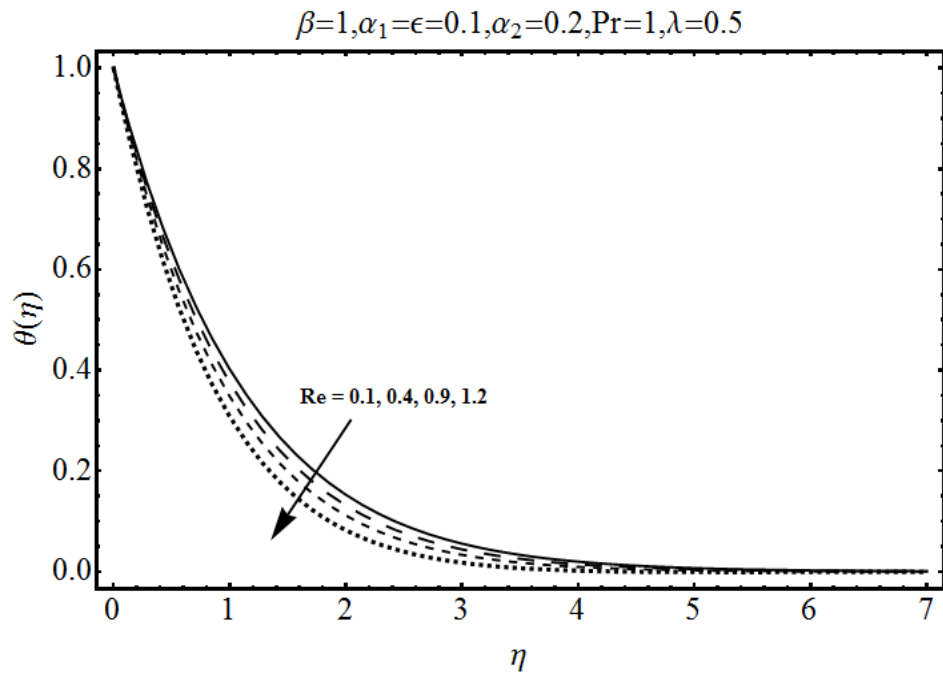
Fig. 7.15: Variation of temperature profile $\theta(\eta)$ for various values of Reynold number Re.
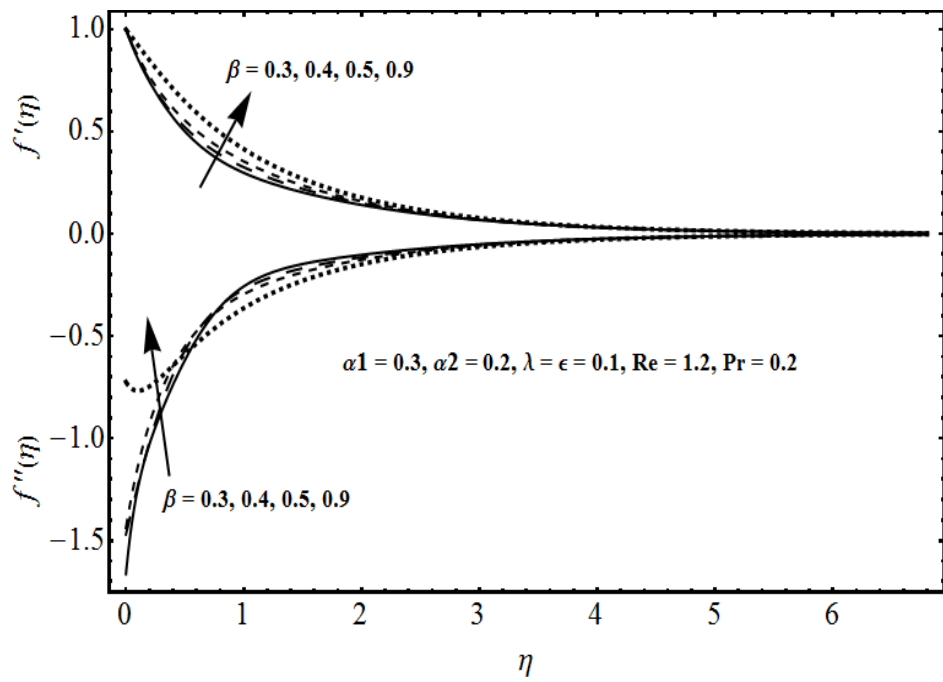
Fig. 7.16: Variation of velocity $f'(\eta)$ and $f''(\eta)$ for several values of third grade parameter β.
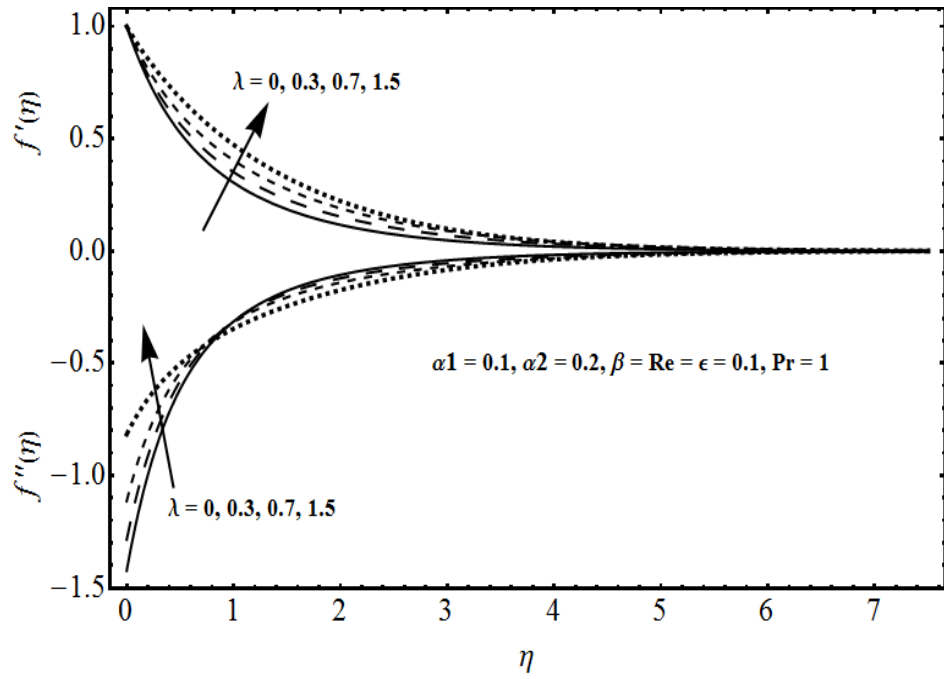
Fig. 7.17: Variation of velocity $f'(\eta)$ and $f''(\eta)$ for several values of mixed convection parameter λ.
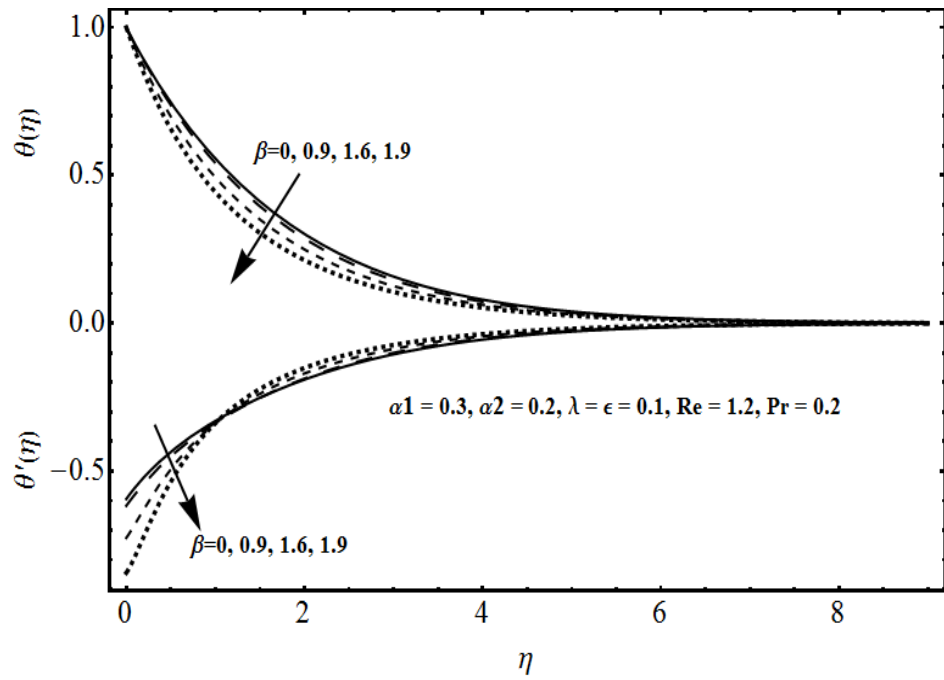
Fig. 7.18: Variation of temperature $\theta(\eta)$ and temperature gradient $\theta'(\eta)$ for several values of third grade parameter β.
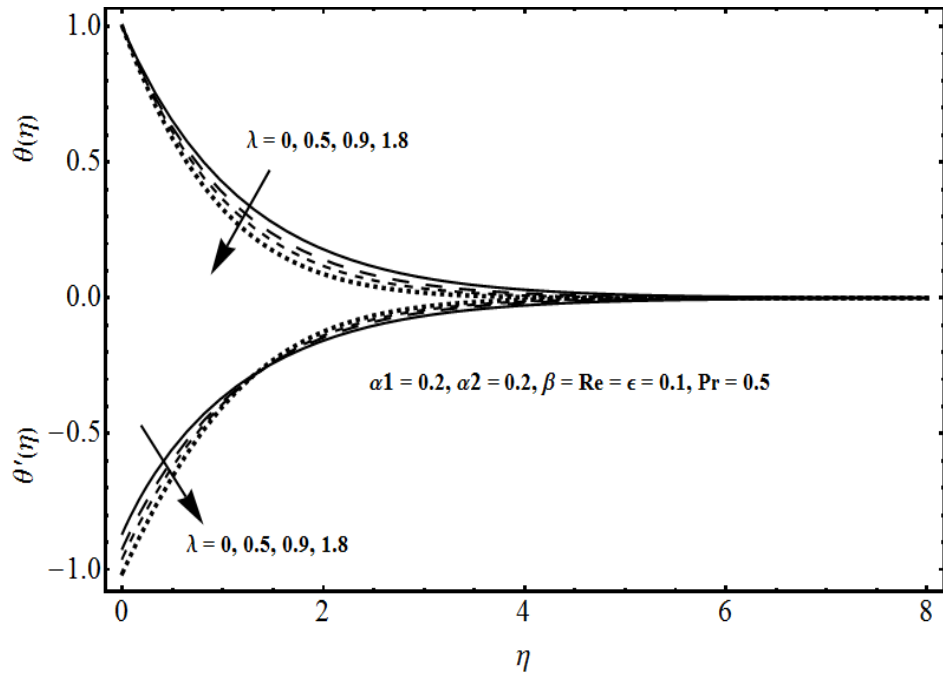
Fig. 7.19: Variation of temperature $\theta\left(\eta\right)$ and temperature gradient $\theta'\left(\eta\right)$ for several values of mixed convection parameter λ.

Table 7.1: Convergence of HAM solutions for different order of approximation when $\alpha_1 = 0.06$, $\alpha_2 = 0.05$, $\beta = 0.1$, $\lambda = 0.2$, $\epsilon = 0.5$, and $\mathrm{Pr} = 2$.

Order of approximation	$-f''\left(0\right)$	$-\theta'\left(0\right)$
1	1.1468	1.0667
2	1.2252	1.0898
5	1.3015	1.1052
8	1.3134	1.1081
15	1.3153	1.1079
20	1.3153	1.1079
30	1.3153	1.1079
50	1.3153	1.1079

Table 7.2: Numerical values of skin friction coefficient and local Nusselt number for different values of physical parameters.

α_1	α_2	β	λ	ϵ	Pr	$-\mathrm{Re}_x^{1/2}\,C_f$	$\mathrm{Re}_x^{-1/2}\,Nu_x$
0.1	0.1	0.3	0.2	0.5	2	2.793	1.125
0.2						3.629	1.120
0.3						4.494	1.117
0.1	0.1	0.3	0.2	0.5	2	2.793	1.125
	0.2					2.965	1.118
	0.3					3.151	1.112

123

α_1	α_2	β	λ	ϵ	Pr	$-\operatorname{Re}_x^{1/2} C_f$	$\operatorname{Re}_x^{-1/2} Nu_x$
0.1	0.1	0.1	0.2	0.5	2	3.143	1.111
		0.2				2.948	1.119
		0.3				2.793	1.125
0.1	0.1	0.3	0.2	0.5	2	2.793	1.125
			0.3			2.711	1.131
			0.4			2.633	1.137
0.1	0.1	0.3	0.2	0.5	2	2.793	1.125
				0.6		2.788	1.077
				0.7		2.783	1.033
0.1	0.1	0.3	0.2	0.5	2	2.793	1.125
					2.1	2.798	1.159
					2.2	2.802	1.192

7.5 Concluding remarks

Effect of variable thermal conductivity in mixed convection flow of third grade fluid past an exponential stretching surface is addressed. The main outcomes of the presented analysis are listed below.

- The skin friction coefficient increases with an increase in the dimensionless parameters, the second grade parameters α_i $(i = 1, 2)$ and the Prandtl number Pr while it decreases for larger third grade parameter β and the mixed convection parameter λ.

- The Nusselt number $\operatorname{Re}_x^{-1/2} Nu_x$ increases with an increase in the third grade parameter β and the mixed convection parameter λ while it decreases when second grade parameters α_i $(i = 1, 2)$ and the Prandtl number Pr are increased.

- Behaviors of third grade parameter β on the velocity and temperature profiles are quite opposite.

- Influence of Pr is to decrease the temperature field $\theta(\eta)$.

- Table 1 ensures that the convergence of the solutions f and θ are obtained at only 15th order of approximation for velocity and 14th order of approximation for temperature.

- Behavior of second grade parameter α_1 on the velocity $f'(\eta)$ and temperature $\theta(\eta)$ are quite reverse.

Chapter 8

Radiative MHD stagnation point flow of third-grade fluid over a stretching cylinder

In this chapter, magnetohydrodynamic (MHD) stagnation point flow of third-grade fluid due to a stretching cylinder is studied. Thermal radiation effects are considered in the analysis of heat transfer phenomenon. Joule heating and viscous dissipation effects are also retained. The resulting nonlinear system is computed for the series solutions. Influence of various physical parameters on the velocity and temperature profiles are scrutinized graphically. Comparison between Newtonian and third-grade fluids is made. Velocity and temperature profiles in the presence/absence of stagnation point are discussed graphically. Numerical values of skin friction and Nusselt number are also computed and interpreted.

8.1   Mathematical formulation

Consider magnetohydrodynamic stagnation point flow of an electrically conducting third-grade fluid due to a stretching cylinder. Heat transfer is analyzed in the presence of Joule heating, thermal radiation and viscous dissipation effects. Cylindrical coordinates are chosen in such a way that $z-$axis is along the axis of stretching cylinder and $r-$axis normal to it. Under the boundary layer approximations (i.e., $u = O(\delta)$, $r = O(\delta)$, $w = O(1)$ and $z = O(1)$) the laws of conservation of mass and momentum give

$$\frac{\partial u}{\partial r} + \frac{u}{r} + \frac{\partial w}{\partial z} = 0, \tag{8.1}$$

$$
\begin{aligned}
u\frac{\partial w}{\partial r} + w\frac{\partial w}{\partial z} &= W_e\frac{dW_e}{dz} + \nu\left(\frac{\partial^2 w}{\partial r^2} + \frac{1}{r}\frac{\partial w}{\partial r}\right) + \frac{\alpha_1^*}{\rho}\left[\frac{w}{r}\frac{\partial^2 w}{\partial r\partial z} + \frac{u}{r}\frac{\partial^2 w}{\partial r^2} + \frac{3}{r}\frac{\partial w}{\partial r}\frac{\partial w}{\partial z}\right. \\
&\quad + \frac{1}{r}\frac{\partial u}{\partial r}\frac{\partial w}{\partial r} + 4\frac{\partial w}{\partial r}\frac{\partial^2 w}{\partial r\partial z} + w\frac{\partial^3 w}{\partial r^2\partial z} + 2\frac{\partial u}{\partial r}\frac{\partial^2 w}{\partial r^2} \\
&\quad \left. + u\frac{\partial^3 w}{\partial r^3} + 3\frac{\partial^2 w}{\partial r^2}\frac{\partial w}{\partial z} + \frac{\partial^2 u}{\partial r^2}\frac{\partial w}{\partial r}\right] + \frac{\alpha_2^*}{\rho}\left[\frac{2}{r}\frac{\partial u}{\partial r}\frac{\partial w}{\partial r} + \frac{2}{r}\frac{\partial w}{\partial r}\frac{\partial w}{\partial z}\right.
\end{aligned}
$$

$$+2\frac{\partial^2 u}{\partial r^2}\frac{\partial w}{\partial r}+2\frac{\partial u}{\partial r}\frac{\partial^2 w}{\partial r^2}+2\frac{\partial^2 w}{\partial r^2}\frac{\partial w}{\partial z}+4\frac{\partial w}{\partial r}\frac{\partial^2 w}{\partial r\partial z}\Big]$$

$$+\frac{\beta_3^*}{\rho}\left[\frac{2}{r}\left(\frac{\partial w}{\partial r}\right)^3+6\left(\frac{\partial w}{\partial r}\right)^2\frac{\partial^2 w}{\partial r^2}\right]+\frac{\sigma B_0^2}{\rho}\left(W_e-w\right), \tag{8.2}$$

$$
u\frac{\partial T}{\partial r}+w\frac{\partial T}{\partial z} = \frac{k}{\rho c_p}\left(\frac{\partial^2 T}{\partial r^2}+\frac{1}{r}\frac{\partial T}{\partial r}\right)+\frac{16\sigma^* T_\infty^3}{3k^*\rho c_p}\left(\frac{\partial^2 T}{\partial r^2}+\frac{1}{r}\frac{\partial T}{\partial r}\right)+\frac{\nu}{c_p}\left(\frac{\partial w}{\partial r}\right)^2
$$

$$+\frac{\alpha_1^*}{\rho c_p}\left[3\frac{\partial u}{\partial r}\left(\frac{\partial w}{\partial r}\right)^2+u\frac{\partial w}{\partial r}\frac{\partial^2 w}{\partial r^2}+w\frac{\partial w}{\partial r}\frac{\partial^2 w}{\partial r\partial z}+3\left(\frac{\partial w}{\partial r}\right)^2\frac{\partial w}{\partial z}\right]$$

$$+2\frac{\beta_3^*}{\rho c_p}\left(\frac{\partial w}{\partial r}\right)^4+\frac{\sigma B_0^2}{\rho c_p}\left(w-W_e\right)^2. \tag{8.3}$$

The subjected conditions can be mentioned as follows:

$$w\left(r,z\right)=W_w\left(z\right)=\frac{W_0 z}{l},\quad u\left(r,z\right)=0,\quad T\left(r,z\right)=T_\infty+b\left(\frac{z}{l}\right),\quad \text{at}\ \ r=R,$$

$$w\left(r,z\right)\longrightarrow W_e\left(z\right)=\frac{W_\infty z}{l},\quad T\left(r,z\right)\longrightarrow T_\infty,\quad \text{at}\ \ r\longrightarrow\infty. \tag{8.4}$$

In the above expressions u and w denote the velocity components in the r and z directions respectively, $(\alpha_1^*,\ \alpha_2^*$ and $\beta_3)$ the fluid parameters, ν the kinematic viscosity, ρ the density of fluid, W_0 and W_∞ are the reference velocities, l the characteristic length, T and T_∞ are the temperatures of the fluid and surrounding respectively, k the thermal conductivity of fluid, σ is the electrical conductivity, B_0 is the strength of an applied magnetic field, σ^* is the Stefan-Boltzmann constant, k^* is the mean absorption coefficient, b is the dimensional constants, c_p is the specific heat at constant pressure, q_r is the radiative heat flux, W_w is stretching velocity and W_e is the free stream velocity. Using

$$\eta=\sqrt{\frac{W_0}{\nu l}}\left(\frac{r^2-R^2}{2R}\right),\ w\left(r,z\right)=\frac{W_0\ z}{l}f'\left(\eta\right),\ u\left(r,z\right)=-\sqrt{\frac{\nu W_0}{l}}\frac{R}{r}f\left(\eta\right),\ \theta=\frac{T-T_\infty}{T_w-T_\infty}, \tag{8.5}$$

incompressibility condition is identically satisfied and the Eqs. (8.2)-(8.4) can be written as follows:

$$\left(1+2\gamma\eta\right)f'''+A^2+2\gamma f''-f'^2+ff''+\alpha_1\left[\left(1+2\gamma\eta\right)\left\{2f'f'''-ff^{(iv)}+3f''^2\right\}+\gamma\left(6f'f''-2ff'''\right)\right]$$

$$+\alpha_2\left[2\left(1+2\gamma\eta\right)f''^2+\gamma\left(2f'f''+2ff'''\right)\right]+\beta\,\mathrm{Re}\left[6\left(1+2\gamma\eta\right)^2f''^2f'''+8\gamma\left(1+2\gamma\eta\right)f''^3\right]$$

$$+Ha^2\sin^2\psi\left(A-f'\right)=0, \tag{8.6}$$

$$\left(1+\frac{4}{3}R_d\right)\left(1+2\gamma\eta\right)\theta''+2\gamma\left(1+\frac{4}{3}R_d\right)\theta'+\Pr Ec\ \left(1+2\gamma\eta\right)f''^2+\Pr\left(f'\ \theta-f\ \theta'\right)$$

$$+\alpha_1\Pr Ec\left[2\gamma ff''^2\ +\left(1+2\gamma\eta\right)f'f''^2-\left(1+2\gamma\eta\right)ff''f'''\right]+$$

$$\beta\Pr Ec\,\mathrm{Re}\left(1+2\gamma\eta\right)f''^4+Ha^2\sin^2\psi\Pr Ec\left(f'-A\right)^2=0, \tag{8.7}$$

$$f\ (0)=0,\ \ f'\left(0\right)=1,\ \ f'\left(\infty\right)\to A,\ \ \theta(0)=1,\ \ \theta(\infty)\to 0, \tag{8.8}$$

where γ is the curvature parameter, Re is the Reynolds number, Ha is the magnetic parameter, $(\alpha_1,\ \alpha_2,\ \beta)$ are the fluid parameters, A is the ratio of velocities, R_d is the radiation parameter, Pr is the Prandtl number and Ec is the Eckert number. These parameters are defined as follows:

$$
\begin{aligned}
\gamma &= \left(\frac{\nu l}{W_0 R^2}\right)^{1/2}, \quad \mathrm{Re} = \frac{Wz}{\nu}, \quad Ha^2 = \frac{\sigma B_0^2 l}{\rho W_0}, \quad \alpha_1 = \frac{\alpha_1^* W_0}{l\mu}, \alpha_2 = \frac{\alpha_2^* W_0}{l\mu}, \\
\beta &= \frac{\beta_3 W_0^2}{l^2 \mu}, \quad A = \frac{W_\infty}{W_0}, \quad R_d = \frac{4\sigma^* T_\infty^3}{k^* k}, \quad \mathrm{Pr} = \frac{\mu c_p}{k}, \quad Ec = \frac{W_0^2 (z/l)^2}{c_p (T_w - T_\infty)}.
\end{aligned}
\tag{8.9}
$$

The local skin friction coefficient is defined by

$$
\begin{aligned}
C_f &= \frac{\tau_{rz}}{\rho U_w^2} = \frac{\tau_{rz}|_{r=R}}{\rho U_w^2}, \\
\mathrm{Re}_z^{1/2} C_f &= \left[f''(0) + 3\alpha_1 f''(0) + 2\beta\,\mathrm{Re}\,f''^3(0) \right].
\end{aligned}
\tag{8.10}
$$

The Nusselt number is

$$
\begin{aligned}
Nu_z &= \frac{zq_w}{k(T_w - T_\infty)} = -\frac{z\left(k + \frac{16\sigma^* T_\infty^3}{3k_1}\right) \frac{\partial T}{\partial y}\Big|_{r=R}}{k(T_w - T_\infty)}, \\
\mathrm{Re}_z^{-1/2} Nu_z &= -\left(1 + \frac{4}{3}R_d\right)\theta'(0),
\end{aligned}
\tag{8.11}
$$

in which $\mathrm{Re}_z = \frac{Wz}{\nu}$ is the local Reynolds number.

8.2 Homotopic solutions

The velocity and temperature in the set of base functions

$$
\left\{ \eta^k \exp\left(-n\eta\right) \Big| k \geq 0,\ n \geq 0 \right\},
\tag{8.12}
$$

are

$$
f(\eta) = a_{0,0}^0 + \sum_{n=0}^{\infty}\sum_{k=0}^{\infty} a_{m,n}^k \eta^k \exp\left(-n\eta\right),
\tag{8.13}
$$

$$
\theta(\eta) = \sum_{n=0}^{\infty}\sum_{k=0}^{\infty} b_{m,n}^k \eta^k \exp\left(-n\eta\right),
\tag{8.14}
$$

where $a_{m,n}^k$ and $b_{m,n}^k$ are the coefficients. The initial guesses and linear operators for the dimensionless momentum and energy equations are (f_0, θ_0) and $(\mathcal{L}_f, \mathcal{L}_\theta)$. The chosen initial guesses and linear operators are given by

$$
f_0(\eta) = A\eta + (1-A)(1 - \exp(-\eta)),
\tag{8.15}
$$

$$
\theta_0(\eta) = \exp(-\eta),
\tag{8.16}
$$

$$
\mathcal{L}_f(f) = \frac{d^3 f}{d\eta^3} - \frac{df}{d\eta}, \quad \mathcal{L}_\theta(\theta) = \frac{d^2\theta}{d\eta^2} - \theta,
\tag{8.17}
$$

with

$$\mathcal{L}_f \ [C_{34} + C_{35} \exp(\eta) + C_{36} \exp(-\eta)] = 0, \tag{8.18}$$

$$\mathcal{L}_\theta \ [C_{37} \exp(\eta) + C_{38} \exp(-\eta)] = 0, \tag{8.19}$$

where $C_i(i = 34 - 38)$ depict the arbitrary constants.

8.2.1 Zeroth-order deformation problems

The zeroth order problems are

$$(1 - q)\mathcal{L}_f[\hat{f}(\eta, q) - f_0(\eta)] = q\hbar_f \mathcal{N}_f \left[\hat{f}(\eta, q) \right], \tag{8.20}$$

$$\hat{f}(\eta; q)\Big|_{\eta = 0} = 0, \quad \left. \frac{\partial \hat{f}'(\eta; q)}{\partial \eta} \right|_{\eta = 0} = 1, \quad \left. \frac{\partial \hat{f}'(\eta; q)}{\partial \eta} \right|_{\eta = \infty} = A, \tag{8.21}$$

$$(1 - q)\mathcal{L}_\theta[\hat{\theta}(\eta, q) - \theta_0(\eta)] = q\hbar_\theta \mathcal{N}_\theta \left[\hat{f}(\eta, q), \hat{\theta}(\eta, q) \right], \tag{8.22}$$

$$\hat{\theta}(\eta; q)\Big|_{\eta = 0} = 1, \quad \hat{\theta}(\eta; q)\Big|_{\eta = \infty} = 0, \tag{8.23}$$

with non-linear operators $\mathcal{N}_f \left[\hat{f}(\eta, q) \right]$ and $\mathcal{N}_\theta \left[\hat{f}(\eta, q), \hat{\theta}(\eta, q) \right]$ defined by

$$
\begin{aligned}
\mathcal{N}_f \left[\hat{f}(\eta; q) \right] = & \ (1 + 2\gamma\eta) \frac{\partial^3 \hat{f}(\eta, q)}{\partial \eta^3} + A^2 + 2\gamma \frac{\partial^2 \hat{f}(\eta, q)}{\partial \eta^2} - \left(\frac{\partial \hat{f}(\eta, q)}{\partial \eta} \right)^2 + \hat{f}(\eta, q) \frac{\partial^2 \hat{f}(\eta, q)}{\partial \eta^2} \\
& + \alpha_1 \left\{ (1 + 2\gamma\eta) \left(2\frac{\partial \hat{f}(\eta, q)}{\partial \eta} \frac{\partial^3 \hat{f}(\eta; q)}{\partial \eta^3} - \hat{f}(\eta, q) \frac{\partial^4 \hat{f}(\eta, q)}{\partial \eta^4} + 3 \left(\frac{\partial^2 \hat{f}(\eta, q)}{\partial \eta^2} \right)^2 \right) \right. \\
& \left. + \gamma \left(6\frac{\partial \hat{f}(\eta, q)}{\partial \eta} \frac{\partial^2 \hat{f}(\eta, q)}{\partial \eta^2} - 2\hat{f}(\eta, q) \frac{\partial^3 \hat{f}(\eta; q)}{\partial \eta^3} \right) \right\} \\
& + \alpha_2 \left\{ 2(1 + 2\gamma\eta) \left(\frac{\partial^2 \hat{f}(\eta, q)}{\partial \eta^2} \right)^2 + \gamma \left(2\frac{\partial \hat{f}(\eta, q)}{\partial \eta} \frac{\partial^2 \hat{f}(\eta, q)}{\partial \eta^2} + 2\hat{f}(\eta, q) \frac{\partial^3 \hat{f}(\eta; q)}{\partial \eta^3} \right) \right\} \\
& + \beta \operatorname{Re} \left[6(1 + 2\gamma\eta)^2 \left(\frac{\partial^2 \hat{f}(\eta, q)}{\partial \eta^2} \right)^2 \frac{\partial^3 \hat{f}(\eta; q)}{\partial \eta^3} + 8\gamma(1 + 2\gamma\eta) \left(\frac{\partial^2 \hat{f}(\eta, q)}{\partial \eta^2} \right)^3 \right] \\
& + Ha^2 \sin^2 \psi \left\{ A - \frac{\partial \hat{f}(\eta, q)}{\partial \eta} \right\}, \tag{8.24}
\end{aligned}
$$

$$
\begin{aligned}
\mathcal{N}_\theta \left[\hat{f}(\eta; q), \hat{\theta}(\eta; q) \right] = & \left(1 + \frac{4}{3}R_d \right)(1 + 2\gamma\eta) \frac{\partial^2 \hat{\theta}(\eta; q)}{\partial \eta^2} + 2\gamma \left(1 + \frac{4}{3}R_d \right) \frac{\partial \hat{\theta}(\eta; q)}{\partial \eta} \\
& + \operatorname{Pr} Ec (1 + 2\gamma\eta) \left(\frac{\partial^2 \hat{f}(\eta, q)}{\partial \eta^2} \right)^2 + \operatorname{Pr} \left(\frac{\partial \hat{f}(\eta; q)}{\partial \eta} \hat{\theta}(\eta; q) - \hat{f}(\eta, q) \frac{\partial \hat{\theta}(\eta; q)}{\partial \eta} \right) \\
& + \alpha_1 \operatorname{Pr} Ec \left[2\gamma \hat{f}(\eta, q) \left(\frac{\partial^2 \hat{f}(\eta, q)}{\partial \eta^2} \right)^2 + (1 + 2\gamma\eta) \frac{\partial \hat{f}(\eta; q)}{\partial \eta} \left(\frac{\partial^2 \hat{f}(\eta, q)}{\partial \eta^2} \right)^2 \right.
\end{aligned}
$$

$$-\left(1+2\gamma\eta\right)\hat{f}(\eta,q)\frac{\partial^2\hat{f}(\eta,q)}{\partial\eta^2}\frac{\partial^3\hat{f}(\eta;q)}{\partial\eta^3}\Bigg] + \beta\Pr Ec\operatorname{Re}\left(1+2\gamma\eta\right)\left(\frac{\partial^2\hat{f}(\eta;q)}{\partial\eta^2}\right)^4$$

$$+Ha^2\sin^2\psi\Pr Ec\left[\frac{\partial\hat{f}(\eta;q)}{\partial\eta}-A\right]^2, \tag{8.25}$$

in which $q \in [0,1]$ indicates the embedding parameter and $\hbar_f$ and $\hbar_\theta$ the nonzero auxiliary parameters.

8.2.2 mth-order deformation problems

The mth-order deformation problems are

$$\mathcal{L}_f\left[f_m\left(\eta\right)-\chi_m f_{m-1}\left(\eta\right)\right]=\hbar_f\mathcal{R}_m^f\left(\eta\right), \tag{8.26}$$

$$\hat{f}_m(\eta;q)\Big|_{\eta\,=\,0}=0, \quad \frac{\partial\hat{f}'_m(\eta;q)}{\partial\eta}\Bigg|_{\eta\,=\,0}=0, \quad \frac{\partial\hat{f}'_m(\eta;q)}{\partial\eta}\Bigg|_{\eta\,=\,\infty}=0, \tag{8.27}$$

$$\mathcal{L}_\theta\left[\theta_m\left(\eta\right)-\chi_m\theta_{m-1}\left(\eta\right)\right]=\hbar_\theta\mathcal{R}_m^\theta\left(\eta\right), \tag{8.28}$$

$$\hat{\theta}_m(\eta;q)\Big|_{\eta\,=\,0}=0, \quad \hat{\theta}_m(\eta;q)\Big|_{\eta\,=\,\infty}=0, \tag{8.29}$$

$$\begin{aligned}
\mathcal{R}_m^f\left(\eta\right) &= \left(1+2\gamma\eta\right)f'''_{m-1}\left(\eta\right)+A^2\left(1-\chi_m\right)+2\gamma f''_{m-1}+\sum_{k=0}^{m-1}\left(f_{m-1-k}f''_k-f'_{m-1-k}f'_k\right)\\
&\quad+\sum_{k=0}^{m-1}\alpha_1\left[\left(1+2\gamma\eta\right)\left(2f'_{m-1-k}f'''_k-f_{m-1-k}f_k^{(iv)}+3f''_{m-1-k}f''_k\right)+\gamma\left(6f'_{m-1-k}f''_k-2f_{m-1-k}f'''_k\right)\right]\\
&\quad+\alpha_2\sum_{k=0}^{m-1}\left[2\left(1+2\gamma\eta\right)f''_{m-1-k}f''_k+\gamma\left(2f'_{m-1-k}f''_k+2f_{m-1-k}f'''_k\right)\right]\\
&\quad+\beta\operatorname{Re}\sum_{k=0}^{m-1}\sum_{l=0}^{k}\left[6\left(1+2\gamma\eta\right)^2f''_{m-1-k}f''_{k-l}f'''_l+8\gamma\left(1+2\gamma\eta\right)f''_{m-1-k}f''_{k-l}f''_l\right]\\
&\quad+Ha^2\sin^2\psi\left[A\left(1-\chi_m\right)-f'_{m-1}\right], \tag{8.30}
\end{aligned}$$

$$\begin{aligned}
\mathcal{R}_m^\theta\left(\eta\right) &= \left(1+\frac{4}{3}R_d\right)\left(1+2\gamma\eta\right)\theta''_{m-1}+2\gamma\left(1+\frac{4}{3}R_d\right)\theta'_{m-1}+\Pr Ec\left(1+2\gamma\eta\right)\sum_{k=0}^{m-1}f''_{m-1-k}f''_k\\
&\quad+\Pr\sum_{k=0}^{m-1}\left(f'_{m-1-k}\theta_k-f_{m-1-k}\theta'_k\right)+\alpha_1\Pr Ec\left[2\gamma\sum_{k=0}^{m-1}f_{m-1-k}\sum_{l=0}^{k}f''_{k-l}f''_l\right.\\
&\quad+\left(1+2\gamma\eta\right)\sum_{k=0}^{m-1}f'_{m-1-k}\sum_{l=0}^{k}f''_{k-l}f''_l-\left(1+2\gamma\eta\right)\sum_{k=0}^{m-1}f_{m-1-k}\sum_{l=0}^{k}f''_{k-l}f'''_l\Bigg]\\
&\quad+\beta\Pr Ec\operatorname{Re}\left(1+2\gamma\eta\right)\sum_{k=0}^{m-1}f''_{m-1-k}\sum_{l=0}^{k}f''_{k-l}\sum_{s=0}^{l}f''_{l-s}f''_s\\
&\quad+Ha^2\sin^2\psi\Pr Ec\left[\sum_{k=0}^{m-1}f'_{m-1-k}f'_k-2Af'_{m-1}-A^2\left(1-\chi_m\right)\right]. \tag{8.31}
\end{aligned}$$

Setting $q = 0$ and $q = 1$, one has

$$\hat{f}(\eta; 0) = f_0(\eta), \qquad \hat{f}(\eta; 1) = f(\eta), \tag{8.32}$$

$$\hat{\theta}(\eta; 0) = \theta_0(\eta), \qquad \hat{\theta}(\eta; 1) = \theta(\eta). \tag{8.33}$$

When q varies from 0 to 1, $\hat{f}(\eta; q)$ and $\hat{\theta}(\eta; q)$ deforms from the initial solutions $f_0(\eta)$ and $\theta_0(\eta)$ to the final solutions $f(\eta)$ and $\theta(\eta)$ respectively. Taylor's series leads to the following relations

$$\hat{f}(\eta; q) = f_0(\eta) + \sum_{m=1}^{\infty} f_m(\eta) q^m, \qquad f_m(\eta) = \frac{1}{m!} \frac{\partial^m \hat{f}(\eta; q)}{\partial q^m}\bigg|_{q=0}, \tag{8.34}$$

$$\hat{\theta}(\eta; q) = \theta_0(\eta) + \sum_{m=1}^{\infty} \theta_m(\eta) q^m, \qquad \theta_m(\eta) = \frac{1}{m!} \frac{\partial^m \hat{\theta}(\eta; q)}{\partial q^m}\bigg|_{q=0}. \tag{8.35}$$

The auxiliary parameters are properly chosen such that the series solutions (8.35) and (8.36) converge at $q = 1$. Therefore

$$f(\eta) = f_0(\eta) + \sum_{m=1}^{\infty} f_m(\eta), \tag{8.36}$$

$$\theta(\eta) = \theta_0(\eta) + \sum_{m=1}^{\infty} \theta_m(\eta). \tag{8.37}$$

Denoting the special solutions by (f_m^*, θ_m^*) one can express the general solutions (f_m, θ_m) of Eqs. (8.26)-(8.29) as follows:

$$f_m(\eta) = f_m^*(\eta) + C_{34} + C_{35} \exp(\eta) + C_{36} \exp(-\eta), \tag{8.38}$$

$$\theta_m(\eta) = \theta_m^*(\eta) + C_{37} \exp(\eta) + C_{38} \exp(-\eta), \tag{8.39}$$

in which the constants $C_i (i = 34 - 38)$ in veiw of the conditions (8.27) and (8.29) are

$$C_{35} = 0 = C_{37}, \quad C_{36} = \frac{\partial f_m^*(\eta)}{\partial \eta}\bigg|_{\eta = 0}, \quad C_{34} = -C_{36} - f_m^*(0), \quad C_{38} = -\theta_m^*(0). \tag{8.40}$$

8.3 Convergence of the homotopy solutions

To get the series solutions through homotopy analysis method, it is important to check the convergence of the desired solutions. Such solutions involve the auxiliary parameters $\hbar_f$ and $\hbar_\theta$. These parameters are useful in adjusting and controlling the convergence region. Therefore $\hbar_f$ and $\hbar_\theta-$curves are plotted for 16th order of approximation in Fig. 8.1 for the suitable ranges of the auxiliary parameters. Here the suitable values for $\hbar_f$ and $\hbar_\theta$ are $-1.3 \leq \hbar_f < -0.4$ and $-0.9 \leq \hbar_\theta < -0.2$.

8.4 Results and discussion

This section illustrates the impact of physical parameters. The results are displayed graphically in the Figs. 8.2-8.19. The conclusions for flow field and other physical quantities of interest are drawn. The

numerical values of the skin friction coefficient and local Nusselt number are presented in the Tables 8.2 and 8.3 for various values of α_1, α_2, β, M, Re, R_d, Pr and Ec. Fig. 8.2 displays the effect of magnetic parameter Ha on velocity profile $f'(\eta)$ by keeping other physical parameters fixed. It is of interest to note that the velocity profile decreases with an increase in magnetic parameter Ha whereas the boundary layer thickness reduces. Clearly by increasing magnetic force, the Lorentz force increases which causes resistance in the fluid flow and consequently the velocity profile decreases. Fig. 8.3 shows the effect of third grade parameter β on the velocity profile $f'(\eta)$. Here it is examined that the velocity increases near the wall for larger values of β whereas it becomes vanishes away from the wall. Figs. 8.4 and 8.5 illustrate the behavior of second grade parameters α_1 and α_2 on the velocity profile $f'(\eta)$ respectively. It is observed that the velocity profile $f'(\eta)$ is an increasing function of α_1. The velocity profile also increases when α_2 is increased (see Fig. 8.5). In fact the second grade parameter are directly proportional to the viscosity and by increasing the second grade parameter the viscosity of the fluid decreases and as a result the velocity profile is increased. The behavior of Reynolds number Re on velocity profile $f'(\eta)$ is shown in Fig. 8.6. It is observed that the velocity profile $f'(\eta)$ decreases with an increase in Reynold number Re. Physically the Reynolds number is defined as the ratio of inertial forces to viscous forces and for larger values of Reynold number the inertial forces are dominant when compared with the viscous forces. Consequently the velocity profile increases. Fig. 8.7 is sketched for the influence of angle of inclination ψ on the velocity profile $f'(\eta)$. The velocity profile and thermal boundary layer decrease for larger values of ψ. In fact due to the larger values of angle of inclination the Lorentz forces are dominant and therefore the velocity profile decreases. Influence of curvature parameter γ is shown in Fig. 8.8. It is revealed that velocity and boundary layer thickness increase when curvature parameter γ increases. In fact with the increase of curvature parameter, the radius of curvature decreases which reduces the contact area of the cylinder with the fluid. Therefore resistance offered by the surface decreases and velocity of the fluid increases. The behavior of A on velocity profile $f'(\eta)$ is shown in Fig. 8.9. It is analyzed that velocity profile $f'(\eta)$ increases for both the cases $A > 1$ and $A < 1$. However the boundary layers in these two cases have opposite behavior. It is noticed that there is no boundary layer for $A = 1$.

Fig. 8.10 is sketched for the behavior of angle of inclination ψ on temperature field $\theta(\eta)$. It is clear from the Fig. that temperature profile increases with an increase in angle of inclination ψ. Because Lorentz force increases with an increase in angle of inclination which is a resistive force. Hence more heat is produced due to the resistive forces. Therefore temperature profile $\theta(\eta)$ increases. Fig. 8.11 portrays the effects of curvature parameter γ on the temperature profile $\theta(\eta)$. It is depicted that temperature profile shows mix behavior near the surface of cylinder while it increases away from the cylinder when $0.5 < \eta < 6$ and it vanishes when $\eta \geq 6$. The thermal boundary layer thickness increases with an increase in curvature parameter γ. Influence of ratio parameter A is analyzed in the Fig. 8.12. It is observed that temperature and thermal boundary layer thickness decrease for larger values of A. The effects of thermal radiation parameter R_d on temperature distribution $\theta(\eta)$ is shown in Fig. 7.13. Temperature and thermal boundary layer thickness increase when radiation parameter is increased. It is due the reason that with the increase of thermal radiation parameter the mean absorption coefficient decreases. This

leads to enhancement of temperature profile. Fig. 8.14 is plotted to see the variation of Prandtl number Pr on the temperature field $\theta(\eta)$. It is revealed that both the temperature and thermal boundary layer thickness are increased for smaller values of Pr. Thermal diffusivity decreases with an increase in Prandtl number and consequently the temperature field decreases. Fluids with high Prandtl number have low thermal diffusivity and fluids subject to low Prandtl number have high Prandtl number. We displayed the temperature field for various values of Eckert number Ec by keeping other parameters fixed in Fig. 8.15. Effect of Eckert number is to increase the thermal boundary layer thickness due to the frictional heating. Fig. 8.16 gives the comparison of velocities for Newtonian, second-grade and third-grade fluids over a cylinder in the presence of magnetohydrodynamics. It is analyzed that the velocity for third-grade fluid is higher than the Newtonian and second-grade fluids. Further the momentum boundary layer thickness is higher for third-grade fluid. Fig. 8.17 is sketched to see the comparison of Newtonian, second-grade and third-grade fluids velocities by a cylinder in the absence of magnetohydrodynamics. It is analyzed that the velocity for third-grade fluid is higher than the Newtonian and second-grade fluids. Further the momentum boundary layer thickness is higher for third-grade fluid. Comparison between velocities of Newtonian and third-grade fluids (with magnetohydrodynamics) over a cylinder is shown in Fig. 8.18 for two cases (i) without stagnation point (ii) with stagnation point. It is depicted that in the presence of magnetohydrodynamics, the velocity profile is higher for third-grade fluid for both the cases. Further it is also noted that the velocity profile is higher for both Newtonian and third-grade fluids in the presence of stagnation point. Fig. 8.19 is drawn for the comparison of velocities between MHD Newtonian and third-grade fluids over a flat plat for two cases (i) without stagnation point (ii) with stagnation point. It is noted that in the presence of MHD, the velocity profile is higher for third-grade fluid for both the cases. On the other hand it is also examined that the velocity profile is higher for both Newtonian and third-grade fluids with stagnation point.

The convergence of series solution is checked and shown in Table 8.1. Note that the series solutions converge at 11th order of approximation up to 5 decimal places for the momentum equation and 12th order of approximation is enough for the temperature. Table 8.2 shows the impact of various parameters on skin friction coefficient. It is observed that skin friction coefficient increases with the increase of curvature parameter γ, magnetic parameter Ha, third-grade parameter β, second-grade parameter α_1, Reynolds number Re and angle of inclination ψ while it decreases with the increase of second-grade parameter α_2 and ratio parameter A. Hence in order to reduce the value of skin friction coefficient which is very useful for industrial applications, one needs to reduce the radius of cylinder and decrease magnetic parameter Ha, third-grade parameter β, second-grade parameter α_1, Reynolds number Re and angle of inclination ψ. Table 8.3 shows the behavior of various parameters on local Nusselt number. It is examined that local Nusselt number increases for larger fluid parameter $(\alpha_1, \alpha_2, \beta)$, Reynolds number Re, radiation parameter R_d, stagnation parameter A and Prandtl number Pr while it decreases with the increase of magnetic parameter Ha, curvature parameter γ, Eckert number Ec and angle of inclination ψ. Therefore higher values of fluid parameters $(\alpha_1, \alpha_2, \beta)$, Reynolds number Re, radiation parameter R_d, stagnation parameter A and Prandtl number Pr and small values of Ha, γ, Ec and ψ can be used to increase the

rate of heat transfer.
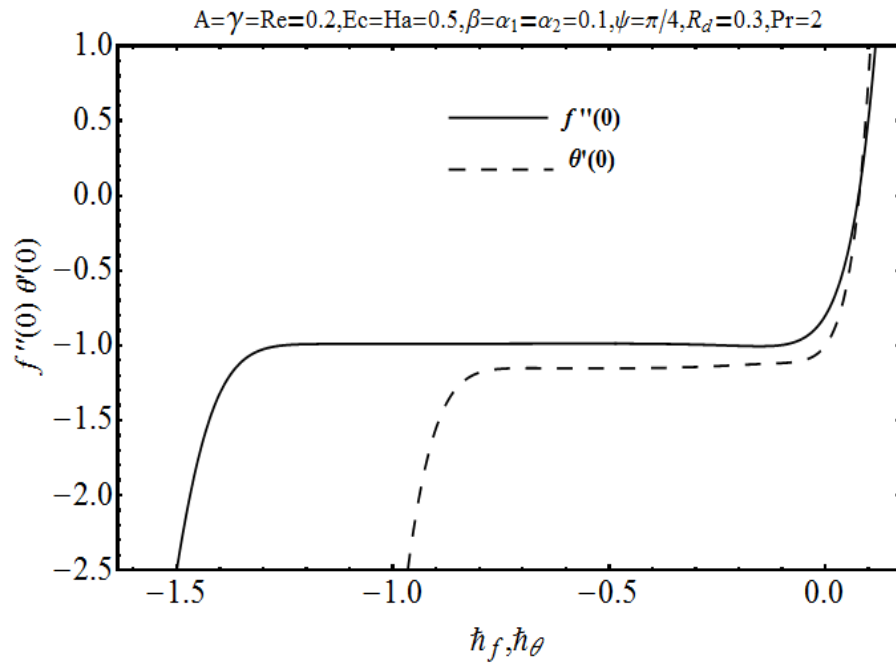
Fig. 8.1 : $\hbar$−curves of the functions $f(\eta)$ and $\theta(\eta)$ at 16th order of approximation.
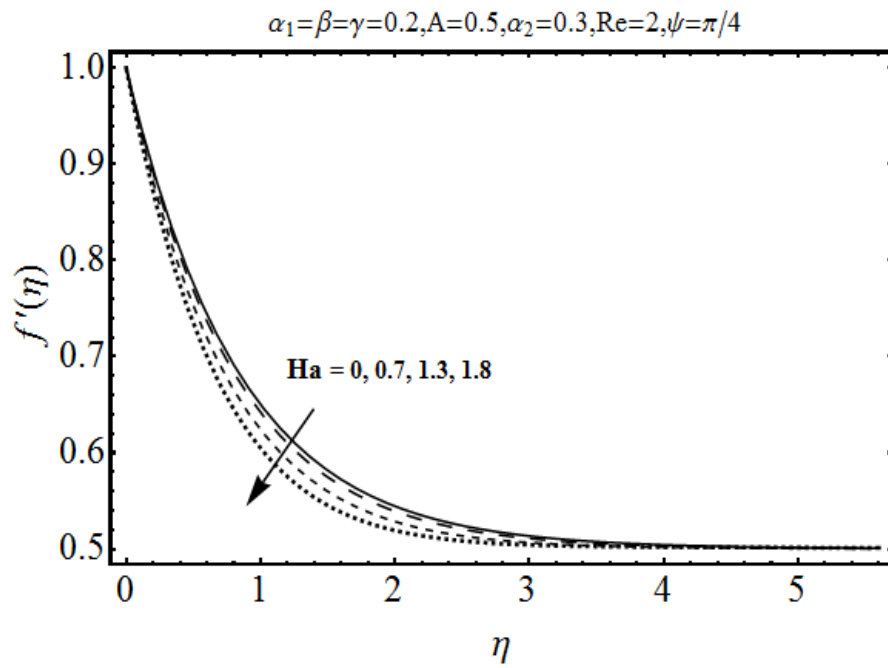
Fig. 8.2: Influence of Ha on $f'(\eta)$.
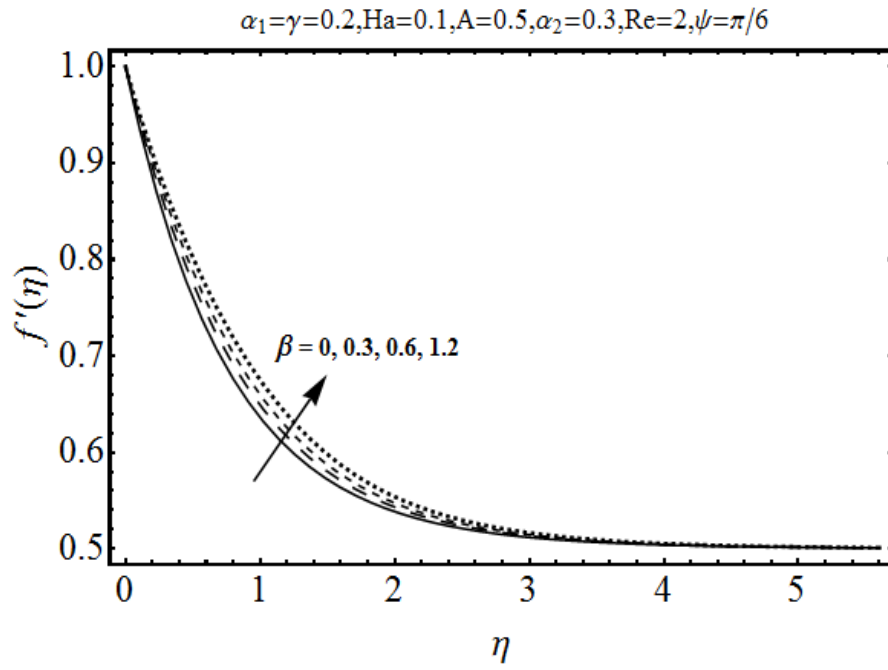
Fig. 8.3: Influence of β on $f'(\eta)$.
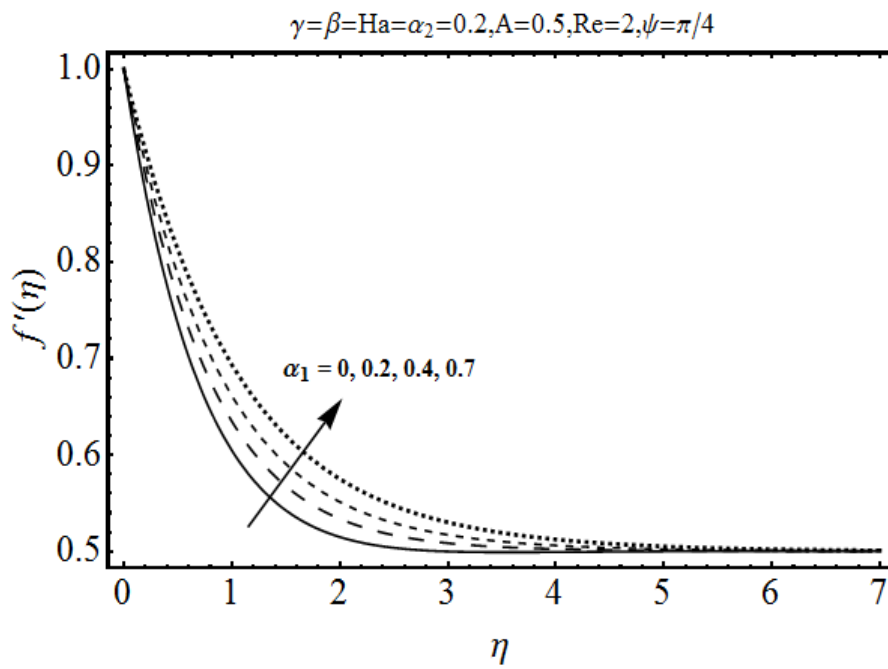
Fig. 8.4: Influence of α_1 on $f'(\eta)$.
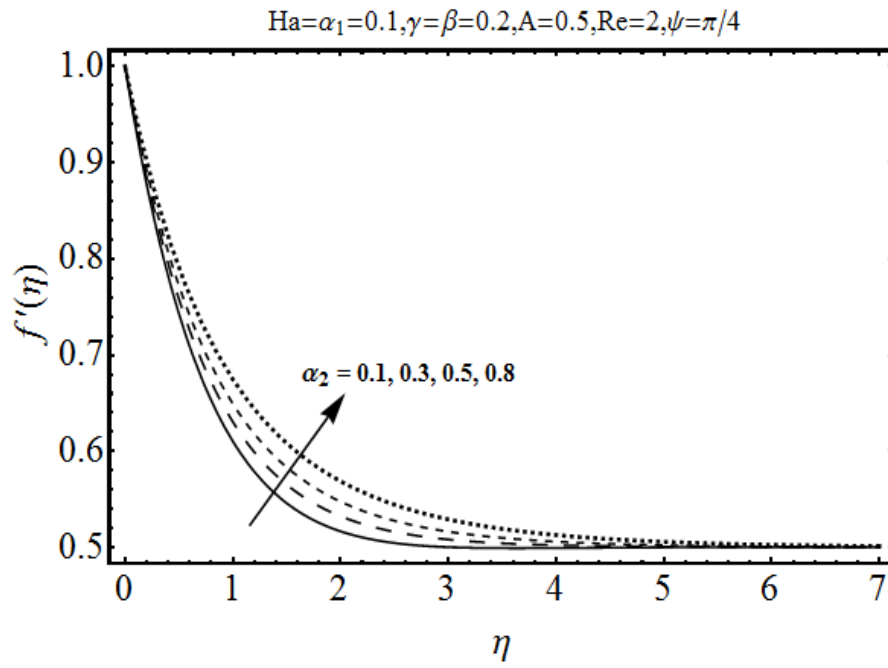
Fig. 8.5: Influence of α_2 on $f'(\eta)$.
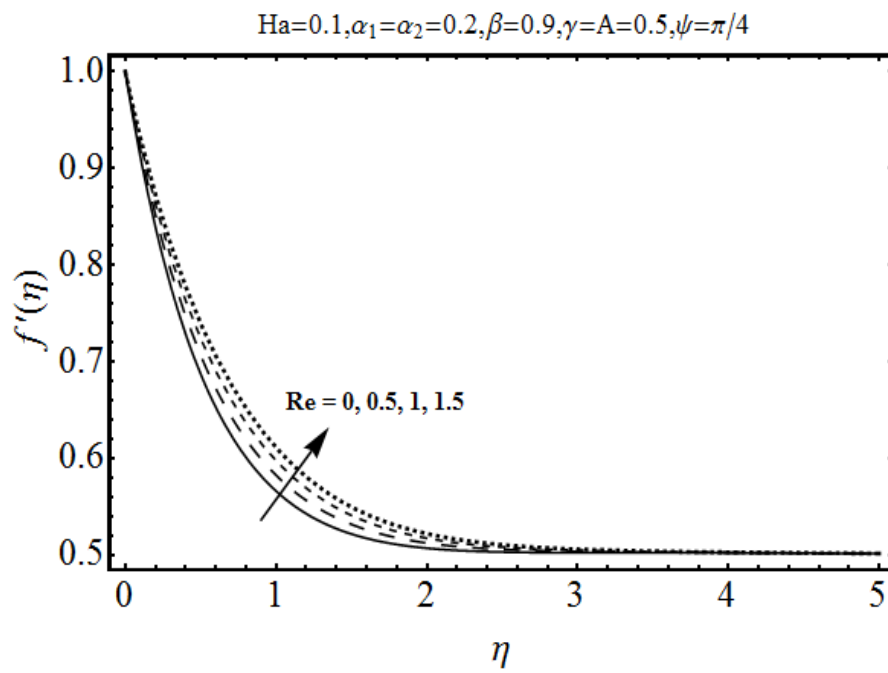
Fig. 8.6: Influence of Re on $f'(\eta)$.
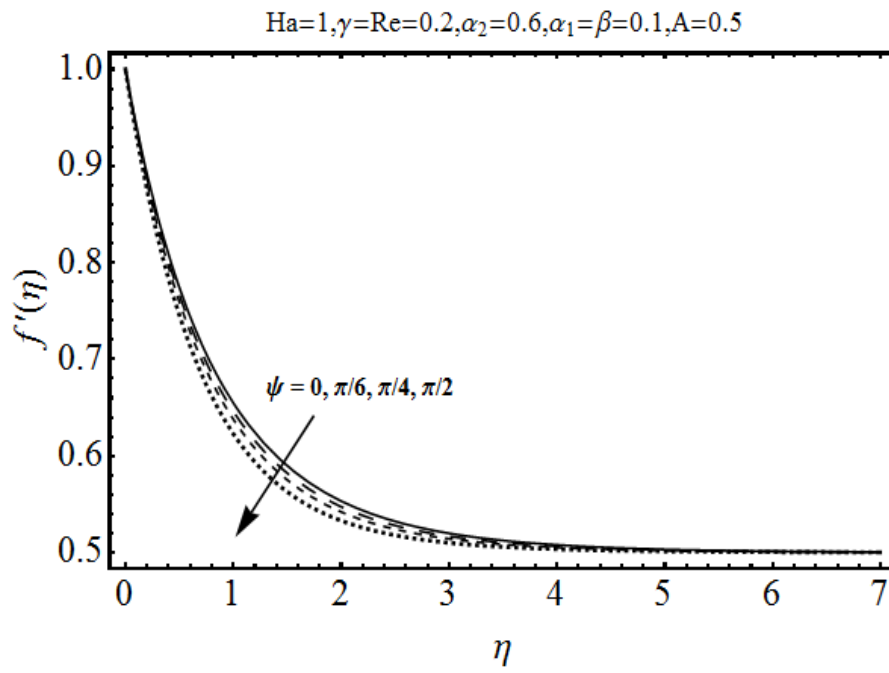
Fig. 8.7: Influence of ψ on $f'(\eta)$.
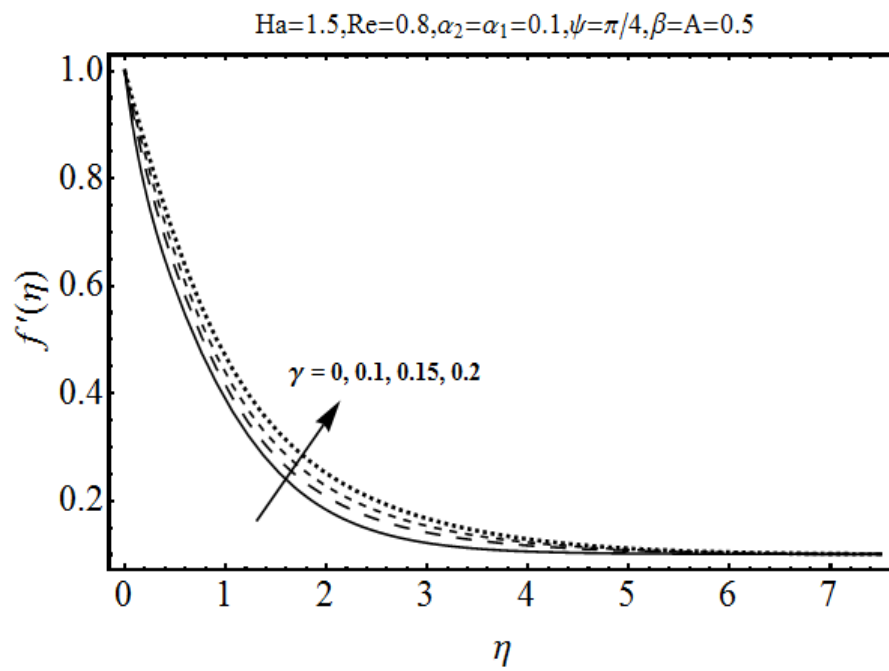
Fig. 8.8: Influence of γ on $f'(\eta)$.
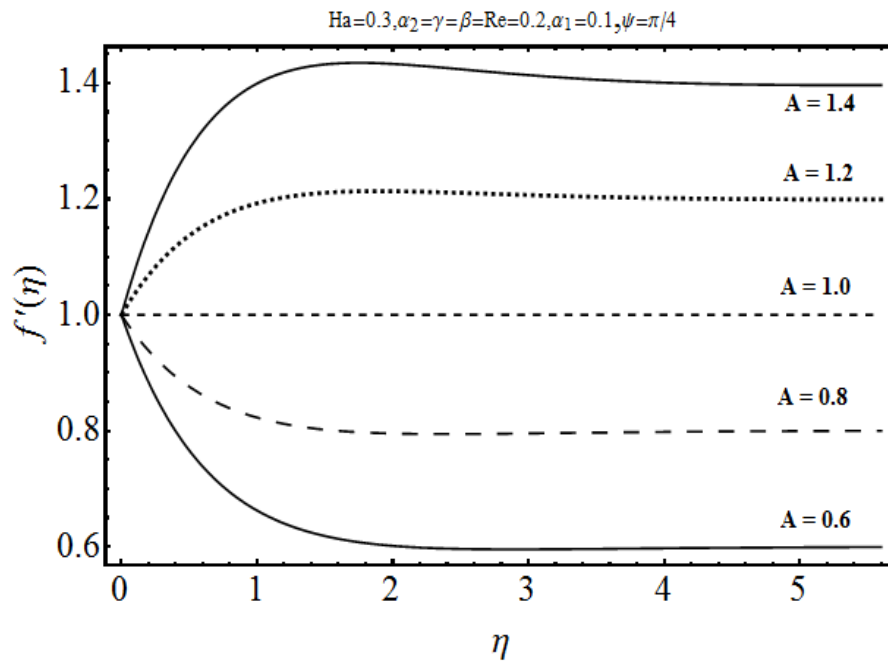
Fig. 8.9: Influence of A on $f'(\eta)$.

Fig. 8.10: Influence of ψ on $\theta(\eta)$.

$\alpha_1=\beta=0.2, R_d=0.1, \text{Re}=\text{Ha}=1, \text{Pr}=2, A=\text{Ec}=0.1, \alpha_2=0.3, \psi=\pi/4$

$\gamma = 0, 0.1, 0.2, 0.3$

Fig. 8.11: Influence of γ on $\theta(\eta)$.

$\alpha_1=\beta=0.2, R_d=0.1, \text{Re}=\text{Ha}=\text{Pr}=1, \gamma=\text{Ec}=0.1, \alpha_2=0.3, \psi=\pi/4$

$A = 0, 0.2, 0.4, 0.7$

Fig. 8.12: Influence of A on $\theta(\eta)$.

$\alpha_1 = \beta = 0.2, \text{Re} = \text{Ha} = \text{Pr} = 1, \gamma = A = \text{Ec} = 0.1, \alpha_2 = 0.3, \psi = \pi/4$

$R_d = 0, 0.4, 0.8, 1.2$
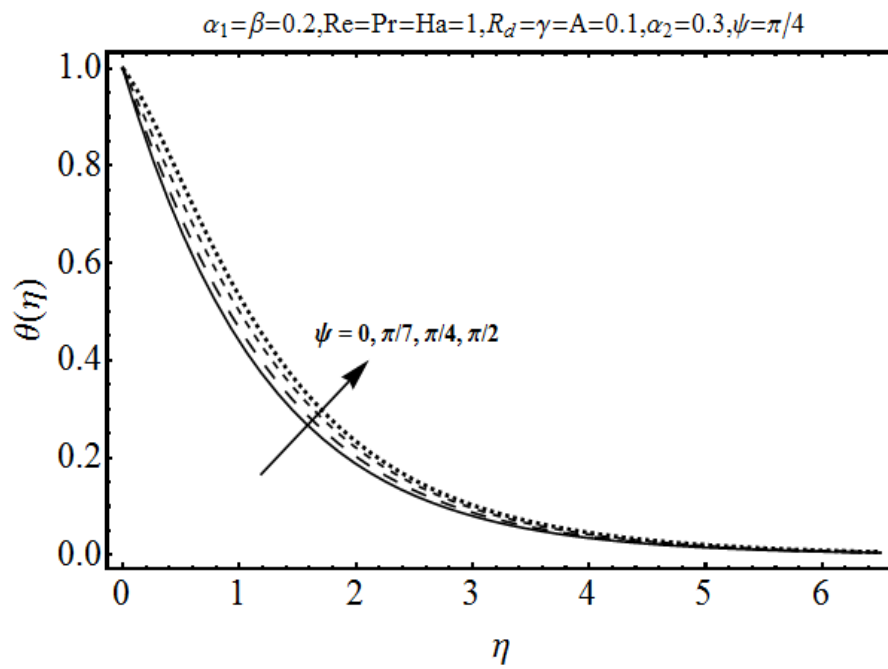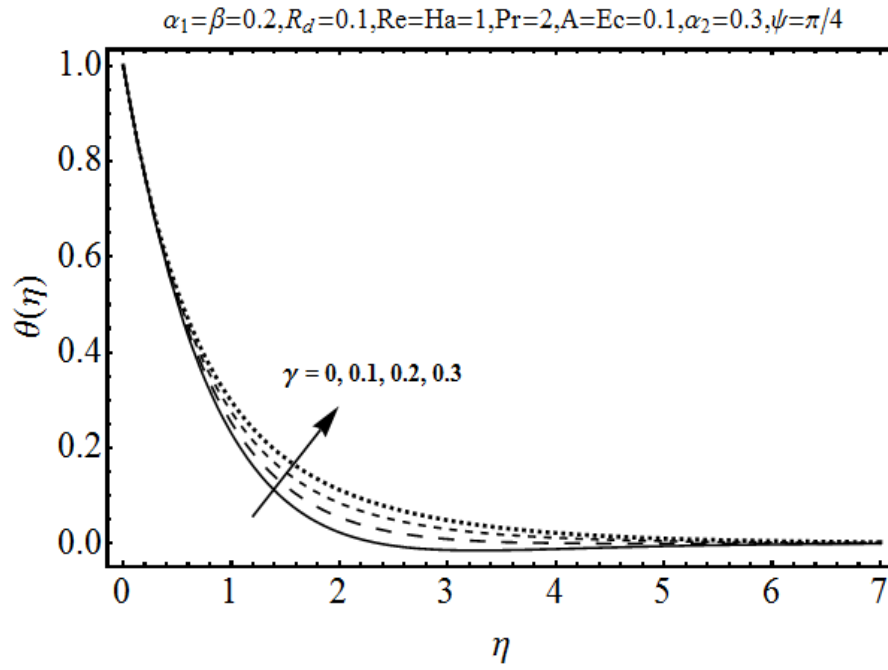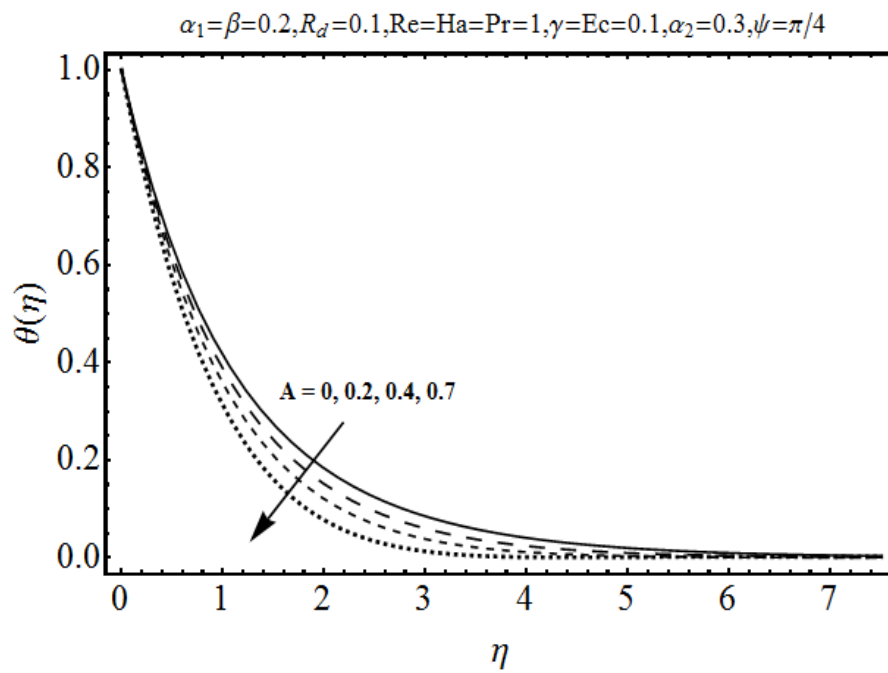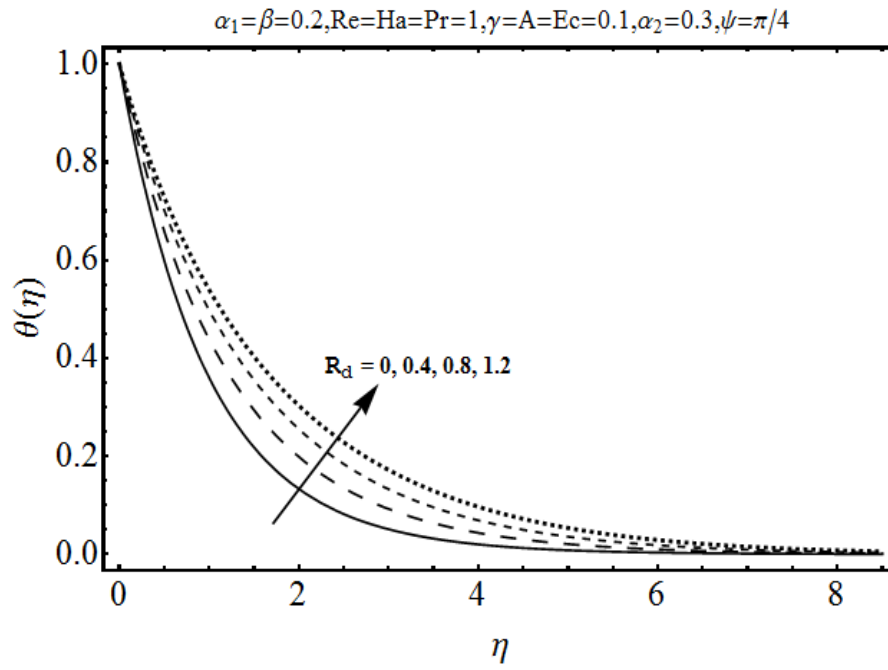
Fig. 8.13: Influence of R_d on $\theta(\eta)$.

$\alpha_1 = \beta = 0.2, \text{Re} = \text{Ha} = 1, R_d = \gamma = A = \text{Ec} = 0.1, \alpha_2 = 0.3, \psi = \pi/4$

$\text{Pr} = 0.1, 0.3, 0.6, 0.9$
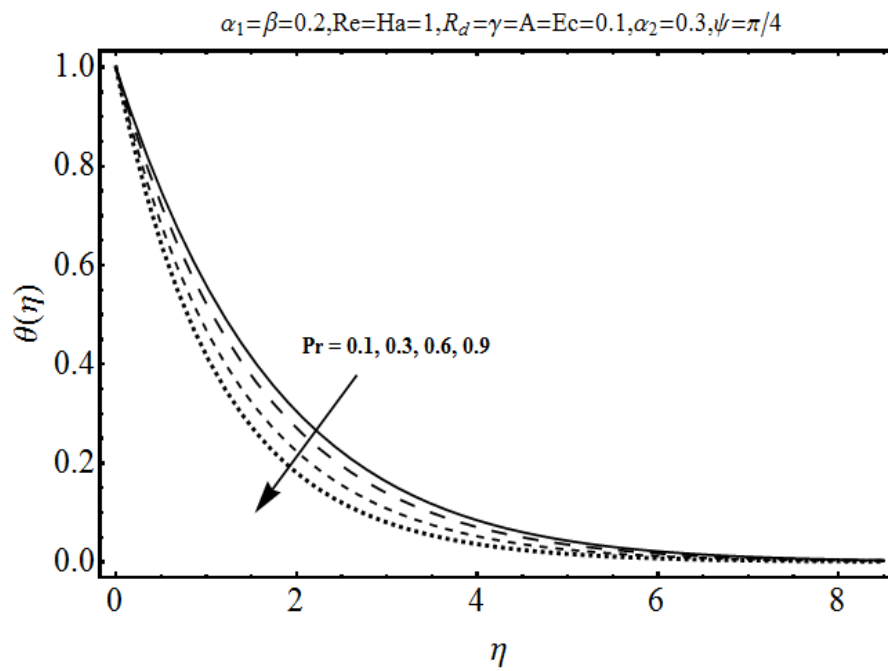
Fig. 8.14: Influence of Pr on $\theta(\eta)$.

$\alpha_1 = \beta = 0.2, \text{Re} = \text{Pr} = \text{Ha} = 1, R_d = \gamma = A = 0.1, \alpha_2 = 0.3, \psi = \pi/4$

$Ec = 0, 0.4, 0.7, 1$
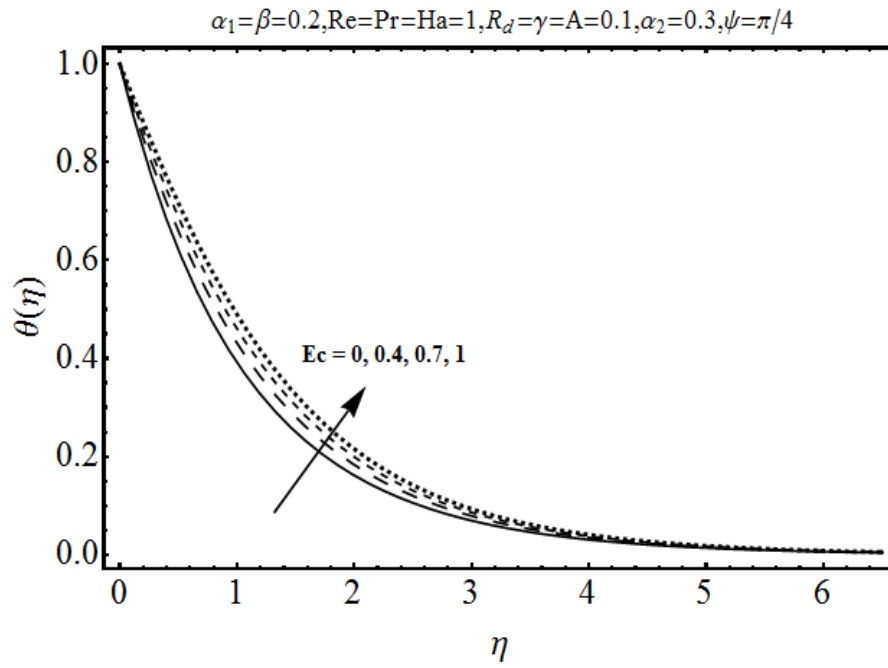
Fig. 8.15: Influence of Ec on $\theta(\eta)$.

For clinder with magnetohydrodynsmic effect

Newtonian Fluid

Second-grade Fluid
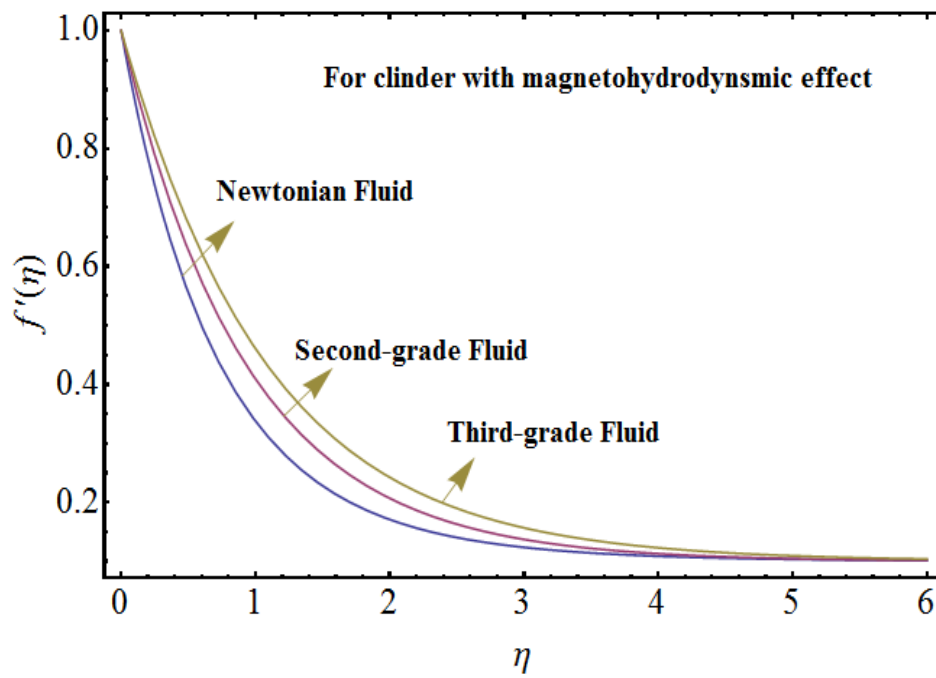
Third-grade Fluid

Fig. 8.16: Comparison of velocity profile for Newtonian, second-grade
and third-grade fluids in the presence of MHD.
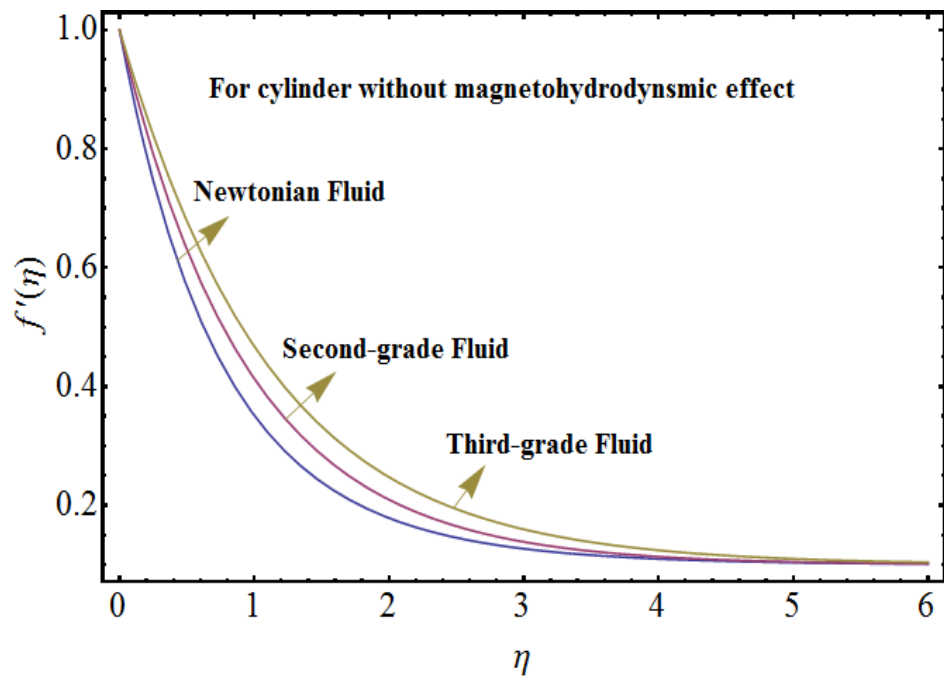
Fig. 8.17: Comparison of velocity profile for Newtonian, second-grade and third-grade fluids in the absence of MHD.
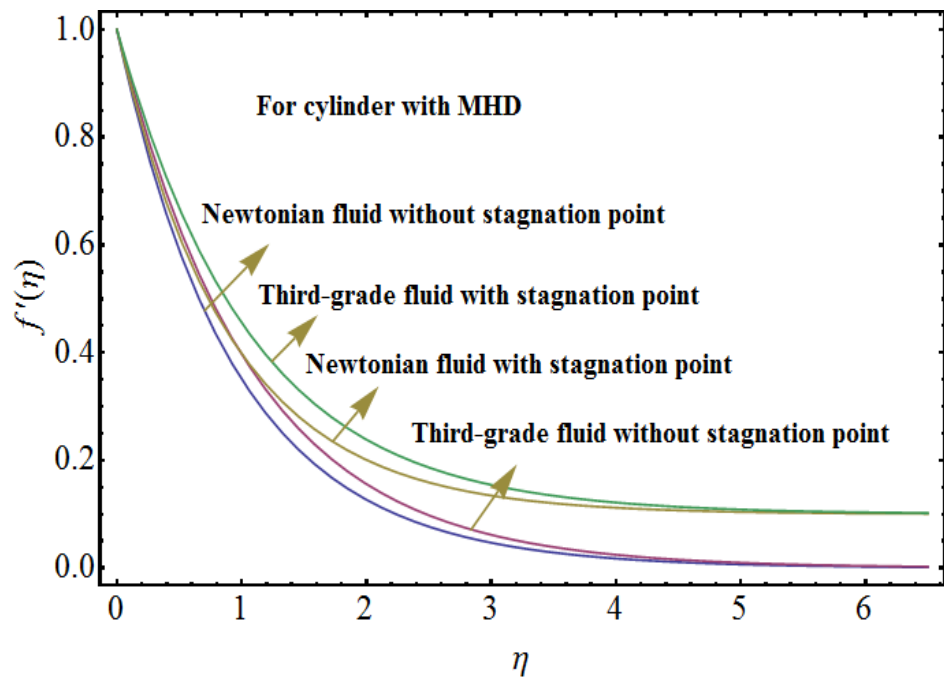
Fig. 8.18: Comparison of velocity profiles for Newtonian and third-grade fluids for cylinder.
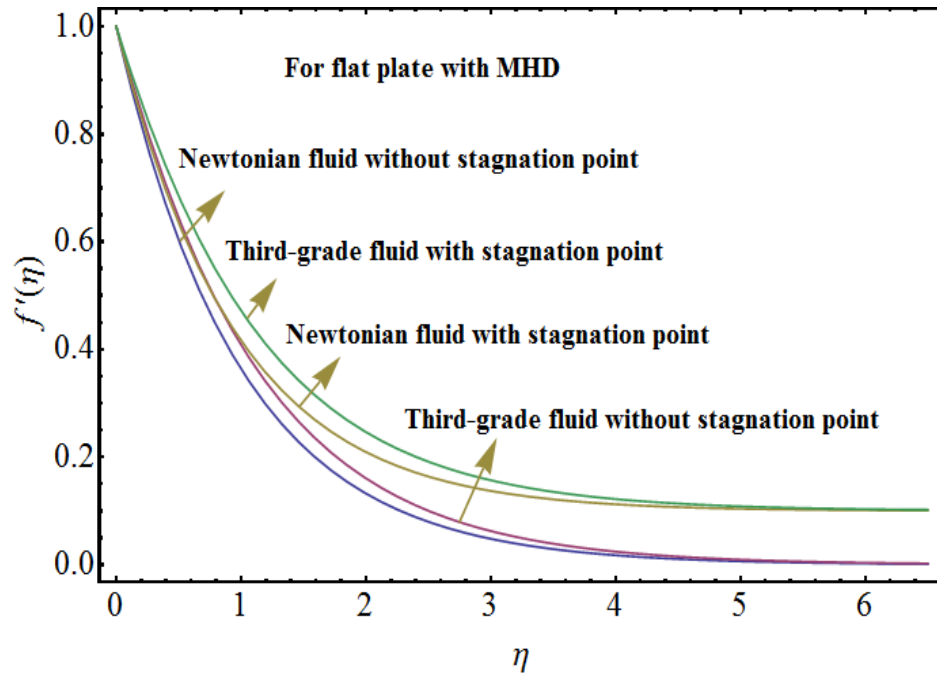
Fig. 8.19: Comparison of velocity profiles for Newtonian and third-grade fluids for flat plate.

Table 8.1: Convergence of homotopy solutions when $\alpha_1 = \alpha_2 = \beta = 0.1$, $Ha = 0.5$, $\gamma = A = \mathrm{Re} = 0.2$, $\psi = \pi/4$, $R_d = 0.3$, $\mathrm{Pr} = 2$, $Ec = 0.5$.

Order of approximation	$-f''(0)$	$-\theta'(0)$
1	0.98019	1.0966
2	1.06910	1.0973
5	1.13430	1.0458
11	1.13740	1.0316
12	1.13740	1.0315
14	1.13740	1.0315
50	1.13740	1.0315

Table 8.2: Numerical values of skin friction coefficient $Re_x^{1/2}C_f$ for different values of physical parameters

α_1	α_2	β	Ha	Re	γ	ψ	A	$-Re_x^{1/2}C_f$
0.0	0.1	0.1	0.5	0.2	0.2	$\pi/4$	0.2	1.4029
0.1								1.5374
0.2								1.6550
0.1	0.0	0.1	0.5	0.2	0.2	$\pi/4$	0.2	1.6491
	0.1							1.5374
	0.2							1.4408
0.1	0.1	0.0	0.5	0.2	0.2	$\pi/4$	0.2	1.5252
		0.1						1.5374
		0.2						1.5487
0.1	0.1	0.1	0.3	0.2	0.2	$\pi/4$	0.2	1.5080
			0.5					1.5374
			0.7					1.5803
0.1	0.1	0.1	0.5	0.0	0.2	$\pi/4$	0.2	1.5252
				0.1				1.5314
				0.2				1.5374
0.1	0.1	0.1	0.5	0.2	0.0	$\pi/4$	0.2	1.0228
					0.1			1.2676
					0.2			1.5374
0.1	0.1	0.1	0.5	0.2	0.2	0	0.2	1.4910
						$\pi/4$		1.5374
						$\pi/2$		1.5820
0.1	0.1	0.1	0.5	0.2	0.2	$\pi/4$	0.0	1.6733
							0.1	1.6200
							0.2	1.5374

Table 8.3: Numerical values of Nusselt number $\mathrm{Re}_x^{-1/2}\,Nu_x$ for different values of physical parameters

α_1	α_2	β	Ha	Re	R_d	γ	ψ	A	Pr	Ec	$\mathrm{Re}_x^{-1/2}\,Nu_x$
0.0	0.1	0.1	0.5	0.2	0.3	0.2	$\pi/4$	0.2	2	0.5	1.3945
0.1											1.4440
0.2											1.4819
0.1	0.0	0.1	0.5	0.2	0.3	0.2	$\pi/4$	0.2	2	0.5	1.3860
	0.1										1.4440
	0.2										1.4957
0.1	0.1	0.0	0.5	0.2	0.3	0.2	$\pi/4$	0.2	2	0.5	1.4354
		0.1									1.4440
		0.2									1.4516
0.1	0.1	0.1	0.3	0.2	0.3	0.2	$\pi/4$	0.2	2	0.5	1.4732
			0.5								1.4440
			0.7								1.4018
0.1	0.1	0.1	0.5	0.0	0.3	0.2	$\pi/4$	0.2	2	0.5	1.4354
				0.1							1.4398
				0.2							1.4440
0.1	0.1	0.1	0.5	0.2	0.0	0.2	$\pi/4$	0.2	2	0.5	1.2022
					0.1						1.2876
					0.3						1.4440
0.1	0.1	0.1	0.5	0.2	0.3	0.0	$\pi/4$	0.2	2	0.5	1.5721
						0.1					1.5112
						0.2					1.4440
0.1	0.1	0.1	0.5	0.2	0.3	0.2	0	0.2	2	0.5	1.4899
							$\pi/4$				1.4440
							$\pi/2$				1.4002
0.1	0.1	0.1	0.5	0.2	0.3	0.2	$\pi/4$	0.0	2	0.5	1.2297
								0.1			1.3312
								0.2			1.4440
0.1	0.1	0.1	0.5	0.2	0.3	0.2	$\pi/4$	0.2	1.0	0.5	1.0444
									1.5		1.2635
									2		1.4440
0.1	0.1	0.1	0.5	0.2	0.3	0.2	$\pi/4$	0.2	2	0.5	1.4440
										0.7	1.2745
										0.9	1.1050

8.5 Concluding remarks

MHD stagnation point flow of third-grade fluid by a stretching cylinder with thermal radiation is examined. Impact of involved parameters is seen. The following observations hold:

- Effect of third grade parameter β is to increase the boundary layer thickness.

- Velocity and temperature profiles increase away from the cylinder when curvature parameter γ increases.

- Effect of fluid parameters and Reynolds number on boundary layer thickness is similar in a qualitative sense.

- Velocity profile decreases while temperature profile increases for larger values of angle of inclination ψ.

- With the increase in Pr the temperature profile and thermal boundary layer thickness decrease.

- Minimum values of skin friction coefficient are achieved for small values of Re, α_1, β, Ha, γ, ψ and larger values of α_2 and A.

- Rate of heat transfer is higher for larger values of α_1, α_2, β, Re, R_d, A and Pr.

Chapter 9

Effect of inclined magnetic field in flow of third grade fluid with variable thermal conductivity

The effects of inclined magnetic field and heat transfer in the flow of a third-grade fluid due to an exponentially stretching sheet is adressed in this chapter. Formulation and analysis are given in the presence of heat source and sink. The variable thermal conductivity is taken temperature dependent. The governing boundary layer equations and boundary conditions are simplified through appropriate transformations. Resulting equations are solved for the approximate solutions. Convergence of governed problems is explicitly discussed. Influences of various dimensionless parameters on the flow and thermal fields are discussed. Numerical values of local skin friction coefficient and the local Nusselt number are analyzed.

9.1 Mathematical formulation

Consider the two-dimensional hydromagnetic flow of incompressible third-grade fluid by an exponentially stretching surface. The heat transfer effects are considered when thermal conductivity varies as a linear function of temperature. Boundary layer flow is considered in the presence of heat generation or absorption. Uniform magnetic field is applied at an angle ψ. There is no external electric field and induced magnetic field is neglected under the assumption of small magnetic Reynolds number. The governing two-dimensional flow and heat transfer equations are

$$\frac{\partial u}{\partial x} + \frac{\partial v}{\partial y} = 0,$$ (9.1)

$$u\frac{\partial u}{\partial x} + v\frac{\partial u}{\partial y} = \nu\frac{\partial^2 u}{\partial y^2} + \frac{\alpha_1^*}{\rho}\left[u\frac{\partial^3 u}{\partial x \partial y^2} + \frac{\partial u}{\partial x}\frac{\partial^2 u}{\partial y^2} + 3\frac{\partial u}{\partial y}\frac{\partial^2 v}{\partial y^2} + v\frac{\partial^3 u}{\partial y^3}\right]$$
$$+ 2\frac{\alpha_2^*}{\rho}\frac{\partial u}{\partial y}\frac{\partial^2 v}{\partial y^2} + 6\frac{\beta_3}{\rho}\left(\frac{\partial u}{\partial y}\right)^2\frac{\partial^2 u}{\partial y^2} - \frac{\sigma\,B_0^2}{\rho}\sin^2(\psi)u,$$ (9.2)

$$u\frac{\partial T}{\partial x} + v\frac{\partial T}{\partial y} = \frac{1}{\rho c_p}\frac{\partial}{\partial y}\left[k(T)\frac{\partial T}{\partial y}\right] + Q(T - T_\infty), \tag{9.3}$$

with the boundary conditions

$$
\begin{aligned}
u &= U_w(x) = U_0 \exp\left(\frac{x}{l}\right), \; v = 0, \; T = T_w = T_\infty + T_0 \exp\left(\frac{x}{2l}\right) \text{ at } y = 0,\\
u &\to 0, \qquad\quad T \to T_\infty \quad \text{as} \quad y \to \infty,
\end{aligned}
\tag{9.4}
$$

where u and v are the velocity components in the $x-$ and $y-$ directions respectively, α_1^*, α_2^* and β_3 are the fluid parameters, ρ is the fluid density, σ is the electric charge density, $K(T)$ is the temperature dependent thermal conductivity, c_p is the specific heat, T and T_∞ are the fluid and ambient temperatures respectively and T_w is the surface temperature.

The temperature dependent thermal conductivity $K(T)$ can be expressed as follows:

$$K(T) = K_\infty\left(1 + \epsilon\frac{T - T_\infty}{\Delta T}\right), \tag{9.5}$$

where ϵ is the small parameter, K_∞ is the thermal conductivity of the fluid far away from the surface and $\Delta T = T_w - T_\infty$. We define the following dimensionless transformations

$$
\begin{aligned}
\eta &= \sqrt{\frac{U_0}{2\nu l}} \exp\left(\frac{x}{2l}\right) y, \; \psi = \sqrt{2\nu l U_0} f(\eta) \exp\left(\frac{x}{2l}\right),\\
u(x,y) &= U_0 \exp\left(\frac{x}{l}\right) f'(\eta), \; v(x,y) = -\sqrt{\frac{\nu U_0}{2l}} \exp\left(\frac{x}{2l}\right)\left[f(\eta) + \eta f'(\eta)\right],\\
\theta &= \frac{T - T_\infty}{T_w - T_\infty}.
\end{aligned}
\tag{9.6}
$$

Here ψ is the stream function, f is the dimensionless stream function and θ is the dimensionless temperature. Using the above transformations, Eq. (8.1) is identically satisfied while Eqs. (9.2)-(9.4) are reduced to

$$
\begin{aligned}
&f''' - 2\left(f'\right)^2 + ff'' + \alpha_1\left\{3f'f''' - ff^{(iv)} - 2\eta f''f''' - 9\left(f''\right)^2\right\}\\
&-\alpha_2\left\{3\left(f''\right)^2 + \eta f''f'''\right\} + 3\beta\left(f''\right)^2 f''' - 2Ha^2\sin^2\psi f' = 0,
\end{aligned}
\tag{9.7}
$$

$$f'(0) = 1, \; f(0) = 0, \; f'(\infty) = 0, \tag{9.8}$$

$$(1 + \epsilon\theta)\theta'' + \epsilon\left(\theta'\right)^2 + \Pr\left(f\,\theta' - f'\theta\right) + 2\Pr\alpha\theta = 0, \tag{9.9}$$

$$\theta(0) = 1, \; \theta(\infty) = 0, \tag{9.10}$$

where α_1, α_2 and β are the fluid parameters, Pr the Prandtl number, ϵ small parameter and α the mixed

convection parameter. These quantities are defined as follows:

$$
\alpha_1 = \frac{U_0 \alpha_1^* \exp\left(\frac{x}{l}\right)}{\nu \rho l}, \quad \alpha_2 = \frac{U_0 \alpha_2^* \exp\left(\frac{x}{l}\right)}{\nu \rho l}, \beta = \frac{U_0^3 \beta_3 \exp\left(\frac{3x}{l}\right)}{\nu^2 \rho l},
$$

$$
\mathrm{Pr} = \frac{\mu_0 c_p}{K}, \quad Ha^2 = \frac{\sigma B_0^2 l}{\rho U_w}, \quad \alpha = \frac{l Q_0}{\rho c_p U_w}. \tag{9.11}
$$

The expressions of skin friction coefficient C_f and local Nusselt number Nu_x are

$$
C_f = \frac{\tau_{xy}}{\rho (cx)^2}, \quad Nu_x = \frac{x q_w}{K (T - T_\infty)}, \tag{9.12}
$$

in which the wall skin friction (τ_{xy}) and the wall heat flux (q_w) are

$$
\tau_{xy} = \left[\mu_0 \frac{\partial u}{\partial y} + \frac{\alpha_1^*}{\rho} \left(2 \frac{\partial u}{\partial x} \frac{\partial u}{\partial y} + v \frac{\partial^2 u}{\partial y^2} + u \frac{\partial^2 u}{\partial x \partial y} \right) + 2 \frac{\beta_3}{\rho} \left(\frac{\partial u}{\partial y} \right)^3 \right]_{y=0}, \quad q_w = -K \left(\frac{\partial T}{\partial y} \right)_{y=0}. \tag{9.13}
$$

After simplification, we have

$$
(\mathrm{Re}_x)^{1/2} C_f = \sqrt{2} \left[f'' + \alpha_1 (\frac{7}{2} f' f'' - \frac{1}{2} f f''') + \beta f''^3 \right]_{\eta=0}, \quad (\mathrm{Re}_x)^{-1/2} Nu_x = -\sqrt{\frac{X}{2}} \theta'(0), \tag{9.14}
$$

where $X = \frac{x}{l}$ and $\mathrm{Re}_x = \frac{U_w x}{\nu}$.

9.2 Homotopic solutions

The initial guesses $f_0(\eta)$ and $\theta_0(\eta)$ and the auxiliary linear operators L_f and L_θ are chosen in the following forms

$$
f_0(\eta) = 1 - \exp(-\eta), \quad \theta_0(\eta) = \exp(-\eta), \tag{9.15}
$$

$$
L_f[f(\eta)] = \frac{d^3 f}{d\eta^3} - \frac{df}{d\eta}, \quad L_\theta[\theta(\eta)] = \frac{d^2 \theta}{d\eta^2} - \theta, \tag{9.16}
$$

with

$$
L_f[C_{39} + C_{40} \exp(\eta) + C_{41} \exp(-\eta)] = 0, \tag{9.17}
$$

$$
L_\theta[C_{42} \exp(\eta) + C_{43} \exp(-\eta)] = 0. \tag{9.18}
$$

where C_i $(i = 39 - 43)$ are the constants to be determined from the boundary conditions.

9.2.1 Zeroth-order deformation problem

The zeroth-order deformation problems are

$$
(1 - q) L_f \left[\hat{f}(\eta, q) - f_0(\eta) \right] = q h_f \mathcal{N}_f \left[\hat{f}(\eta, q) \right], \tag{9.19}
$$

$$
\hat{f}(0, q) = 0, \quad \left. \frac{\partial \hat{f}(\eta, q)}{\partial \eta} \right|_{\eta=0} = 1, \quad \left. \frac{\partial \hat{f}(\eta, q)}{\partial \eta} \right|_{\eta \to \infty} = 0, \tag{9.20}
$$

$$(1 - q) L_\theta \left[\hat{\theta} (\eta, q) - \theta_0 (\eta) \right] = q h_\theta \mathcal{N}_\theta \left[\hat{\theta} (\eta, q) . \hat{f} (\eta, q) \right], \tag{9.21}$$

$$\left. \hat{\theta} (\eta, q) \right|_{\eta=0} = 1, \qquad \left. \hat{\theta} (\eta, q) \right|_{\eta \to \infty} = 0. \tag{9.22}$$

In the above expression $q \in [0, 1]$ denotes an embedding parameter and $\hbar_f \neq 0$ and $\hbar_\theta \neq 0$ are the auxiliary parameters. The non-linear operators $\mathcal{N}_f$ and $\mathcal{N}_\theta$ are given by

$$\mathcal{N}_f [f (\eta, q)] = \frac{\partial^3 \hat{f}}{\partial \eta^3} - 2 \left(\frac{\partial \hat{f}}{\partial \eta} \right)^2 + f \frac{\partial^2 \hat{f}}{\partial \eta^2} + \alpha_1 \left[3 \frac{\partial \hat{f}}{\partial \eta} \frac{\partial^3 \hat{f}}{\partial \eta^3} - f \frac{\partial^4 \hat{f}}{\partial \eta^4} - 2\eta \frac{\partial^2 \hat{f}}{\partial \eta^2} \frac{\partial^3 \hat{f}}{\partial \eta^3} - 9 \left(\frac{\partial^2 \hat{f}}{\partial \eta^2} \right)^2 \right]$$
$$-\alpha_2 \left[3 \left(\frac{\partial^2 \hat{f}}{\partial \eta^2} \right)^2 + \eta \frac{\partial^2 \hat{f}}{\partial \eta^2} \frac{\partial^3 \hat{f}}{\partial \eta^3} \right] + 3\beta \left(\frac{\partial^2 \hat{f}}{\partial \eta^2} \right)^2 \frac{\partial^3 \hat{f}}{\partial \eta^3} - 2Ha^2 \sin^2 \psi \frac{\partial \hat{f}}{\partial \eta}, \tag{9.23}$$

$$\mathcal{N}_\theta [\theta (\eta, q), f (\eta, q)] = (1 + \epsilon\theta) \frac{\partial^2 \hat{\theta}}{\partial \eta^2} + \epsilon \left(\frac{\partial \hat{\theta}}{\partial \eta} \right)^2 + \Pr \left(\hat{f} \frac{\partial \hat{\theta}}{\partial \eta} - \frac{\partial \hat{f}}{\partial \eta} \hat{\theta} \right) + 2 \Pr \alpha \ \hat{\theta}. \tag{9.24}$$

When $q = 0$ and $q = 1$, then

$$\hat{f} (\eta, 0) = f_0 (\eta), \ \hat{\theta} (\eta, 0) = \theta_0 (\eta) \ \text{and} \ \hat{f} (\eta, 1) = f (\eta), \ \hat{\theta} (\eta, 1) = \theta (\eta). \tag{9.25}$$

In view of Taylor series, one can express $\hat{f} (\eta, q)$ and $\hat{\theta} (\eta, q)$ in the following forms:

$$\hat{f} (\eta, q) = f_0 (\eta) + \sum_{m=1}^{\infty} f_m (\eta) q^m, \quad \hat{f}_m (\eta) = \frac{1}{m!} \left. \frac{\partial^m f (\eta, q)}{\partial q^m} \right|_{q=0}, \tag{9.26}$$

$$\hat{\theta} (\eta, q) = \theta_0 (\eta) + \sum_{m=1}^{\infty} \theta_m (\eta) q^m, \quad \hat{\theta}_m (\eta) = \frac{1}{m!} \left. \frac{\partial^m \theta (\eta, q)}{\partial q^m} \right|_{q=0}, \tag{9.27}$$

where the convergence depends upon $\hbar_f$ and $\hbar_\theta$. The convergence of the series (9.26) and (9.27) is strictly based upon $\hbar_f$ and $\hbar_\theta$. The values of $\hbar_f$ and $\hbar_\theta$ are chosen in such a way that the series (9.26) and (9.27) are convergent at $q = 1$ and hence

$$\hat{f} (\eta) = f_0 (\eta) + \sum_{m=1}^{\infty} f_m (\eta), \tag{9.28}$$

$$\hat{\theta} (\eta) = \theta_0 (\eta) + \sum_{m=1}^{\infty} \theta_m (\eta). \tag{9.29}$$

9.2.2   mth-order deformation problems

The mth-order deformation problems are

$$L_f \left[\hat{f}_m (\eta) - \chi_m \hat{f}_{m-1} (\eta) \right] = h_f \mathcal{R}_m^f (\eta), \tag{9.30}$$

$$\hat{f}_m (0, q) = 0, \quad \left. \frac{\partial \hat{f}_m (\eta, q)}{\partial \eta} \right|_{\eta=0} = 0, \quad \left. \frac{\partial \hat{f}_m (\eta, q)}{\partial \eta} \right|_{\eta \to \infty} = 0, \tag{9.31}$$

$$L_\theta \left[\hat{\theta}_m (\eta) - \chi_m \hat{\theta}_{m-1} (\eta) \right] = \hbar_\theta \mathcal{R}_m^\theta (\eta), \tag{9.32}$$

$$\hat{\theta}_m (\eta, q) \Big|_{\eta=0} - \gamma \; \theta_m (\eta, q)|_{\eta=0} = 0, \qquad \hat{\theta}_m (\eta, q) \Big|_{\eta \to \infty} = 0. \tag{9.33}$$

$$
\begin{aligned}
\mathcal{R}_m^f (\eta) &= f_{m-1}''' - 2 \sum_{k=0}^{m-1} f_{m-1-k}' f_k' + \sum_{k=0}^{m-1} f_{m-1-k} f_k'' + \alpha_1 \sum_{k=0}^{m-1} \left[3 f_{m-1-k}' f_m''' - f_{m-1-k} f_k^{(iv)} \right. \\
&\quad \left. -2\eta \; f_{m-1-k}'' \; f_k''' - 9 f_{m-1-k}'' \; f_k'' \right] + \alpha_2 \sum_{k=0}^{m-1} \left[3 f_{m-1-k}'' f_k'' + \eta f_{m-1-k}'' f_k''' \right] \\
&\quad + 3\beta \operatorname{Re} \sum_{k=0}^{m-1} f_{m-1-k}'' \sum_{l=0}^{k} f_{k-l}'' f_l''' - 2 Ha^2 \sin^2 (\psi) \, f_{m-1}',
\end{aligned}
\tag{9.34}
$$

$$\mathcal{R}_m^\theta (\eta) = \theta_{m-1}'' + \epsilon \sum_{k=0}^{m-1} \theta_{m-1-k} \theta_k'' + \epsilon \sum_{k=0}^{m-1} \theta_{m-1-k}' \theta_k' + \operatorname{Pr} \sum_{k=0}^{m-1} \left(f_{m-1-k} \theta_k' - f_{m-1-k}' \theta_k \right) + 2 \operatorname{Pr} \alpha \, \theta_{m-1},$$
$$\tag{9.35}$$

The general solutions (f_m, θ_m) of the mth order Eqs. (30)-(33) in terms of special solutions (f_m^*, θ_m^*) are

$$f_m (\eta) = f_m^* + C_{39} + C_{40} \exp (\eta) + C_{41} \exp (-\eta), \tag{9.36}$$

$$\theta_m (\eta) = \theta_m^* + C_{42} \exp (\eta) + C_{43} \exp (-\eta), \tag{9.37}$$

where arbitrary constants are determined through the boundary conditions (8.30) and (8.32) in the values given below:

$$
\begin{aligned}
C_{41} &= C_{42} = 0, \qquad C_{40} = \left. \frac{\partial f_m^* (\eta)}{\partial \eta} \right|_{\eta=0}, \qquad C_{39} = -C_{40} - f_m^* (0), \\
C_{43} &= -\theta_m^* (0).
\end{aligned}
$$

9.3 Convergence of the homotopy solutions

In homotopy analysis method, the convergence region is essential to determine the meaningful series solutions of the governing problems. The auxiliary parameters $\hbar_f$ and $\hbar_\theta$ are used to control the convergence region of series solutions (9.28) and (9.29). Therefore the $\hbar$-curves are plotted at 18th order of approximations in Fig. 9.1. From Fig. 9.1 we observed that the suitable ranges of $\hbar_f$ and $\hbar_\theta$ are $-1.4 \leq \hbar_f < -0.5$ and $-1.5 \leq \hbar_\theta < -0.2$.

9.4 Results and discussion

The theme of this section is to analyze the effect of various physical parameters on the velocity and temperature profiles. Variation of magnetic parameter Ha on the velocity profile is displayed in Fig. 9.2 by keeping other parameters fixed. It is found that velocity profile decreases via larger Ha. Physically by increasing magnetic field the Lorentz force increases. More resistance is offered to the motion of fluid and thus the velocity of the fluid is reduced. Fig. 9.3 illustrates the effect of third-grade parameter β

on the velocity profile $f'(\eta)$. It is analyzed that the velocity profile increases near the wall for larger values of β and it vanishes away from the wall. Moreover the momentum boundary layer thickness is also increasing function of β. In fact β is inversly proportional to the viscosity. For larger values of β, the viscosity of the fluid decreases and hence the velocity profile increases. Fig. 9.4 is drawn to see the effect of fluid parameter α_2 on the velocity profile $f'(\eta)$. The velocity profile decreases near the wall and it shows mixing behavior away from the wall when $\eta \geq 3$. Momentum boundary layer thickness is also decreased. Similar behavior is observed in Fig. 9.5 for the fluid parameter α_2 (see Fig. 9.4). Fig. 9.6 is plotted to see the behavior of angle of inclination ψ on velocity profile $f'(\eta)$. It is clearly seen that velocity profile decreases by increasing values of angle of inclination ψ. It is due to the fact that with an increase in angle of inclination, the effect of magnetic field on fluid particles increases which enhances the Lorentz force. Consequently the velocity profile decreases. It is also noted that for $\psi = 0$ the magnetic field has no effect on the velocity profile while maximum resistance is offered for the fluid particles when $\psi = \pi/2$. Behavior of magnetic parameter Ha on temperature profile $\theta(\eta)$ is sketched in Fig. 9.7 for both heat generation and absorption cases. It is analyzed that temperature profile is increased by increasing magnetic parameter Ha for both cases i.e. heat generation and heat absorption. Larger values of magnetic parameter corresponds to an increase in Lorentz force. Hence temperature profile increases. It is also observed that the thermal boundary layer thickness is increasing function of magnetic parameter. Analysis of third-grade parameter β on temperature profile $\theta(\eta)$ is displayed in Fig. 9.8 for heat generation and absorption cases. It is observed that temperature profile is decreased for larger values of third-grade parameter β in both heat generation and absorption. Because viscosity of the fluid decreases for larger values of β, resistance offered to fluid particles decreases and less heat is produced. Consequently the temperature profile decreases. Fig. 9.9 is presented for the behavior of fluid parameter α_1 for heat generation and absorption on temperature profile $\theta(\eta)$. It is found that for both cases the temperature profile increases near the surface of the wall and it increases rapidly away from the surface. Fig. 9.10 is plotted for the influence of α_2 on temperature profile $\theta(\eta)$ when $\alpha = 0.4$ and $\alpha = -0.4$. It is analyzed that temperature and thermal boundary layer thickness increase for higher values of fluid parameter α_2 for heat source and sink. Fig. 9.11 shows the variation of angle of inclination ψ on temperature profile for both heat generation and absorption. It is noted that temperature profile is higher for larger values of angle ψ for both heat generation and absorption. In fact higher values of angle ψ corresponds to larger magnetic field which opposes the fluid motion. Hence temperature profile increases. Fig. 9.12 presents the influence of small parameter ϵ on the temperature profile in heat generation and absorption cases. Increasing the value of small parameter ϵ produces higher temperatures for both cases. There is also an increase in the thermal boundary layer thickness when small parameter ϵ increases. Fig. 9.13 is plotted to see the effects of Prandtl number Pr on the fluid temperature $\theta(\eta)$ for both cases of heat generation and absorption. It is observed that the fluid temperature $\theta(\eta)$ decays through Prandtl number Pr. Further the thermal boundary layer thickness decreases. In fact the Prandtl number is the ratio of momentum diffusivity to thermal diffusivity and the thermal diffusivity becomes smaller (for larger Prandtl number) which reduces the temperature and associated boundary layer thickness.

Fig. 9.14 shows the behavior of heat generation/absorption parameter α on temperature distribution. It is noted that temperature distribution is higher for larger values of heat generation parameter while it decreases with an increase in heat absorption parameter. In fact more heat is produced during the heat generation process which is responsible in the enhancement of temperature distribution. Fig. 9.15 displays the behavior of skin friction coefficient corresponding to Newtonian and non-Newtonian fluids and Hartman number M. It is analyzed that skin friciton coefficient for Newtonian fluid is less than second and third grade fluids. It is also noted that skin friction coefficient increases for higher values of Hartman number in the case of Newtonian and non-Newtonian fluids. Figs. 9.16 and 9.17 show impact of Newtonian and non-Newtonian fluids and ϵ for the case of heat generation/absorption. Nusselt number is higher for the third grade fluid when compared with Newtonian and second grade fluids in both cases of heat generation and heat absorption. Further Nusselt number shows decreasing behavior for higher ϵ.

Table 9.1 shows the convergence of series solutions numerically. It is noted that 7th order of approximation is enough for velocity and 12th order of approximation is sufficient for the temperature. Table 9.2 depicts the numerical values of skin friction coefficient for various values of α_1, α_2, β, Ha and ψ. It is analyzed that the surface drag force increases for larger values of α_1, α_2, β, M and ψ. Table 9.3 displays the numerical values of local Nusselt number for different values of α_1, α_2, β, Ha, Pr, ψ and ϵ in the case of heat absorption when $\alpha = -0.1$. It is seen that local Nusselt number decreases with the increase of α_1, α_2, Ha, and ψ while it increases when β, Pr and ϵ are increased. Table 9.4 is constructed to see the numerical values of local Nusselt number for different values of α_1, α_2, β, Ha, Pr, ψ and ϵ in the case of heat generation when $\alpha = 0.1$. It is noted that rate of heat transfer increases for larger β and Pr while it decreases when α_1, α_2, Ha, ϵ, and ψ are increased. Table 9.5 shows the comparison of local Nusselt number with the previous results. It is concluded that present results are in good agreement with the previous results.

$\beta=\alpha_1=0.1, \alpha_2=0.2, \text{Re}=0.1, \text{Ha}=0.2, \lambda=\gamma=0.2, \text{Pr}=1.5, \psi=\pi/4, \epsilon=0.2$
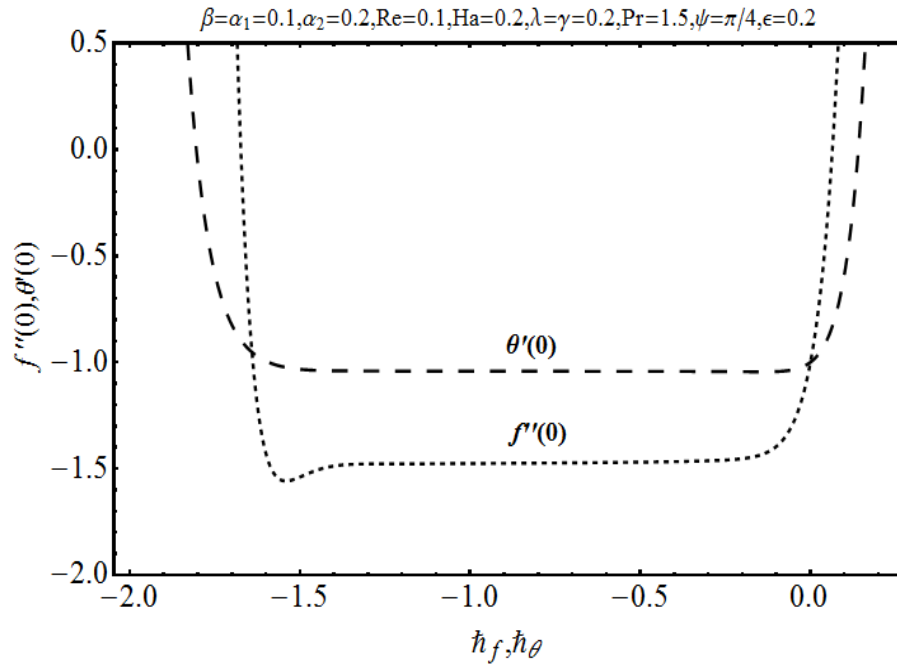
Fig. 9.1: $\hbar$-curve for the functions $f(\eta)$ and $\theta(\eta)$.
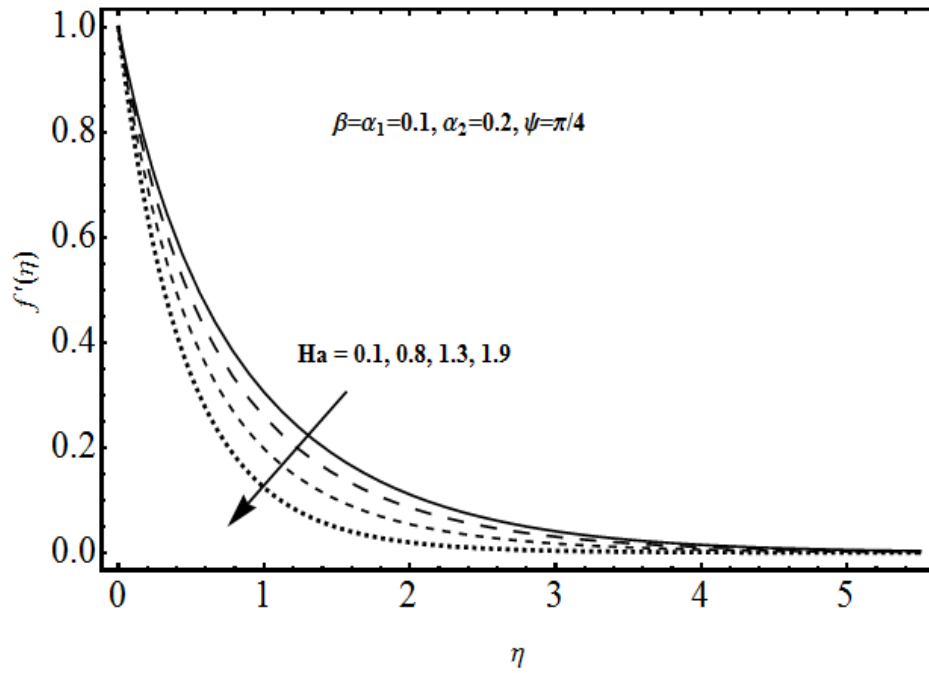
Fig. 9.2: Variation of velocity component $f'(\eta)$ for magnetic parameter Ha.
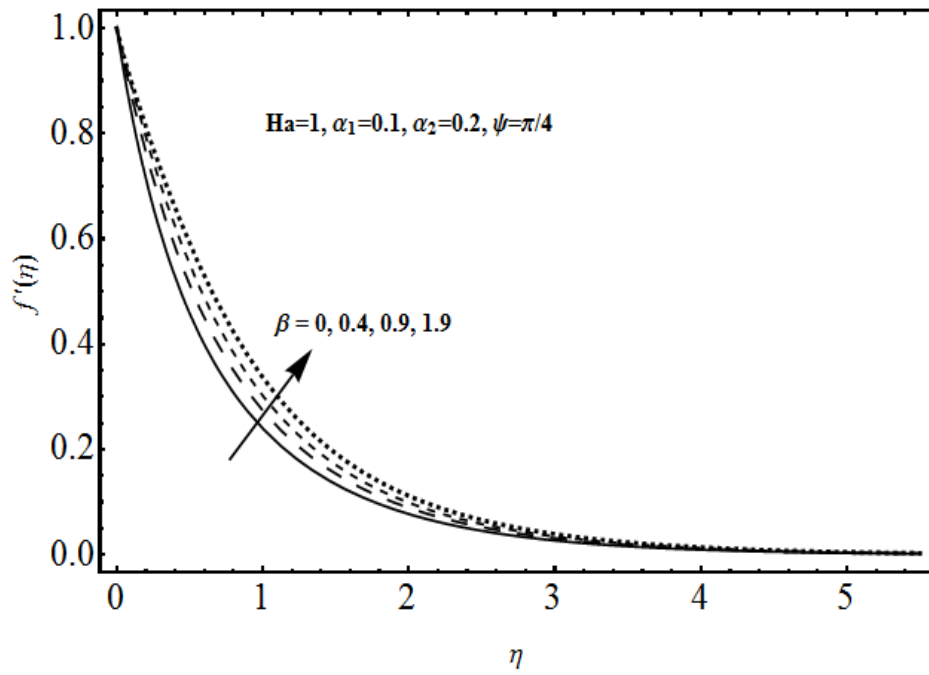
Fig. 9.3: Variation of velocity component $f'(\eta)$ for third-grade parameter β.
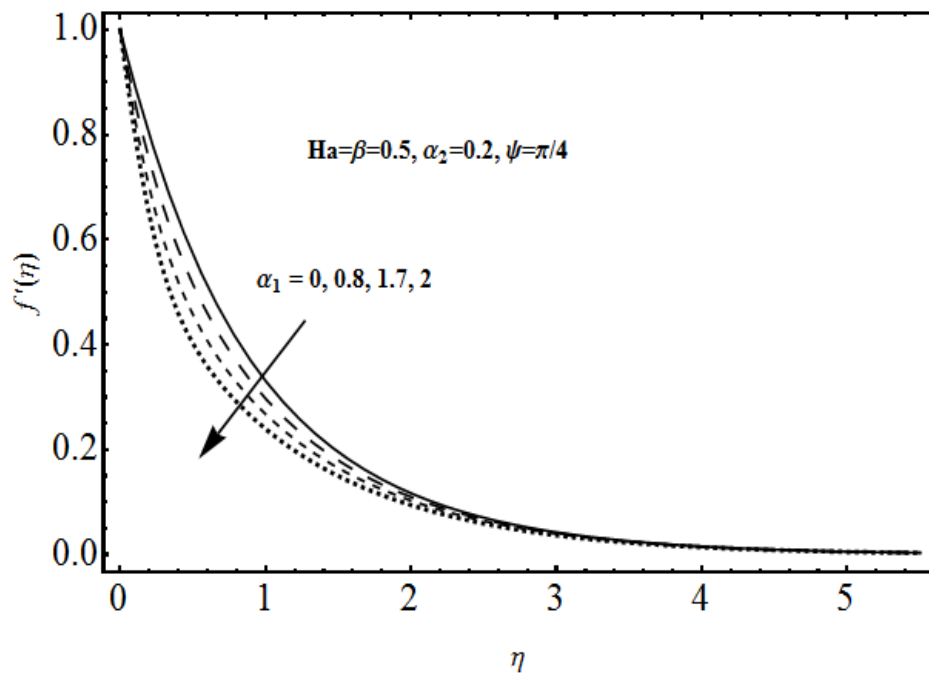
Fig. 9.4: Variation of velocity component $f'(\eta)$ for second-grade parameter α_1.
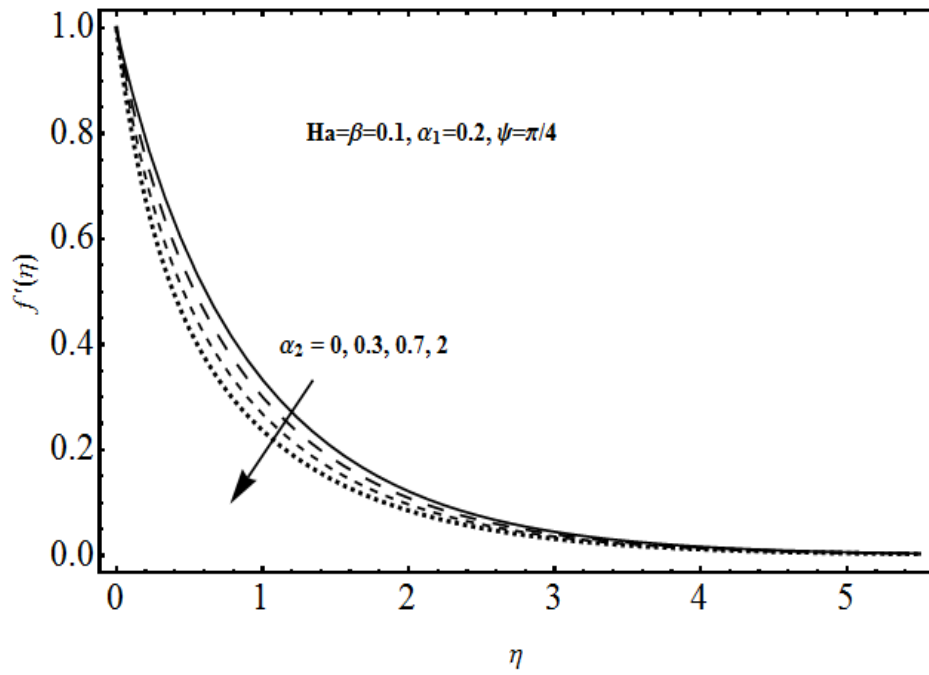
Fig. 9.5: Variation of velocity component $f'(\eta)$ for second-grade parameter α_2.
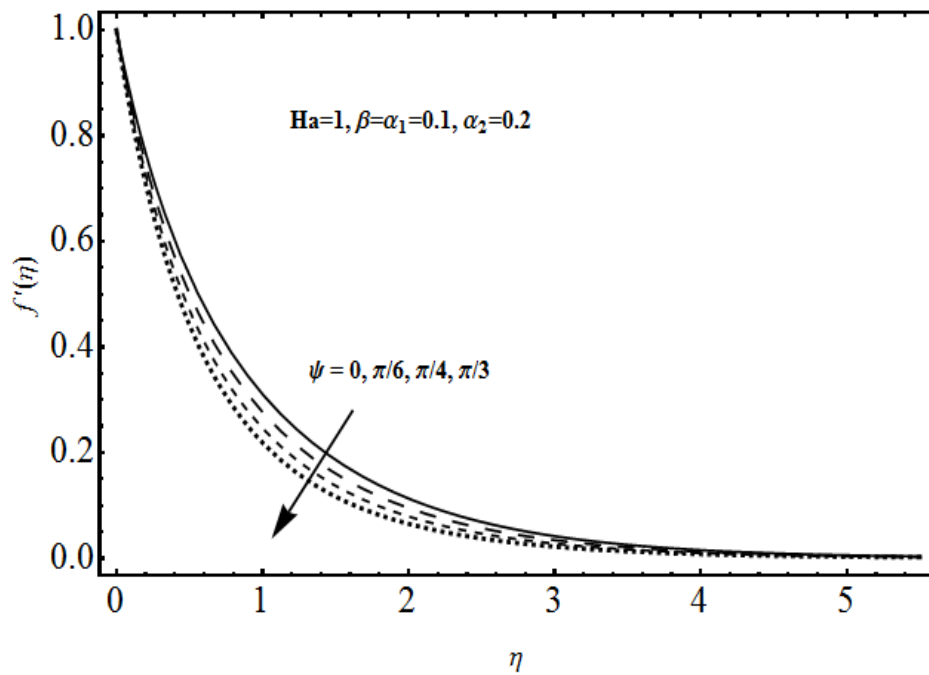
Fig. 9.6: Variation of velocity component $f'(\eta)$ for inclination parameter ψ.
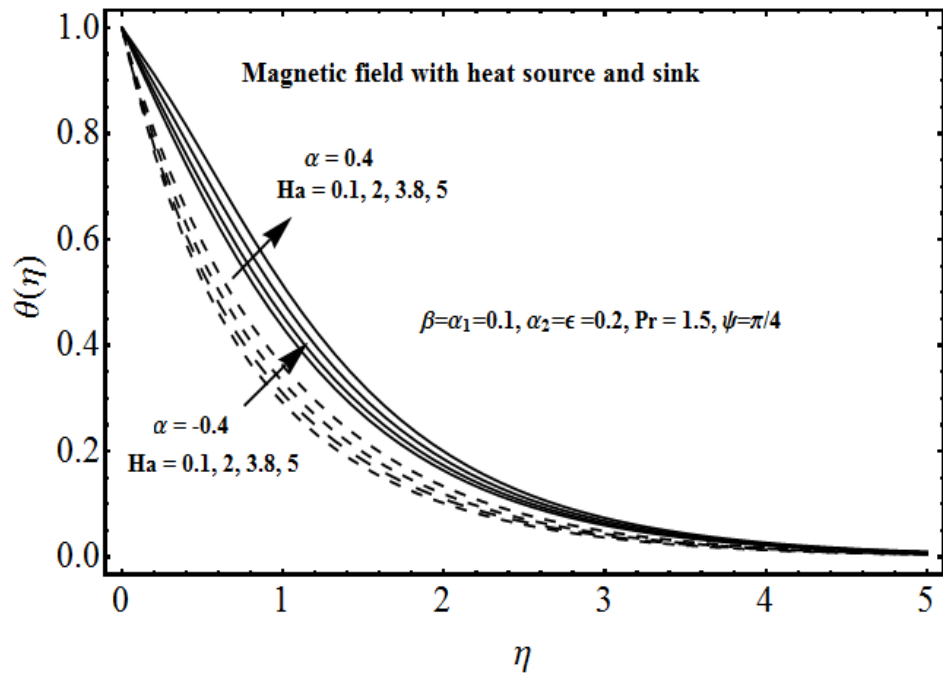
Fig. 9.7: Variation of temperature $\theta\left(\eta\right)$ for magnetic parameter Ha.
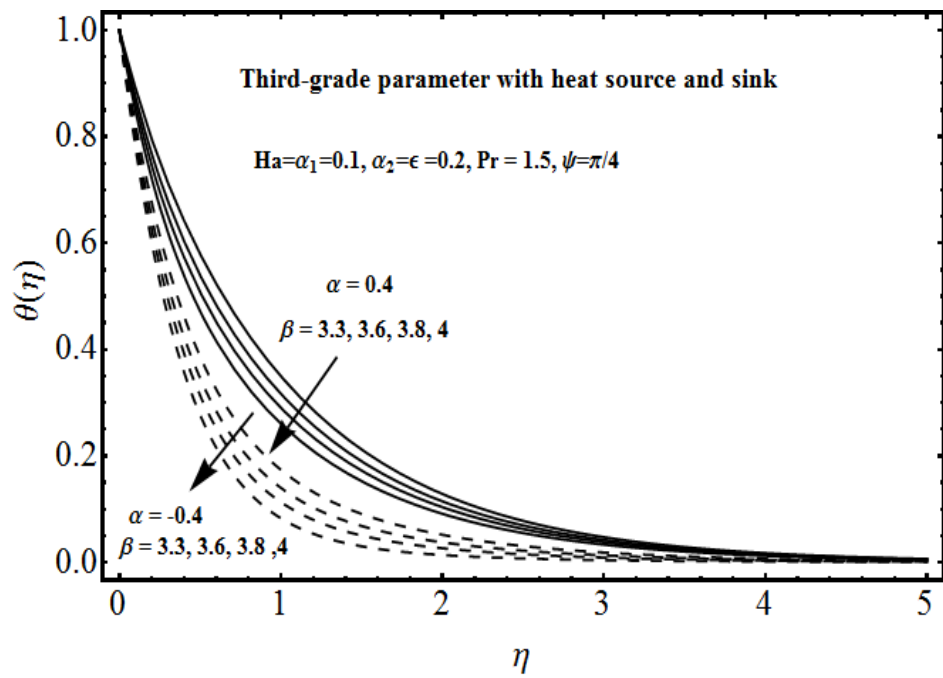
Fig. 9.8: Variation of temperature $\theta\left(\eta\right)$ for third-grade parameter β.
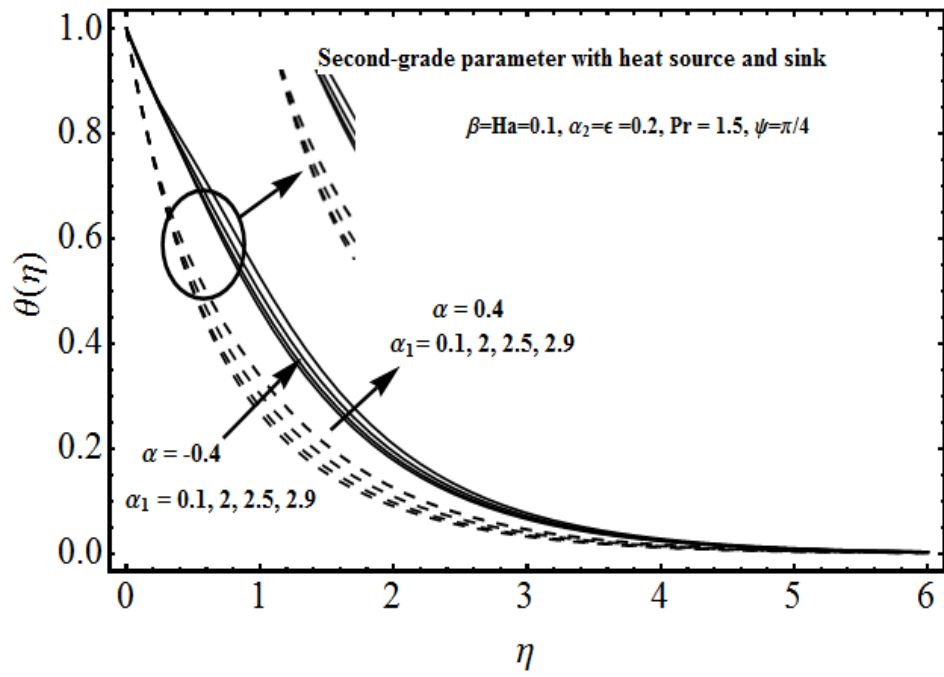
Fig. 9.9: Variation of temperature $\theta\,(\eta)$ for second-grade parameter α_1.
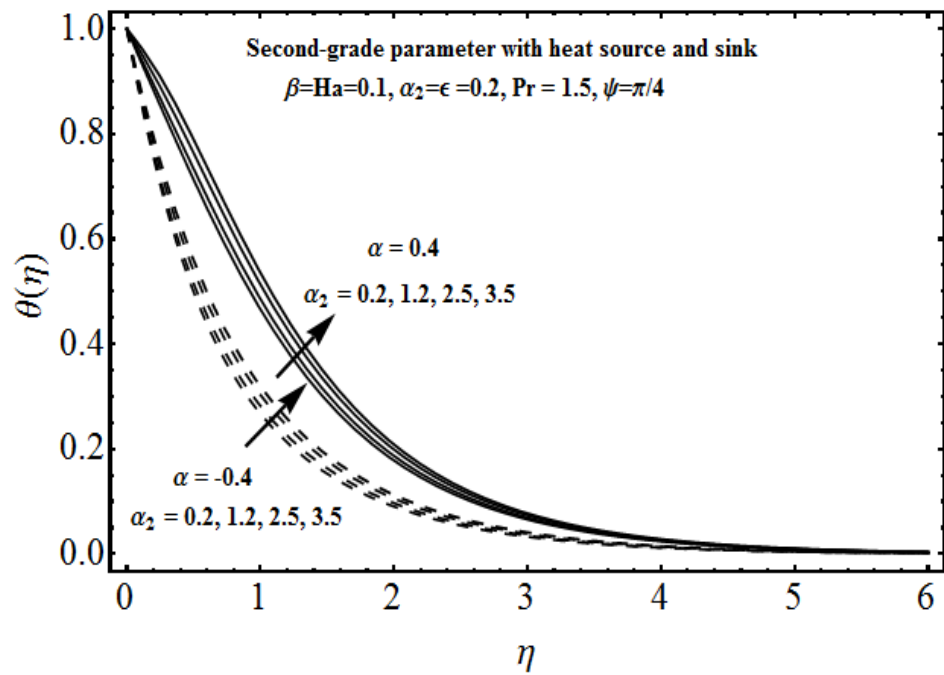
Fig. 9.10: Variation of temperature $\theta\,(\eta)$ for second-grade parameter α_2.
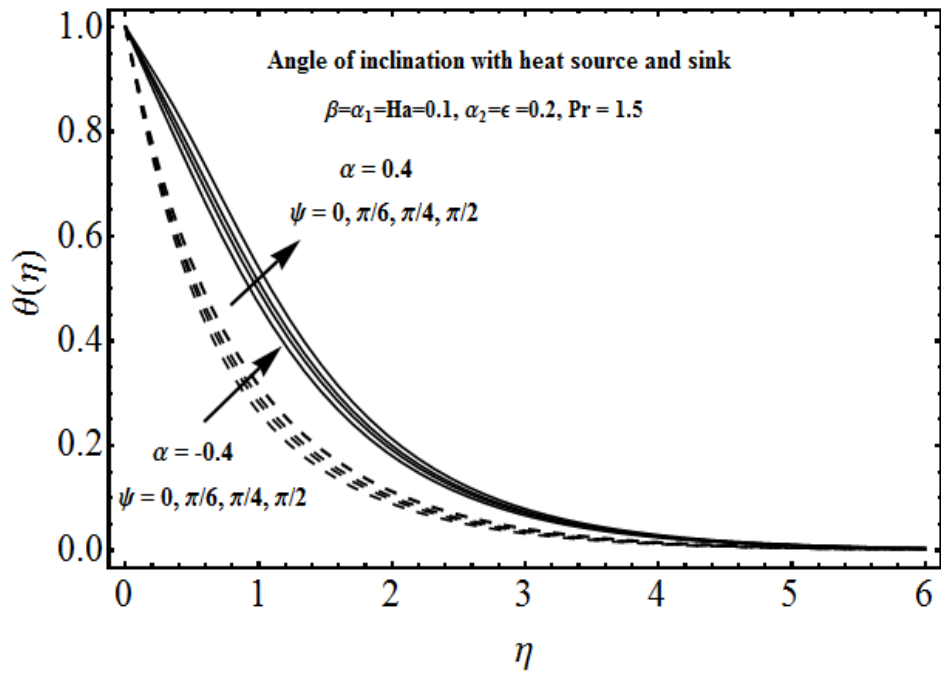
Fig. 9.11: Variation of temperature $\theta(\eta)$ for angle of inclination ψ.
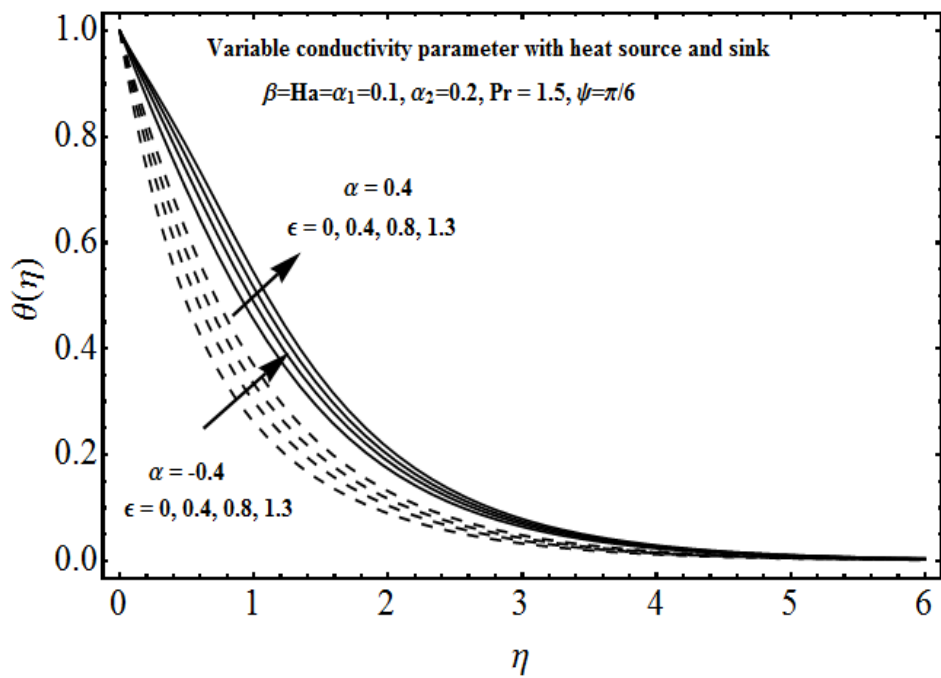
Fig. 9.12: Variation of temperature $\theta(\eta)$ for variable conductivity

parameter ϵ.
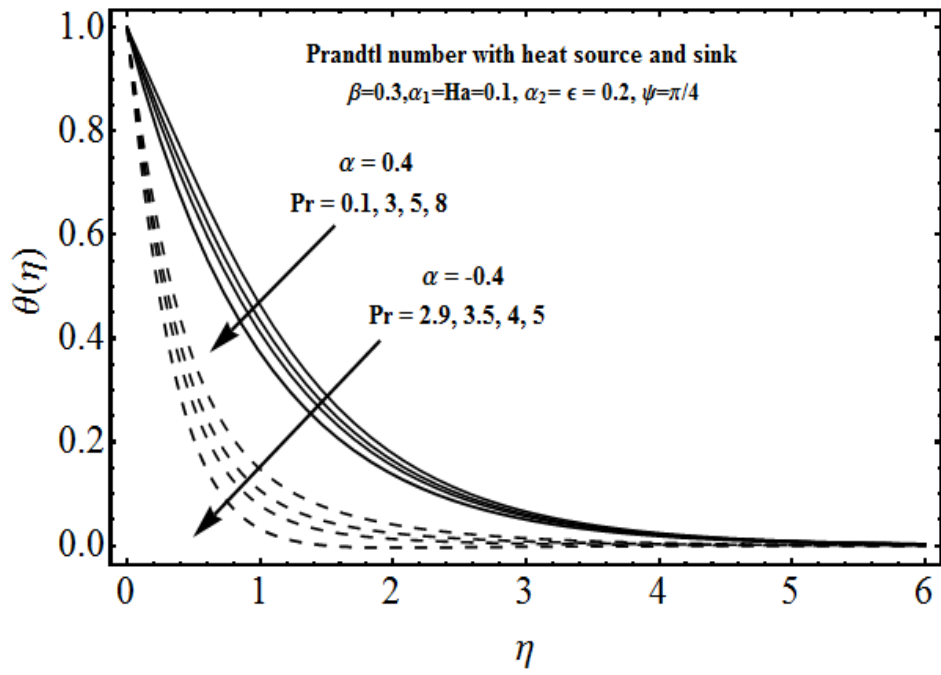
Fig. 9.13: Variation of temperature $\theta(\eta)$ for Prandtl number Pr.
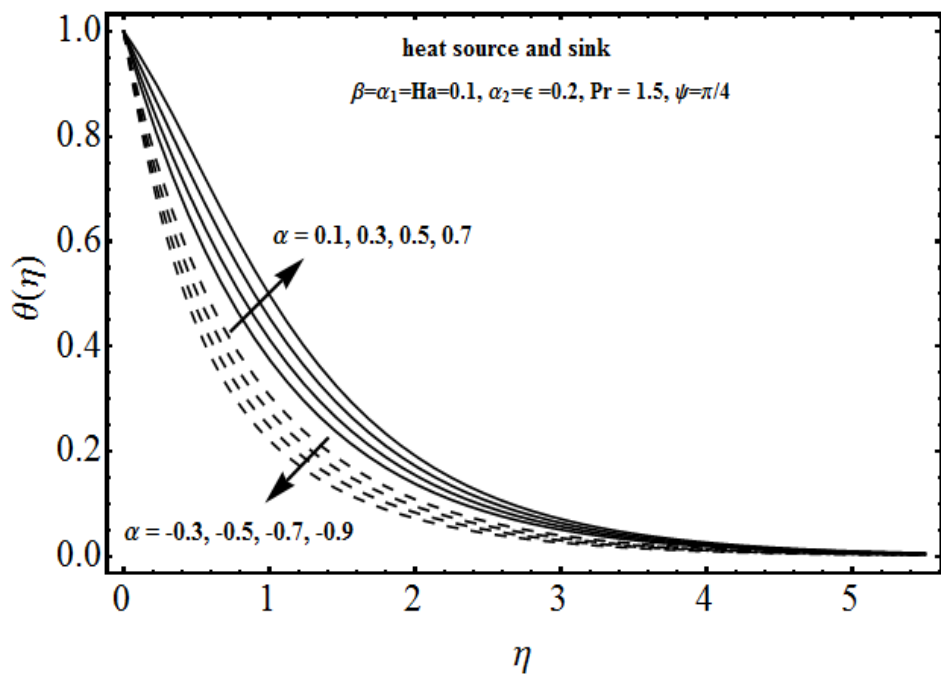
Fig. 9.14: Variation of temperature $\theta(\eta)$ for heat source and sink

parameter α.

Table 9.1: Convergence of HAM solutions for different order of approximation when $\alpha_1 = 0.01$, $\alpha_2 = 0.02$, $\beta = 0.04$, $\mathrm{Re} = 0.1$, $Ha = 0.7$, $\lambda = 0.2$, $\gamma = 0.2$, $Ec = 0.5$ and $\mathrm{Pr} = 2$.

Order of approximation	$-f''(0)$	$-\theta'(0)$
1	1.419	0.1371
2	1.534	0.1245
5	1.613	0.1099
7	1.616	0.1072
12	1.616	0.1057
18	1.616	0.1057
26	1.616	0.1057
30	1.616	0.1057

Table 9.2: Numerical values of local Nusselt number $\mathrm{Re}_x^{-1/2} Nu_x$ for different values of physical parameters.

α_1	α_2	β	Ha	ψ	$-\mathrm{Re}_x^{1/2} C_x$
0.1	0.2	0.1	0.2	$\pi/4$	3.1690
0.2					4.1530
0.3					5.1460
0.4					6.1350
0.1	0.1	0.1	0.2	$\pi/4$	2.9610
	0.2				3.1690
	0.3				3.3960
	0.4				3.6410
0.1	0.2	0.1	0.2	$\pi/4$	3.1690
		0.2			3.1780
		0.3			3.1910
		0.4			3.2040
0.1	0.2	0.1	0.2	$\pi/4$	3.1690
			0.3		3.2220
			0.4		3.2950
			0.5		3.3880
0.1	0.2	0.1	0.2	0	3.1250
				$\pi/4$	3.1690
				$\pi/3$	3.1910
				$\pi/2$	3.2120

Table 9.3: Numerical values of local Nusselt number $\mathrm{Re}_x^{-1/2} Nu_x$ for different values of physical parameters for heat sink when $\alpha = -0.1$.

α_1	α_2	β	Re	Ha	Pr	ψ	ϵ	$\mathrm{Re}_x^{-1/2} Nu_x$
0.1	0.2	0.1	0.1	0.2	1.5	$\pi/4$	0.2	0.8404
0.2								0.8378
0.3								0.8366
0.4								0.8362
0.1	0.1	0.1	0.1	0.2	1.5	$\pi/4$	0.2	0.8457
	0.2							0.8404
	0.3							0.8350
	0.4							0.8296
0.1	0.2	0.1	0.1	0.2	1.5	$\pi/4$	0.2	0.8404
		0.2						0.8471
		0.3						0.8524
		0.4						0.8569
0.1	0.2	0.1	0.1	0.2	1.5	$\pi/4$	0.2	0.8404
				0.3				0.8377
				0.4				0.8339
0.1	0.2	0.1	0.1	0.5	1.1	$\pi/4$	0.2	0.6877
					1.2			0.7251
					1.3			0.7611
					1.4			0.7958
0.1	0.2	0.1	0.1	0.2	1.5	0	0.2	0.8426
						$\pi/4$		0.8404
						$\pi/3$		0.8392
						$\pi/2$		0.8381
0.1	0.2	0.1	0.1	0.2	1.5	$\pi/4$	0.2	0.8404
							0.3	0.7944
							0.4	0.7543

Table 9.4: Numerical values of local Nusselt number $\mathrm{Re}_x^{-1/2}\,Nu_x$ for different values of physical parameters for heat source when $\alpha = 0.1$.

α_1	α_2	β	Re	Ha	Pr	ψ	ϵ	X	$\mathrm{Re}_x^{-1/2}\,Nu_x$
0.1	0.2	0.1	0.2	0.1	1.5	$\pi/4$	0.2	1	0.6399
0.2									0.6379
0.3									0.6359
0.1	0.1	0.1	0.2	0.1	1.5	$\pi/4$	0.2	1	0.6484
	0.2								0.6399
	0.3								0.6308
0.1	0.2	0.1	0.2	0.1	1.5	$\pi/4$	0.2	1	0.6399
		0.2							0.6499
		0.3							0.6581
0.1	0.2	0.1	0.2	0.1	1.5	$\pi/4$	0.2	1	0.6399
			0.2						0.6363
			0.3						0.6303
0.1	0.2	0.1	0.1	0.5	1.1	$\pi/4$	0.2	1	0.5019
					1.2				0.5340
					1.3				0.5739
0.1	0.2	0.1	0.1	0.2	1.5	0	0.2	1	0.6412
						$\pi/4$			0.6360
						$\pi/2$			0.6313
0.1	0.2	0.1	0.1	0.2	1.5	$\pi/4$	0.2	1	0.6361
							0.3		0.5977
							0.4		0.5642
0.1	0.2	0.1	0.1	0.2	1.5	$\pi/4$	0.2	0.7	0.5321
								0.8	0.5688
								1.0	0.6361

9.5   Concluding remarks

Effect of inclined magnetic field on flow of variable thermal conductivity in third-grade fluid is investigated. Main observations are listed below.

- Effects of α_1, α_2 and ψ on the fluid temperature are quite similar.

- The velocity field $f'(\eta)$ decreases by increasing magnetic parameter while temperature profile $\theta(\eta)$ enhances for both heat generation/absorption.

- Table 1 ensures that the convergence of the functions $f(\eta)$ and $\theta(\eta)$ are obtained at only 7th and 12th order of approximations respectively.

- Effects of Ha and ψ on the velocity field are qualitatively similar.

- Effect of fluid parameter and angle of inclination are quite opposite.

- An increase in Pr corresponds to decrease in the temperature profile for both heat generation and absorption.

- Effects of fluid parameter β on the temperature field are quite similar for heat generation and absorption.

- Numerical values of local Nusselt number decays for both heat generation and absorption cases for larger α_1, α_2 and Ha.

- Skin-friction coefficient increases for larger values of α_1, α_2, β, Ha and ψ.

Chapter 10

Newtonian heating effects in an axisymmetric stagnation point flow of third grade fluid subject to Soret and Dufour effects

This chapter focuses on the mathematical modeling and analysis of magnetohydrodynamic (MHD) mixed convection stagnation point flow by radially stretching surface. Problem formulation involves the constitutive equations of an incompressible third-grade fluid. In addition heat transfer analysis is examined in presence of Joule heating and Soret and Dufour effects. Adequate transformations lead to the nonlinear ordinary differential systems. Homotopic approach is employed for the convergent series solutions of the resulting problems. Interval of convergence is explicitly determined. The velocity, temperature and concentration are analyzed with respect to different parameters of interest. The skin friction coefficient, Nusselt and Sherwood numbers are numerically examined.

10.1   Mathematical formulation

We examine the magnetohydrodynamic (MHD) mixed convection boundary layer stagnation point flow of an incompressible third-grade fluid towads a radially stretching surface. Simultaneous effects of heat and mass transfer are considered. Constant magnetic field is applied along the $z-$axis. There is no external electric field. Induced magnetic field is neglected under the assumption of small magnetic Reynolds number. Hall effects are also assumed negligible. Joule heating, Soret and Dufour effects are present. The velocity component in the flow near stagnation point is given by $U_e(r) = ar$ and velocity of stretching sheet is $U_m(r) = cr$ (where a and c are the positive constants). Under the aforementioned assumptions, the governing boundary layer flow equations are given by:

$$\frac{\partial u}{\partial r} + \frac{u}{r} + \frac{\partial w}{\partial z} = 0, \tag{10.1}$$

$$u\frac{\partial u}{\partial r} + w\frac{\partial u}{\partial z} = U_e\frac{dU_e}{dr} + \nu\frac{\partial^2 u}{\partial z^2} + \frac{\alpha_1^*}{\rho}\left[\frac{\partial u}{\partial z}\frac{\partial^2 w}{\partial z^2} + 3\frac{\partial u}{\partial r}\frac{\partial^2 u}{\partial z^2} + w\frac{\partial^3 u}{\partial z^3} + u\frac{\partial^3 u}{\partial r\partial z^2}\right.$$

$$\left. + 2\frac{\partial w}{\partial z}\frac{\partial^2 u}{\partial z^2} + 4\frac{\partial u}{\partial z}\frac{\partial^2 u}{\partial r\partial z}\right] + \frac{\alpha_2^*}{\rho}\left[2\frac{\partial w}{\partial z}\frac{\partial^2 w}{\partial z^2} + 2\frac{\partial u}{\partial r}\frac{\partial^2 u}{\partial z^2}\right.$$

$$\left. + \frac{1}{r}\left(\frac{\partial u}{\partial z}\right)^2 + 6\frac{\partial u}{\partial z}\frac{\partial^2 u}{\partial r\partial z} + 2\frac{\partial w}{\partial z}\frac{\partial^2 u}{\partial z^2}\right] + \frac{\beta_3^*}{\rho}\left[6\left(\frac{\partial u}{\partial z}\right)^2\frac{\partial^2 u}{\partial z^2}\right]$$

$$+ \frac{\sigma B_0^2}{\rho}\left(U_e - u\right) + g\beta_T\left(T - T_\infty\right) + g\beta_c\left(C - C_\infty\right), \tag{10.2}$$

$$u\frac{\partial T}{\partial r} + w\frac{\partial T}{\partial z} = \frac{K}{\rho c_p}\frac{\partial^2 T}{\partial z^2} + \frac{D_m K_T}{\rho c_p}\frac{\partial^2 T}{\partial y^2} + \frac{\sigma B_0^2}{\rho c_p}u^2, \tag{10.3}$$

$$u\frac{\partial C}{\partial r} + w\frac{\partial C}{\partial z} = D_m\frac{\partial^2 C}{\partial z^2} + \frac{D_m K_T}{T_m}\frac{\partial^2 T}{\partial y^2}, \tag{10.4}$$

where u and w are the velocity components along the radial and axial directions respectively, ν is the fluid kinematic viscosity, ρ is the fluid density, σ is the electrical conductivity of fluid, β_T is the thermal expansion coefficient, β_c is the concentration expansion coefficient, K is the thermal conductivity, T_∞ is the ambient temperature, C_∞ is the ambient concentration, B_0 is the strength of magnetic field, D is the mass diffusivity, g is the gravitational acceleration and c_p is the specific heat.

The relevent conditions for the present flow consideration are

$$u\left(r,0\right) = U_w(r) = cr, \ w(r,0) = 0, \ \frac{\partial T(r,0)}{\partial z} = -h_s T(r,0), \ C(r,0) = C_w,$$

$$u \to U_e(r) = ar, \ T \to T_\infty, \ C \to C_\infty \text{ as } z \to \infty, \tag{10.5}$$

where h_s is heat transfer parameter and c is stretching rate. Setting

$$u\left(r,z\right) = crf'\left(\eta\right), \ w\left(r,z\right) = -2\sqrt{c\nu}f\left(\eta\right), \ \theta = \frac{T - T_\infty}{T_\infty},$$

$$\theta = \frac{C - C_\infty}{C_w - C_\infty}, \ \eta = \sqrt{\frac{c}{\nu}}z, \tag{10.6}$$

the incompressibility condition is automatically satiesfied while the other equations and conditions yield

$$f''' + 2ff'' - \left(f'\right)^2 + \alpha_1\left[2\left(f''\right)^2 - 2ff^{(iv)}\right] + \alpha_2\left[3\left(f''\right)^2 - 2f'f'''\right]$$

$$+ 6\beta\,\mathrm{Re}\left(f''\right)^2 f''' + Ha^2\left[A - f'\right] + A^2 + Gs\,\theta + Gc\,\phi = 0, \tag{10.7}$$

$$\theta'' + 2\Pr f\,\theta' + Ha^2\Pr Ec f'^2 + \Pr Du\,\phi'' = 0, \tag{10.8}$$

$$\phi'' + 2Sc\,f\phi' + Sc\,Sr\,\theta'' = 0, \tag{10.9}$$

$$f'\left(0\right) = 1, \ f\left(0\right) = 0, \ \theta'(0) = -\gamma_1\left(1 + \theta\left(0\right)\right), \ \phi\left(0\right) = 1,$$

$$f'\left(\infty\right) = A, \qquad \theta(\infty) = 0, \qquad \phi\left(\infty\right) = 0. \tag{10.10}$$

Here prime denotes differentiation with respect to η, α_1 and α_2 are the dimensionless normal stress moduli, β is the dimensionless third grade fluid parameter, Ha is the Hartman number, Re is the Reynolds number, A is the ratio of free stream to the stretching velocities, Gs is the thermal Grashof number, Gc is the solutal Grashof number, Pr is the Prandtl number, Ec is the Eckert number, Du is the Dufour number, Sr is the Soret number, Sc is the Schmidt number and γ_1 is the conjugate parameter for Newtonian heating. The definitions of these parameters are

$$
\begin{aligned}
\alpha_1 &= \frac{\alpha_1^* c}{\rho \nu}, \ \alpha_2 = \frac{\alpha_2^* c}{\rho \nu}, \ \beta = \frac{\beta_3 c^2}{\rho \nu}, \ Ha^2 = \frac{\sigma B_0^2}{\rho c}, \\
\text{Re} &= \frac{cr^2}{\nu}, \ A = \frac{a}{c}, \ Gs = \frac{g \beta_T T_\infty}{c^2 r}, \ Gc = \frac{g \beta_c \left(C_w - C_\infty\right)}{c^2 r}, \\
\text{Pr} &= \frac{\mu c_p}{K}, \ Ec = \frac{c^2 r^2}{c_p T_\infty}, \ Du = \frac{D_m K_T \left(C_w - C_\infty\right)}{\nu c_s c_p T_\infty}, \\
Sr &= \frac{D_m K_T T_\infty}{\nu T_m \left(C_w - C_\infty\right)}, \ Sc = \frac{\nu}{D_m} \ \gamma_1 = h_s \sqrt{\frac{\nu}{a}}.
\end{aligned}
\tag{10.11}
$$

The skin friction coefficient (C_f), local Nusselt number and local Sherwood numbers are defined by

$$
C_f = \frac{\tau_{rz}}{\frac{1}{2}\rho \left(cr\right)^2}, \ Nu_r = \frac{r q_w}{K \left(T - T_\infty\right)}, \ Sh = \frac{r j_w}{K \left(C - C_\infty\right)},
\tag{10.12}
$$

with

$$
\tau_{rz} = \left[\mu \frac{\partial u}{\partial z} + \alpha_1^* \left(w \frac{\partial^2 u}{\partial z^2} + 3 \frac{\partial u}{\partial r} \frac{\partial u}{\partial z} \right) + \alpha_2^* \left(2 \frac{\partial u}{\partial r} \frac{\partial u}{\partial z} + 2 \frac{\partial w}{\partial z} \frac{\partial u}{\partial z} \right) + 2 \beta^* \left(\frac{\partial u}{\partial z} \right)^3 \right],
\tag{10.13}
$$

$$
q_w = -K \left(\frac{\partial T}{\partial z} \right)_{z=0},
\tag{10.14}
$$

$$
j_w = -K \left(\frac{\partial C}{\partial z} \right)_{z=0}.
\tag{10.15}
$$

In dimensionless form, we obtain

$$
\left(\text{Re}_r\right)^{-1/2} C_f = f''(0) + 3\alpha_1 f''(0) - 2\alpha_2 f''(0) + 2\beta \left(f''(0) \right)^3,
\tag{10.16}
$$

$$
\left(\text{Re}_r\right)^{-1/2} Nu_r = \gamma \left(1 + \frac{1}{\theta(0)} \right),
\tag{10.17}
$$

$$
\left(\text{Re}_r\right)^{-1/2} Sh = -\phi'(0),
\tag{10.18}
$$

in which $\text{Re}_r^{1/2} = \sqrt{r^2 c / \nu}$ denotes the local Reynolds number.

10.2 Homotopic solutions

To obtain homotopy solutions, we express the velocity, temperature and concentration distributions by a set of base functions

$$\left\{ \eta^k \exp\left(-n\eta\right) | k \geq 0, n \geq 0 \right\}, \tag{10.19}$$

in the forms

$$f_m\left(\eta\right) = \sum_{n=0}^{\infty} \sum_{k=0}^{\infty} a_{m,n}^k \eta^k \exp\left(-n\eta\right), \tag{10.20}$$

$$\theta_m(\eta) = \sum_{n=0}^{\infty} \sum_{k=0}^{\infty} b_{m,n}^k \eta^k \exp\left(-n\eta\right), \tag{10.21}$$

$$\phi_m(\eta) = \sum_{n=0}^{\infty} \sum_{k=0}^{\infty} c_{m,n}^k \eta^k \exp\left(-n\eta\right), \tag{10.22}$$

where $a_{m,n}^k$, $b_{m,n}^k$ and $c_{m,n}^k$ are the coefficients to be determined. We have chosen the following initial guesses $f_0\left(\eta\right)$, $\theta_0\left(\eta\right)$ and $\phi_0\left(\eta\right)$ and the auxiliary linear operators $\mathcal{L}_f$, $\mathcal{L}_\theta$ and $\mathcal{L}_\phi$ by the rule of solution expression and the boundary conditions (10.14):

$$
\begin{aligned}
f_0\left(\eta\right) &= A\eta + \left(1 - A\right)\left(1 - \exp\left(-\eta\right)\right), \\
\theta_0\left(\eta\right) &= \frac{\gamma_1 \exp\left(-\eta\right)}{1 - \gamma_1}, \ \gamma_1 \neq 1, \\
\phi_0\left(\eta\right) &= \exp\left(-\eta\right),
\end{aligned}
\tag{10.23}
$$

$$\mathcal{L}_f\left[f\left(\eta\right)\right] = \frac{d^3 f}{d\eta^3} - \frac{df}{d\eta}, \quad \mathcal{L}_\theta\left[\theta\left(\eta\right)\right] = \frac{d^2\theta}{d\eta^2} - \theta, \quad \mathcal{L}_\phi\left[\phi\left(\eta\right)\right] = \frac{d^2\phi}{d\eta^2} - \phi. \tag{10.24}$$

The above linear operators have the following properties:

$$\mathcal{L}_f\left[C_{44} + C_{45} \exp\left(\eta\right) + C_{46} \exp\left(-\eta\right)\right] = 0, \tag{10.25}$$

$$\mathcal{L}_\theta\left[C_{47} \exp\left(\eta\right) + C_{48} \exp\left(-\eta\right)\right] = 0, \tag{10.26}$$

$$\mathcal{L}_\phi\left[C_{49} \exp\left(\eta\right) + C_{50} \exp\left(-\eta\right)\right] = 0. \tag{10.27}$$

where $C_i \left(i = 44 - 50\right)$ are the arbitrary constants.

10.2.1 Zeroth-order deformation problems

The related zeroth-order deformation problems can be written as follows:

$$\left(1 - q\right) \mathcal{L}_f\left[\hat{f}\left(\eta, q\right) - f_0\left(\eta\right)\right] = q\hbar_f \mathcal{N}_f\left[\hat{f}\left(\eta, q\right)\right], \tag{10.28}$$

$$\left(1 - q\right) \mathcal{L}_\theta\left[\hat{\theta}\left(\eta, q\right) - \theta_0\left(\eta\right)\right] = q\hbar_\theta \mathcal{N}_\theta\left[\hat{\theta}\left(\eta, q\right), \hat{f}\left(\eta, q\right), \hat{\phi}\left(\eta, q\right)\right], \tag{10.29}$$

$$\left(1 - q\right) \mathcal{L}_\phi\left[\hat{\phi}\left(\eta, q\right) - \phi_0\left(\eta\right)\right] = q\hbar_\phi \mathcal{N}_\phi\left[\hat{\phi}\left(\eta, q\right), \hat{f}\left(\eta, q\right), \hat{\theta}\left(\eta, q\right)\right], \tag{10.30}$$

$$\hat{f}(\eta, q)\big|_{\eta=0} = 0, \qquad \frac{\partial \hat{f}(\eta, q)}{\partial \eta}\bigg|_{\eta=0} = 1, \qquad \frac{\partial \hat{f}(\eta, q)}{\partial \eta}\bigg|_{\eta \to \infty} = A, \qquad (10.31)$$

$$\frac{\partial \hat{\theta}(\eta, q)}{\partial \eta}\bigg|_{\eta=0} = -\gamma \left(1 + \hat{\theta}(\eta, q)\right)\big|_{\eta=0}, \qquad \hat{\theta}(\eta, q)\big|_{\eta \to \infty} = 0, \qquad (10.32)$$

$$\hat{\phi}(\eta, q)\big|_{\eta=0} = 1, \qquad \hat{\phi}(\eta, q)\big|_{\eta \to \infty} = 0, \qquad (10.33)$$

$$
\begin{aligned}
\mathcal{N}_f\left[\hat{f}(\eta, q)\right] &= \frac{\partial^3 \hat{f}}{\partial \eta^3} + 2f \frac{\partial^2 \hat{f}}{\partial \eta^2} - \left(\frac{\partial \hat{f}}{\partial \eta}\right)^2 + A^2 + \alpha_1 \left[2\left(\frac{\partial^2 \hat{f}}{\partial \eta^2}\right)^2 - 2f \frac{\partial^4 \hat{f}}{\partial \eta^4}\right] \\
&\quad + \alpha_2 \left[3\left(\frac{\partial^2 \hat{f}}{\partial \eta^2}\right)^2 - 2\frac{\partial \hat{f}}{\partial \eta}\frac{\partial^3 \hat{f}}{\partial \eta^3}\right] + 6\beta \ \text{Re} \left(\frac{\partial^2 \hat{f}}{\partial \eta^2}\right)^2 \frac{\partial^3 \hat{f}}{\partial \eta^3} \\
&\quad + Ha^2 \left[A - \frac{\partial \hat{f}}{\partial \eta}\right] + Gs\ \theta + Gc\ \phi,
\end{aligned}
\qquad (10.34)
$$

$$\mathcal{N}_\theta\left[\hat{\theta}(\eta, q), \hat{f}(\eta, q), \hat{\phi}(\eta, q)\right] = \frac{\partial^2 \hat{\theta}}{\partial \eta^2} + 2\Pr\ f \frac{\partial \hat{\theta}}{\partial \eta} + M^2\ \Pr\ Ec \left(\frac{\partial \hat{f}}{\partial \eta}\right)^2 + \Pr\ Du \frac{\partial^2 \hat{\phi}}{\partial \eta^2}, \qquad (10.35)$$

$$\mathcal{N}_\phi\left[\hat{\phi}(\eta, q), \hat{f}(\eta, q), \hat{\theta}(\eta, q)\right] = \frac{\partial^2 \hat{\phi}}{\partial \eta^2} + 2\ Sc\ f \frac{\partial \hat{\phi}}{\partial \eta} + Sc\ Sr \frac{\partial^2 \hat{\theta}}{\partial \eta^2}. \qquad (10.36)$$

In view of Taylor series, one can express that

$$\hat{f}(\eta, q) = f_0(\eta) + \sum_{m=1}^{\infty} f_m(\eta) q^m, \qquad \hat{f}_m(\eta) = \frac{1}{m!}\frac{\partial^m f(\eta, q)}{\partial q^m}\bigg|_{q=0}, \qquad (10.37)$$

$$\hat{\theta}(\eta, q) = \theta_0(\eta) + \sum_{m=1}^{\infty} \theta_m(\eta) q^m, \qquad \hat{\theta}_m(\eta) = \frac{1}{m!}\frac{\partial^m \theta(\eta, q)}{\partial q^m}\bigg|_{q=0}, \qquad (10.38)$$

$$\hat{\phi}(\eta, q) = \phi_0(\eta) + \sum_{m=1}^{\infty} \phi_m(\eta) q^m, \qquad \hat{\phi}_m(\eta) = \frac{1}{m!}\frac{\partial^m \phi(\eta, q)}{\partial q^m}\bigg|_{q=0}. \qquad (10.39)$$

In the above expressions $q \in [0, 1]$ and $\hbar_f \neq 0$, $\hbar_\theta \neq 0$, $\hbar_\phi \neq 0$ are respectively the embedding and auxiliary parameters. When q varies from 0 to 1, then $\hat{f}(\eta, q)$, $\hat{\theta}(\eta, q)$, $\hat{\phi}(\eta, q)$ vary from initial guesses $f_0(\eta)$, $\theta_0(\eta)$ and $\phi_0(\eta)$ to final solutions $f(\eta)$, $\theta(\eta)$ and $\phi(\eta)$. Note that the convergence of the series (10.37)-(10.39) strictly depend upon $\hbar_f$, $\hbar_\theta$ and $\hbar_\phi$. The values of $\hbar_f$, $\hbar_\theta$ and $\hbar_\phi$ are chosen in such a way that the series (10.37)-(10.39) are convergent at $q = 1$ and hence

$$\hat{f}(\eta) = f_0(\eta) + \sum_{m=1}^{\infty} f_m(\eta), \qquad (10.40)$$

$$\hat{\theta}(\eta) = \theta_0(\eta) + \sum_{m=1}^{\infty} \theta_m(\eta), \qquad (10.41)$$

$$\hat{\phi}(\eta) = \phi_0(\eta) + \sum_{m=1}^{\infty} \phi_m(\eta). \qquad (10.42)$$

10.2.2 mth-order deformation problems

The problems at this order are

$$\mathcal{L}_f \left[\hat{f}_m(\eta) - \chi_m \hat{f}_{m-1}(\eta) \right] = \hbar_f \mathcal{R}_m^f(\eta),$$

$$\hat{f}_m(0,q) = 0, \quad \left. \frac{\partial \hat{f}_m(\eta,q)}{\partial \eta} \right|_{\eta=0} = 0, \quad \left. \frac{\partial \hat{f}_m(\eta,q)}{\partial \eta} \right|_{\eta \to \infty} = 0, \tag{10.43}$$

$$\mathcal{L}_\theta \left[\hat{\theta}_m(\eta) - \chi_m \hat{\theta}_{m-1}(\eta) \right] = \hbar_\theta \mathcal{R}_m^\theta(\eta),$$

$$\left. \frac{\partial \hat{\theta}_m(\eta,q)}{\partial \eta} \right|_{\eta=0} + \gamma_1 \left. \hat{\theta}_m(\eta,q) \right|_{\eta=0} = 0, \quad \left. \hat{\theta}_m(\eta,q) \right|_{\eta \to \infty} = 0, \tag{10.44}$$

$$\mathcal{L}_3 \left[\hat{\phi}_m(\eta) - \chi_m \hat{\phi}_{m-1}(\eta) \right] = \hbar_\phi \mathcal{R}_m^\phi(\eta),$$

$$\left. \frac{\partial \hat{\phi}_m(\eta,q)}{\partial \eta} \right|_{\eta=0} = 0, \quad \left. \hat{\phi}_m(\eta,q) \right|_{\eta \to \infty} = 0, \tag{10.45}$$

$$\begin{aligned}
\mathcal{R}_m^f(\eta) &= f'''_{m-1}(\eta) + 2 \sum_{k=0}^{m-1} f_{m-1-k} f''_k - \sum_{k=0}^{m-1} f'_{m-1-k} f'_k + Ha^2 A (1 - \chi_m) + A^2 (1 - \chi_m) \\
&\quad + \alpha_1 \sum_{k=0}^{m-1} \left(2 f''_{m-1-k} f''_k - 2 f_{m-1-k} f_k^{(iv)} \right) + \alpha_2 \sum_{k=0}^{m-1} \left(3 f''_{m-1-k} f''_k - 2 f'_{m-1-k} f'''_k \right) \\
&\quad + 6\beta \operatorname{Re} \sum_{k=0}^{m-1} \sum_{l=0}^{k} f''_{m-1-k} f''_{k-l} f'''_l - M^2 f'_{m-1} + Gs\, \theta_{m-1} + Gc\, \phi_{m-1},
\end{aligned} \tag{10.46}$$

$$\mathcal{R}_m^\theta(\eta) = \theta''_{m-1}(\eta) + 2 \Pr \sum_{k=0}^{m-1} f_{m-1-k} \theta'_k + M^2 \Pr Ec \sum_{k=0}^{m-1} f'_{m-1-k} f'_k + \Pr Du\, \phi''_{m-1}(\eta), \tag{10.47}$$

$$\mathcal{R}_m^\phi(\eta) = \phi''_{m-1}(\eta) + 2 Sc \sum_{k=0}^{m-1} f_{m-1-k} \phi'_k + Sc\, Sr\, \theta''_{m-1}(\eta), \tag{10.48}$$

The general solutions (f_m, θ_m, ϕ_m) of Eqs. (10.46) to (10.48) in terms of special solutions $(f_m^*, \theta_m^*, \phi_m^*)$ are given by

$$f(\eta) = f^* + C_{44} + C_{45} \exp(\eta) + C_{46} \exp(-\eta), \tag{10.49}$$

$$\theta(\eta) = \theta^* + C_{47} \exp(\eta) + C_{48} \exp(-\eta), \tag{10.50}$$

$$\phi(\eta) = \phi^* + C_{49} \exp(\eta) + C_{50} \exp(-\eta). \tag{10.51}$$

10.3 Convergence of the homotopy solutions

We note that the series solutions (10.28) to (10.30) contain auxiliary parameters $\hbar_f$, $\hbar_\theta$ and $\hbar_\phi$. The convergence of the obtained series solutions strongly depend upon these parameters. For convergence analysis, we sketched the $\hbar$-curves for 12th-order of approximations in Fig. 10.2. It is found that ranges

for admissible values of $\hbar_f$, $\hbar_\theta$ and $\hbar_\phi$ are $-2.1 \leq \hbar_f, \hbar_\theta < -0.1$, and $-1.8 \leq \hbar_\phi < -0.1$. Table 1 shows the convergence of series solutions through numerical values. It is observed that the 24th order of approximations are enough for f and ϕ whereas 26th order of approximations are required for θ.

10.4 Results and discussion

This section is prepared to enlighten the effects of embedded parameters on the velocity, temperature, concentration, skin friction coefficient, local Nusselt number and local Sherwood number.

10.4.1 Velocity profile

Influence of the fluid parameters α_1 and α_2 on velocity profile is displayed in the Figs. 10.3 and 10.4. It is noted that an increase in the values of α_1 and α_2 significantly enhances the velocity profile $f'(\eta)$. In fact α_1 and α_2 are inversely proportional to the viscosity so by increasing the parameters α_1 and α_2 the viscosity decreases which shows that the velocity increases. Fig. 10.5 displays representative velocity field for various values of parameter β. It is seen that velocity profile is decreasing function of β. Furthermore the boundary layer thickness is smaller for higher values of β. Fig. 10.6 depicts the behavior for velocity field via magnetic parameter $Ha = 0, 0.7, 1.2$ and 1.7. The application of transverse magnetic field gives rise to a resistive force namely the Lorentz force. Effects of this force slow down the motion of the fluid. Hence by increasing the strength of the magnetic field, there is decrease in fluid velocity and momentum boundary layer thickness. Fig. 10.7 is sketched for the influence of Reynolds number Re on the velocity profile $f'(\eta)$. It is observed that the velocity profile increases for larger Re. Behavior of Prandtl number Pr on velocity profile is shown in Fig. 10.8. Velocity field increases for higher values of Prandtl number Pr. Furthermore the momentum boundary layer thickness is smaller for larger values of Pr. Influence of Eckert number Ec on the velocity profile is presented in Fig. 10.9. This Fig. demonstrates that velocity and momentum boundary layer thickness increase through an increase in Ec. Fig. 10.10 elucidates the effects of Dufour number Du on the velocity. Clearly an increase in Dufour number leads to an increase in the fluid velocity. In Fig. 10.11 the velocity profile for different values of the solutal Grashof number Gc is described. It is observed that an increase in Gc corresponds to a rise in the velocity field. In addition, curves show that the velocity increases rapidly near the surface and have maximum value at $\eta = 0$ and then it vanishes away from the surface. Influence of the different values of Grashof number Gs on the velocity profile are described in Fig. 10.12. It is found that the velocity profile is much for larger Grashof number Gs. Here the Grashof number defines the effects of free convection. Physically $Gs > 0$ means heating of the fluid of cold boundary surface, $Gs < 0$ means cooling of the fluid of heated boundary surface and $Gs = 0$ corresponds to the absence of free convection. Fig. 10.13 is sketched to see the effect of γ on the velocity distribution. It is noted that the velocity profile is increased by increasing γ. Fig. 10.14 displays representative velocity profiles for different values of ratio A. The increasing value of A means that free stream velocity is more when compared with the stretching velocity. Larger A increases pressure and straining motion near the stagnation point and therefore velocity and boundary

layer thickness are increased. Same behavior is shown for $A < 1$ on the velocity profile while the boundary layer thickness has opposite effect for both cases. Also no boundary layer is formed for $A = 1$.

10.4.2 Temperature profile

Fig. 10.15 displays the impact of α_1 on the temperature field. Here the temperature and thermal boundary layer thickness are increased for larger α_1. The same behavior is observed in Fig. 10.16 for the parameter α_2. The temperature increases significantly for the larger values of β (see Fig. 10.17). Fig. 10.18 depicts that by increasing the magnetic parameter Ha the dimensionless temperature $\theta(\eta)$ increases. Dimensionless temperature is also increasing function of Reynolds number Re (see in Fig. 10.19). Fig. 10.20 is sketched to see the influence of Prandtl number Pr on temperature $\theta(\eta)$. It reveals that temperature $\theta(\eta)$ is increasing function of Pr. Fig. 10.21 shows the behavior of Eckert number Ec on $\theta(\eta)$. Here $Ec = 0$ ensures the absence of Joule heating while $Ec \neq 0$ corresponds to the presence of Joule heating. Dimensionless temperature $\theta(\eta)$ enhances by increasing Ec. In fact Ec is the ratio of the kinetic energy to the enthalpy. Hence an increase in Ec yields increase in kinetic energy and thus temperature $\theta(\eta)$ increases. Fig. 10.22 is drawn to see the influence of Dufour number Du on the temperature profile $\theta(\eta)$. It is observed that the temperature profile is increased by increasing Du. The variation of temperature $\theta(\eta)$ with respect to the solutal Grashof number Gc is presented in Fig. 10.23. This Fig. depicts that temperature increases when Gc is increased. We also note that the increase of parameter Gc causes an increase in the thermal boundary layer thickness. Variations of Gs on temperature are qualitatively similar to that of Gc (see Figs. 10.23 and 10.24). Increasing Schmidt number Sc leads to an increase in the fluid temperature (see Fig. 10.25). Influence of Soret number Sr on the dimensionless temperature can be observed from Fig. 10.26. It is noticed that the temperature profile and thermal boundary layer thickness decrease by increasing Sr. Influence of conjugate parameter γ on the temperature profile is displayed in Fig. 10.27. Higher values of γ correspond to larger Newtonian heating which shows an increase in the temperature and thermal boundary layer thickness. The characteristics of the ratio parameter A on the temperature profile $\theta(\eta)$ are described in Fig. 10.28. It is observed that temperature decreases for larger ratio parameter A. However thermal boundary layer thickness is higher for smaller values of ratio parameter A.

10.4.3 Concentration profile

Effects of the embedded parameters on concentration field $\phi(\eta)$ are studied in the Figs. 10.29-10.36. The variation of Reynolds number on the concentration profile is sketched in the Fig. 10.29. Here the concentration field decreases when Reynolds number Re increases. Also the solutal boundary layer thickness decreases. Effect of Dufour number Du on the concentration profile $\phi(\eta)$ is shown in Fig. 10.30. Increasing Du leads to a small decrease in the concentration boundary layer thickness. The variation in dimensionless concentration profiles for different values of Gc is presented in Fig. 10.31. It is noted from the Fig. that concentration profile is decreasing function of Gc while the same behavior is observed for Gs on $\phi(\eta)$ in Fig. 10.32. In Fig. 10.33 the influence of the various values of Sr on concentration profile

is displayed. Here the concentration profile is clearly increasing function of Sr. The opposite behavior is observed for the values of Schmidt number Sc on the concentration profile (see in Fig. 10.34). Fig. 10.35 represents the influence of conjugate parameter γ on the concentration profile $\phi(\eta)$ versus η. It is examined that with an increase in γ the concentration profile increases. Fig. 10.36 illustrates the effects of A on concentration profile $\phi(\eta)$ versus η. Obviously an increase in A reduces the concentration profile. The solutal boundary layer thickness is also decreased.

Table 10.1 is prepared to analyze the convergence of series solutions. Tables 10.2-10.4 provide the numerical values of skin friction coefficient, local Nusselt number and local Sharwood number for different values of involved parameters. The magnitude of skin friction coefficient is reduced when α_2, Re, A, Gs, Gc, Du, Sr, Pr and Ec are increased. However the skin friction increases for α_1, β, Ha and Sc (see Table 10.2). From Table 10.3 we can observe that the magnitude of local Nusselt number is more for larger values of α_1, α_2, β, A, Gs and Sr. On the other hand it is reduced by the increase of Ha, Gc, Du, Sc, Pr and Ec. The magnitude of local Sherwood number increases for α_1, A, Gs, Gc, Sc and Pr while it decreases when α_2, β, Re, Ha, Sr, Ec and Du are increased (see Table 10.4).
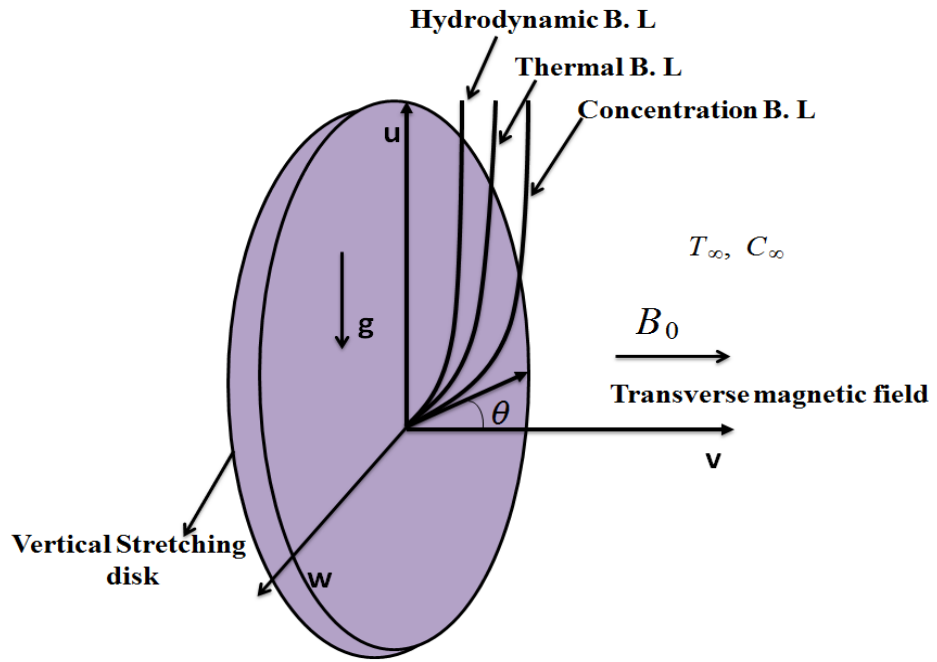
Fig. 10.1: Physical flow model.

Fig. 10.2: $\hbar-$curves for the functions $f(\eta)$, $\theta(\eta)$ and $\phi(\eta)$.

α_1 = 0.1, 0.5, 1.0, 1.7

Fig. 10.3: Influence of α_1 on $f'(\eta)$.

α_1=A=Sc=γ_1=Gs=0.2,Re=0.3,Pr=1,Ec=Gc=0.5,β=Ha=Sr=0.1

α_2 = 0.0, 0.9, 1.6, 2.5
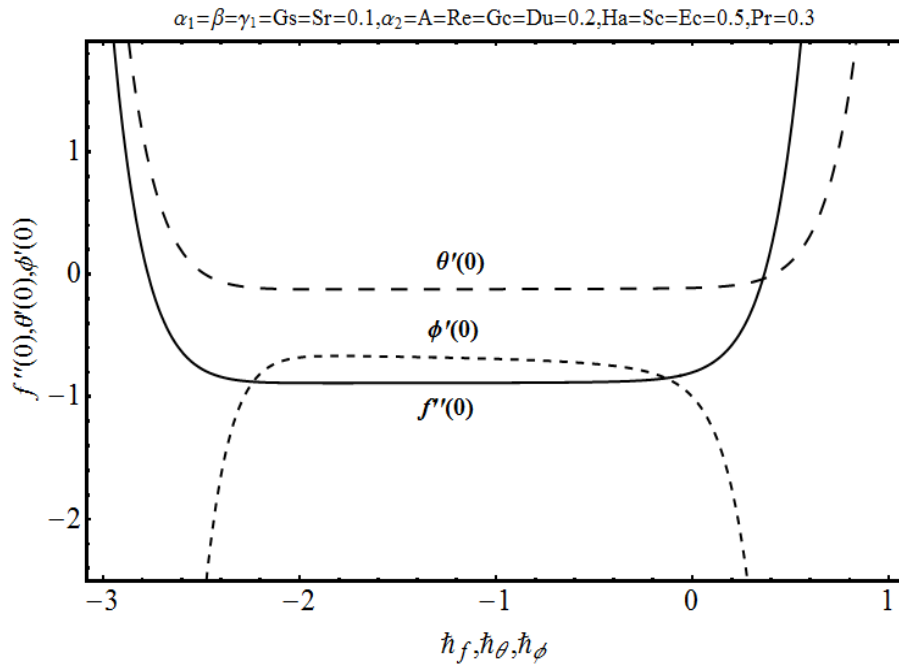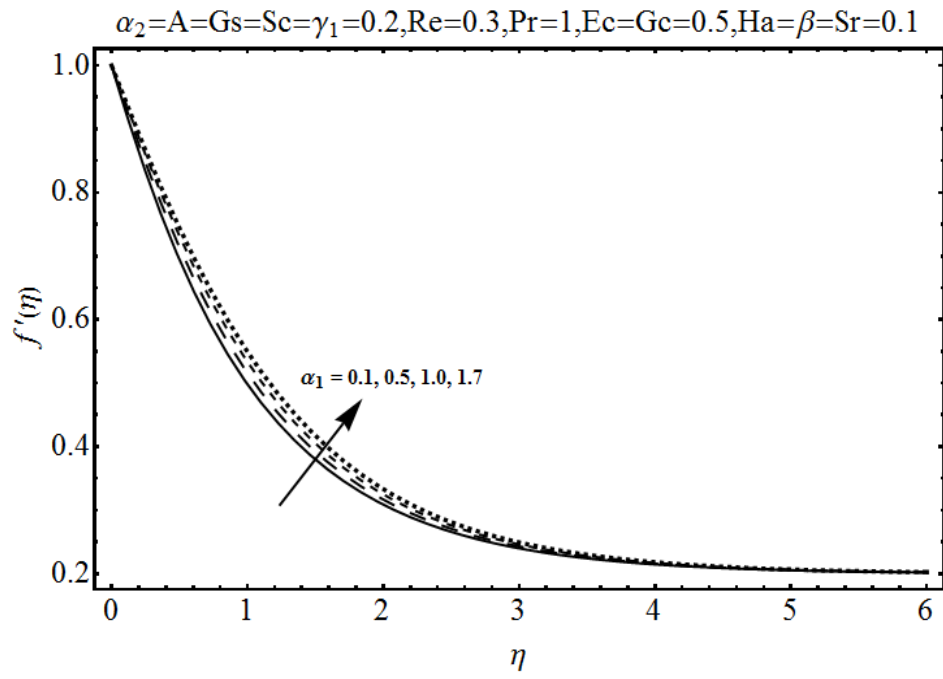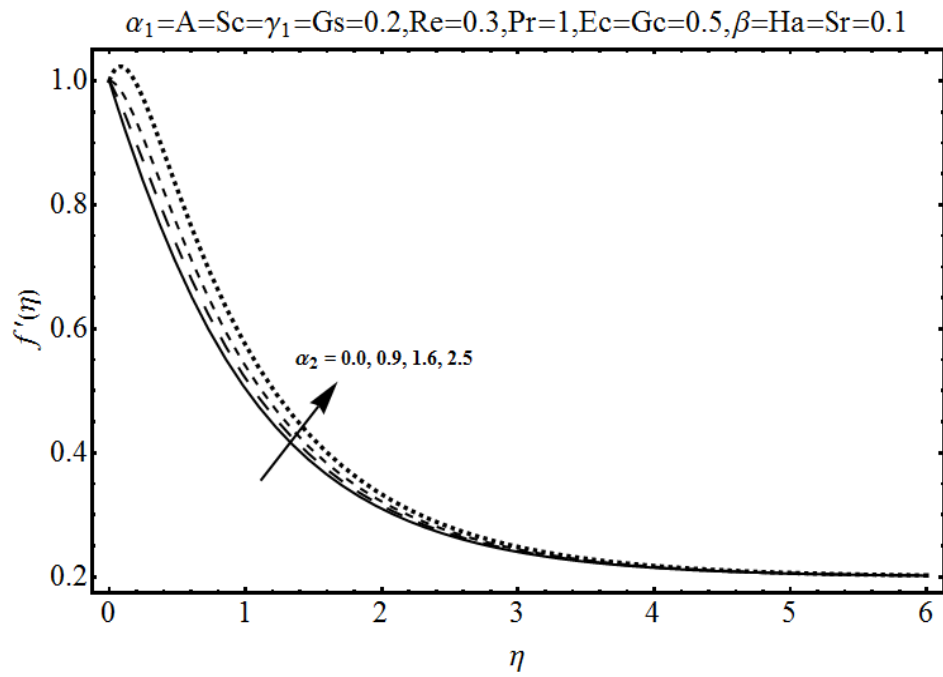
Fig. 10.4: Influence of α_2 on $f'(\eta)$.

174
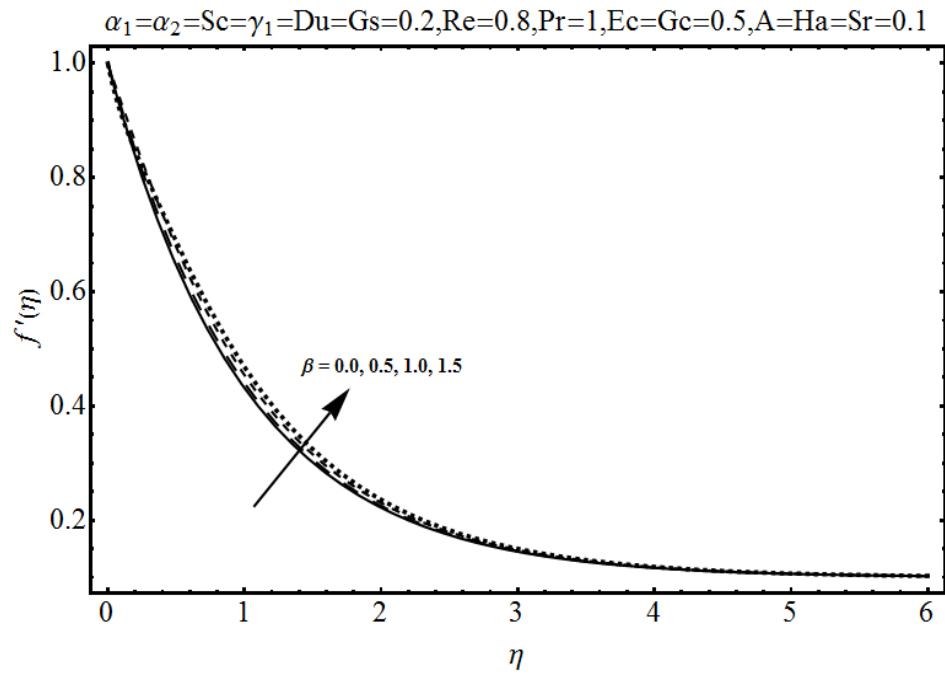
Fig. 10.5: Influence of β on $f'(\eta)$.
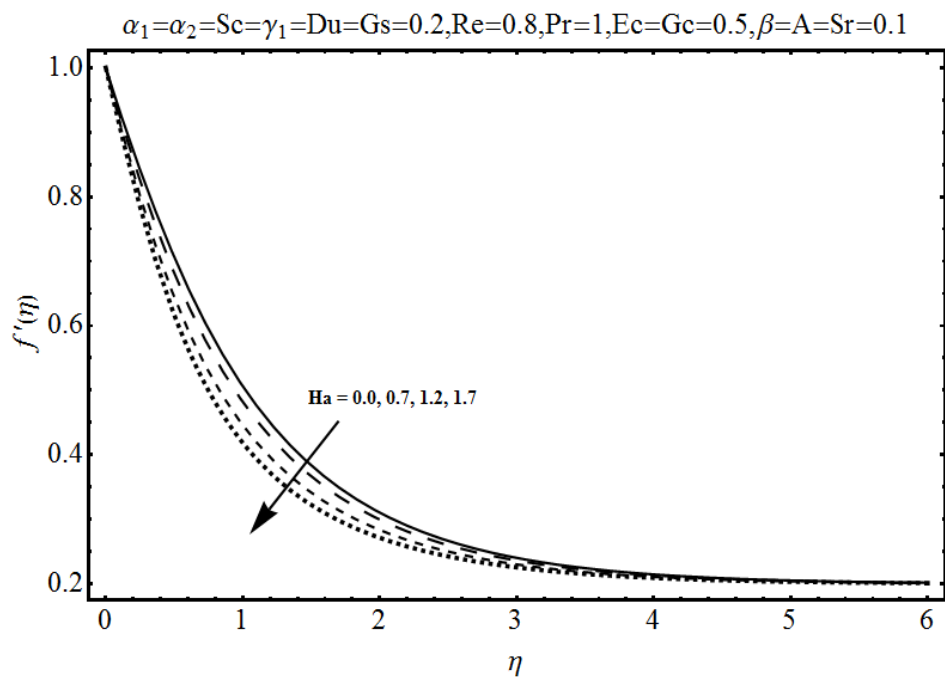
Fig. 10.6: Influence of Ha on $f'(\eta)$.

$\alpha_1 = \alpha_2 = A = Du = \gamma_1 = Gs = Sc = 0.2, \beta = Sr = 0.1, Ha = 2.5, Pr = 1, Ec = Gc = 0.5$
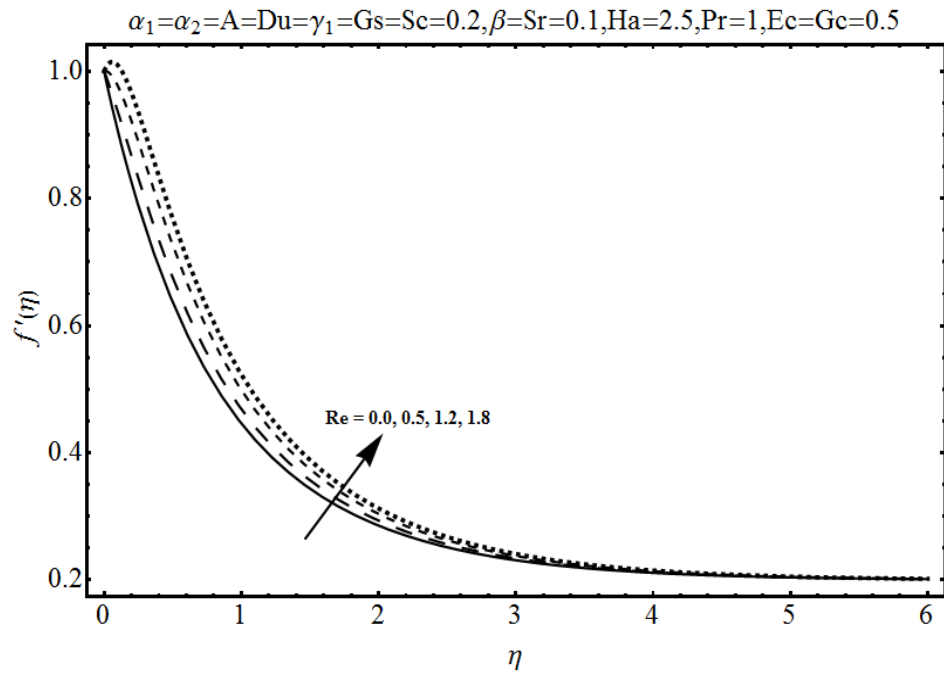
Fig. 10.7: Influence of Re on $f'(\eta)$.

$\alpha_1 = \alpha_2 = A = Du = Gs = \gamma_1 = Sc = 0.2, \beta = Gc = Sr = 0.1, Ha = 3, Re = Ec = 0.5$

Fig. 10.8: Influence of Pr on $f'(\eta)$.

$\alpha_1 = \alpha_2 = A = Gs = Sc = \gamma_1 = 0.2, \beta = Sr = 0.1, Ha = 3, Re = 0.3, Pr = 1.5, Gc = 0.5$

Ec = 0.0, 0.5, 0.9, 1.5
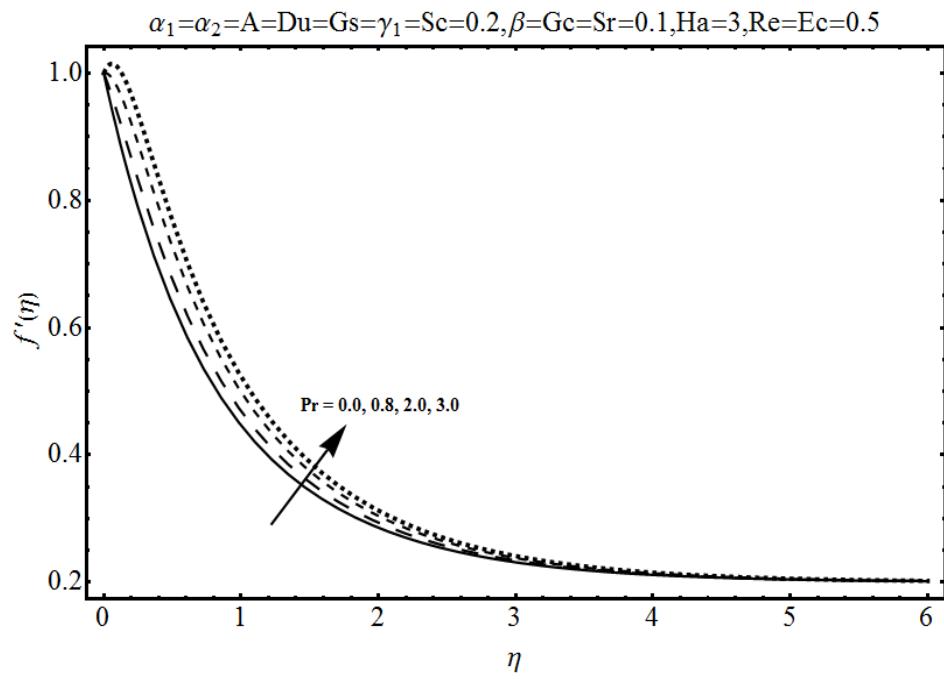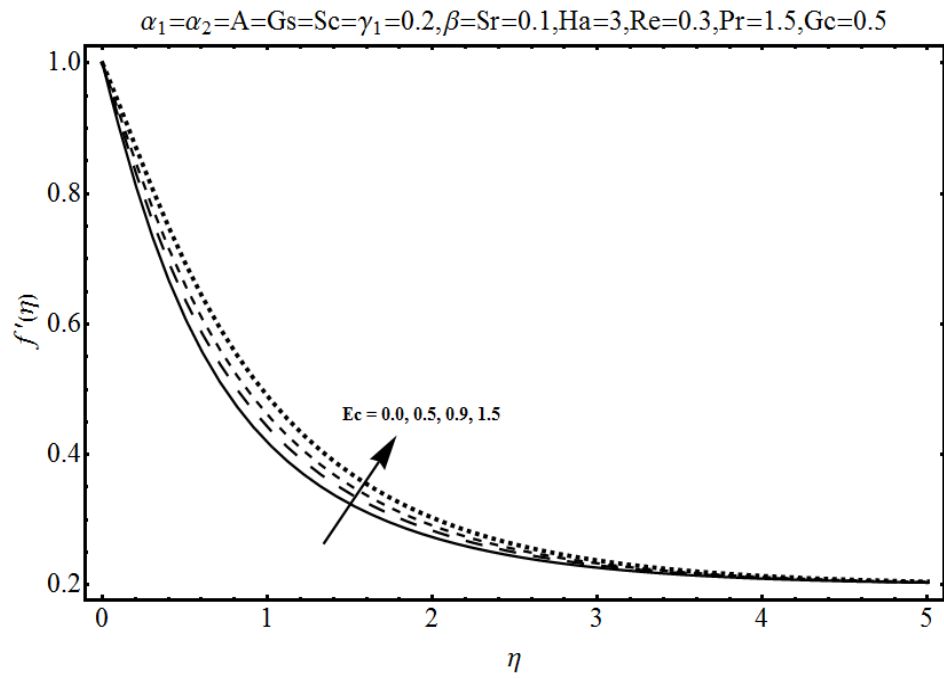
Fig. 10.9: Influence of Ec on $f'(\eta)$.

$\alpha_1 = \alpha_2 = A = Gs = Sc = \gamma_1 = 0.2, \beta = 0.3, Re = Ha = 1, Pr = 1.5, Sr = Ec = Gc = 0.5$

Du = 0.0, 0.8, 1.3, 2.0
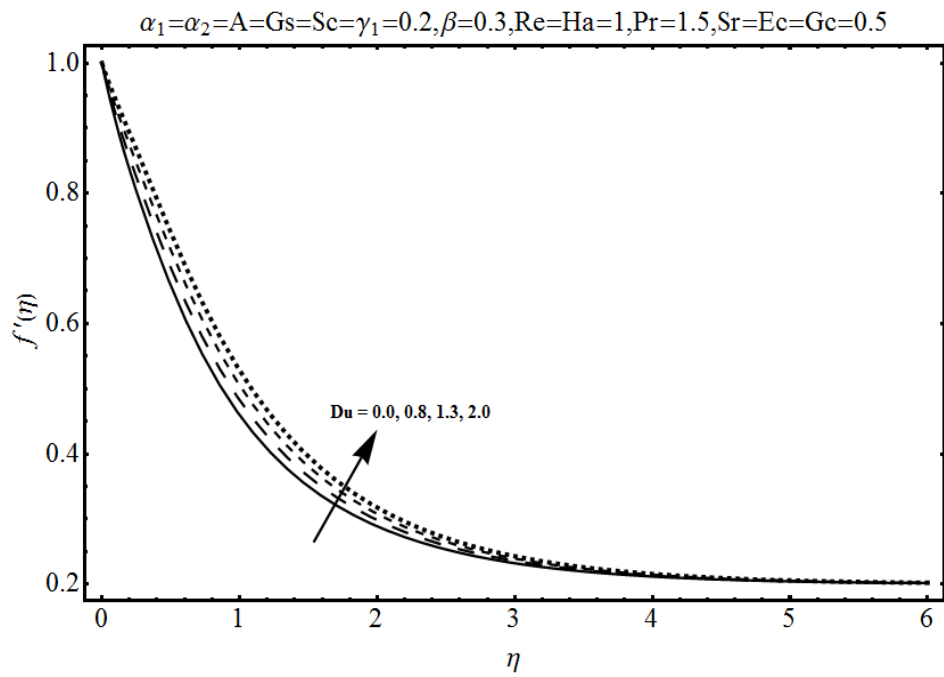
Fig. 10.10: Influence of Du on $f'(\eta)$.

177

$\alpha_1 = \alpha_2 = A = Gs = Sc = Du = \gamma_1 = 0.2, \beta = Sr = 0.1, Ha = 3, Re = 0.3, Pr = 1, Ec = 0.5$

Gc = 0, 2, 4, 6
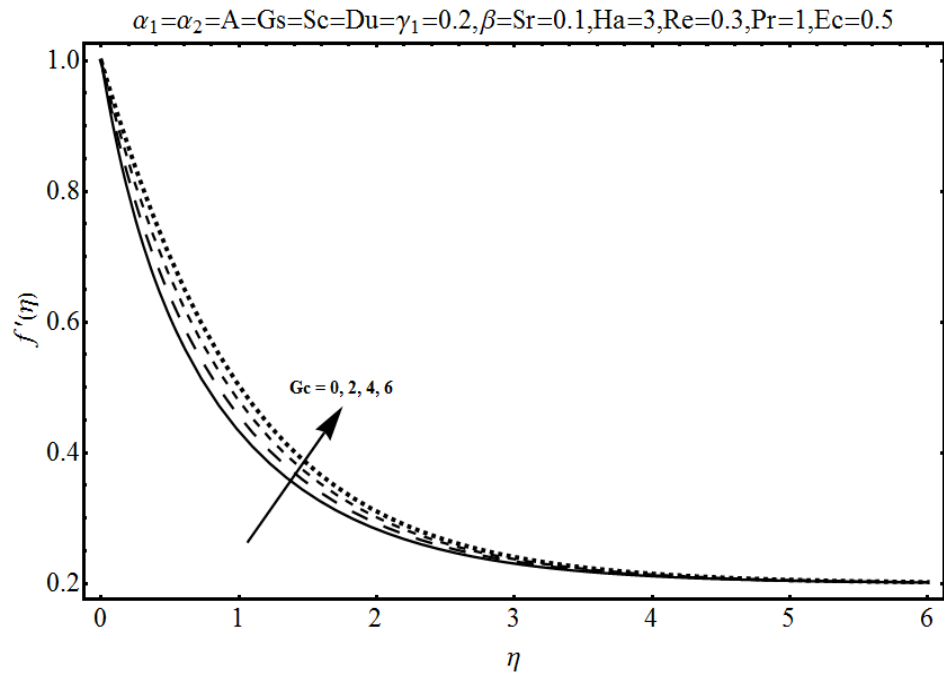
Fig. 10.11: Influence of Gc on $f'(\eta)$.

$\alpha_1 = \alpha_2 = A = Sc = Du = \gamma_1 = 0.2, \beta = Sr = 0.1, Ha = 3, Re = 0.3, Pr = 1, Ec = Gc = 0.5$

Gs = 0.0, 0.2, 0.4, 0.6
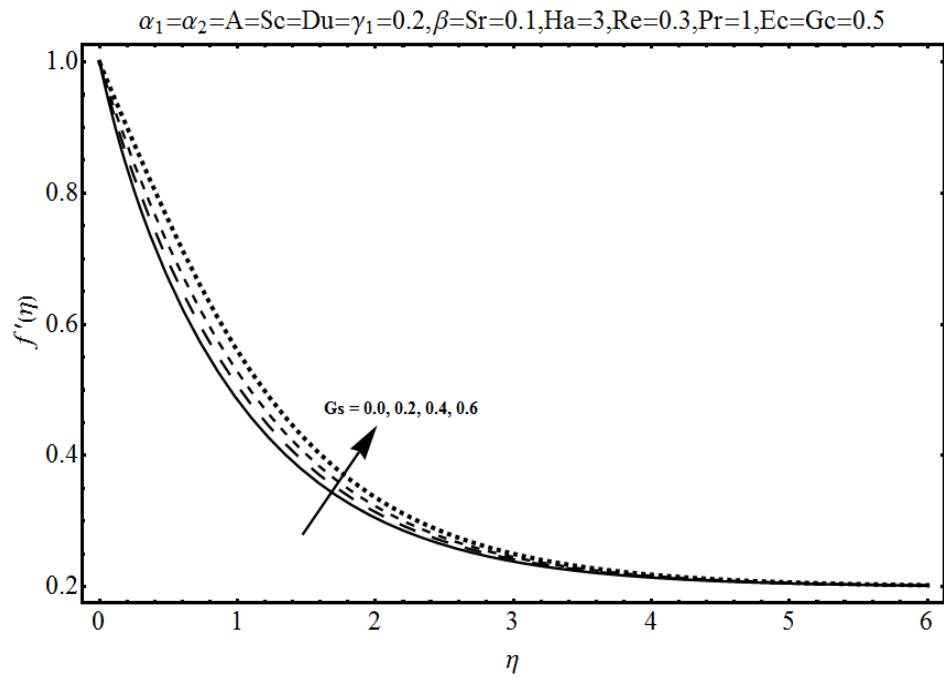
Fig. 10.12: Influence of Gs on $f'(\eta)$.
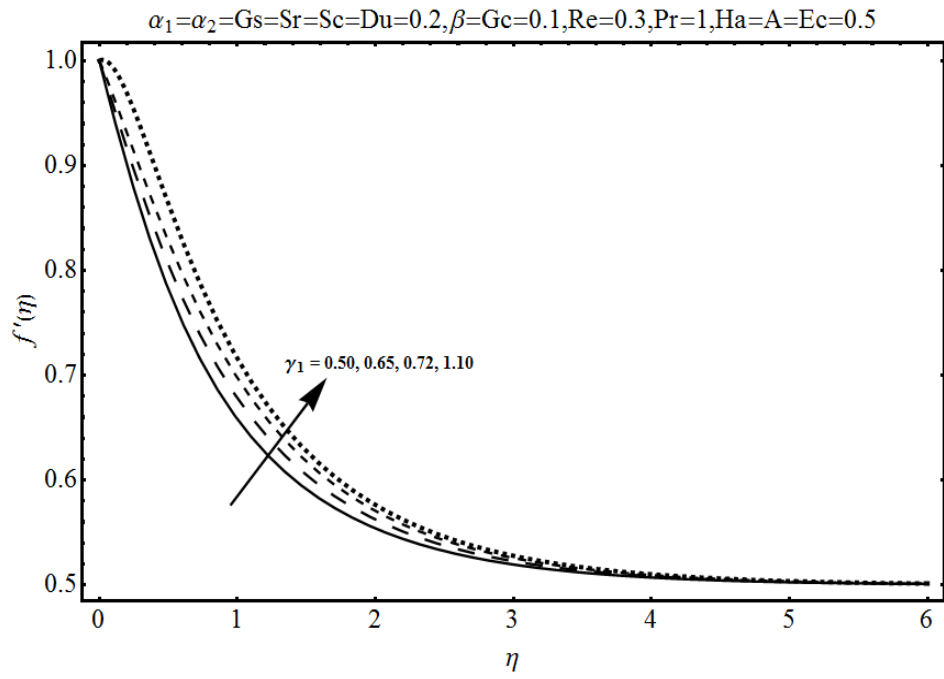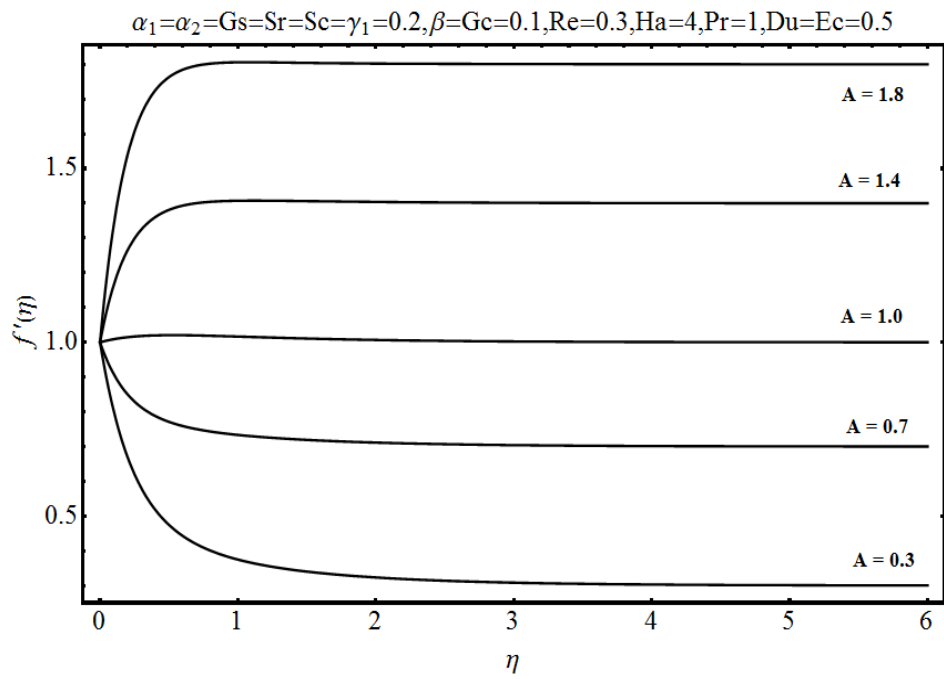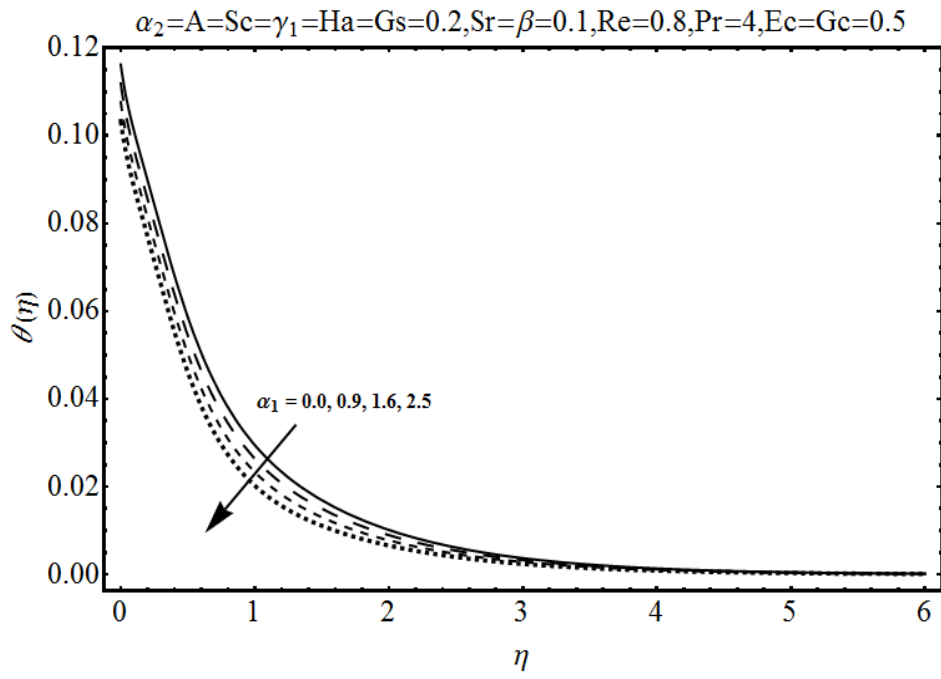
$\alpha_1=\alpha_2=Gs=Sr=Sc=Du=0.2, \beta=Gc=0.1, Re=0.3, Pr=1, Ha=A=Ec=0.5$

$\gamma_1 = 0.50, 0.65, 0.72, 1.10$

Fig. 10.13: Influence of γ_1 on $f'(\eta)$.

$\alpha_1=\alpha_2=Gs=Sr=Sc=\gamma_1=0.2, \beta=Gc=0.1, Re=0.3, Ha=4, Pr=1, Du=Ec=0.5$

A = 1.8

A = 1.4

A = 1.0

A = 0.7

A = 0.3

Fig. 10.14: Influence of A on $f'(\eta)$.

α_2=A=Sc=γ_1=Ha=Gs=0.2,Sr=β=0.1,Re=0.8,Pr=4,Ec=Gc=0.5

α_1 = 0.0, 0.9, 1.6, 2.5

Fig. 10.15: Influence of α_1 on $\theta(\eta)$.

α_1=A=Sc=γ_1=Gs=0.2,Re=Ha=Sr=β=0.1,Pr=2.5,Ec=Gc=0.5

α_2 = 0.0, 0.6, 1.5, 2.5

Fig. 10.16: Influence of α_2 on $\theta(\eta)$.

$$\alpha_1=\alpha_2=A=Sc=\gamma_1=Gs=0.2, Pr=4, Re=0.3, Ec=Gc=0.5, Ha=Sr=0.1$$

$\beta = 0.0, 1.0, 2.0, 3.5$

Fig. 10.17: Influence of β on $\theta\left(\eta\right)$.

$$\alpha_1=\alpha_2=A=\gamma_1=Sc=Gs=0.2, Sr=\beta=0.1, Re=0.3, Pr=2, Ec=Gc=0.5$$

$Ha = 0.0, 1.0, 1.5, 2.7$
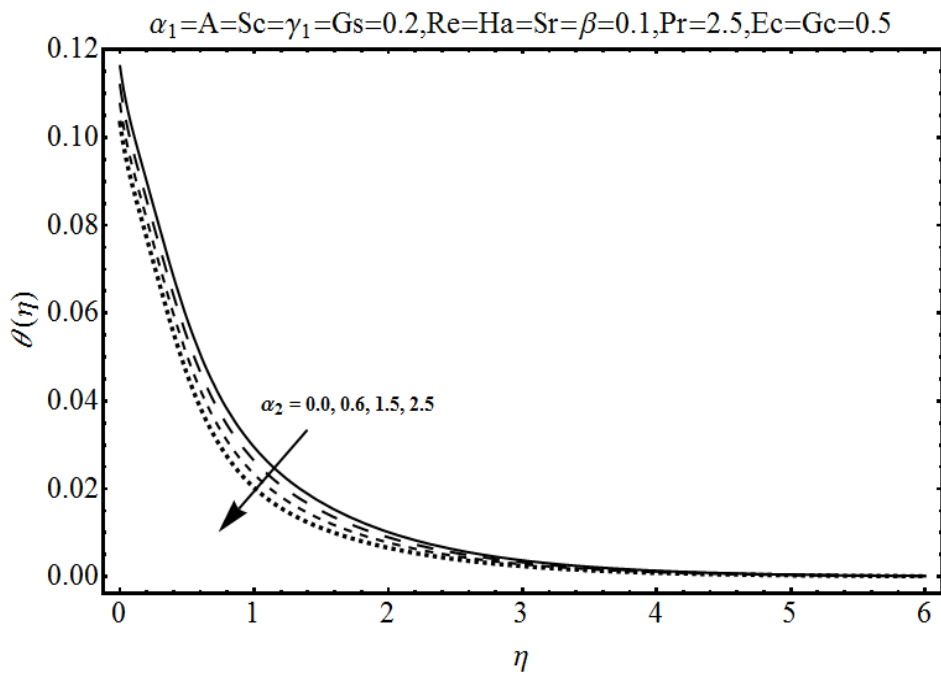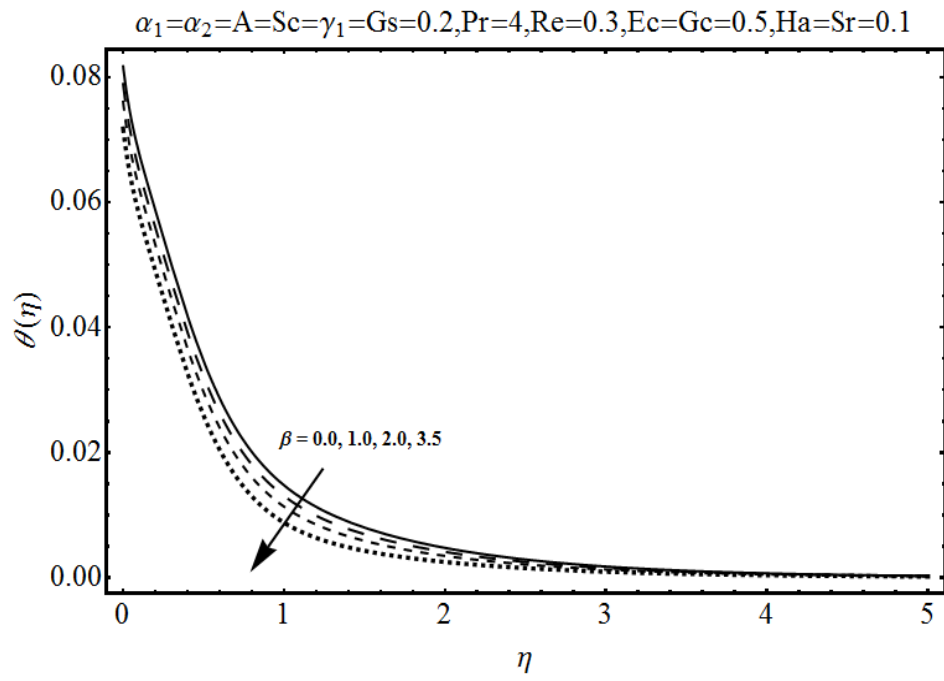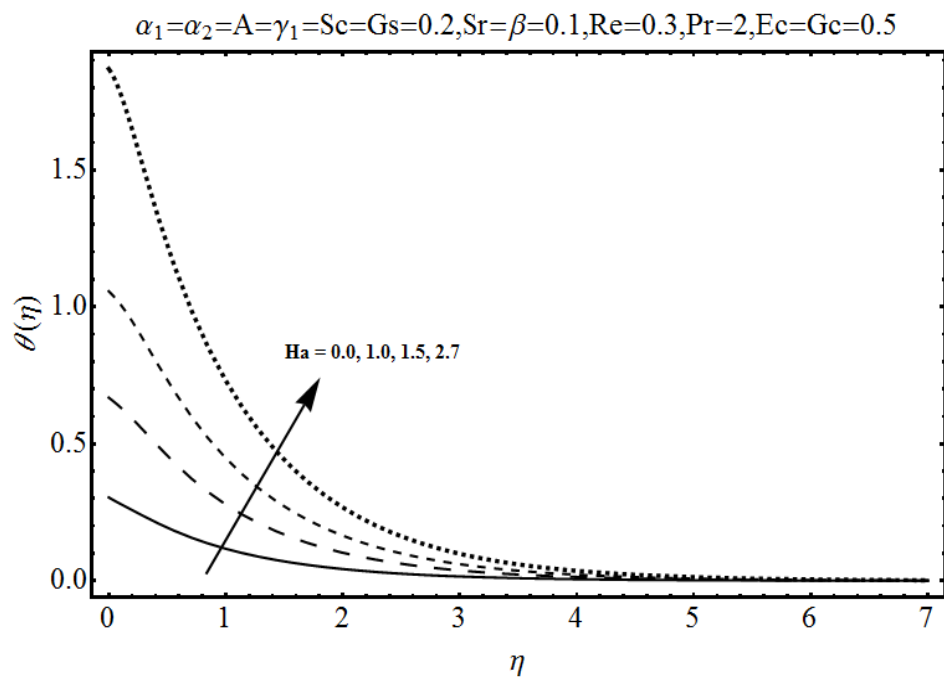
Fig. 10.18: Influence of Ha on $\theta\left(\eta\right)$.

$\alpha_1=\alpha_2=\gamma_1=A=Gs=Sc=0.2,\beta=Sr=0.1,Ha=3,Pr=1,Ec=Gc=0.5$

Re = 0.0, 2.0, 4.0, 6.0
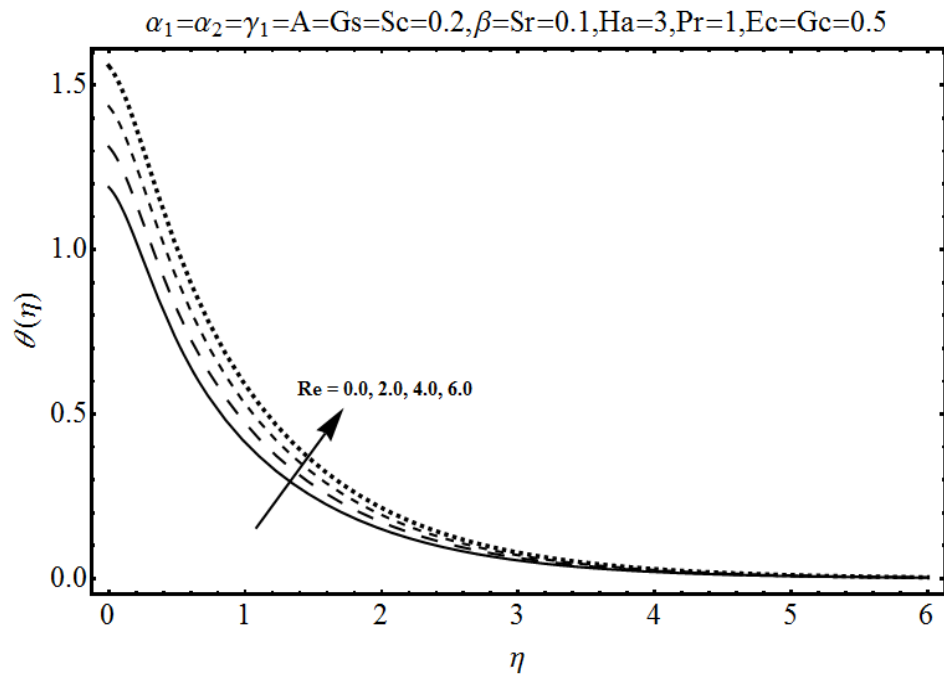
Fig. 10.19: Influence of Re on $\theta(\eta)$.

$\alpha_1=\alpha_2=A=\gamma_1=Gs=Sc=0.2,\beta=Sr=0.1,Ha=2,Re=0.3,Ec=Gc=0.5$

Pr = 0.1, 0.3, 0.7, 1.4
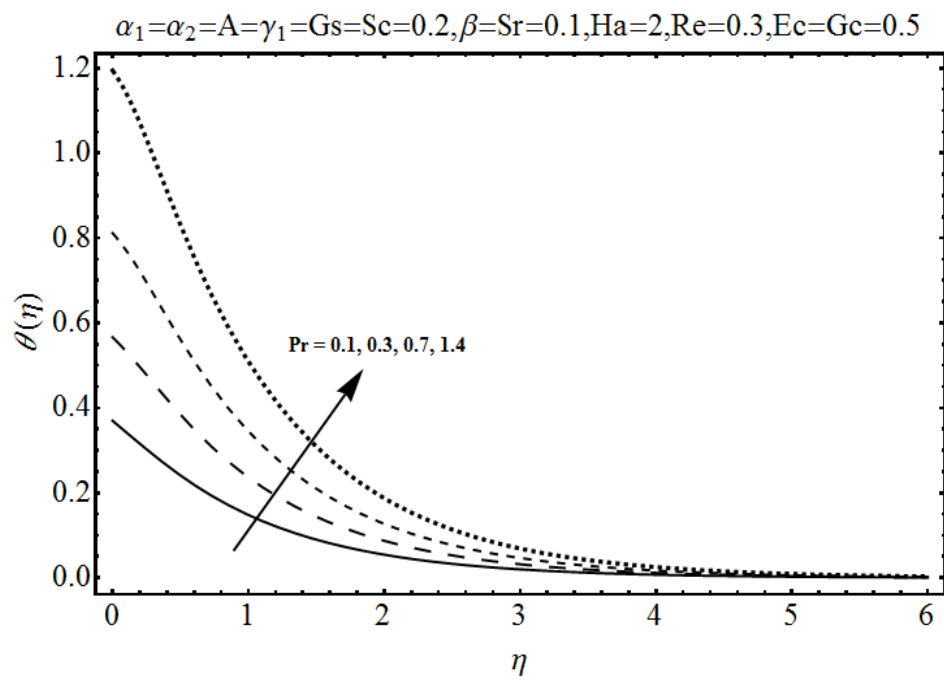
Fig. 10.20: Influence of Pr on $\theta(\eta)$.
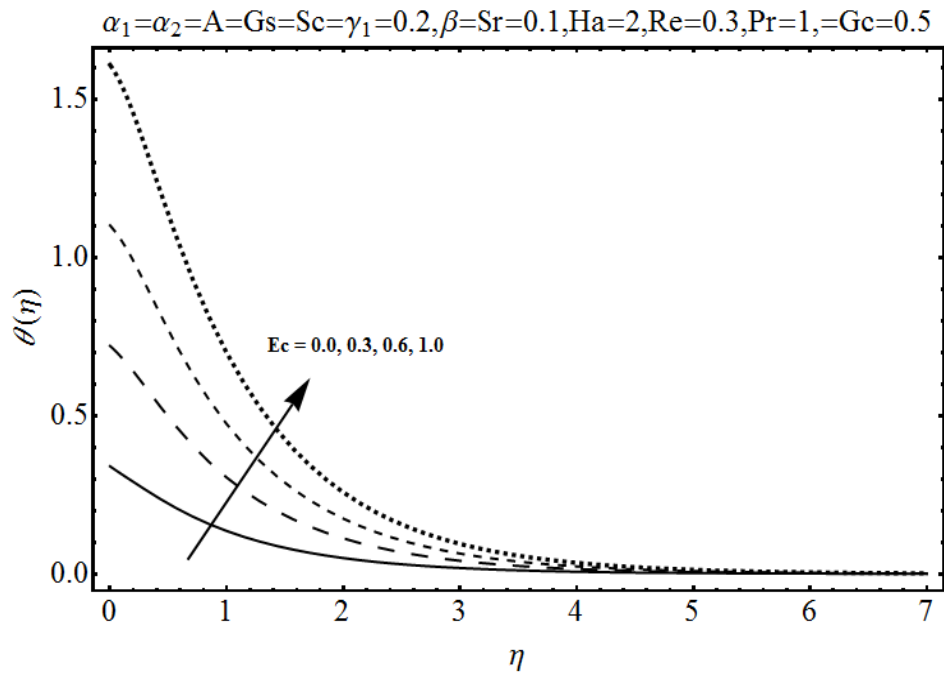
Fig. 10.21: Influence of Ec on $\theta(\eta)$.
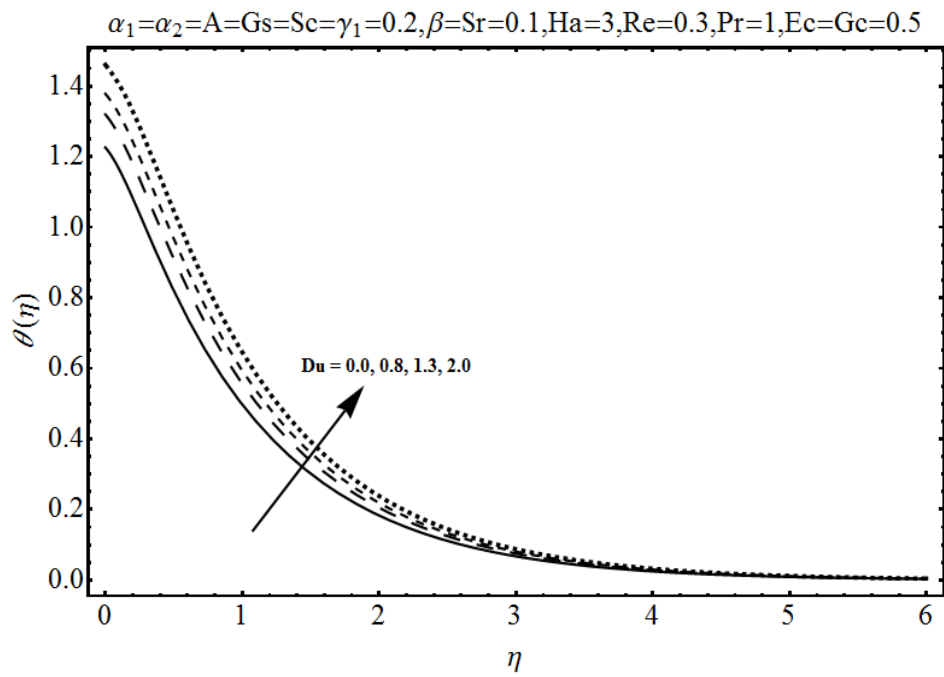
Fig. 10.22: Influence of Du on $\theta(\eta)$.

$\alpha_1 = \alpha_2 = A = Gs = Sc = Du = \gamma_1 = 0.2, \beta = Sr = 0.1, Ha = 3, Re = 0.3, Pr = 1, Ec = 0.5$

Gc = 0.0, 0.5, 1.0, 1.5
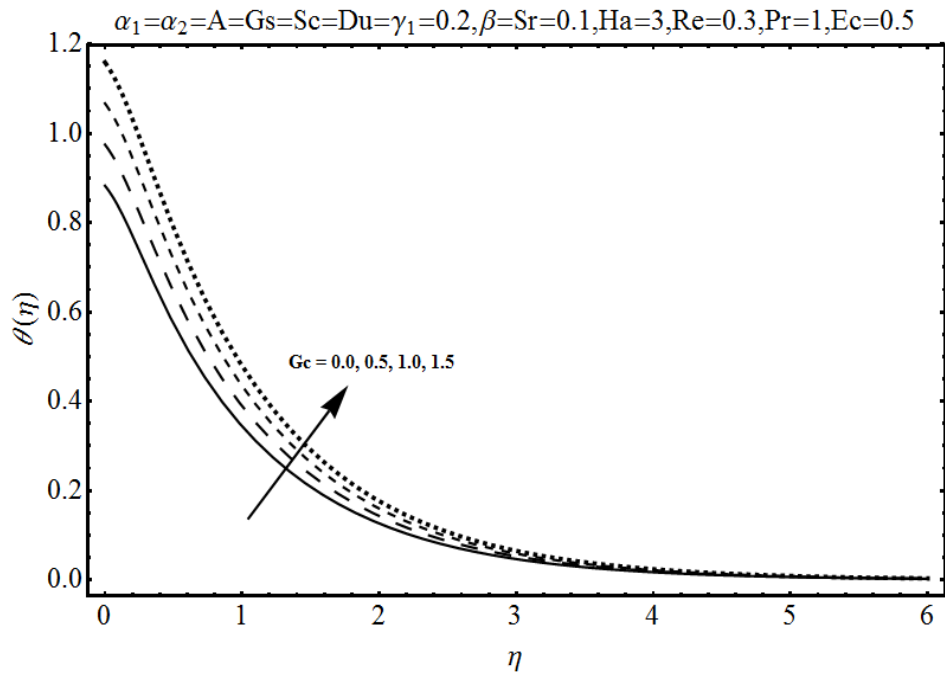
Fig. 10.23: Influence of Gc on $\theta(\eta)$.

$\alpha_1 = \alpha_2 = A = Sc = Du = \gamma_1 = 0.2, \beta = Sr = 0.1, Ha = 3, Re = 0.3, Pr = 2.5, Ec = Gc = 0.5$

Gs = 0.0, 1.0, 2.0, 3.0
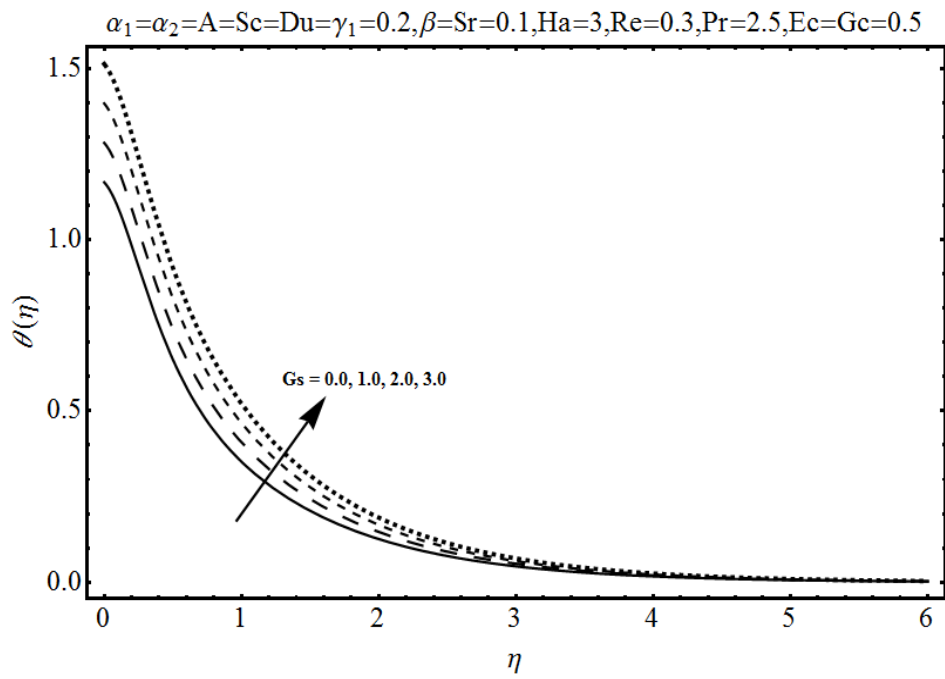
Fig. 10.24: Influence of Gs on $\theta(\eta)$.

$$\alpha_1 = \alpha_2 = A = Gs = Du = \gamma_1 = 0.2, \beta = Sr = Gc = 0.1, Re = 0.3, Pr = 2.5, Ha = Ec = 0.5$$

Sc = 0.5, 2.0, 4.0, 6.0

Fig. 10.25: Influence of Sc on $\theta(\eta)$.

$$\alpha_1 = \alpha_2 = A = Gs = Du = Sc = Ha = \gamma_1 = 0.2, \beta = Gc = 0.1, Re = 0.3, Pr = 2.5, Ec = 0.5$$

Sr = 0.5, 2.0, 4.0, 6.0
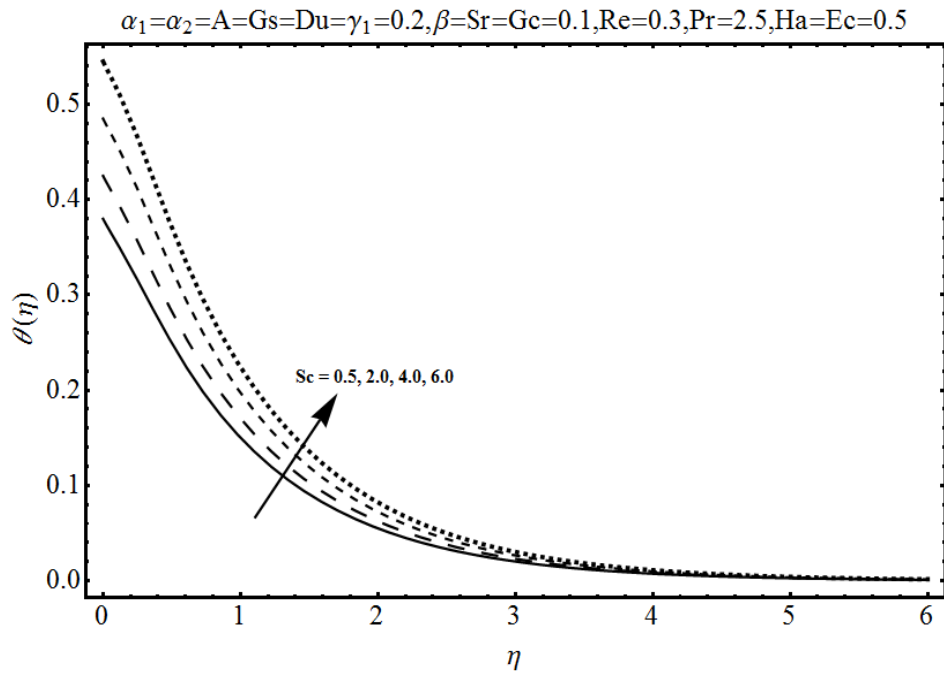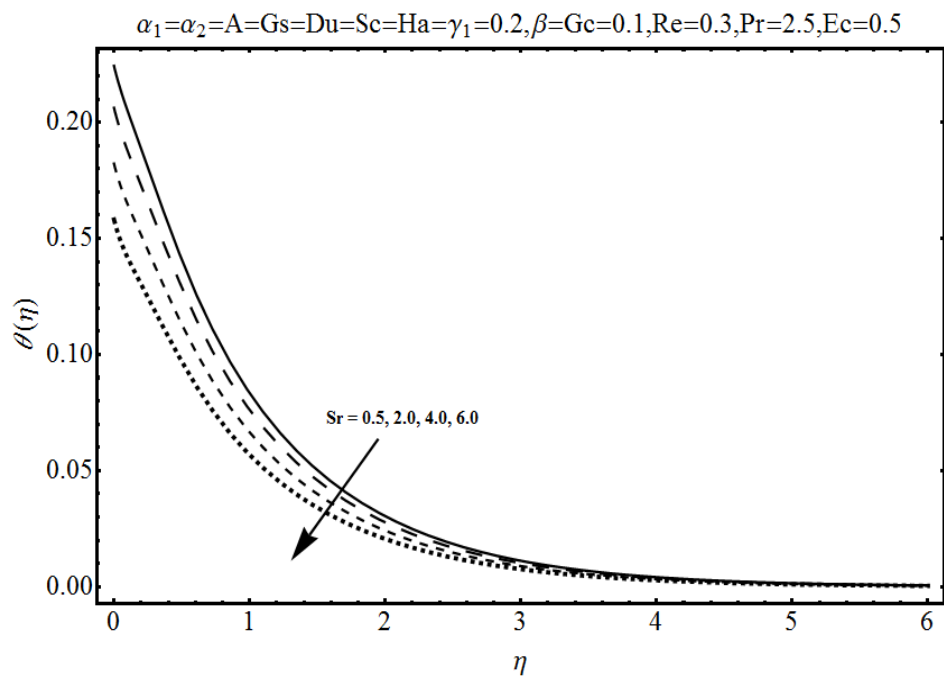
Fig. 10.26: Influence of Sr on $\theta(\eta)$.

$$\alpha_1 = \alpha_2 = A = Gs = Sr = Sc = Du = Ha = 0.2, \beta = Gc = 0.1, Re = 0.3, Pr = 1, Ec = 0.5$$

$\gamma_1 = 0.4, 0.5, 0.6, 0.7$
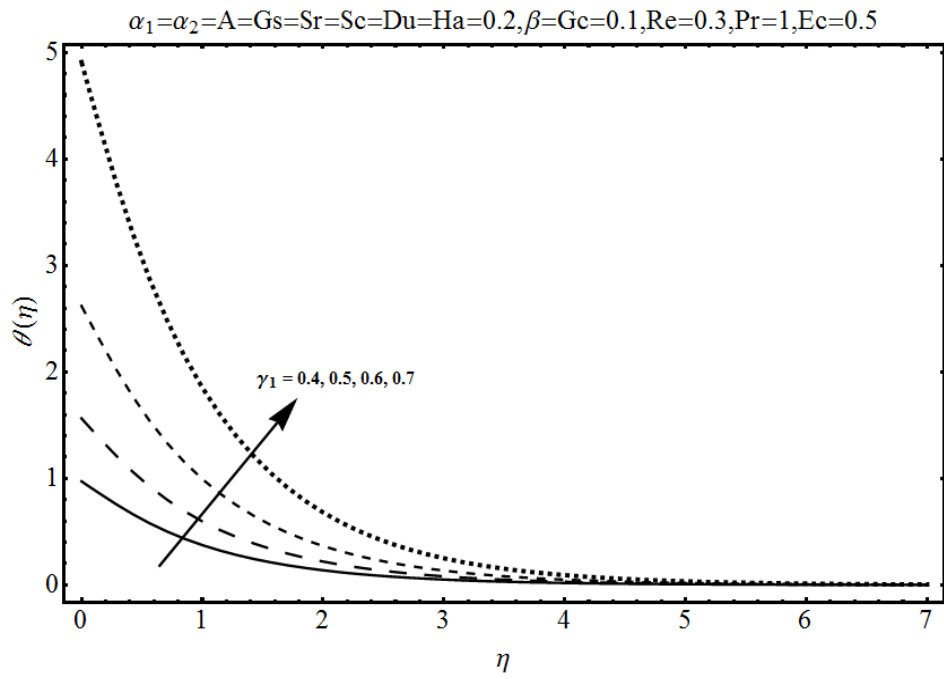
Fig. 10.27: Influence of γ_1 on $\theta(\eta)$.

$$\alpha_1 = \alpha_2 = Gs = Sr = Sc = Du = \gamma_1 = 0.2, Ha = \beta = Gc = 0.1, Re = 0.3, Pr = 1, Ec = 0.5$$

$A = 0.0, 1.5, 2.5, 3.5$
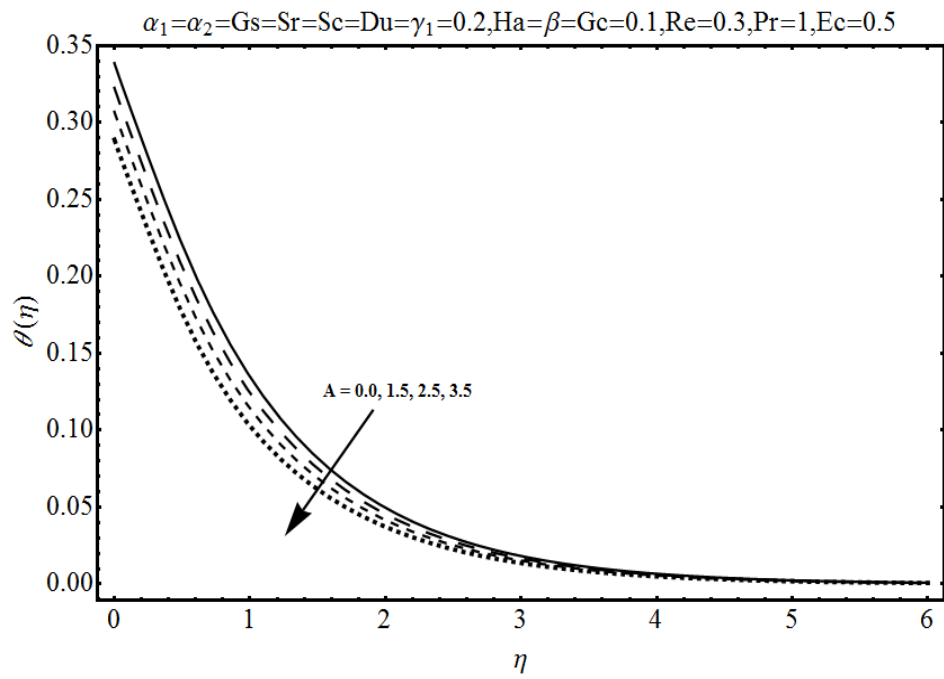
Fig. 10.28: Influence of A on $\theta(\eta)$.
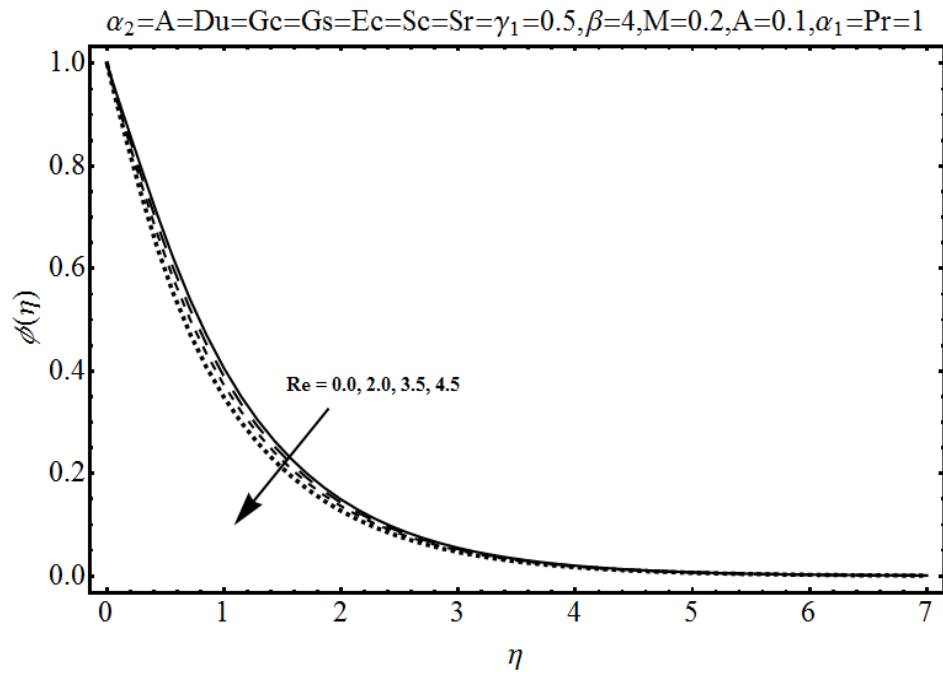
Fig. 10.29: Influence of Re on $\phi(\eta)$.
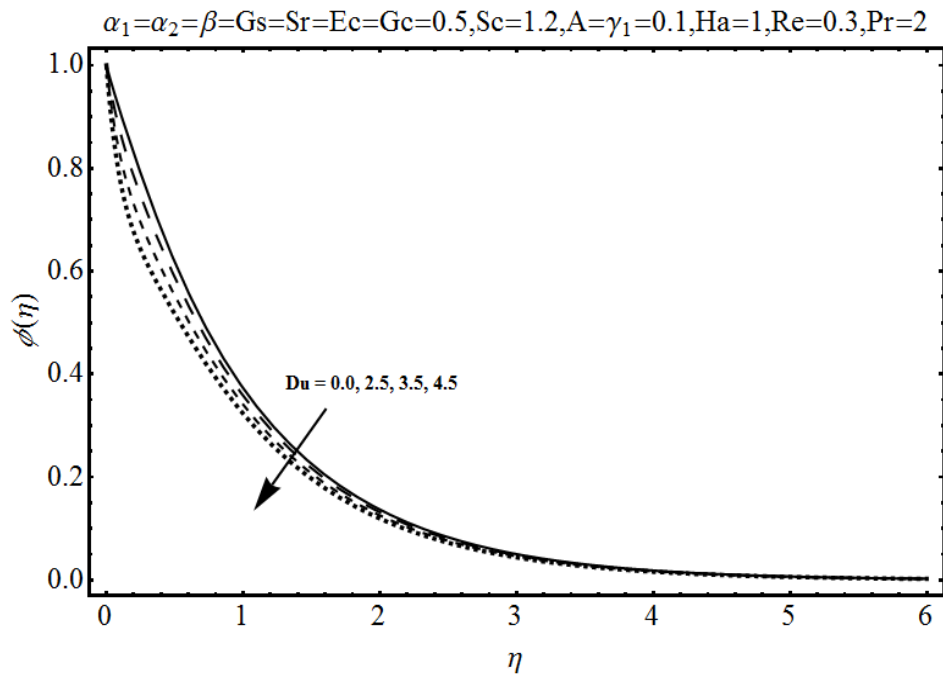
Fig. 10.30: Influence of Re on $\phi(\eta)$.

$\alpha_1 = \alpha_2 = Sr = Re = 0.2, \beta = 0.1, \gamma_1 = 0.68, Sc = 2.5, Ha = 3, Pr = 2, A = 0.8, Du = Gs = Ec = 0.5$

Gc = 0.0, 0.5, 2.0, 3.5
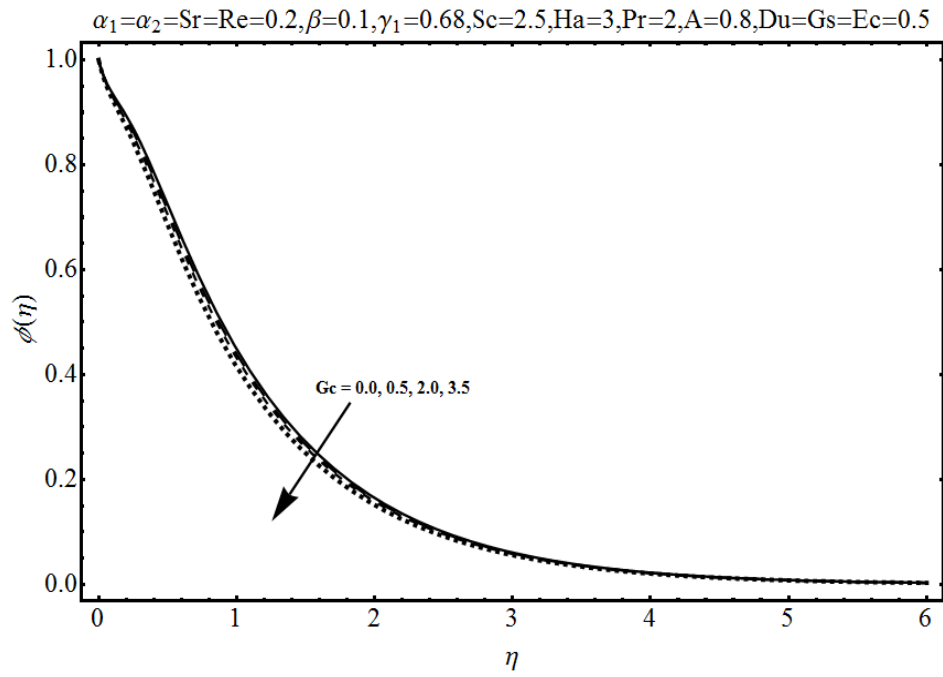
Fig. 10.31: Influence of Gc on $\phi(\eta)$.

$\alpha_1 = \alpha_2 = 0.2, \gamma_1 = 0.68, Sr = 0.4, Sc = M = 2, Re = 0.7, Pr = 2, Du = \beta = A = Ec = Gc = 0.5$

Gs = 0.0, 1.0, 2.0, 3.0
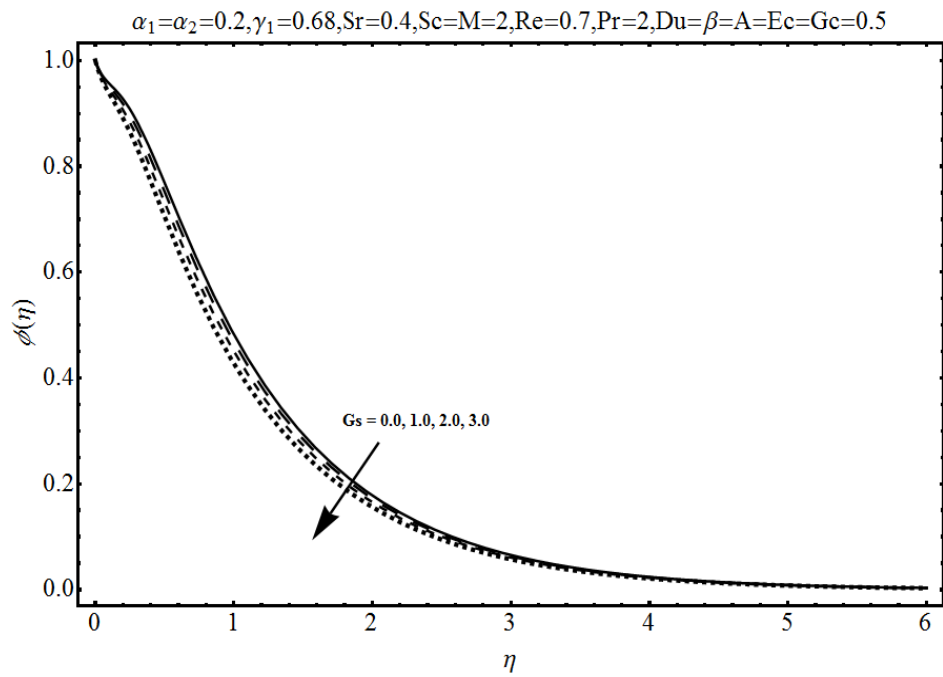
Fig. 10.32: Influence of Gc on $\phi(\eta)$.

$\alpha_1 = \alpha_2 = Du = Ha = \gamma_1 = 0.2, \beta = 1.2, Sc = 3, Re = 0.8, Pr = 1, Gc = 0.1, Gs = A = Ec = 0.5$

Sr = 0.0, 2.0, 4.0, 6.0
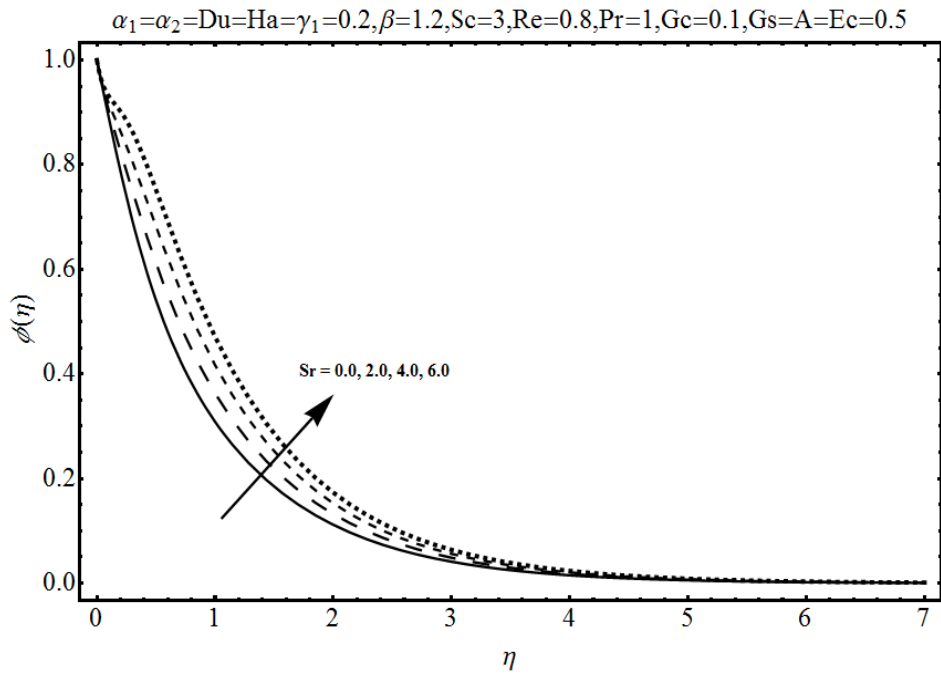
Fig. 10.33: Influence of Sr on $\phi(\eta)$.

$\alpha_1 = \alpha_2 = A = Gs = \gamma_1 = Du = 0.2, \beta = Sr = Gc = 0.1, Re = 0.3, Pr = 1, Ha = Ec = 0.5$

Sc = 0.0, 2.0, 4.0, 6.0
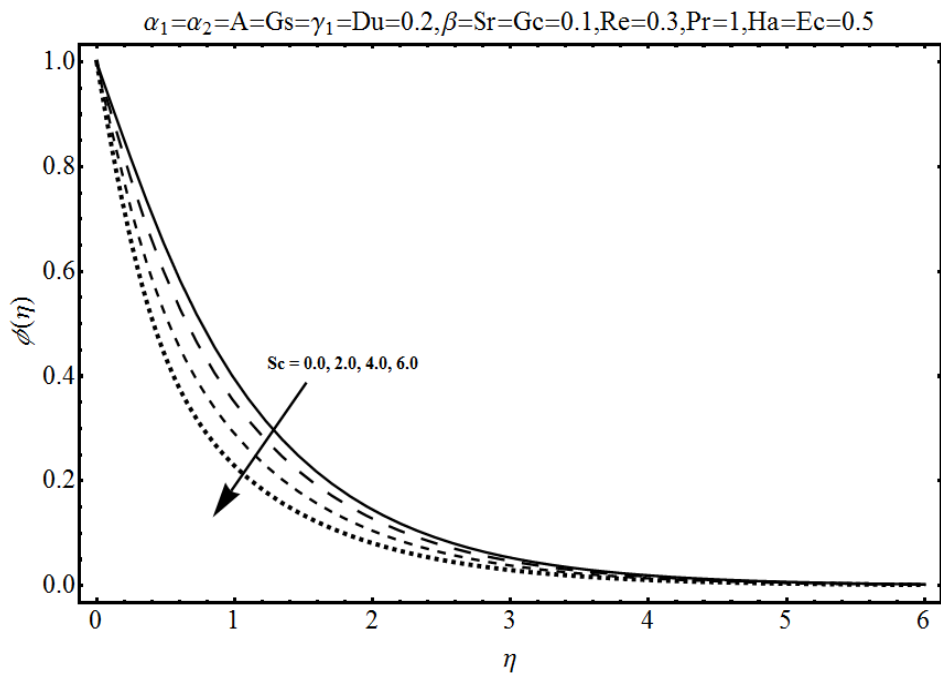
Fig. 10.34: Influence of Sc on $\phi(\eta)$.

α_2=A=Gs=Du=0.2,Ha=3,Gc=0.1,Pr=Sr=1.5,Re=0.3,α_1=A=Sc=β=Ec=0.5

$\gamma_1 = 0.0, 0.3, 0.5, 0.7$

Fig. 10.35: Influence of γ_1 on $\phi(\eta)$.

α_2=Gs=Sr=γ_1=0.2,β=0.4,Gc=Re=0.1,Sc=0.8,Pr=2,Ha=4,α_1=Du=Ec=0.5

$A = 0.0, 2.0, 2.5, 3.5$
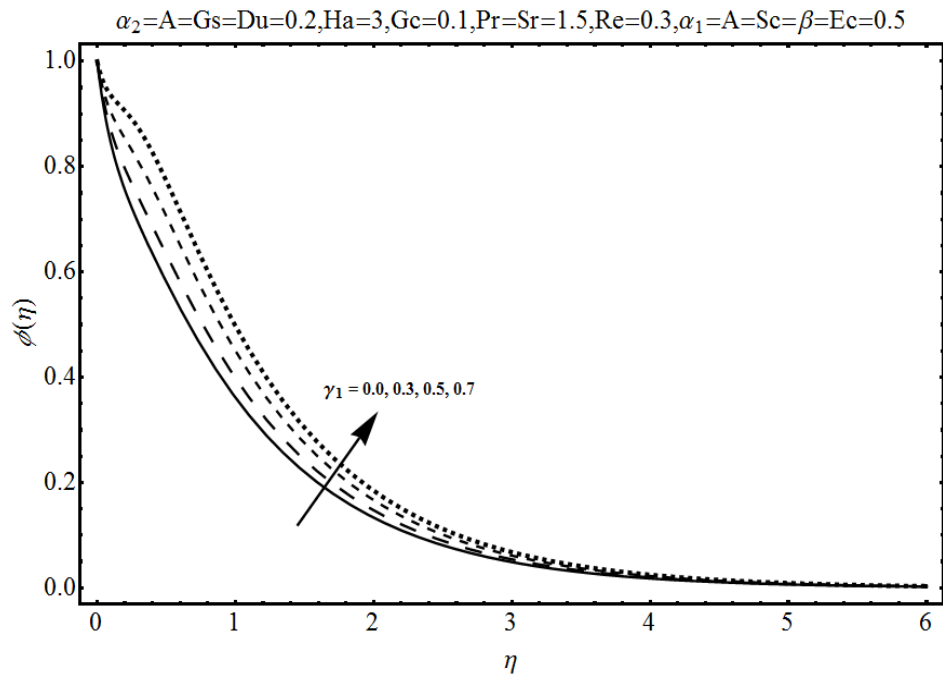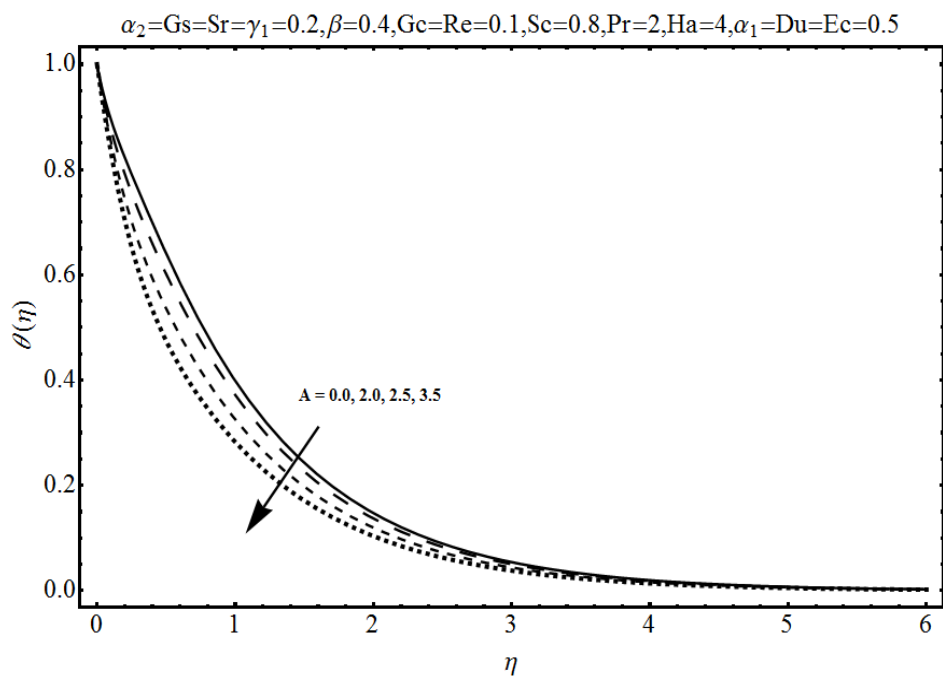
Fig. 10.36: Influence of A on $\phi(\eta)$.

Table 10.1: Convergence of homotopy solutions when $\alpha_1 = 0.1$, $\alpha_2 = 0.2$, $\gamma_1 = 0.1$, $\beta = Sr = Gs = 0.1$, $\text{Re} = Gc = Du = A = 0.2$, $M = Ec = Sc = 0.5$, $\text{Pr} = 0.3$.

Order of approximation	$-f''(0)$	$-\theta'(0)$	$-\phi'(0)$
1	0.8758	0.1165	0.7569
2	0.8739	0.1170	0.7709
5	0.8845	0.1199	0.7009
10	0.8875	0.1219	0.6746
16	0.8884	0.1233	0.6579
24	0.8886	0.1238	0.6541
26	0.8886	0.1247	0.6541
40	0.8886	0.1247	0.6541

Table 10.2: Numerical values of skin friction coefficients $Re_r^{1/2}C_f$ for different values of physical parameters.

α_1	α_2	β	Re	Ha	A	Gs	Gc	Du	Sr	Sc	Pr	Ec	$-Re_r^{1/2}C_f$
0.1	0.2	0.1	0.2	0.5	0.2	0.1	0.2	0.2	0.1	0.5	0.3	0.5	1.794
0.2													1.926
0.22													1.953
0.1	0.2	0.1	0.2	0.5	0.2	0.1	0.2	0.2	0.1	0.5	0.3	0.5	1.794
	0.3												1.559
	0.4												1.316
0.1	0.2	0.1	0.2	0.5	0.2	0.1	0.2	0.2	0.1	0.5	0.3	0.5	1.794
		0.2											1.886
		0.3											1.974
0.1	0.2	0.1	0.2	0.5	0.2	0.1	0.2	0.2	0.1	0.5	0.3	0.5	1.794
			0.3										1.774
			0.4										1.760
0.1	0.2	0.1	0.2	0.5	0.2	0.1	0.2	0.2	0.1	0.5	0.3	0.5	1.794
				0.6									1.859
				0.7									1.938
0.1	0.2	0.1	0.2	0.5	0.2	0.1	0.2	0.2	0.1	0.5	0.3	0.5	1.794
					0.2								1.770
					0.3								1.750
0.1	0.2	0.1	0.2	0.5	0.2	0.1	0.2	0.2	0.1	0.5	0.3	0.5	1.794
							0.3						1.701
							0.4						1.611

α_1	α_2	β	Re	Ha	A	Gs	Gc	Du	Sr	Sc	Pr	Ec	$-Re_r^{1/2}C_f$
0.1	0.2	0.1	0.2	0.5	0.2	0.1	0.2	0.2	0.1	0.5	0.3	0.5	1.794
								0.3					1.792
								0.4					1.789
0.1	0.2	0.1	0.2	0.5	0.2	0.1	0.2	0.2	0.1	0.5	0.3	0.5	1.794
									1				1.792
									2				1.788
0.1	0.2	0.1	0.2	0.5	0.2	0.1	0.2	0.2	0.1	0.5	0.3	0.5	1.794
										1.1			1.799
										1.9			1.814
0.1	0.2	0.1	0.2	0.5	0.2	0.1	0.2	0.2	0.1	0.5	0.3	0.5	1.794
											0.9		1.787
											1.8		1.781
0.1	0.2	0.1	0.2	0.5	0.2	0.1	0.2	0.2	0.1	0.5	0.3	0.5	1.794
												0.9	1.790
												1.8	1.784

Table 10.3: Numerical values of Nusselt number $Re_r^{-1/2}Nu_r$ for different values of physical parameters.

α_1	α_2	β	Re	Ha	A	Gs	Gc	Du	Sr	Sc	Pr	Ec	$-Re_x^{-1/2}Nu_r$
0.1	0.2	0.3	0.1	0.1	0.2	0.5	0.5	0.5	0.5	0.5	1	0.5	0.7107
0.5													0.7123
0.8													0.7159
0.1	0.2	0.3	0.1	1	0.2	0.5	0.5	0.5	0.5	0.5	1	0.5	0.7107
	0.6												0.7138
	1.0												0.7172
0.1	0.2	0.3	0.1	0.1	0.2	0.5	0.5	0.5	0.5	0.5	1	0.5	0.7107
		0.6											0.7122
		0.9											0.7221
0.1	0.2	0.3	0.1	0.1	0.2	0.5	0.5	0.5	0.5	0.5	1	0.5	0.7107
			0.5										0.7123
			0.9										0.7141
0.1	0.2	0.1	0.2	1	0.2	0.5	0.5	0.5	0.5	0.5	1	0.5	0.7018
				1.2									0.6813
				1.4									0.6652

α_1	α_2	β	Re	a	A	Gs	Gc	Du	Sr	Sc	Pr	Ec	$-Re_x^{-1/2}Nu_r$
0.1	0.2	0.1	0.2	1	0.2	0.5	0.5	0.5	0.5	0.5	1	0.5	0.7018
					0.3								0.7020
					0.4								0.7022
1	1	2	0.2	1	0.2	0.5	0.5	0.5	0.5	0.5	1	0.5	0.7100
						0.6							0.7157
						0.7							0.7170
1	1	2	0.2	1	0.2	0.5	0.5	0.5	0.5	0.5	1	0.5	0.7100
							0.6						0.6690
							0.7						0.5027
1	1	2	0.2	1	0.2	0.5	0.5	0.5	0.5	0.5	1	0.5	0.7100
								0.6					0.6670
								0.7					0.6649
1	1	2	0.2	1	0.2	0.5	0.5	0.5	0.5	0.5	1	0.5	0.7018
									0.6				0.7128
									0.7				0.7137
1	1	2	0.2	1	0.2	0.5	0.5	0.5	0.5	0.5	1	0.5	0.7018
										0.6			0.6687
										0.7			0.6673
0.1	0.2	0.1	0.2	1	0.2	0.5	0.5	0.5	0.5	0.5	1	0.5	0.7018
											1.1		0.6878
											1.2		0.6655
0.1	0.2	0.1	0.2	1	0.2	0.5	0.5	0.5	0.5	0.5	1	0.5	0.7018
			0.3									0.6	0.6963
												0.7	0.6597

Table 10.4: Numerical values of Sharwood number $Re_r^{-1/2}Sh_r$ for different values of physical parameters.

α_1	α_2	β	Re	Ha	A	Gs	Gc	Du	Sr	Sc	Pr	Ec	$-Re_r^{-1/2}Sh_r$
0.1	0.2	0.3	0.1	0.9	0.2	0.5	0.5	0.5	0.5	0.5	1	0.5	0.4363
0.3													0.4375
0.6													0.5572
0.1	0.2	0.3	0.1	0.9	0.2	0.5	0.5	0.5	0.5	0.5	1	0.5	0.4363
	0.3												0.4321
	0.4												0.4307

α_1	α_2	β	Re	Ha	A	Gs	Gc	Du	Sr	Sc	Pr	Ec	$-Re_r^{-1/2}Sh_r$
0.1	0.2	0.3	0.1	0.9	0.2	0.5	0.5	0.5	0.5	0.5	1	0.5	0.4363
		0.2											0.4250
		0.3											0.4130
0.1	0.2	0.3	0.1	0.9	0.2	0.5	0.5	0.5	0.5	0.5	1	0.5	0.4363
			0.2										0.4265
			0.3										0.4168
0.1	0.2	0.3	0.1	0.9	0.2	0.5	0.5	0.5	0.5	0.5	1	0.5	0.4363
				1.0									0.4180
				1.1									0.4045
0.1	0.2	0.1	0.2	0.9	0.2	0.5	0.5	0.5	0.5	0.5	1	0.5	0.4363
					0.3								0.4481
					0.4								0.5744
0.1	0.2	0.3	0.1	0.9	0.2	0.5	0.5	0.5	0.5	0.5	1	0.5	0.4363
						0.6							0.4463
						0.7							0.4575
0.1	0.2	0.3	0.1	0.9	0.2	0.5	0.5	0.5	0.5	0.5	1	0.5	0.4363
							0.6						0.4418
							0.7						0.4486
0.1	0.2	0.3	0.1	0.9	0.2	0.5	0.5	0.5	0.5	0.5	1	0.5	0.4363
								0.6					0.3837
								0.7					0.3634
0.1	0.2	0.3	0.1	0.9	0.2	0.5	0.5	0.5	0.5	0.5	1	0.5	0.4363
									0.6				0.3835
									0.7				0.3457
0.1	0.2	0.3	0.1	0.9	0.2	0.5	0.5	0.5	0.5	0.5	1	0.5	0.4363
										0.6			0.4738
										0.7			0.5149
0.1	0.2	0.3	0.1	0.9	0.2	0.5	0.5	0.5	0.5	0.5	1	0.5	0.4299
											1.1		0.4445
											1.2		0.4484
0.1	0.2	0.3	0.1	0.9	0.2	0.5	0.5	0.5	0.5	0.5	1	0.5	0.4363
												0.6	0.4237
												0.7	0.4162

10.5 Concluding remarks

We examined the axisymmetric stagnation point flow of third-grade fluid towards a radially stretching surface with Newtonian heating. The main findings can be summarized as follows:

- Velocity increases while temperature decreases when the fluid parameters α_1, α_2 and β increased.

- Influence of Hartman number (Ha) on the velocity and temperature profile is opposite.

- There is opposite behavior of ratio parameter (A) on the temperature and concentration.

- Temperature and thermal boundary layer thickness are reduced when larger values of Prandtl number are employed.

- Effects of Schmidt and Soret numbers on temperature profile are opposite.

- Influence of Sc on temperature and concentration is opposite.

- Influence of thermal Grashof and solutal Grashof numbers on temperature profile is similar while it has opposite behavior for concentration profile.

- Dufour number Du increases the temperature of fluid.

- Nusselt number decreases with the increase of Ha, Gc, Du, Sc, Pr and Ec.

- Both temperature and concentration increase when conjugate parameter γ_1 is enhanced.

Chapter 11

Characteristics of homogeneous-heterogeneous reactions and Newtonian heating in flow of third grade fluid

The main objective of this chapter is to model and analyze the characteristics of homogeneous-heterogeneous reactions in the magnetohydrodynamic (MHD) flow of third grade fluid over a stretching surface. Both magnetic and electric fields are taken into account. Advanced heat transfer technique (i.e., Newtonian heating) and heat generation/absorption effects are used in the formulation. Homogeneous and heterogeneous reactions are considered within the fluid and at the boundary respectively. Production of heat during chemical reaction is assumed negligible. Approximate convergent solutions are constructed. Influences of various pertinent parameters on the velocity, temperature and concentration distributions are analyzed and discussed. Numerical values of skin friction and local Nusselt number are computed. Concentration distributions for homogeneous and heterogeneous reaction parameters are found opposite.

11.1   Mathematical formulation

We consider the steady flow of an incompressible third-grade fluid by an impermeable stretching surface. Electromagnetic flow analysis is examined with homogeneous-heterogeneous reactions. In addition the effect of heat generation/absorption is present. Cartesian coordinate system is chosen in such a way that $x-$axis is along the stretching sheet and $y-$axis normal to it. Stretching velocity of the surface is originated by applying two forces which are equal in magnitude but opposite in direction when origin is kept fixed. Fluid is electrically conducting via uniform magnetic field $\vec{B} = (0, B_0, 0)$ and uniform electric field $\vec{E} = (0, 0, -E_0)$. Newtonian heating condition is also taken into account. The heat released by the reaction is assumed negligible. The homogeneous reaction for cubic autocatalysis can be represented as

follows:

$$\mathbf{A} + 2\mathbf{B} \rightarrow 3\mathbf{B}, \qquad \text{rate} = k_1 a b^2. \tag{11.1}$$

First-order isothermal reaction on the catalyst surface is presented in the form

$$\mathbf{A} \rightarrow \mathbf{B}, \qquad \text{rate} = k_2 a, \tag{11.2}$$

in which a and b are the concentrations of chemical species $\mathbf{A}$ and $\mathbf{B}$ while k_1 and k_2 denote the rate constants. These equations of reactions ensure that the reaction rate is zero in the external flow and at the outer edge of the boundary layer. Using the boundary layer approximations the relevant equations through aforementioned assumptions are

$$\frac{\partial u}{\partial x} + \frac{\partial v}{\partial y} = 0, \tag{11.3}$$

$$\begin{aligned} u\frac{\partial u}{\partial x} + v\frac{\partial u}{\partial y} &= \nu \frac{\partial^2 u}{\partial y^2} + \frac{\alpha_1^*}{\rho}\left[u\frac{\partial^3 u}{\partial x \partial y^2} + \frac{\partial u}{\partial x}\frac{\partial^2 u}{\partial y^2} + 3\frac{\partial u}{\partial y}\frac{\partial^2 v}{\partial y^2} + v\frac{\partial^3 u}{\partial y^3} \right] \\ &\quad + 2\frac{\alpha_2^*}{\rho}\frac{\partial u}{\partial y}\frac{\partial^2 v}{\partial y^2} + 6\frac{\beta_3}{\rho}\left(\frac{\partial u}{\partial y}\right)^2\frac{\partial^2 u}{\partial y^2} + \frac{\sigma}{\rho}\sin^2\psi\left(E_0 B_0 - B_0^2 u\right), \end{aligned} \tag{11.4}$$

$$u\frac{\partial T}{\partial x} + v\frac{\partial T}{\partial y} = \frac{k}{\rho c_p}\frac{\partial^2 T}{\partial y^2} + \frac{\sigma}{\rho c_p}\left(B_0 u - E_0\right)^2 + \frac{Q_0}{\rho c_p}\left(T - T_\infty\right), \tag{11.5}$$

$$u\frac{\partial a}{\partial x} + v\frac{\partial a}{\partial y} = D_A\frac{\partial^2 a}{\partial y^2} - k_1 a b^2, \tag{11.6}$$

$$u\frac{\partial b}{\partial x} + v\frac{\partial b}{\partial y} = D_B\frac{\partial^2 b}{\partial y^2} + k_1 a b^2, \tag{11.7}$$

with

$$u = U_w(x) = U_0\exp\left(\frac{x}{l}\right), \quad v = 0 \quad \frac{\partial T}{\partial y} = -h_s T, \quad D_A\frac{\partial a}{\partial y} = k_2 a, \quad D_B\frac{\partial b}{\partial y} = -k_s a \text{ at } y = 0,$$

$$u \rightarrow 0, \quad T \rightarrow T_\infty, \quad a \rightarrow a_0, \quad b \rightarrow 0 \quad \text{as} \quad y \rightarrow \infty. \tag{11.8}$$

In above expressions u and v denote the velocity components in the axial and radial directions respectively, σ the electrical conductivity, B_0 the magnetic field, E_0 the electric field, $(\alpha_1^*, \alpha_2^*, \beta_3)$ the fluid material parameters, U_w the stretching velocity, ν the kinematic viscosity, k the thermal conductivity, ρ the density, c_p the specific heat, Q_0 the heat generation/absorption coefficient, D_A and D_B the diffusion species coefficients of A and B, h_s the heat transfer coefficient, T_∞ the ambient fluid temperature, l the characteristic length and a_0 the positive dimensional constant.

Considering the following transformations

$$\eta = \sqrt{\frac{U_0}{2\nu l}}\exp\left(\frac{x}{2l}\right)y, \Psi = \sqrt{2\nu l U_0}f(\eta)\exp\left(\frac{x}{2l}\right),$$

$$u(x, y) = U_0 \exp\left(\frac{x}{l}\right) f'(\eta), \quad v(x, y) = -\sqrt{\frac{\nu U_0}{2l}} \exp\left(\frac{x}{2l}\right) [f(\eta) + \eta f'(\eta)],$$

$$\theta(\eta) = \frac{T - T_\infty}{T_\infty}, \quad g(\eta) = \frac{a}{a_0}, \quad h(\eta) = \frac{b}{a_0}, \tag{11.9}$$

incompressibility condition is satisfied automatically and Eqs. (11.4) to (11.8) are reduced to

$$f''' - 2(f')^2 + ff'' + \alpha_1 \left\{3f'f''' - ff^{(iv)} - 2\eta f''f''' - 9(f'')^2\right\} - \alpha_2 \left\{3(f'')^2 + \eta f''f'''\right\}$$
$$+ 3\beta \operatorname{Re} (f'')^2 f''' + 2Ha^2 \sin^2 \psi (E_1 - f') = 0, \tag{11.10}$$

$$\theta'' + \Pr f\theta' + 2Ha^2 \Pr Ec \sin^2 \psi \left[(f')^2 + E_1^2 - 2E_1 f'\right] + 2\Pr \alpha\theta = 0, \tag{11.11}$$

$$\frac{1}{Sc} g'' + fg' - Kgh^2 = 0, \tag{11.12}$$

$$\frac{\delta_1}{Sc} h'' + fh' + Kgh^2 = 0, \tag{11.13}$$

$$f'(0) = 1, \quad f(0) = 0, \quad \theta'(0) = -\gamma_1 (1 + \theta(0)), \quad g'(0) = K_2 g(0), \quad \delta_1 h'(0) = -K_2 g(0),$$
$$f'(\infty) \to 0, \quad \theta(\infty) \to 0, \quad g(\infty) \to 1, \quad h(\infty) \to 0, \tag{11.14}$$

where $(\alpha_1, \alpha_2, \beta)$ depict the fluid parameters, Ha the magnetic parameter, E_1 the electric parameter, Pr the Prandtl number, Ec the Eckert number, γ_1 the conjugate parameter, K the strength of homogeneous reaction parameter, K_2 the strength of heterogeneous reaction parameter, α the heat generation/absorption parameter, δ_1 the ratio of mass diffusion coefficient and Sc the Schmidt number. These quantities are defined as follows:

$$\alpha_1 = \frac{U_0 \alpha_1^* \exp\left(\frac{x}{l}\right)}{\mu l}, \quad \alpha_2 = \frac{U_0 \alpha_2^* \exp\left(\frac{x}{l}\right)}{\mu l}, \quad \beta = \frac{U_0^2 \beta_3 \exp\left(\frac{2x}{l}\right)}{\mu l^2},$$

$$Ha^2 = \frac{\sigma B_0^2}{\rho U_w}, \quad E_1 = \frac{E_0}{B_0 U_w}, \quad \Pr = \frac{\mu c_p}{K}, \quad Ec = \frac{U_w^2}{c_p (T_w - T_\infty)}, \quad \gamma_1 = h_s \sqrt{\frac{\nu}{a}},$$

$$K = \frac{k_1 a_0^2}{c}, \quad K_2 = \frac{k_2 l \operatorname{Re}_x^{-1/2}}{D}, \quad \alpha = \frac{lQ_0}{\rho c_p U_w}, \quad \delta_1 = \frac{D_B}{D_A}, \quad \operatorname{Re}_x = \frac{U_w x}{\nu}, \tag{11.15}$$

where the diffusion coefficients of chemical species **A** and **B** are of comparable size. This argument provides us to make further assumption that the diffusion coefficients D_A and D_B are equal i.e. $\delta_1 = 1$ and thus [12]:

$$g(\eta) + h(\eta) = 1. \tag{11.16}$$

Now Eqs. (11.12) and (11.13) yield

$$\frac{1}{Sc} g'' + fg' - Kg(1 - g)^2 = 0, \tag{11.17}$$

with the boundary conditions

$$g'(0) = K_2 g(0), \quad g(\eta) \to 1 \quad \text{as} \quad \eta \to \infty. \tag{11.18}$$

Skin friction coefficient and local Nusselt number are defined by:

$$C_f = \frac{\tau_w}{\rho U_w^2}, \qquad Nu_x = \frac{x q_w}{k(T - T_\infty)}, \tag{11.19}$$

$$\tau_{xy} = \left[\mu_0 \frac{\partial u}{\partial y} + \frac{\alpha_1^*}{\rho} \left(2 \frac{\partial u}{\partial x} \frac{\partial u}{\partial y} + v \frac{\partial^2 u}{\partial y^2} + u \frac{\partial^2 u}{\partial x \partial y} \right) + 2 \frac{\beta_3}{\rho} \left(\frac{\partial u}{\partial y} \right)^3 \right]_{y=0}, \quad q_w = -K \left(\frac{\partial T}{\partial y} \right)_{y=0}. \tag{11.20}$$

Dimensionless skin friction coefficient and local Nusselt number are

$$\frac{1}{\sqrt{2}} C_{fx} \operatorname{Re}_x^{1/2} = f''(0) + \frac{7}{2} \alpha_1 f''(0) + \beta \left[f''(0) \right]^3, \tag{11.21}$$

$$\sqrt{\frac{2}{X}} Nu_x \operatorname{Re}_x^{-1/2} = \gamma_1 \left(1 + \frac{1}{\theta(0)} \right), \tag{11.22}$$

where $\operatorname{Re}_x = U_w x / \nu$ is the Reynolds number.

11.2 Homotopic solutions

The initial guess and linear operator. Hence the initial guesses $(f_0(\eta), \theta_0(\eta), g_0(\eta))$ and linear operators $(\mathcal{L}_f, \mathcal{L}_\theta, \mathcal{L}_g)$ for the momentum, energy and concentration equations are expressed in the forms

$$f_0(\eta) = 1 - \exp(-\eta), \quad \theta_0(\eta) = \frac{\gamma_1 \exp(-\eta)}{(1 - \gamma_1)}, \quad g_0(\eta) = 1 - \frac{1}{2} \exp(-K_2 \eta), \tag{11.23}$$

$$\mathcal{L}_f(f) = \frac{d^3 f}{d\eta^3} - \frac{df}{d\eta}, \quad \mathcal{L}_\theta(\theta) = \frac{d^2 \theta}{d\eta^2} - \theta, \quad \mathcal{L}_g(g) = \frac{d^2 g}{d\eta^2} - g, \tag{11.24}$$

with

$$\mathcal{L}_f \left[C_{51} + C_{52} \exp(\eta) + C_{53} \exp(-\eta) \right] = 0, \tag{11.25}$$

$$\mathcal{L}_\theta \left[C_{54} \exp(\eta) + C_{55} \exp(-\eta) \right] = 0, \tag{11.26}$$

$$\mathcal{L}_g \left[C_{56} \exp(\eta) + C_{57} \exp(-\eta) \right] = 0, \tag{11.27}$$

where C_i $(i = 51, ..., 57)$ are the arbitrary constants. The zeroth and mth order deformation problems are:

11.2.1 Zeroth-order problem

$$(1 - q) \mathcal{L}_f \left[\widehat{f}(\eta; q) - f_0(\eta) \right] = q \hbar_f \mathcal{N}_f \left[\widehat{f}(\eta; q) \right], \tag{11.28}$$

$$\widehat{f}'(0; q) = 1, \quad \widehat{f}(0; q) = 0, \quad \widehat{f}'(\infty; q) = 0, \tag{11.29}$$

$$(1 - q) \mathcal{L}_\theta \left[\widehat{\theta} (\eta; q) - \theta_0 (\eta) \right] = q \hbar_\theta \mathcal{N}_\theta \left[\widehat{\theta} (\eta; q) , \widehat{f} (\eta; q) \right], \tag{11.30}$$

$$\widehat{\theta}' (0; q) = -\gamma_1 \left(1 + \widehat{\theta} (0; q) \right), \quad \widehat{\theta} (\infty; q) = 0, \tag{11.31}$$

$$(1 - q) \mathcal{L}_g \left[\widehat{g} (\eta; q) - g_0 (\eta) \right] = q \hbar_g \mathcal{N}_g \left[\widehat{g} (\eta; q) , \widehat{f} (\eta; q) \right], \tag{11.32}$$

$$\frac{\partial \widehat{g}(0; q)}{\partial \eta} = K_2 g (0; q) \qquad \widehat{g} (\infty; q) = 1, \tag{11.33}$$

$$
\begin{aligned}
\mathcal{N}_f \left[\widehat{f} (\eta, q) , \widehat{\theta} (\eta; q) \right] &= \frac{\partial^3 \widehat{f} (\eta; q)}{\partial \eta^3} - 2 \left(\frac{\partial \widehat{f} (\eta; q)}{\partial \eta} \right)^2 + \widehat{f} (\eta; q) \frac{\partial^2 \widehat{f} (\eta; q)}{\partial \eta^2} + \alpha_1 \left\{ 3 \frac{\partial \widehat{f} (\eta; q)}{\partial \eta} \frac{\partial^3 \widehat{f} (\eta; q)}{\partial \eta^3} \right. \\
&\quad \left. - \widehat{f} (\eta; q) \frac{\partial^4 \widehat{f} (\eta; q)}{\partial \eta^4} - 2\eta \frac{\partial^2 \widehat{f} (\eta; q)}{\partial \eta^2} \frac{\partial^3 \widehat{f} (\eta; q)}{\partial \eta^3} - 9 \left(\frac{\partial^2 \widehat{f} (\eta; q)}{\partial \eta^2} \right)^2 \right\} \\
&\quad - \alpha_2 \left\{ 3 \left(\frac{\partial^2 \widehat{f} (\eta; q)}{\partial \eta^2} \right)^2 + +\eta \frac{\partial^2 \widehat{f} (\eta; q)}{\partial \eta^2} \frac{\partial^3 \widehat{f} (\eta; q)}{\partial \eta^3} \right\} \\
&\quad + 3\beta \operatorname{Re} \left(\frac{\partial^2 \widehat{f} (\eta; q)}{\partial \eta^2} \right)^2 \frac{\partial^3 \widehat{f} (\eta; q)}{\partial \eta^3} + 2Ha^2 \sin^2 \psi \left(E - \frac{\partial \widehat{f} (\eta; q)}{\partial \eta} \right), \tag{11.34}
\end{aligned}
$$

$$
\begin{aligned}
\mathcal{N}_\theta \left[\widehat{\theta} (\eta; p) , \widehat{f} (\eta; p) \right] &= \frac{\partial^2 \widehat{\theta}(\eta, p)}{\partial \eta^2} + \operatorname{Pr} \widehat{f} (\eta; p) \frac{\partial \widehat{\theta} (\eta; p)}{\partial \eta} + 2Ha^2 \sin^2 \psi Ec \left\{ \left(\frac{\partial \widehat{f} (\eta; p)}{\partial \eta} \right)^2 + E_1^2 \right. \\
&\quad \left. - 2E_1 \frac{\partial \widehat{f} (\eta; p)}{\partial \eta} \right\} + 2 \operatorname{Pr} \alpha \widehat{\theta}(\eta, p), \tag{11.35}
\end{aligned}
$$

$$\mathcal{N}_g \left[\widehat{g} (\eta; q) , \widehat{f} (\eta; q) \right] = \frac{1}{Sc} \frac{\partial^2 \widehat{g}(\eta, q)}{\partial \eta^2} + \widehat{f} (\eta; q) \frac{\partial \widehat{g} (\eta; q)}{\partial \eta} - K g(\eta; q) (1 - g(\eta; q))^2, \tag{11.36}$$

where $p \in [0, 1]$ is embedding parameter and $\hbar_f$, $\hbar_\theta$ and $\hbar_g$ the non-zero auxiliary parameters.

11.2.2 mth-order deformation problems

$$\mathcal{L}_f [f_m (\eta) - \chi_m f_{m-1} (\eta)] = \hbar_f \mathcal{R}_m^f (\eta), \tag{11.37}$$

$$f'_m (0) = 0, \qquad f'_m (\infty) = 0, \qquad f_m (0) = 0, \tag{11.38}$$

$$\mathcal{L}_\theta [\theta_m (\eta) - \chi_m \theta_{m-1} (\eta)] = \hbar_\theta \mathcal{R}_m^\theta (\eta), \tag{11.39}$$

$$\theta'_m (0) + \gamma_1 \theta_m (0) = 0, \quad \theta_m (\infty) = 0, \tag{11.40}$$

$$\mathcal{L}_g [g_m (\eta) - \chi_m g_{m-1} (\eta)] = \hbar_g \mathcal{R}_m^g (\eta), \tag{11.41}$$

$$g'_m(0) = K_s g_m (0), \; g_m(\infty) = 0, \tag{11.42}$$

$$\mathcal{R}_m^f (\eta) = f'''_{m-1} (\eta) - 2 \sum_{k=0}^{m-1} f'_{m-1-k} f'_k + \sum_{k=0}^{m-1} f_{m-1-k} f''_k + \alpha_1 \sum_{k=0}^{m-1} \left[3 f'_{m-1-k} f'''_m - f_{m-1-k} f_k^{(iv)} \right.$$

$$-2\eta f''_{m-1-k}f'''_k - 9f''_{-1-k}f''_k\big] - \alpha_2 \sum_{k=0}^{m-1} \big[3f''_{m-1-k}f''_k + \eta f''_{m-1-k}f'''_k\big]$$

$$+3\beta \operatorname{Re} \sum_{k=0}^{m-1} f''_{m-1-k} \sum_{l=0}^{k} f''_{k-l}f'''_l + 2Ha^2 \sin^2\psi \left[E_1(1-\chi_m) - f'_{m-1}\right], \qquad (11.43)$$

$$\mathcal{R}_m^\theta(\eta) = \theta''_{m-1}(\eta) + \operatorname{Pr} \sum_{k=0}^{m-1} f_{m-1-k}\theta'_k + 2Ha^2 \operatorname{Pr} Ec \sin^2\psi \left[\sum_{k=0}^{m-1} f'_{m-1-k}f'_k + E_1^2(1-\chi_m) - 2E_1 f'_{m-1}\right]$$
$$+ 2\operatorname{Pr}\alpha\theta_{m-1}, \qquad (11.44)$$

$$\mathcal{R}_m^g(\eta) = \frac{1}{Sc}g''_{m-1} + \sum_{k=0}^{m-1} f_{m-1-k}g'_k - K_1 g_{m-1} - K_1 \sum_{k=0}^{m-1} \left(g_{m-1-k} \sum_{l=0}^{k} g_{k-l}g_l - 2g_{m-1-k}g_k\right). \qquad (11.45)$$

For $q = 0$ and $q = 1$, we can write

$$\widehat{f}(\eta; 0) = f_0(\eta), \quad \widehat{f}(\eta; 1) = f(\eta), \qquad (11.46)$$

$$\widehat{\theta}(\eta; 0) = \theta_0(\eta), \quad \widehat{\theta}(\eta; 1) = \theta(\eta), \quad \widehat{g}(\eta; 0) = g_0(\eta), \quad \widehat{g}(\eta; 1) = g(\eta), \qquad (11.47)$$

and with the variation of q from 0 to 1, $\widehat{f}(\eta; q)$, $\widehat{\theta}(\eta; q)$ and $\widehat{g}(\eta; q)$ vary from the initial solutions $f_0(\eta)$, $\theta_0(\eta)$ and $g_0(\eta)$ to the final solutions $f(\eta)$, $\theta(\eta)$ and $g(\eta)$ respectively. The values of auxiliary parameters is selected in such a manner that the series solutions converge. The general solutions (f_m, θ_m, g_m) of Eqs. $(11.37 - 11.42)$ via special solutions $(f_m^*, \theta_m^*, g_m^*)$ are

$$f_m(\eta) = f_m^\star(\eta) + C_{51} + C_{52}e^\eta + C_{53}e^{-\eta}, \qquad (11.48)$$

$$\theta_m(\eta) = \theta_m^\star(\eta) + C_{54}e^\eta + C_{55}e^{-\eta}, \qquad (11.49)$$

$$g_m(\eta) = g_m^\star(\eta) + C_{56}e^\eta + C_{57}e^{-\eta}. \qquad (11.50)$$

11.3   Convergence of the homotopy solutions

Homotopic technique offers us great freedom to adjust and control the convergence region of the series solutions. The region parallel to $\hbar$−axis is known as convergence region. Hence we have plotted the $\hbar$−curves in the Figs. 11.2(a-c). It is noted that the admissible ranges of the auxiliary parameters $\hbar_f$, $\hbar_\theta$ and $\hbar_g$ are $-0.8 \leq \hbar_f \leq -0.3$, $-1.5 \leq \hbar_\theta \leq -0.5$ and $-1.2 \leq \hbar_g \leq -0.2$.

11.4   Results and discussion

The main emphasis of this section is to analyze the characteristics of different pertinent parameters on the axial velocity, temperature and concentration distributions. Characteristics of magnetic parameter Ha on the velocity distribution are illustrated in Fig. 11.3. It is concluded that velocity profile decreases for $M = 0.1, 0.8, 1.3, 1.9$. Further boundary layer thickness also decreases. In fact higher values of magnetic

parameter Ha corresponds to larger Lorentz force which provides more resistance to the fluid motion and thus the velocity distribution decreases. Fig. 11.4 shows the behavior of third grade parameter β on the velocity distribution. Here we analyzed that velocity distribution enhances for larger values of third grade parameter. Higher values of third grade parameter corresponds to low viscosity which is responsible in enhancement of the velocity profile. Influence of electric parameter E_1 on the velocity distribution is displayed in Fig. 11.5. The velocity distribution is higher for larger values of electric field. In fact the Lorentz force (arising due to the electric field acts like an accelerating force) reduces the frictional resistance which causes to shift the stream line away from the stretching surface. Effect of Reynold number Re on the velocity profile is sketched in Fig. 11.6. Velocity profile increases near the surface of sheet while it vanishes gradually far away from the surface. In fact for higher values of Reynolds number (which is the ratio of inertial forces to the viscous forces) the friction between the fluid and surface reduces. Therefore velocity profile increases. Analysis of ψ on the velocity profile is shown in Fig. 11.7. Here both velocity profile and associated boundary layer thickness are decreasing functions of ψ. It is due to the fact that with an increase in angle of inclination, the effect of magnetic field on fluid particles increases which enhances the Lorentz force and consequently the velocity profile decreases. It is also noted that for $\psi = 0$ the magnetic field has no effect on the velocity profile while maximum resistance is possible for the fluid particles when $\psi = \pi/2$.

Behavior of magnetic parameter Ha on the temperature distribution is shown in Fig. 11.8. It is concluded that higher values of megnatic parameter give rise to the temperature distribution. Larger values of magnetic parameter corresponds to increase in Lorentz force which is a resistive force. Therefore temperature distribution increases. Effect of conjugate parameter γ_1 on temperature field is displayed in Fig. 11.9. Temperature distribution increases for larger values of conjugate paramter γ_1 while thermal boundary layer thickness decreases. Behavior of electric field parameter E_1 on the temperature distribution is shown in Fig. 11.10. Temperature distribution is increasing function of electric field parameter. Further higher values of electric field parameter result in enhancement of thermal boundary layer thickness. Influence of heat generation on temperature profile is presented in Fig. 11.11. Temperature profile increases with an increase in heat generation parameter $\alpha > 0$. It is also noted that thermal boundary layer thickness increases for heat generation. In case of heat generation more heat is produced and it leads to an enhancement of temperature. Characteristics of Eckert number Ec on temperature distribution is sketched in Fig. 11.12. It is shown that temperature distribution increases for larger values of Eckert number. Eckert number is the ratio of kinetic energy to the enthalpy. Higher Eckert number corresponds to an increase in heat by friction. Hence less heat is transferred from surface to the fluid and as a result the temperature distribution becomes higher. Fig. 11.13 shows the variation of angle of inclination on temperature distribution. It is noted that temperature distribution is higher for larger values of angle of inclination. In fact higher values of angle of inclination corresponds to larger magnetic field which opposes the fluid motion. Hence temperature distribution increases.

Analysis of strength of homogeneous reaction K_1 on the concentration profile is displayed in Fig. 11.14. Concentration profile decreases while boundary layer thickness increases for higher values of

strength of homogeneous reaction parameter. Behavior of strength of heterogeneous reaction parameter K_2 on the concentration distribution is analyzed in Fig. 11.15. Concentration distribution increases for higher values of heterogeneous reaction parameter K_2. Effect of Schmidt number Sc on concentration distribution is shown in Fig. 11.16. Increasing behavior of concentration distribution is noted for larger Schmidt number. It is also analyzed that the solutal boundary layer thickness decreases. Note that the Schmidt number is the ratio of momentum diffusivity to mass diffusivity. Hence higher values of Schmidt number correspond to small mass diffusivity and thus the concentration profile increases.

Table 11.1 shows the convergence analysis of the series solutions for momentum, energy and concentration equations. It is concluded that 15th order of approximations is sufficient for convergence analysis of momentum equation while 30th order of approximations are enough for energy and concentration equations. Table 11.2 presents behavior of various parameters on skin friction coefficient. Higher values of α_1, α_2, M and ψ result in enhancement of skin friction coefficient while it decreases for larger values of β, Re and E_1. Table 11.3 shows the characteristics of various pertinent parameters on Nusselt number. It is noted that Nusselt number increases for higher values of α_1, α_2, M, K_2, ψ and α while it decreases with the increase in γ_1, Sc and K_1.
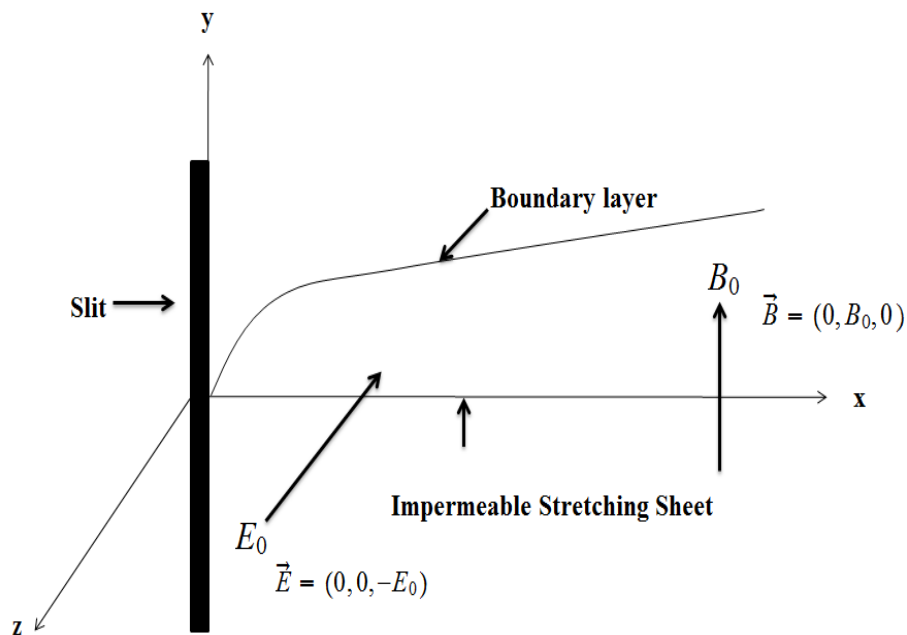

Fig. 11.1: Flow sketch.
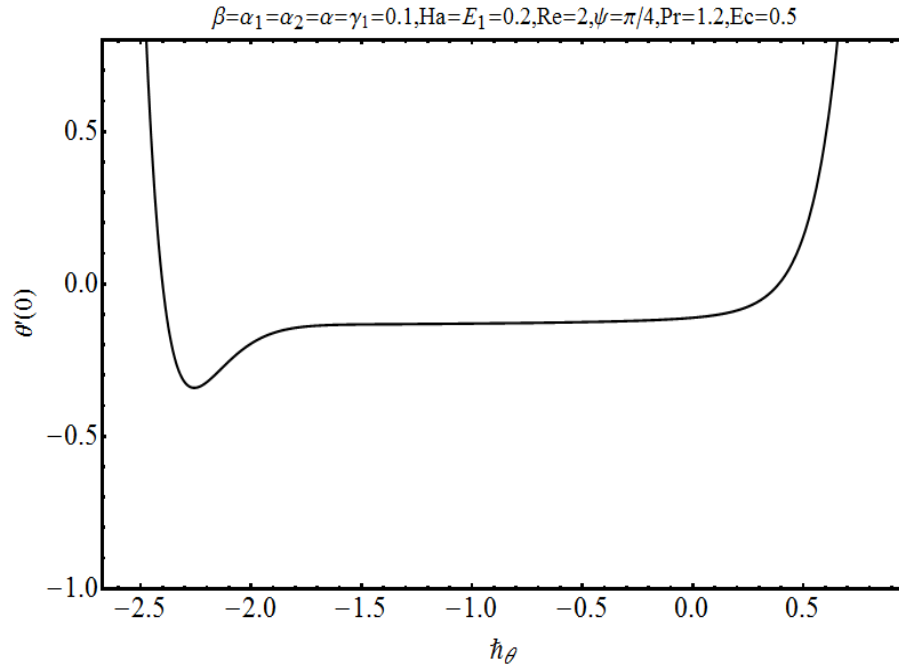
Fig. 11.2(a): $\hbar-$curve for $f(\eta)$.
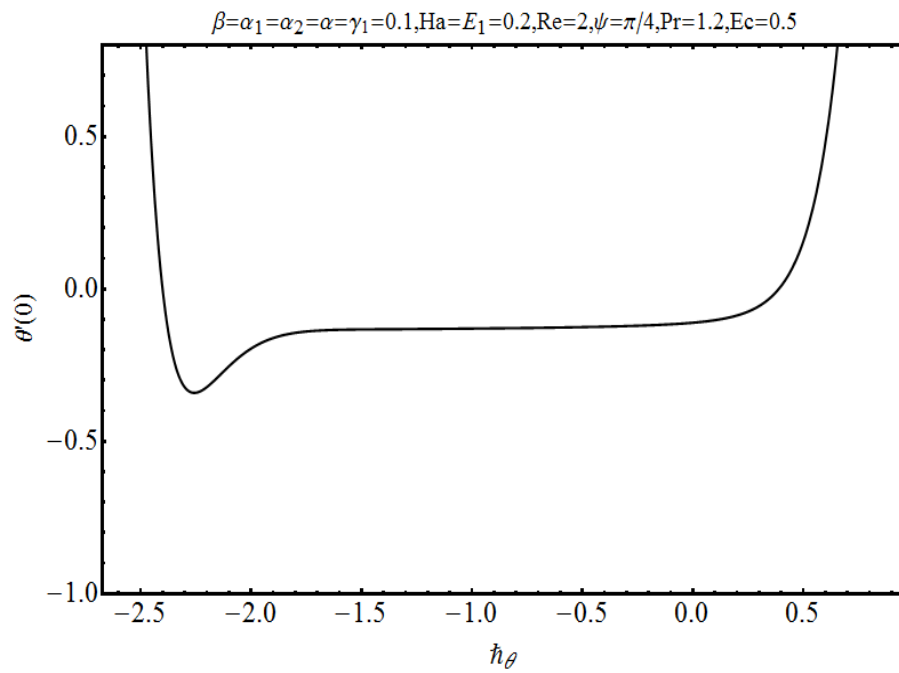
Fig. 11.2(b): $\hbar-$curve for $\theta(\eta)$.
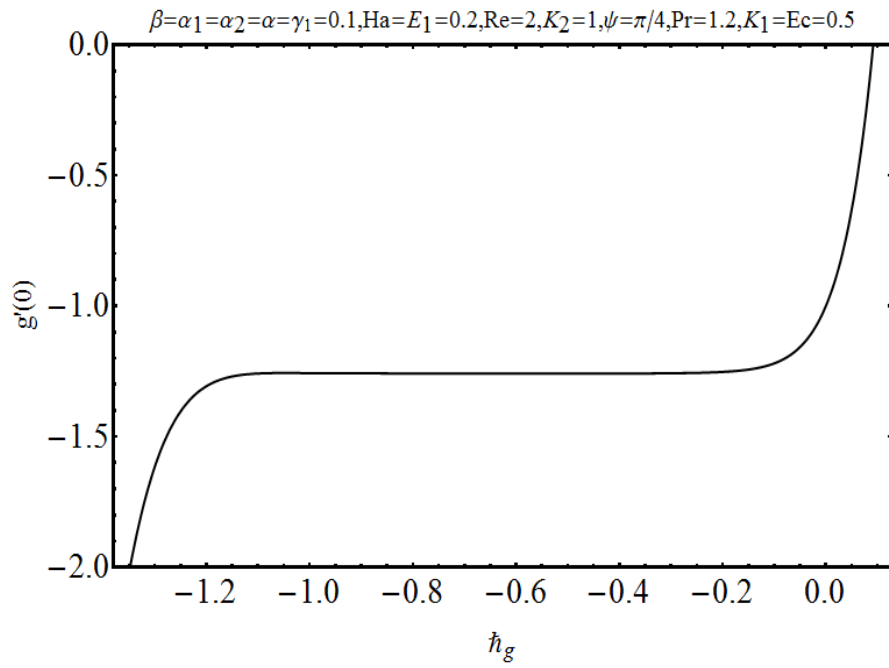
Fig. 11.2(c): $\hbar-$curve for $g\left(\eta\right)$.

Fig. 11.3: Effect of Ha on $f'\left(\eta\right)$.

Fig. 11.4: Effect of β on $f'(\eta)$.

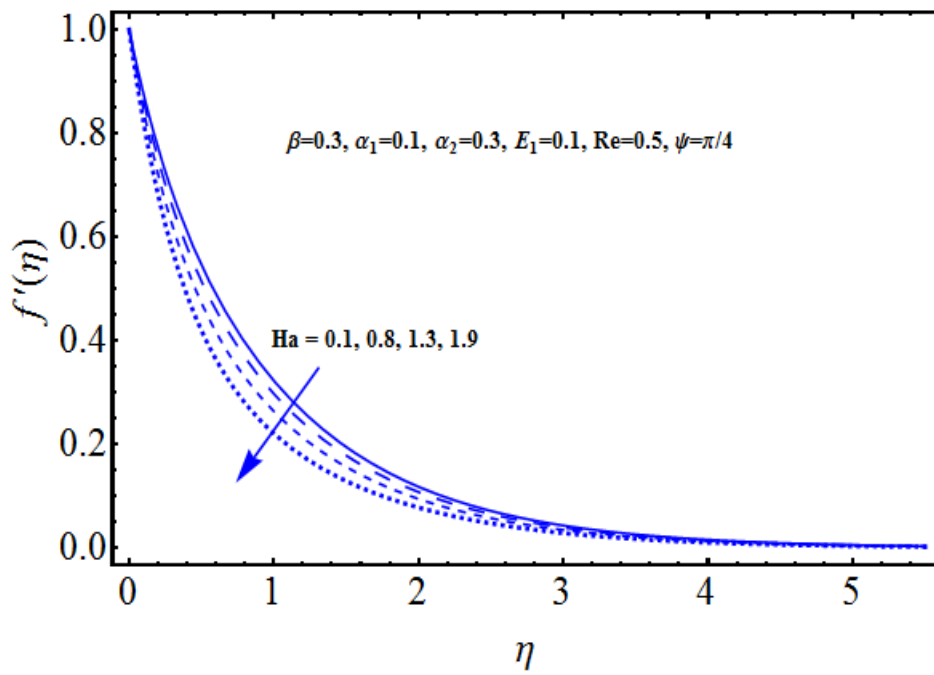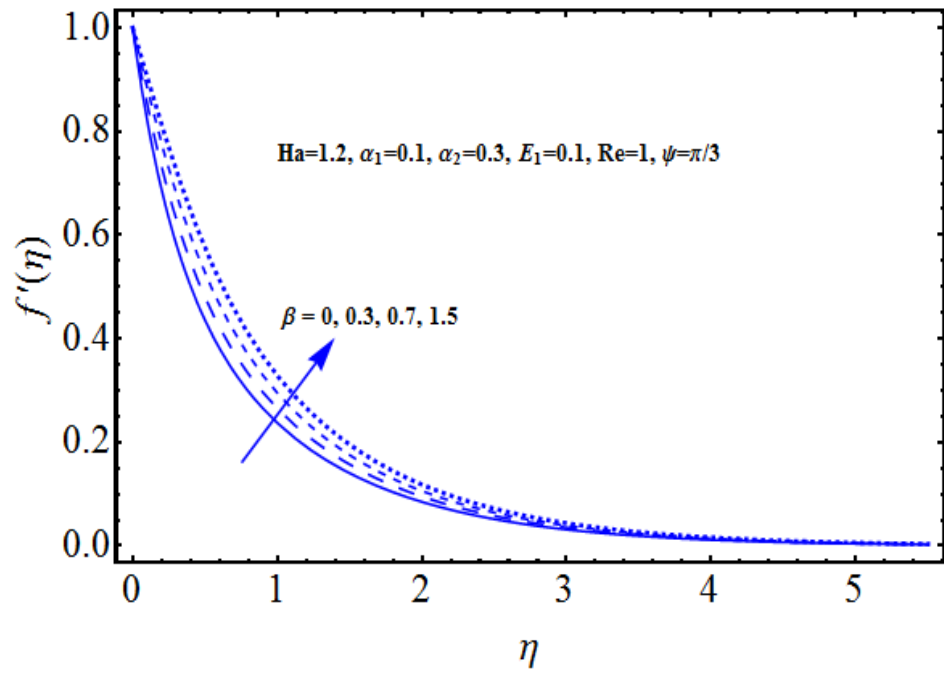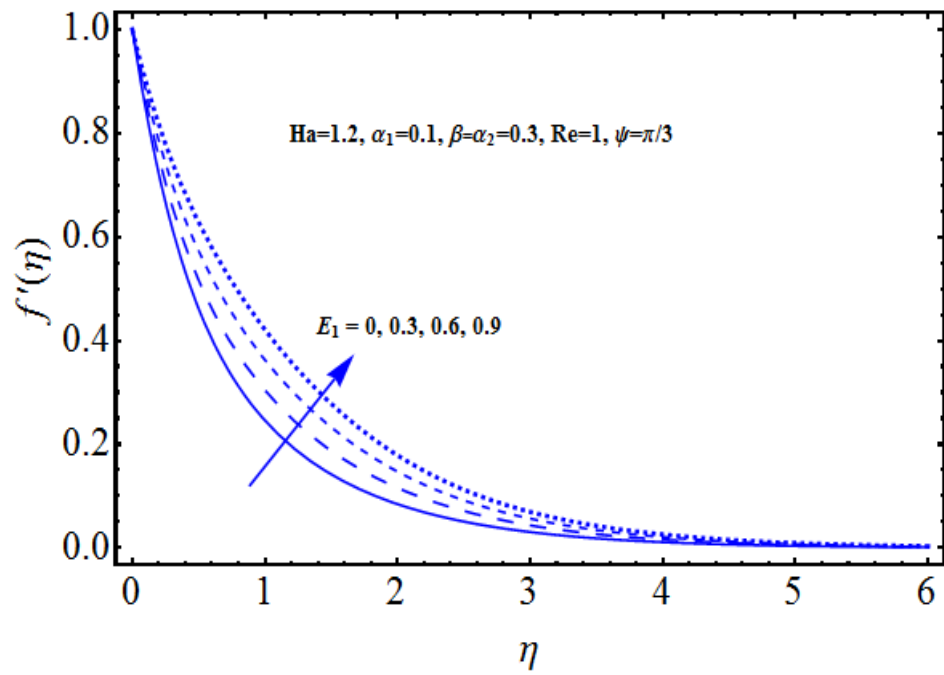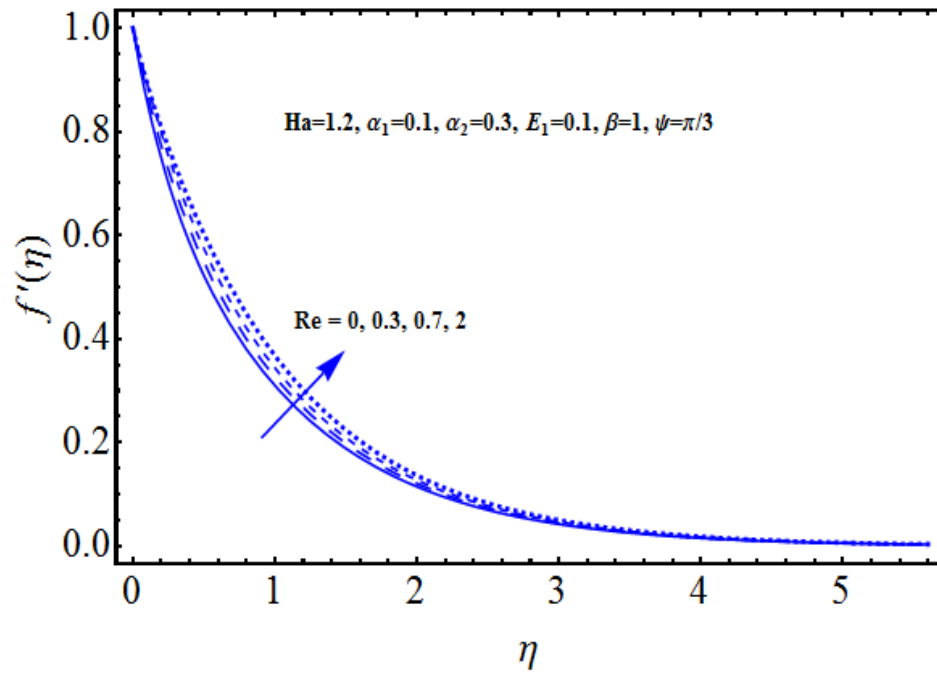Fig. 11.5: Effect of E_1 on $f'(\eta)$.

Fig. 11.6: Effect of Re on $f'(\eta)$.
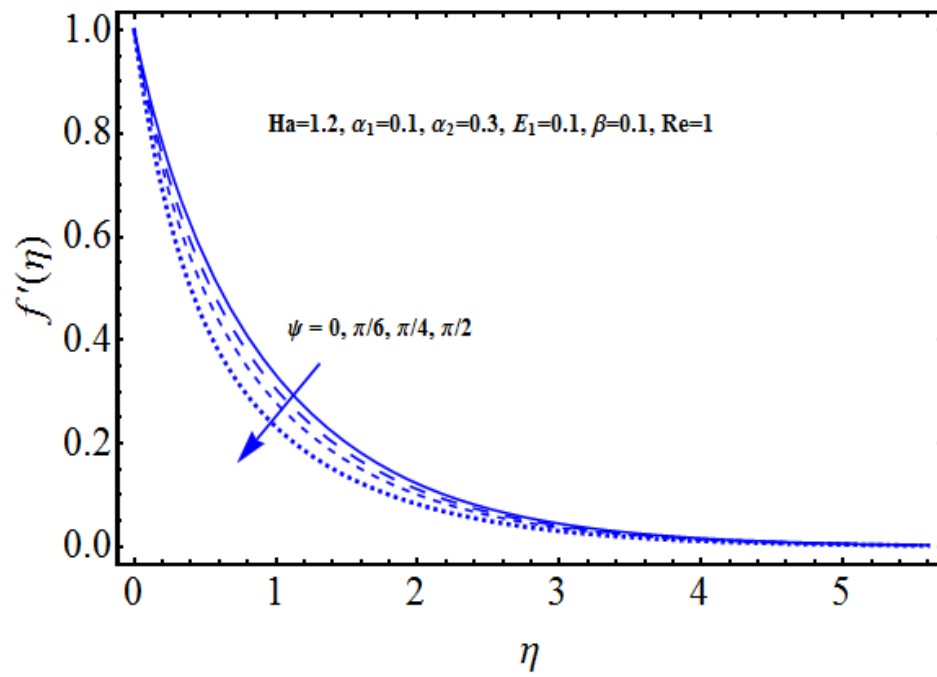
Fig. 11.7: Effect of ψ on $f'(\eta)$.

Fig. 11.8: Effect of Ha on $\theta(\eta)$.

Fig. 11.9: Effect of γ_1 on $\theta(\eta)$.

Fig. 11.10: Effect of E_1 on $\theta(\eta)$.

Fig. 11.11: Effect of α on $\theta(\eta)$.

Fig. 11.12: Effect of Ec on $\theta\left(\eta\right)$.

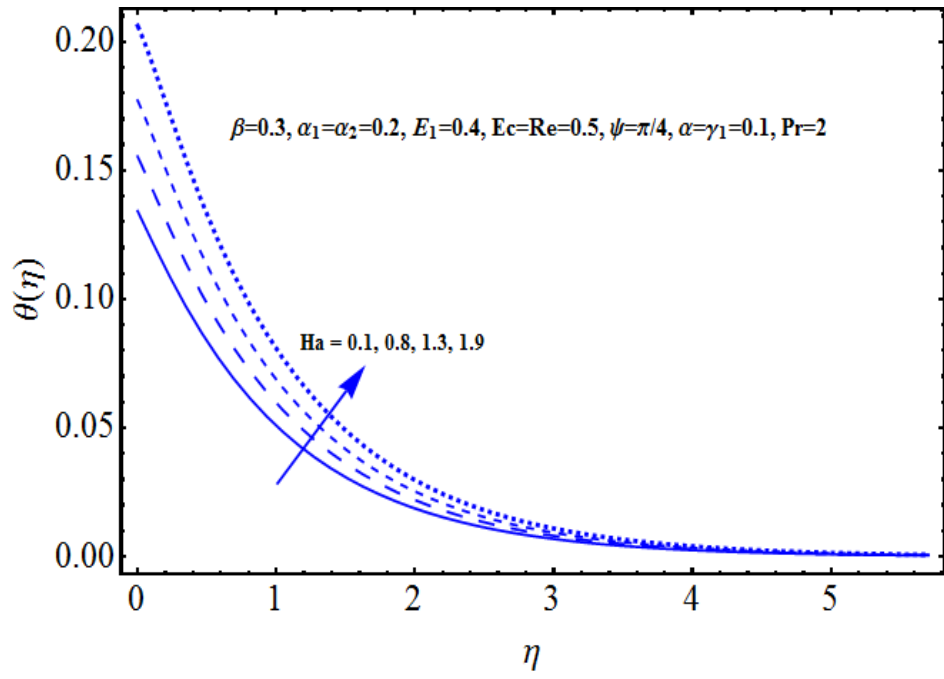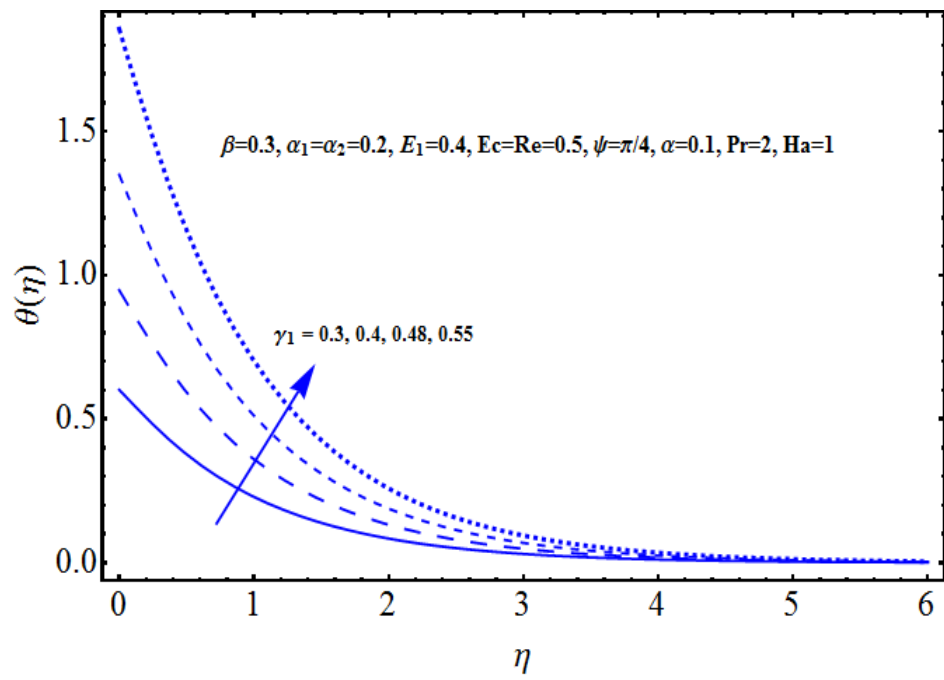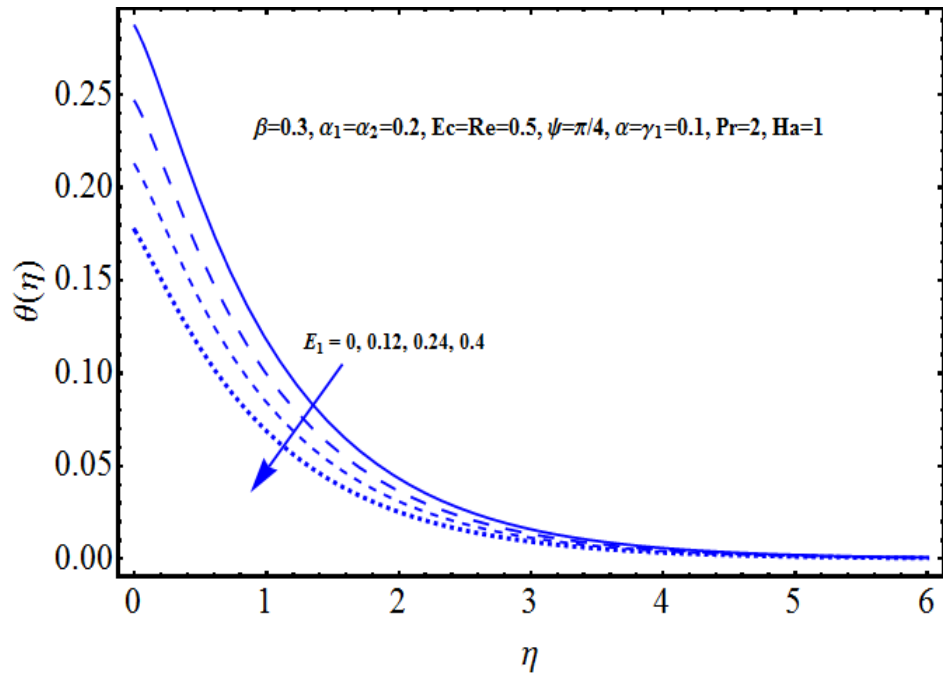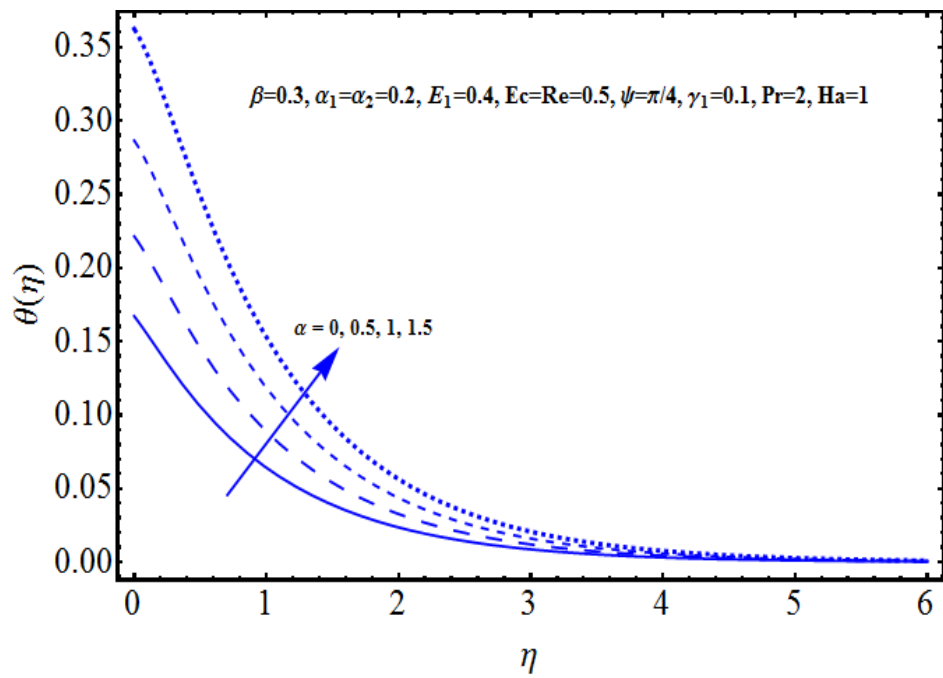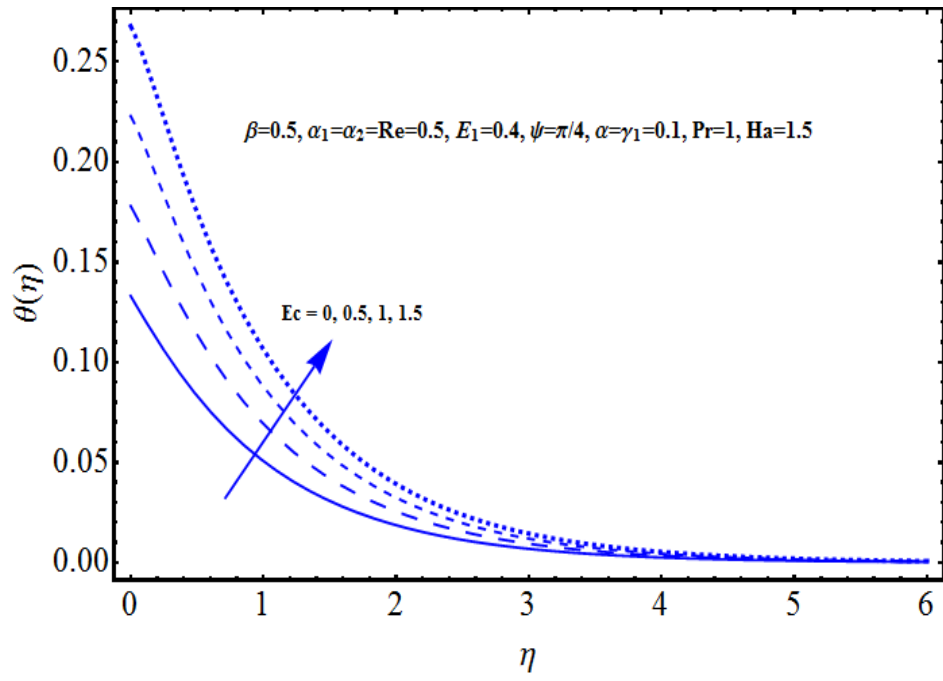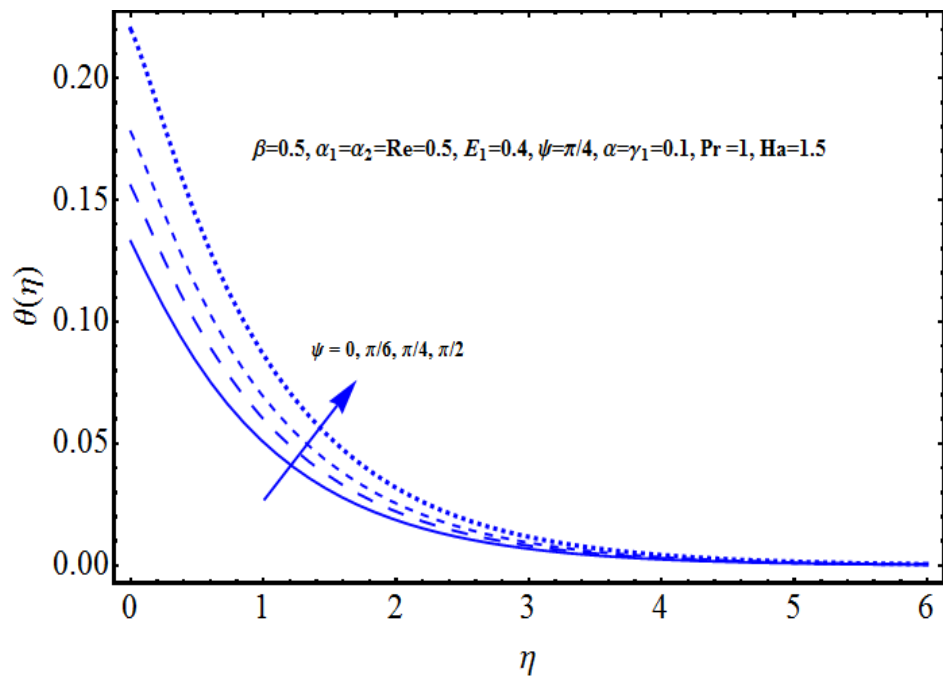Fig. 11.13: Effect of ψ on $\theta\left(\eta\right)$.
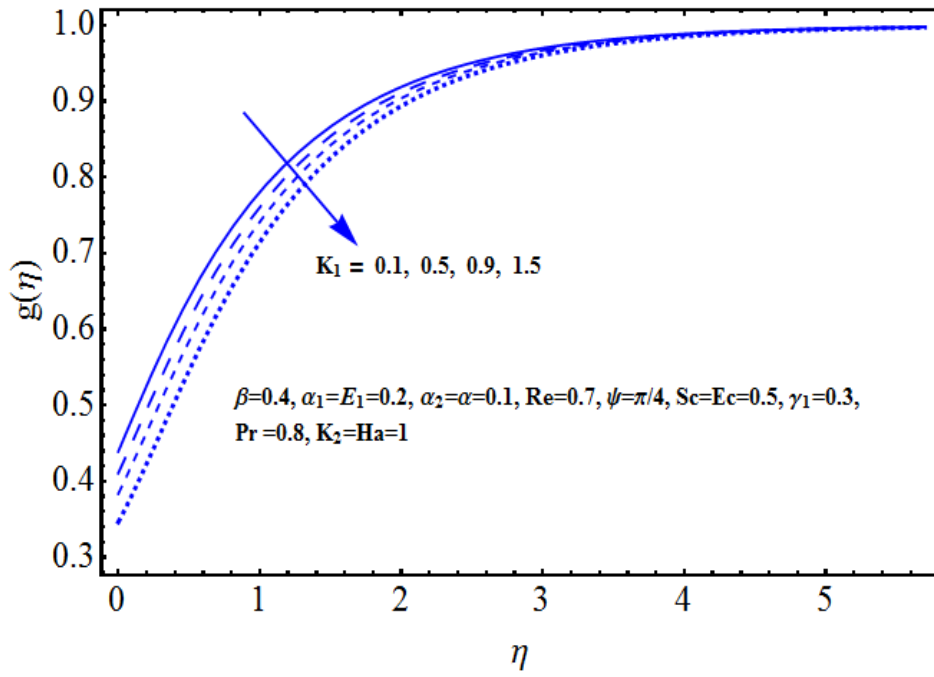
Fig. 11.14: Effect of K_1 on $g(\eta)$.
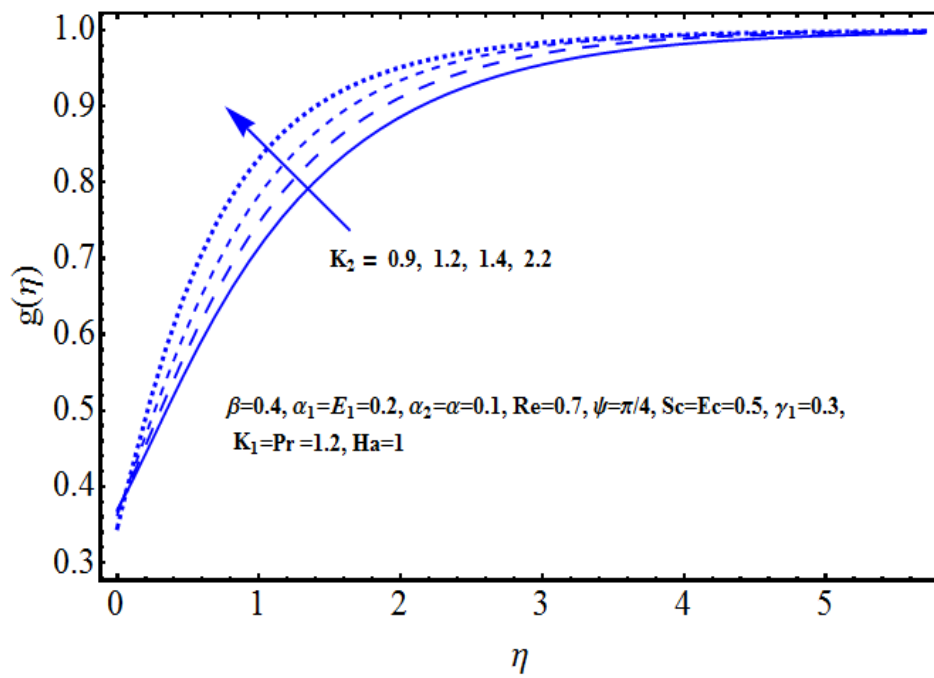
Fig. 11.15: Effect of K_2 on $g(\eta)$.
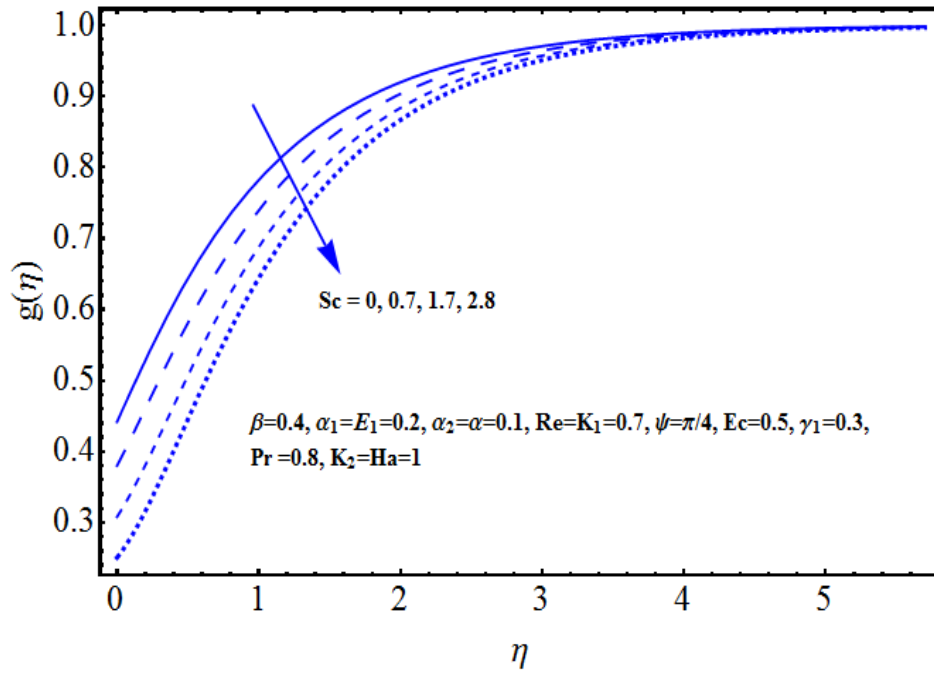
Fig. 11.16: Effect of Sc on $g(\eta)$.

Table 11.1: Convergence of series solutions for various order of approximations when $\alpha_1 = \alpha_2 = \beta = \gamma = \alpha = 0.1$, $Ha = E_1 = 0.1$, $Re = 2$, $\psi = \pi/4$, $Pr = Sc = 1.2$, $K_1 = 0.5$, $K_2 = 1$ and $Ec = 0.1$.

Order of approximations	$-f''(0)$	$-\theta'(0)$	$g'(0)$
1	1.135	0.1124	0.4259
5	1.248	0.1163	0.2622
10	1.258	0.1197	0.1846
15	1.259	0.1212	0.1613
20	1.259	0.1239	0.1302
30	1.259	0.1262	0.1193
60	1.259	0.1262	0.1193

Table 11.2: Numerical values of skin friction coefficient for different parameters.

α_1	α_2	β	Re	Ha	E_1	ψ	$-\frac{1}{\sqrt{2}} Re_x^{1/2} C_f$
0.0	0.1	0.1	2	0.2	0.2	$\pi/4$	1.861
0.1							2.673
0.2							3.546
0.1	0.0	0.1	2	0.2	0.2	$\pi/4$	2.531
	0.1						2.673
	0.2						2.824

α_1	α_2	β	Re	Ha	E_1	ψ	$-\frac{1}{\sqrt{2}} \mathrm{Re}_x^{1/2} C_f$
0.1	0.1	0.0	2	0.2	0.2	$\pi/4$	2.914
		0.1					2.673
		0.2					2.576
0.1	0.1	0.1	1	0.2	0.2	$\pi/4$	2.937
			1.5				2.778
			2				2.673
0.1	0.1	0.1	2	0.0	0.2	$\pi/4$	2.654
				0.2			2.673
				0.5			2.759
0.1	0.1	0.1	2	0.2	0.0	$\pi/4$	2.685
					0.1		2.683
					0.2		2.673
0.1	0.1	0.1	2	0.2	0.2	$\pi/6$	2.664
						$\pi/4$	2.673
						$\pi/2$	2.690

Table 12.3: Numerical values of Nusselt number for different parameters when $\alpha_1 = 0.2$ and $\alpha_2 = 0.1$.

β	γ_1	M	E_1	α	Pr	ψ	Ec	Sc	K_1	K_2	$\gamma_1(1+\frac{1}{\theta(0)})$
0.0	0.2	0.1	0.2	0.1	0.1	$\pi/4$	0.5	1.2	0.7	1	0.10708
0.2											0.10691
0.5											0.10675
0.2	0.8										0.62383
	1.2										0.74344
	1.4										0.79425
	1.2	0.0									0.66032
		0.1									0.74341
		0.3									0.85912
		0.1	0.0								0.82771
			0.2								0.74344
			0.4								0.67655
			0.2	0.0							0.74387
				0.1							0.74349
				0.3							0.7399

β	γ_1	M	E_1	α	Pr	ψ	Ec	Sc	K_1	K_2	$\gamma_1(1+\frac{1}{\theta(0)})$
0.1	1.2	0.1	0.2	0.1	0.1	$\pi/4$	0.5	1.2	0.7	1	0.73312
					0.2						0.74345
					0.4						0.78147
						$\pi/6$					0.10674
						$\pi/4$					0.10717
						$\pi/2$					0.10756
							0.1				0.12794
							0.2				0.11736
							0.3				0.10674
								0.0			0.10638
								0.5			0.10708
								1.0			0.10749
								1.2	0.5		0.12794
									0.7		0.11736
									0.9		0.10674
										0.0	0.10638
										0.5	0.10708
										1.0	0.10749

11.5   Concluding remarks

Here we have explored the characteristics of electromagnetic flow of third-grade fluid induced by an impermeable stretching surface with homogeneous-heterogeneous reactions and heat generation/absorption. The key points are summarized as follows:

- Electric field has opposite behavior for the velocity and temperature distributions.

- Velocity distribution increases for higher values of third grade fluid parameter.

- Conjugate parameter results in enhancement of temperature and thermal boundary layer thickness.

- Temperature distribution and thermal boundary layer thickness are increasing function of heat generation parameter. Results for heat absorption are reverse.

- Concentration distribution decreases for higher values of strength of homogeneous reaction K_1.

- Larger values of strength of heterogeneous reaction K_2 result in enhancement of concentration profile.

Bibliography

[1] J. B. R. Loureiroa and A. P. S. Freirea, Asymptotic analysis of turbulent boundary layer flow of purely viscous non-Newtonian fluids, J. Non-Newtonian Fluid Mech. 199, 20-28 (2013).

[2] M. Keimanesha, M. M. Rashidi, A. J. Chamkha and R. Jafari, Study of a third grade non-Newtonian fluid flow between two parallel plates using the multi-step differential transform method. Comp. Math. Appl. 62, 2871-2891 (2011).

[3] M. Mustafa, T. Hayat and S. Obaidat, Stagnation-point flow and heat transfer of a Casson fluid towards a stretching sheet. ZNA 67, 70-76 (2012).

[4] S. Abbasbanday and T. Hayat, On series solution for unsteady boundary layer equations in a special third grade fluid. Commun. Nonlinear Sci. Numer. Simulat. 16, 3140-3146 (2011).

[5] A. A. M. Mahmoud, Slip velocity effect on a non-Newtonian power-law fluid over a moving permeable surface with heat generation. Math. Comp. Modell. 54, 1228-1237 (2011).

[6] T. Hayat, S. Asad, M. Qasim and A. A. Hendi, Boundary layer flow of a Jeffrey fluid with convective boundary conditions, Int. J. Numer. Meth. Fluids 69, 1350-1362 (2012).

[7] M. Renardy and X. Wang, Boundary layer for the upper convected Maxwell fluid. J. Non-Newtonian Fluid Mech. 189-190, 14-18 (2012).

[8] M. Ramzan, M. Farooq, A. Alsaedi and T. Hayat, MHD three dimensional flow of couple stress fluid with Newtonian heating. Eur. Phys. J. Plus 128, 49 (2013).

[9] B. Sahoo and F. Labropulu, Steady Homann flow and heat transfer of an electrically conducting fluid. Comp. Math. Appl. 63, 1244-1255 (2012).

[10] O. U. Mehmood, S. Shafie and N. Mustapha, Peristaltic transport of Walters-B fluid in an asymmetric channel. Int. J. Appl. Math. Mech. 7 (21), 1-19 (2011).

[11] E. Ghasemi, M. Bayat and M. Bayat, Viscoelastic MHD flow of Walters liquid-B fluid and heat transfer over a non-isothermal stretching sheet. Int. J. Phys. Sci. 6 (21), 5022-5039 (2011).

[12] M. M. Nandeppanavar, M. S. Abel and J. Tawade, Heat transfer in a Walters-B fluid over an impermeable stretching sheet with non-uniform heat source/sink and elastic deformation. Comm. Nonlinear Sci. Numer. Simulat. 15, 1791-1802 (2010).

[13] V. Sharma and U. Gupta, Stability of stratifid elastico-viscous Walters (model B) fluid in the presence of horizontal magnetic field and rotation. Studia Geotechnica et. Mechanica 32 (2), 41-54 (2010).

[14] J. E. Dunn and R. L. Fosdick, Thermodynamics stability and boundedness of fluids of complexity 2 and fluids of second-grade. Arch. Ratio Mech. Anal. 56, 191–252 (1974).

[15] R. L. Fosdick and K. R. Rajagopal, Anomalous feature in the model of second order fluids. Arch. Ratio Mech. Anal. 70, 145–152 (1979).

[16] K. L. Hsiao, Conjugate heat transfer of magnetic mixed convetion with radiative and viscous dissipation effects for second grade viscoelastic fluid past a stretching sheet. Appl. Thermal Eng. 27, 1895-1903 (2007).

[17] T. Hayat, M. Nawaz, M. Sajid and S. Asghar, The effect of thermal radiation on the flow of a second grade fluid. Comp. Math. Appl. 58, 369-379 (2009).

[18] B. Sahoo and Y. Do, Effects of slip on sheet driven flow and heat transfer of a third grade fluid past a stretching sheet. Int. Commun. Heat Mass Transfer 37, 1064-1071 (2010).

[19] S. Abbasbandy and T. Hayat, On series solution for unsteady boundary layer equations in a special third grade fluid. Commun. Nonlinear Sci. Numer. Simulat. 16, 3140-3148 (2011).

[20] T. Hayat, A. Shafiq, M. Nawaz and A. Alsaedi, On non-linear flow of third-grade fluid between the stretching/shrinking sheets. J. Aerosp. Eng. 10.1061/(ASCE)AS.1943-5525.0000244, (2012).

[21] T. Hayat, R. Naz, S. Asghar and S. Mesloub, Soret–Dufour effects on three-dimensional flow of third grade fluid. Nuclear Eng. Design 243, 1-14 (2012).

[22] H. Alfven, Existence of electromagnetic-hydrodynamic waves. Nature 150, 405-406 (1942).

[23] J. Hartmann and I. Hg-Dynamics, Theory of the laminar flow of an electrically conducting liquid in a homogeneous magnetic field. K. Dan. Vidensk. Selsk. Mat.-Fys. Medd. 15, 1-27 (1937).

[24] M. M. Rashidi, S. Abelman and N. F. Mehr, Entropy generation in steady MHD flow due to a rotating disk in a nanofluid. Int. J. Heat Mass Trans. 62, 515-525 (2013).

[25] S. A. Shehzad, A. Alsaedi and T. Hayat, Hydromagnetic steady flow of Maxwell fluid over a bidirectional stretching surface with prescribed surface temperature and prescribed surface heat flux. Plos One 8 (7), e68139 (2013).

[26] M. Turkyilmazoglu, Exact solutions for the incompressible viscous magnetohydrodynamic fluid of a rotating disk flow. Int. J. Nonlinear Mech. 46, 306-311 (2011).

[27] T. Hayat, S. A. Shehzad, M. B. Ashraf and A. Alsaedi, Magnetohydrodynamic mixed convection flow of thixotropic fluid with thermophoresis and Joule heating. J. Thermo Phys. Heat Transfer 27, 733-740 (2013).

[28] M. Sheikholeslami, M. Gorji Bandpay and D. D. Ganji, Magnetic field effects on natural convection around a horizontal circular cylinder inside a square enclosure filled with nanofluid. Int. Commun. Heat Mass Transfer 39, 978-986 (2012).

[29] B. S. Dandapat and A. Mukhopadhyay, Finite amplitude long wave instability of a film of conducting fluid flowing down an inclined plane in presence of electromagnetic field. Int. J. Appl. Mech. Eng. 8, 379-383 (2003).

[30] T. Hayat, A. Shafiq, M. Nawaz and A. Alsaedi, MHD axisymmetric flow of third grade fluid between porous disks with heat transfer. Appl. Math. Mech. 33 (6), 749-764 (2012).

[31] K. Ahmad and R. Nazar, Unsteady magnetohydrodynamic mixed convection stagnation point flow of a viscoelastic fluid on a vertical surface. JQMA 6 (2), 105-117 (2010).

[32] M. Hatami, M. Sheikholeslami, M. Hosseini and D. D. Ganji, Analytical investigation of MHD nanofluid flow in non-parallel walls. J. Mol. Liq. 194, 251-259 (2014).

[33] M. Sheikholeslami, D. D. Ganji, M. Gorji-Bandpy and S. Soleimani, Magnetic field effect on nanofluid flow and heat transfer using KKL model. J. Taiwan Inst. Chem. Eng. 45, 795-807 (2014).

[34] M. C. Raju, N. A. Reddy and S. V. K. Varma, Analytical study of MHD free convection dissipative boundary layer flow past a porous vertical surface in the presence of thermal radiation, chemical reaction and constant suction. Ain Shams Eng. J. 5 (4), 1361–1369 (2014).

[35] M. Awais, T. Hayat, A. Alsaedi and S. Asghar, Time dependent three dimensional boundary layer flow of a Maxwell fluid. Comp. Fluids 91, 21-27 (2014).

[36] N. Freidoonimehr, M. M. Rashidi and S. Mahmud, Unsteady MHD free convective flow past a permeable stretching vertical surface in a nanofluid. Int. J. Thermal Sci. 87, 136-145 (2015).

[37] M. Sheikholeslami, D. D. Ganji, M. Y. Javed and R. Ellahi, Effect of radiation on magnetohydrodynamic nanofluid flow and heat transfer by means of two phase model. JMMM 374, 36-43 (2015).

[38] M. Sheikholeslami and D. D. Ganji, Nanofluid flow and heat transfer between parallel plates considering Brownian motion using DTM. Comput. Methods Appl. Mech. Eng. 283, 651-663 (2015).

[39] R. I. Peroso and G. A. Domoto. Inward spherical solidofication-solution by the method of strained co-ordinates. Int. J. Heat Mass Transfer 16 (5), 1037-1043 (1973).

[40] M. Epstein, The effect of melting on heat transfer to submerged bodies. Heat Mass Transfer 2, 97-104 (1975).

[41] M. Epstein and D. H. Cho, Melting heat transfer in steady laminar flow over a flat plate. ASME J. Heat Transfer 98, 531-533 (1976).

[42] M. Kazmierczak, D. Poulikakos and D. Sadowski, Melting of a vertical plate in porous medium controlled by forced convection of a dissimilar fluid. Int. Commun. Heat Mass Transfer 14, 507-517 (1987).

[43] W. T. Cheng and C. H. Lin, Melting effect on mixed convective heat transfer with aiding and opposing external flows from the vertical plate in a liquid-saturated porous medium. Int. J. Heat Mass Transfer 50, 3026-3034 (2007).

[44] W. T. Cheng and C. H. Lin, Unsteady mass transfer in mixed convective heat flow from a vertical plate embedded in a liquid-saturated porous medium with melting effect. Int. Commun. Heat Mass Transfer 35, 1350-1354 (2008).

[45] A. Ishak, R. Nazar, N. Bachok, and I. Pop, Melting heat transfer in steady laminar flow over a moving surface. Heat Mass Transfer 46 (4), 463-468 (2010).

[46] N. Bachok, A. Ishak and I. Pop, Melting heat transfer in boundary layer stagnation point flow towards a stretching/shrinking sheet. Phys. Lett. A. 374 (40), 4075-4079 (2010).

[47] N. A. Yacob, A. Ishak and I. Pop, Melting heat transfer in boundary layer stagnation-point flow towards a stretching/shrinking sheet in a micropolar fluid. Comp. Fluids 47, 16-21 (2011).

[48] R. S. Gorla, A. Chamkha and A. Aloraier, Melting heat transfer in a nanofluid flow past a permeable continuous moving surface. J. Naval Arch. Marine Eng. 8, 83-92 (2011).

[49] R. G. Abdel-Rahman, M. M. Khader and A. M. Megahed, Melting phenomenon in magneto hydro-dynamics steady flow and heat transfer over a moving surface in the presence of thermal radiation. Chin. Phys. B 22 (3), 030202 (2013).

[50] T. Hayat, Z. Iqbal, M. Mustafa and A. A. Hendi, Melting heat transfer in the stagnation point flow of third-grade fluid past a stretching sheet with viscous dissipation. Thermal Sci. 17 (3), 865-875 (2013).

[51] T. Hayat, M. Hussain, M. Awais and S. Obaidat, Melting heat transfer in a boundary layer flow of a second grade fluid under Soret and Dufour effects. Int. J. Numer. Meth. Heat Fluid Flow 23 (7), 1155-1168 (2013).

[52] M. Awais, T. Hayat, M. Mustafa, K. Bhattacharyya and M. Asif Farooq, Analytic and numeric solutions for stagnation-point flow with melting, thermal-diffusion and diffusion-thermo effects. Int. J. Numer. Meth. Heat Fluid Flow 24 (2), 438-454 (2014).

[53] T. Hayat, M. Farooq and A. Alsaedi, Melting heat transfer in the stagnation-point flow of Maxwell fluid with double-diffusive convection. Int. J. Numer. Meth. Heat Fluid Flow 24 (3), 760-774 (2014).

[54] K. Das, Radiation and melting effects on MHD boundary layer flow over a moving surface. Ain Shams Eng. J. 5, 1207-1214 (2014).

[55] J. H. Merkin, Natural convection boundary layer flow on a vertical surface with Newtonian heating. Int. J. Heat Fluid Flow 15, 392-398 (1994).

[56] D. Lesnic, D. B. Ingham and I. Pop, Free convection from a horizontal surface in a porous medium with Newtonian heating. J. Porous Media 3, 227-232 (2000).

[57] D. Lesnic, D. B. Ingham, I. Pop and C. Storr, Free convection boundary-layer flow above a nearly horizontal surface in a porous medium with Newtonian heating. Heat Mass Transfer 40, 665 (2004).

[58] M. Z. Salleh, R. Nazar and I. Pop, Forced convection boundary layer flow at a forward stagnation point with Newtonian heating. Chem. Eng. Comm. 196, 987-996 (2009).

[59] M. Z. Salleh, R. Nazar and I. Pop, Boundary layer flow and heat transfer over a stretching sheet with Newtonian heating. J. Taiwan Inst. Chem. Eng. 41, 651-655 (2010).

[60] M. J. Uddin, W. A. Khan and A. I. Ismail, MHD free convective boundary layer flow of nanofluid past a flat vertical plate with Newtonian heating boundary condition. PLOS One 7 (11), e49499 (2012).

[61] T. Hayat, M. Farooq, Z. Iqbal and A. Alsaedi, Mixed convection Falkner Skan flow of a Maxwell fluid. ASME J. Heat Transfer 134, 114504 (2012).

[62] T. Hayat, Z. Iqbal and M. Mustafa, Flow of second grade fluid over a stretching surface with Newtonian heating. J. Mech. 28, 209-216 (2012).

[63] O. D. Makinde, Computational modelling of MHD unsteady flow and heat transfer towards a flat plate with Navier slip and Newtonian heating. Brazilian J. Chem. Eng. 29, 159-166 (2012).

[64] M. Ramzan, M. Farooq, A. Alsaedi and T. Hayat, MHD three dimensional flow of couple stress fluid with Newtonian heating. Euro. Phy. J. Plus 128, 49 (2013).

[65] O. D. Makinde, Effects of viscous dissipation and Newtonian heating on boundary layer flow of nanofluids over a flat plate. Int. J. Numer. Meth. Heat Fluids Flow 23, 1291-1303 (2013).

[66] N. M. Sarif, M. Z. Salleh and R. Nazar, Numerical solution of flow and heat transfer over a stretching sheet with Newtonian heating using the Keller Box method. Procedia Engineering 53, 542-554 (2013).

[67] M. A. Chaudhary and J. H. Merkin, A simple isothermal model for homogeneous heterogeneous reactions in boundary layer flow. I equal diffusivities. Fluid Dyn. Research 16, 311-333 (1995).

[68] M. A. Chaudhary and J. H. Merkin, A simple isothermal model for homogeneous-heterogeneous reactions in boundary-layer flow. II Different diffusivities for reactant and autocatalyst. Fluid Dyn. Research 16, 335-359 (1995).

[69] M. A. Chaudhary and J. H. Merkin, Homogeneous-heterogeneous reactions in boundary-layer flow: Effects of loss of reactant. Math. Computer Model 24, 21-28 (1996).

[70] W. A. Khan and I. Pop, Flow near the two-dimensional stagnation point on an infinite permeable wall with a homogeneous-heterogeneous reaction. Commun. Nonlinear Sci. Numer. Simulat. 15, 3435-3443 (2010).

[71] N. Bachok, A. Ishak and I. Pop, On the stagnation-point flow towards a stretching sheet with homogeneous–heterogeneous reactions effects. Commun. Nonlinear Sci. Numer. Simulat. 16, 4296-4302 (2011).

[72] S. Shaw, P. K. Kameswaran and P. Sibanda, Homogeneous-heterogeneous reactions in micropolar fluid flowfrom a permeable stretching or shrinking sheet in a porous medium. Bound. Value Prob. 2013, 77 (2013).

[73] P. K. Kameswaran, S. Shaw, P. Sibanda, and P. V. S. N. Murthy, Homogeneous-heterogeneous reactions in a nanofluid flow due to a porous stretching sheet. Int. J. Heat Mass Transfer 57, 465-472 (2013).

[74] S. J. Liao, Beyond Perturbation: Introduction to Homotopy Analysis Method, Chapman and Hall, CRC Press, Boca Raton (2003).

[75] S. J. Liao, Homotopy analysis method in non-linear differential equations, Springer and Higher Education Press, Heidelberg (2012).

[76] S. Abbasbandy, E. Shivanian and K. Vajravelu, Mathematical properties of $\hbar$-curve in the frame work of the homotopy analysis method. Commun. Nonlinear Sci. Numer. Simulat. 16, 4268-4275 (2011).

[77] A. Mastroberardino, Homotopy analysis method applied to electrohydrodynamic flow. Commun. Nonlinear Sci. Numer. Simulat. 16, 2730–2736 (2011).

[78] S. Abbasbandy and A. Shirzadi, A new application of the homotopy analysis method: Solving the Sturm–Liouville problems. Commun. Nonlinear Sci. Numer. Simulat. 16, 112-126 (2011).

[79] M. Turkyilmazoglu, Solution of the Thomas-Fermi equation with a convergent approach. Commun. Nonlinear Sci. Numer. Simulat. 17, 4097-4103 (2012).

[80] O. A. Beg, M. M. Rashidi, T. A. Beg and M. Asadi, Homotopy analysis of transient magneto-bio-fluid dynamics of micropolar squeeze film in a porous medium: A model for magneto-bio-rheological lubrication. J. Mech. Medicine Biology 12 1250051 (2012).

[81] M. M. Rashidi, S. A. M. Pour, T. Hayat and S. Obaidat, Analytic approximate solutions for steady flow over a rotating disk in porous medium with heat transfer by homotopy analysis method. Comp. Fluids 54, 1-9 (2012).

[82] T. Hayat, A. Qayyum, F. Alsaedi, M. Awais and A. M. Dobaie, Thermal radiation effects in squeezing flow of a Jeffery fluid. Eur. Phys. J. Plus. 128, 85 (2013).

[83] S. A. Shehzad, T. Hayat, M. S. Alhuthali and S. Asghar, MHD three-dimensional flow of Jeffrey fluid with Newtonian heating. J. Central South Uni. 21, 1428-1433 (2014).

[84] Q. Xue, Model for thermal conductivity of carbon nanotube based composites. Phys. B Condens Matter 368, 302-307 (2005).

[85] H. Andersson, Slip flow past a stretching surface. Acta Mech. 158, 121-125 (2002).

[86] M. A. Mahmoud, Chemical reaction and variable viscosity effects on flow and mass transfer of a non-Newtonian visco-elastic fluid past a stretching surface embedded in a porous medium. Meccanica 45, 835-846 (2010).

[87] M. A. Mahmoud and S. E. Waheed, MHD flow and heat transfer of a micropolar fluid over a stretching surface with heat generation (absorption) and slip velocity. J. Egyp. Math. Soc. 20, 20-27 (2012).

[88] T. Hayat and M. Qasim, Influence of thermal radiation and Joule heating on MHD flow of a Maxwell fluid in the presence of thermophoresis. Int. J. Heat Mass Transfer 53, 4780-4788 (2010).

[89] M. Awais, T. Hayat and A. Alsaedi, Investigation of heat transfer in flow of Burgers fluid during a melting process. J. Egyp. Math. Soc. 23, 410-415 (2015).

[90] T. R. Mahapatra and A. S. Gupta, Heat transfer in stagnation point flow towards a stretching sheet. Heat Mass Transfer 38, 517–521 (2002).

[91] T. Hayat, M. Farooq, A. Alsaedi and Z. Iqbal, Melting heat transfer in the stagnation point flow of Power-Eyring fluid. J. Thermo. Heat Transfer 27 (4), 761-766 (2013).